CRANFIELD INSTITUTE OF TECHNOLOGY

SCHOOL OF AUTOMOTIVE STUDIES

Ph.D. THESIS

M.S.I. ALVI

THE STRESS DISTRIBUTION IN THE JOINTS OF VEHICLE CHASSIS FRAMES SUBJECT TO TORSION

Supervisor: G. H. TIDBURY

February, 1978

This thesis is dedicated to my parents, elders, family members and friends who have always remembered me in their prayers and without their encouragement I could not have completed this work.

ABSTRACT

The problem of warping inhibition in the joints of commercial vehicle chassis frames is very important for the estimation of stress distribution in the joints and the overall torsional stiffness of frames. The joints being the weakest parts in the entire frame require that the stress levels should be estimated when designing a frame for required torsional stiffness. Plate theory has been applied to analyse stress distributions in the joints of a ladder frame in torsion. The frame consists of channel section cross members welded to the web of the side members. The degree of cross member warping inhibition in the welded joints has also been estimated analytically by using the concept of the strip beam theory. The analytical values of stresses have been compared with photoelastic measurements on photoelastic models of isolated joints and a complete ladder frame.

ACKNOWLEDGEMENTS

I would like to express my sincere thanks to my supervisor, Mr G H Tidbury, for his timely guidance, inspiration and encouragement which has played a major part in the completion of this work. I want to thank the authorities of The School of Automotive Studies for providing me with the facilities to carry out my Ph.D. studies there.

I would also like to express my gratitutde to the Vice Chancellor of The University of Engineering and Technology, Lahore, Pakistan, for granting me study leave.

My special thanks to my friend Ing. Dusan Kecman for helping me to get important information from the work published in Russian without which this work would have been narrow and almost incomplete. I wish to show my gratitude to Dr Majid Sadeghi and Mr K P Nair for their help.

I would also like to thank Messrs Reg Aldridge and John Heathorn and other members of the workshop staff who helped in making aluminium moulds and advised me on overcoming the difficulties encountered during the casting of the Araldite models.

Finally, my grateful thanks to my typist, Mrs E Denton, who did an excellent job to bring this work to its final shape.

CONTENTS

LIST OF FIGURES

LIST OF PHOTOGRAPHS

NOTATION

$x_1x_2x_3$	Catesian co-ordinate axes
u_i	Displacement components
τ_{ij}	Stress components
n_{ij}	Force components
q_i	Shear force components
m_{ij}	Component of moments
E	Young's Modulus
G	Shear Modulus
ν	Poisson Ratio
f_σ	Material Fringe Value
σ_z	Direct stress in the cross member profile.
ℓ	Half the length of the cross member
t	Cross member section thickness.
L	Half the length of the side member.
h	Side member section thickness.
k_o	Cross member flange warping force intensity.
$\overset{*}{C}$	Strip beam theory constant.
$\overset{*}{C}_{av}$	Average value of $\overset{*}{C}$ used in this work
K	Cross member warping restraint factor.
α_m =	$\frac{m\pi}{2L}$
ϕ_1 =	$\text{Cosh}\alpha_m x_2$
ϕ_2 =	$\sinh\alpha_m x_2$
ϕ_3 =	$x_2\phi_1$
ϕ_4 =	$x_2\phi_2$
p =	Cross member end warping force per unit length

Dimensions of the joint are defined in relevant figures.

Other variables and constants are defined in the text during theoretical development of the analysis.

INTRODUCTION

A chassis frame is an essential structural part of any commercial automobile vehicle with regard to its load carrying capacity. Besides payload it is subjected to various kinds of loads including static, dynamic and shock loads, etc. during vehicle operation. As such a chassis frame should require maximum attention during the design of a vehicle structure.

Chassis frames in trucks, trailers and semi-trailers generally consist of two side (or longitudinal) members and several cross members arranged in a ladder configuration. Because of this arrangement they are also described as ladder frames. The side members and cross members are usually of open channel or I-sections but sometimes closed, tubular sections are employed as cross members.

There is a great variety of designs of joints between the cross members and side members both as to joint configuration and the method of attachment of cross member to side member. The design of chassis frames has been based on the bending loads and torsional loads. The side members are generally designed to resist bending loads due to payloads and the cross members mainly stand torsional loads which arise due to many reasons during vehicle operation.

A chassis frame is expected to exhibit a torsional stiffness which should meet the operational requirements of the vehicle. Because of this consideration more emphasis has been given to the proper control of the overall torsional stiffness values in chassis frames. However the fact should not be ignored that the frame members should not be subjected to high stresses that could lead to their failure thus making the frame ineffective.

The weakest parts of the frame are its joints which are also the regions of high stresses due to many factors. It is necessary that the desired torsional stiffness of a frame should not produce very high stress in the joints which could cause the failure of the joints.

The major factor for the cause of high stresses in the frame joints is due to the warping inhibition in them. Open section beams warp in torsion which,when restrained, produce high localised stresses. The degree of warping inhibition in a joint also controls the overall frame torsional stiffness. So it is important for a designer, before designing a frame for required torsional stiffness, to estimate the following

1. The degree of warping inhibition in the joints analytically or experimentally.

2. The distribution of stresses in joints.

Various automatic structural programmes to analyse frames have been developed which give a good estimation of the overall

torsional stiffness but stress estimations in the joints are not accurate enough. A few attempts have been made to investigate stresses in joints by analytic methods. Most information regarding stresses in joints has been obtained by using experimental methods on actual frames. Such information cannot be generalised for joints of other dimensions and configuration. In order to improve knowledge in this area an investigation has been carried out in the present work to analyse stress distributions and the degree of warping inhibition in the joints of a ladder frame in torsion. The frame consists of channel section cross members welded to the web of channel section side members. The equations of plate theory have been employed in this analysis and the theoretical stress values have been compared with experimental stresses obtained by using reflection techniques of photoelasticity on photoelastic models.

CHAPTER 1 LITERATURE SURVEY

A general survey of the literature published in English indicates that investigations in commercial vehicle chassis frames have been conducted mostly for estimating torsional stiffness of these frames rather than stresses occurring in the area of a joint. In dealing with frames consisting of open sections, torsional stiffness and stresses in them are mainly affected by the amount of warping inhibitions in the joint. The stresses occurring in the cross members have been obtained from warping inhibition investigations. Research work in this field has received greater attention in East European countries and a number of references are available specially in the Russian language. Probably Vlasov's [1] major work in thin walled beams attracted attention in those countries. English translations of work published in Russia in the field are not available and the author reviewed some of the references appearing later in this section with the help of a colleague conversant with the Russian language.

The joints of ladder type frames have been investigated by various research workers employing the following methods.

i) Vlasov's approach for analysing open section thin walled beams subject to arbitrary loadings.

ii) Wagner Kappus' approach for analysing open section thin walled beams subject to torsional loads.

iii) Finite element methods available for structural analysis.

iv) Analytical approach based on classical plate theory.

The analysis of entire frames has been mostly carried out by employing computerised automatic programmes available for a variety of structural engineering problems. In certain cases, the conventional programmes have been modified to include special effects associated with the behaviour of thin walled beams subjected to torsional loads.

The analysis of joints requires an accurate estimation of warping inhibition in every joint as its value depends on many factors including methods of attachment employed for connecting cross members to the side members. The stresses in a joint depend upon the manner in which the load is transferred from cross member to the side member and vice versa. Most of the research conducted in the analysis of chassis frames depended on the estimation of warping inhibition by simple experimental tests on isolated joints. Very few attempts have been made to estimate this effect theoretically. A survey of the published literature is presented in the following pages. The author has considered it useful to briefly point out the salient features of work published in Russian or German for future reference.

1.1. ANALYTICAL METHODS

The torsional stiffness of chassis frames has been estimated in some

cases by analytical methods employing Vlasov's theory of thin walled beams [1]. The amount of partial restraint in a frame joint of open section members has been determined by purely experimental procedures for the analytical methods in most cases but a few have employed theoretical estimation of these effects. The main objective of analytical methods has been torsional stiffness rather than stress distribution in the joints although in some cases stresses in the cross members have been compared.

1.1.1. The application of Vlasov's theory in joint analysis

Doich [2] suggested a method of calculating stresses and torsional stiffness in bus chassis frames. He assumed that a beam with elastically restrained ends could be considered as an assembly of several beams with rigid ends. The fictitious lengths of such beams were calculated from restrained torsion considerations at the joint. They were employed to determine angle of twist at any section of the composite beam when subjected to known torsional moments and bimoments at each end. Equality of angle of twist at any section was considered as a condition for the composite beam and he obtained an equivalent uniform average cross section beam to replace the composite one. The equivalent beam dimensions were used to calculate stresses/angle of twist in the beam. But the fictitious lengths of the elemental beams can only be calculated if the coefficients of warping restraint at both ends of a composite beam are known. He has suggested that strain gauge measurements at various points on the actual frame should be made to determine these coefficients. His method can be useful only for existing frames where such measurements are possible. Gel'fgat and Oshnokov [3] proposed a simplified method of calculating torsional stiffness by considering the equilibrium of bimoments in a joint. However, they assumed the joints as rigid ones which does over-estimate the bimoments near the joints and does not help towards an understanding of the interaction between side members and cross members. Hanke [4] analysed a ladder frame joint consisting of a channel section cross member symmetrically attached to the web of a channel section side member. He considered that in a perfectly coupled joint (i.e. rigid) the total work done by the stresses induced in the joint due to torsion was zero. He included the work done due to bimoment stresses in this equation and obtained a condition of bimoment equilibrium at the joint which was similar to that proposed in [3]. The angle of twist per unit length of all members ending in the joint was assumed to be equal. He used the equations of [1] to calculate the distribution of bimoment and the angle of twist etc. for each member of the joint. He introduced an experimentally determined coupling coefficient to deal with joints with imperfect coupling to include the degree of warping inhibition. He has suggested that coupling coefficients should be determined experimentally by measuring the angle of twist and bimoment in various members of an isolated joint. Zaks [5] investigated the effect of cross member end warping loads on the side member in a joint from the consideration of equilibrium of bimoments in the two parts of the side member assumed to be connected to each other in the joint. He derived a bimoment equilibrium equation at the joint in a more general form including the asymmetry of the cross member attachment to the side member. He also assumed a perfect kinematic coupling between various members meeting in the joint. This is another name for rigid joints which in actual practice seldom exist and due to local

deformations of the webs and flanges of the various members the kinematic coupling does not remain perfect. Zaks used the coupling coefficients of [4] to overcome this difficulty. He has also included the length of the side member in the derivation of the bimoment equation. The coupling coefficients are affected by the length of the members if the beams are very short otherwise they are constant for particular joints. Zaks and Belokurov [6] found that warping in a joint was also dependent upon the direction in which twisting moments were applied to the cross member and side member ends in the joint. They investigated the case when equal torques of the same sense were applied to the cross member and side member ends in a joint, the warping produced was three times greater than in the case in which torques were applied in opposite sense to each other. They concluded that a soft joint would result when the members were subjected to torques of the same sense while a stiff joint would result in the other case. The automobile frame joints would behave as "soft joints" as torques of the same nature were induced. Warping of any member in the joint depends on the inhibition offered by others which must depend on the displacements produced due to the applied loads. They found that joints in which cross members were attached with vertical webs behaved in a much stiffer manner compared to the joints where cross member webs were attached horizontally. Zaks and Belokurov [7] further invesitgated the effect of the cross member web orientation in the joint on the torsional stiffness of a ladder frame consisting of I-section cross members. They found that the torsional stiffness of the frame increased as the angle between the cross member web and the longitudinal axis of the side member was increased but the stresses increased too. They proposed that this was not a proper method of controlling the torsional stiffness. Instead they suggested a method to increase frame stiffness by using cross members of partly closed and partly open section members. Closed sections towards the ends and open section in the middle of the cross members were used. Such composite section cross members were used in a ladder frame and they found that the value of the torsional stiffness was five times greater than with open section cross members. High stresses were found at the sections where open and closed sections of a cross member joined. Zaks and Belokurov [8] investigated another composite shape of cross members in a ladder frame with Z-section side members. The middle part of the cross member was closed in this case. This resulted in a soft joint.

Zaks, Zaharov and Belokurov [9] reported that in the case of short beams of open sections, Vlasov's [1] assumption of zero shear at the mid plane was not valid. In short cross member beams the effect of mid plane shear must be included in the calculations. Zaks and Zaharov [10] further investigated the effect of mid plane shear in short open section beams and observed that the end conditions of a beam produced more effects on displacements than stresses. Neglecting displacements due to mid plane shear in the case of short beams led to a big difference between experimental and theoretical values. The ratio of beam length to beam depth was kept very small (i.e. only 0.5) in their analysis.

1.1.2 The application of plate theory in joint analysis.

Zaks [11] employed the equations of classical plate theory to analyse

stresses in an automobile chassis joint consisting of a channel section side member and a symmetrical I-section cross member. He made a comparison of the results of this analysis with the results calculated using Vlasov's thin walled beam theory. Both results were then compared with experimental values for various locations of cross member web on the side member. He found that in every case results predicted by plate theory were more accurate in the region of the joint than those obtained by Vlasov's theory. Both methods showed a good comparison in regions away from the joint which were not affected by the localised affects of the joint. Zaks concluded that the plate theory gave more accurate results than Vlasov's theory if stress distributions were required in the region of the joint. Both theoretical approaches employed by him gave proportional values in terms of cross member flange end warping force intensity. The value of warping force intensity in turn depends on the amount of warping inhibiton which he measured experimentally. Then he applied plate theory for a symmetric I-section cross member where flange warping loads were antisymmetrically distributed on the side member and there was no contribution from cross member web. It will be shown in the present work that plate theory can be applied for a channel section cross member to estimate stresses in the side member as well as the cross member which Zaks has ignored because warping force intensity was not estimated analytically. It seems that further use of plate theory in the joint analysis for a channel section cross member has not been undertaken because of unsymmetry of loading and distribution of the cross member web warping load. Kobrin, Kilimnik and Titov [12] used the equations of plate theory developed by Zaks [11] to investigate the state of stress of chassis frame side member walls at the points of load transfer. They also restricted themselves to the analysis of a symmetric problem and obtained good agreement with experimentally measured values.

1.1.3. Joint analysis using simple models

Takahashi [13] invesitgated the torsional strength of truck frames by using simple idealised models. He observed that when a channel section cross member was attached to an equal channel section side member and were joined flange to flange, the whole load is transferred through flanges only and the webs do not share in the transfer. In order to idealise this mode of load transfer he idealised a channel section by a rectangular frame consisting of four rods joined together. He demonstrated the load transfer path by using paper models and then used the rectangular frame model of a joint to represent this effect. In the case of full depth cross members which are attached to the flanges and web, maximum warping inhibition of the cross member takes place. It is not clear how he ignored the warping force of the cross member web. It is only possible if it is allowed to warp freely. It is accepted that the zero warping line on a channel section flange does not lie in the middle but Takahashi has assumed that it is in the middle. He has successfully shown that the problem of a chassis frame with full depth channel section cross members could be analysed in a simple manner by using a rod frame model of the actual frame. Simple expressions for torsional, bending and axial rigidities of the rod were employed to obtain accurate stresses and displacements. He used

a relatively new method known as "Vibration Method" with a hand held extensometer.to measure strains on various parts of the frame. He obtained a good agrement between theoretical results and measured values.

1.2. THE APPLICATION OF FINITE ELEMENT TECHNIQUES IN CHASSIS FRAME ANALYSIS

With the development of computer storage facilities a large variety of general purpose programs using finite element techniques have been developed for the analysis of structural problems. Chassis frames are analysed using these programs and some of the work done in this field is reviewed below.

1.2.1. Analysis without consideration of restrained torsion effects

Ali, Hedges and Mills [14] analysed a chassis type structure consisting of open and closed section beams employing finite element techniques. A stiffness matrix for a beam element was derived and a displacement method was used. All frame beams were idealised into beam elements connected at nodal points. No allowance was made for restrained torsion of open section beams. Upper and lower limits for displacements of various parts of the structure were established and comparison was made with measured values. This work was extended to compute stresses in the structure by Hedges, Norville and Gurdogan [15]. They found that in some cases stress values were over-estimated by 50% as compared to measured values. They concluded that for an accurate analysis beam section properties must be estimated correctly. Ali, Hedges and Mills [16] modified the stiffness matrix of [14] to include inertia terms and applied the modified stiffness matrix to investigate the dynamic response of the frame used in [14]. From these references it is clear that accurate stress estimation can only be made if restrained torsion of open sections is considered in a realistic manner in finite element idealisations.

1.2.2. Estimation of the degree of warping restraint

Tidbury, Marshall and Roach [17] used a simple analytical approach to estimate degree of warping inhibition of an open section cross member by a channel section side member in the joint of a ladder frame. They assumed that only the side member web provided a resistance to the warping of the cross member if the joint fixing was confined to the web. The side member web was split into independent strip beams. The beams were further assumed to be simply supported at the flange/web corner when a single force due to the warping of cross member flange act on a strip beam. Linear variations of flange warping force on each strip beam were approximated by point loads. Displacement was calculated at the load point and the ratio of the strip displacement to the normal force was assumed constant for all the beams. This constant was used to determine an effective torsion constant of the cross member. Effective torsion constant for the side member of the frame was calculated by treating the portion of its web between two cross members as a plate under torsion separated from its flange. The cross section of the web was constrained to remain plane at sections where the cross members were attached to it. The values of the effective torsion constants of the cross members and the

side members were used in the modified Erz formula to obtain the overall torsional stiffness of the frame. The value of the frame torsional stiffness compared well with the measured values. Awudu [18] applied the strip beam approach on isolated joints to check its validity. He obtained a good correlation between the strip beam and experimental values in respect of percentage warping for large sections but for sections with small flanges he found that their experimental torque deflection curves fell outside the free warping curves. The strip beam approach was the first effort, to the best of the author's knowledge, to estimate the degree of warping inhibition in a joint. Obviously a very simplified approach cannot fulfil the rigorous theoretical considerations but in certain practical applications it provided an accurate estimation of overall frame torsional stiffness. It has its limitations and does not work when the cross member web is attached parallel to the longitudinal axis of the side member [19]. Tidbury [19] has derived a general expression for the angle of twist of an open section beam in terms of end bimoments when the degree of partial warping inhibition at its two ends was not equal. He has also pointed out many practical cases where certain forces act on a chassis frame to introduce bimoment stresses in the side member besides twisting the frame. Azodi [20] has investigated the effect of a longitudinal force on a channel section side member to which an actual chassis frame would be subjected due to the braking force. He found that in such a case bimoment stresses induced in the side frame were high as compared to the bending stresses. Megson and Alade [21] estimated the warping inhibition of a cross member by the side member using finite element approach. Plate and membrane elements were used in the idealisation of a joint between a channel section side member and a channel section cross member. The side member web was assumed to be a rectangular plate simply supported along all the edges. Wagner torsion bending theory was modified to include the effect of partial warping inhibition in a joint. It was assumed that partial warping displacement of the beam end was proportional to its free warping. The validity of this assumption was verified by finite element analysis of the joint. Theoretical and experimental values for stresses and angle of twist on the cross members of isolated joints were compared. Good agreement was obtained except for stresses when the value of the cross member warping restraint factor was smaller than 0.44 [22]. Warping inhibition of the side member due to the cross member was estimated by applying the moment couple method of [23] and effective values of torsion constants of the side and cross members were used in an automatic structural program to estimate the overall torsional stiffness of a ladder frame. Theoretical and experimentally measured values compared very well. It has been shown in the present work that the cross member warping restraint factors of [17] and [21] are directly related to each other as in an elastic system displacement will be always be proportional to the applied force. The linearity of warping displacement and warping force has always been assumed in all the previously mentioned researches except in [21]. The values of cross member warping restraint factors [21] were found by finite element method and must be accurate in comparison to the strip beam approach which is a very simplified approach. It is not clear from [22], how the side member warping restraint factors were evaluated. The automatic structural program used for determining the torsional stiffness of the frame required effective torsion constants of cross

members and side members of the frame as an input to the computer. [22] is a valuable work in the analysis of ladder frames and graphs showing values of cross member (Channel and I-sections) warping restraint factors are very useful for practical purposes.

1.2.3. Stiffness matrix including restrained torsion terms

Ivanov [24] derived a stiffness matrix for a beam element with four degrees of freedom including warping. He compared the finite element results of displacements and stresses with analytical results using Vlasov's theory and observed only 1% difference. He applied this stiffness matrix to analyse an actual truck frame. In the finite element idealisation of the frame, beam elements were placed along shear centre lines with nodes at the intersection of shear centre axes of the side members and cross members. The frame joints were assumed rigid and he obtained good agreement between the theoretical and measured values. It is not certain whether the joints used in the actual frame behaved as rigid joints. Ivanov [25] used the stiffness matrix of [24] to analyse semi trailer frames for torsional and bending loads applied separately. The frame consisted of channel section cross members which were placed unsymmetrically on the webs of I-section side members. Because of the eccentricity of shear centre axes and also between the shear centres and centres of gravity of the side members and cross members it was not possible to calculate end loads from the computed values at nodal points. Further simplifying assumptions had to be made to overcome this problem and stresses did not compare well with the measured values as compared to the displacements. Flexibility of the joint was not accounted for in this analysis. Romanov, Slomka and Sablocki [26] also included additonal terms in a general stiffness matrix to account for the effect of restrained torsion in the analysis of commercial vehicle chassis frames of open section profiles. Beam elements were used in the finite element idealisation of the frame and a displacement method was employed for analysis. It was assumed initially that the frame joints were rigid and nodes coincided with the intersection of the shear centre axes of side members and cross members. It was further assumed that the beam cross section was deformable. They found that real torsional stiffness of each node was the important factor in the accurate estimation of overall frame torsional stiffness. An elasticity coefficient was used in the analysis at each nodal point to account for the flexibility of the joint. These coefficients were experimentally measured from tests on isolated joints. Beerman [27] included the elasticity of nodal points in the finite element analysis in a slightly different form. He used triangular elements in the nodal areas with 5 degrees of freedom per node thus 15 degrees of freedom for every element. He employed displacement compatibility conditions at the nodal points. The effective lengths of the cross members were used in the analysis. He has mentioned that in some practical tests warping restraint factors of greater than one were obtained.

The difficulties involved in the stress analysis of chassis frames by finite element techniques using beam elements are due to the following points:

(a) Beam elements are to be placed along the shear centre axes of the beams with nodal points at the intersection of shear centre axes. In cases where cross members are not placed symmetrically on the side member web it cannot be achieved and as a result of this bimoment equilibrium of the joint is not maintained.

(b) Because of the arrangement suggested in point (a), eccentricity exists between shear centre axes and centroidal axes of the beams except for I-section beams. Because of this eccentricity bending stresses are not predicted accurately. It is reported because of this discrepancy that some results are obtained accurately with respect to shear centres axes as reference axes while in some other cases centroidal and mid plane axes could lead to better estimates.

(c) Elasticity of the nodal points require experimental tests to determine the degree of warping inhibition in a joint.

1.3 OTHER APPROACHES

Kobrin and Gorbonos [28] carried out a statistical analysis to determine the optimum values of design parameters of side rails in truck frames. The analysis was based on the information collected from the existing design of truckframes used by various major industrial plants of the world. The design criteria for the side rails was found to be bending due to payloads and the channel section was the usual choice. They found the optimum ratio between the flange and web height to be around 0.3. Torsional stiffness and minimum weight requirements were the major factors besides payloads that controlled the values of the section modulus. The authors intended to carry out a similar analysis of the existing designs of truck frames to establish optimum values for the cross members and their joints with the side members. Such an analysis will be very useful in the design of chassis frames.

Lasevich, Skolnikov and Podlegaeva [29] proposed a method for the selection of optimum sections for commercial vehicle chassis frames. They used the maximum allowable direct stress and the minimum weight as the criteria in the selection of optimum sections. The maximum total stress in a section was the algebraic sum of all effects including the bimoment stress and this relation was used to determine appropriate dimensions of the section concerned. They found since all the stress contributing factors were functions of the section geometry except bimoment which was also a function of frame geometry, so the algebraic equation could not be directly solved. They used an iterative calculation procedure on computer for solving the equation and compared various sections on the basis of minimum weight. They found even neglecting bimoment stresses in the first approximation led to eroneous results.

1.4 APPROACH SELECTED FOR THE PRESENT ANALYSIS

It has been shown by the literature survey that the problem of stress

analysis of chassis frame joints needed further investigation. As the method of attachment of the two members varied from joint to joint it was not possible to develop an analytical model which could take care of all the designs. Since a ladder type frame consisting of channel section side members and cross members with welded joints presented a fundamental problem, it was decided to investigate the problem of stress estimation in welded joints. It was intended that such an analysis would be useful in the design of chassis frames as it would provide an information regarding stress distributions in various parts of the joints.

As the purpose of the present investigation was to determine stress distributions in the frame joints so it was necessary to use an analytical approach which could give good estimation of stresses preferably without experimental assistance. It has been shown by Zaks [11] that the plate theory gave better estimation of stress distributions in joints consisting of a symmetric I-section attached to the web of a channel section, than Vlasov's theory of thin walled beams. It has been also reported in many papers that for unsymmetric joints the condition of bimoment equilibrium was violated. The plate theory does not possess such a limitation and can be applied to asymmetric positioning of the cross member in a joint. Vlasov's theory of thin walled beams is based on the assumption of non-deformability of the section shape and the absence of shear strains from the middle surface of the section. Since the deformations in the vicinity of a joint are affected by localised effects so it is doubtful that the assumptions would be valid in the joint. Because of these considerations, it was decided to apply the plate theory to analyse a welded joint between two channel sections in a general manner.

It was also decided to estimate the degree of warping inhibition in a welded joint analytically so that the quantitative estimation of stresses/displacements in such a joint was possible.

As it is necessary to verify the results of any proposed analytic approach, it was decided to use photoelastic method of experimental stress analysis for such a verification.

CHAPTER 2 THEORETICAL INVESTIGATION

2.1. BRIEF DESCRIPTION

The state of stress in a joint of a chassis frame of ladder type construction largely depends upon warping inhibition. High values of localised stresses develop in the region of a joint which can weaken the joint severely if bracket mounting holes are present in the same area. It is important to locate areas of high stresses in the joint for the overall safety of a chassis frame.

The problem of a joint consisting of channel section members with crossmember attached to the web of the side member is theoretically analysed in this chapter. The theoretical model of a channel section sidemember is assumed to be made by joining three flat plates. It is subjected to the external forces which result from the warping of a channel section cross member due to applied torque at its free end. The resulting stresses/displacements in the side member are analysed by employing the equations of classical plate theory. The warping restraint factor for the cross member has been evaluated from the present analysis. In order to obtain stress/displacement distribution on any part of the side member, a computer programme was written using the results of the present analysis and results were computed for some cases. The programme is in Basic language and can be run on HP9830A.model.

2.1.1. Sequence of calculations

The sequence of the mathematical formulation of the problem and its analytical treatment is described below.

i) The general equations of classical plate theory have been employed to express results of plate bending and plate stretching problems in terms of initial parameters of a plate. The forces/displacements and moments etc., are assumed to be single trigonometric Fourier series forms to satisfy simply supported boundary conditions along the two parallel edges of plate, i.e. $x_1 = 0$ and $x_1 = 2L$ in Fig.(2.1a). Since a channel section side member has been considered to be made up by joining three plates along their edges, its analysis becomes easy if the resulting equations of plate bending and plate stretching problems are presented in such forms that can be applied directly to the junction of plates. It is advantageous to express the resulting equations of plate problems in terms of the initial parameters of a plate defined along one edge of the plate. Then stresses/forces/moments on any part of the plate can be obtained if these initial parameters are given specified values, subject to the boundary conditions along the edge at which they are defined originally. The equations for plate bending and plate stretching problems are expressed in Appendices I and II in terms of these parameters. Zaks [11] has used a similar approach to express

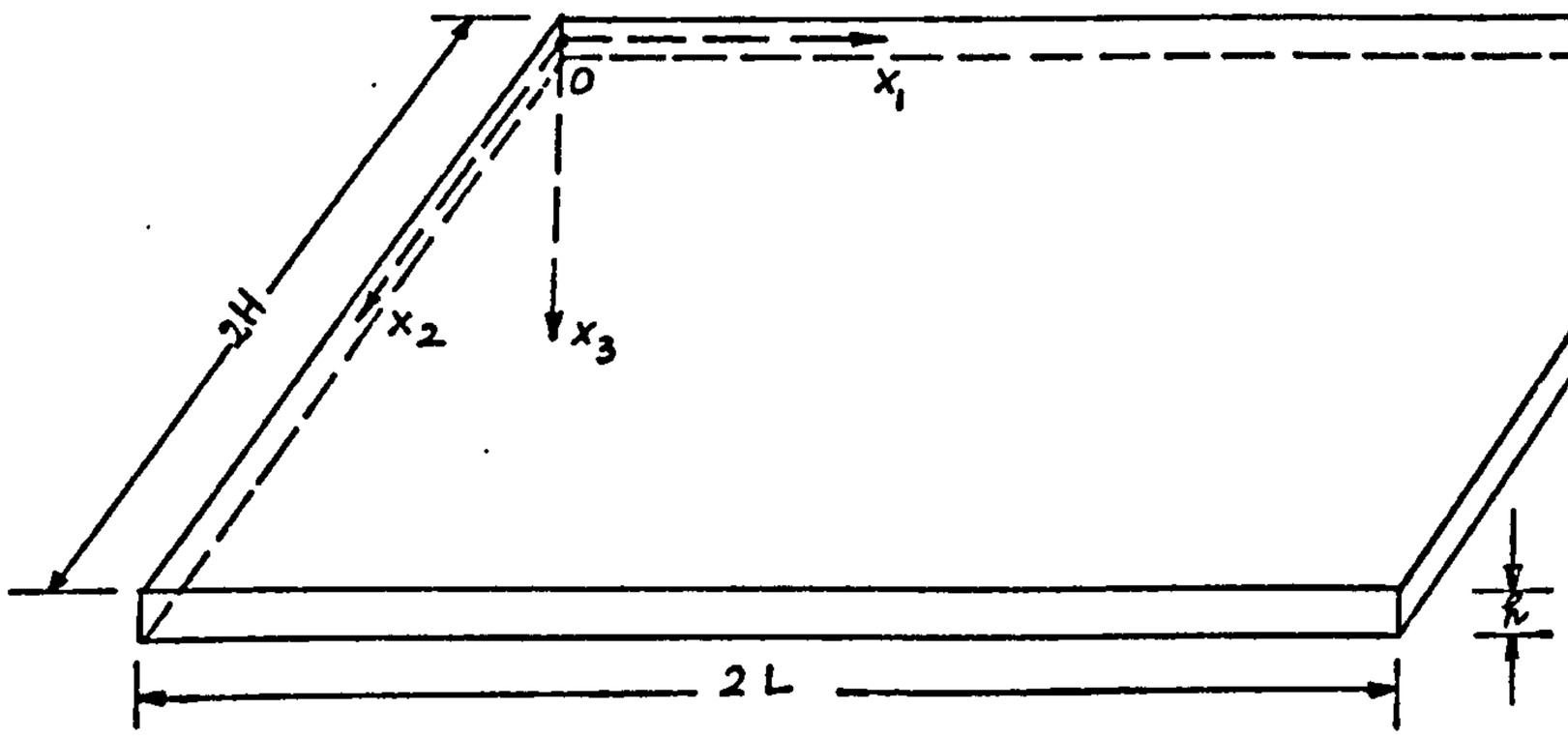

Fig.2.1a A rectangular plate referred to a Cartesian co-ordinate system

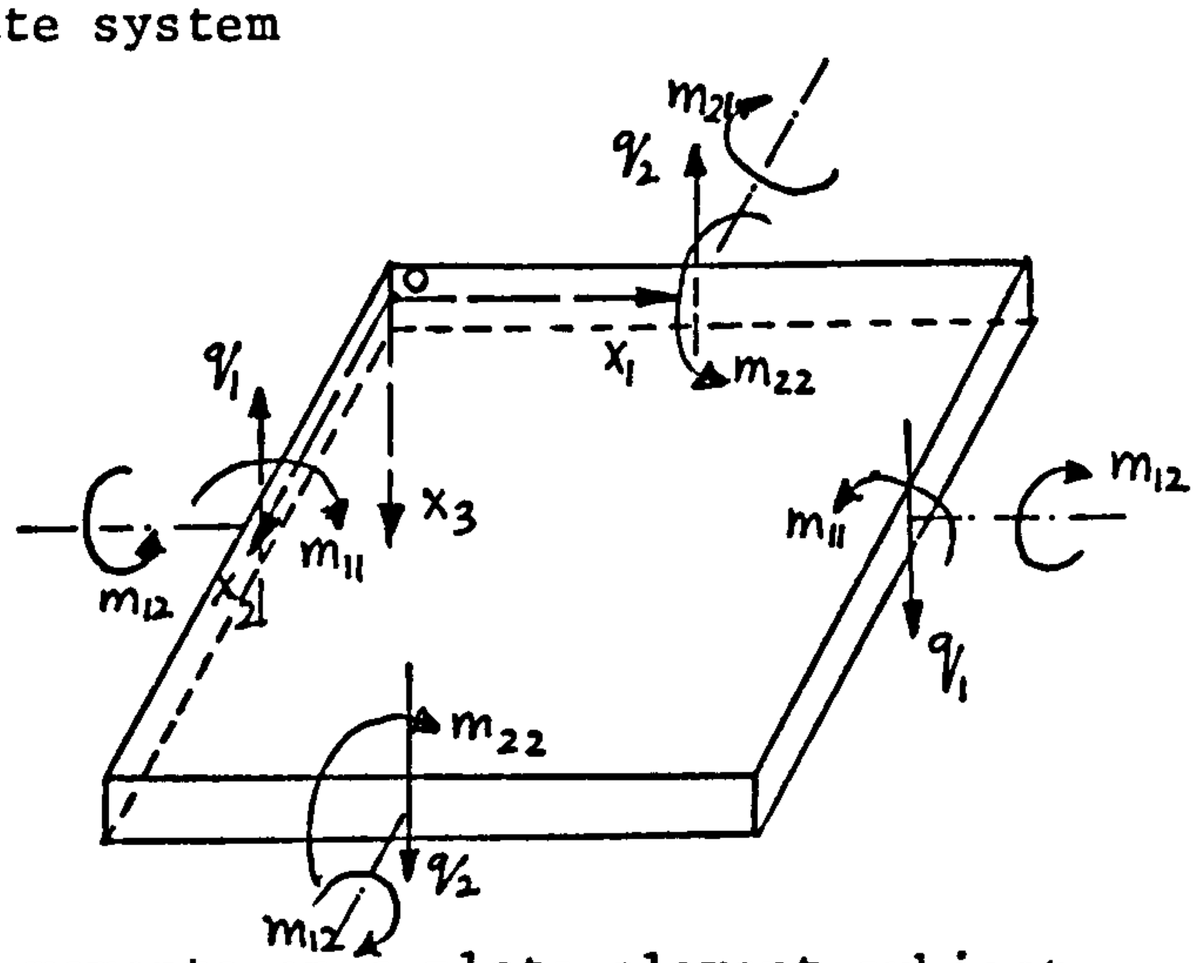

Fig.2.1b Forces and moments on a plate element subject to bending loading.

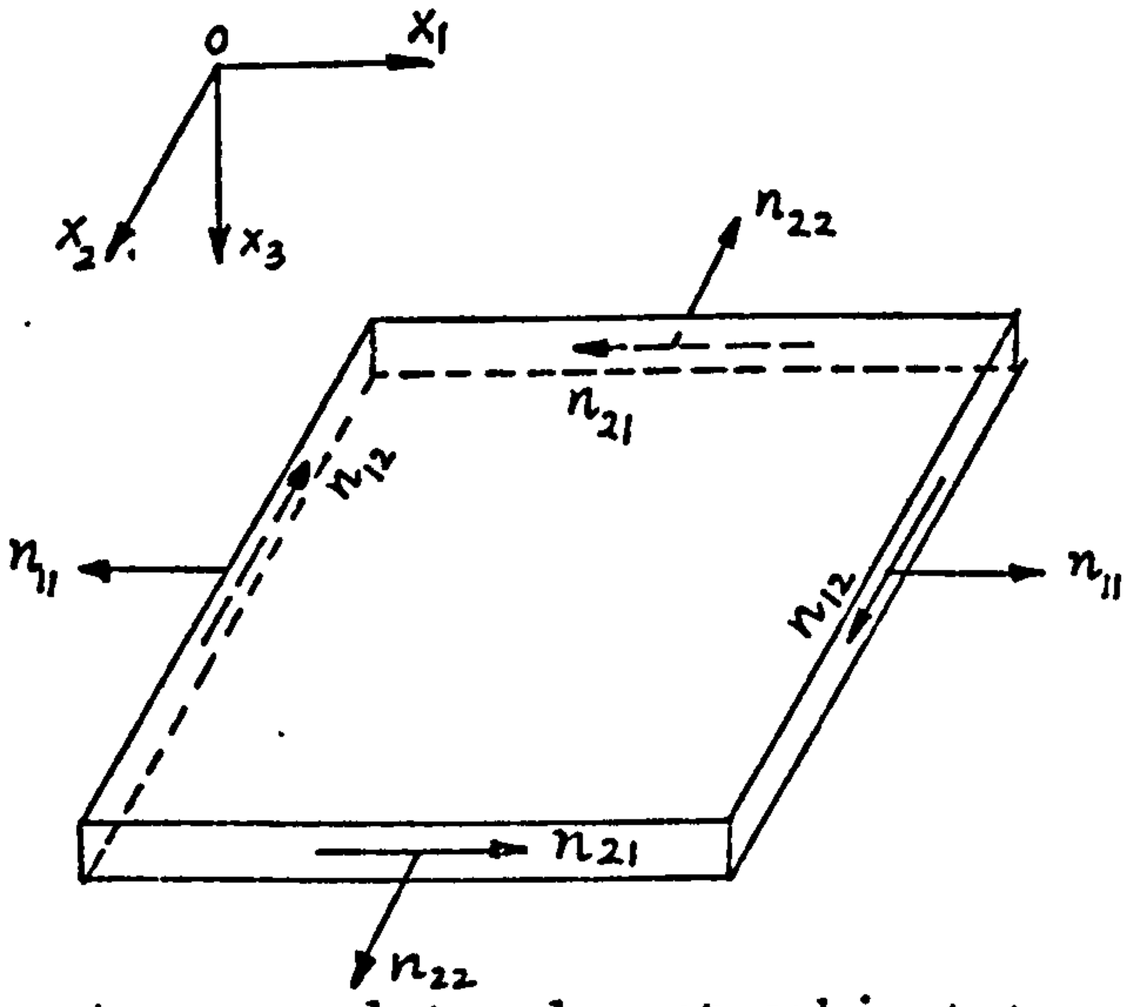

Fig.2.1c Force components on a plate element subject to stretching.

the resulting equations in terms of the initial parameters of a plate. But his results are only applicable to a plate problem if the external loads are antisymmetrically applied to a plate. The form of equations (AI.23) and (AII.19) of Appendices I and II is such that they can be directly applied to a plate problem for any arbitrary loading. These equations express the Fourier coefficients of various series as shown in the Appendices and they do not include any term for external forces. Any external load acting on a plate has to be expanded in a single trigonometric Fourier series. The form of this series is determined from the relevant form of the internal component of the force/moment acting in the plate. The Fourier coefficient of this series is included in equations (AI.23) and (AII.19) to satisfy boundary conditions of the problem. Once the values of Fourier coefficients are obtained then they are used in the respective Fourier series to obtain the values of the desired quantities.

ii) In section 2.2, the side member web of a joint has been considered as a rectangular flat plate with all edges simply supported. This plate is subjected to the cross member end warping forces. The effect of cross member flange warping forces and web warping forces has been analysed separately. The warping forces are represented by distributed forces as shown in fig. (2.2a). Distribution of these forces on the side member web is given by equations (2.2), (2.3) and (2.18).

Simply supported boundary conditions are expressed by equations (2.4) and (2.5) along the four edges of the side member web. Since the web will bend due to the external warping forces, all the equations of the plate bending problem of Appendix I are applicable to this problem. Boundary conditions along $x_1 = 0$ and $x_1 = 2L$ expressed by equations (2.4) are automatically satisfied as the assumed form of $u_3(x_1,x_2)$ as given by equation (AI.10) ensures this. The conditions expressed by equations (2.5) are to be satisfied along the other two parallel edges of the plate i.e. along $x_2 = 0$ and $x_2 = 2H$. Since the initial parameters as employed in Appendix I are defined along the edge $x_2 = 0$, so the equations (2.5) along $x_2 = 0$ for the problem under consideration will result in equation (2.7). This means that out of four initial parameters, there are only two non zero parameters for this problem which are to be evaluated from the equations (2.5) at $x_2 = 2H$. The external warping forces must also be taken into account while satisfying the boundary conditions. As warping forces and resultant vertical shear forces v_2 are acting identically on the plate so the warping forces must have an identical form of Fourier series as v_2. Equations (2.10), (2.11) and (2.23) represent Fourier series forms of warping forces of the top flange, bottom flange and web of the cross member respectively. Their respective Fourier coefficients are expressed by equations (2.12) and (2.24). The contribution of these external forces is considered by adding respective terms in the equations (AI.23) while applying them to the boundary conditions (2.5) at $x_2 = 2H$. The resulting form of these boundary conditions after necessary substitutions is given by equations (2.9) for the flange warping forces, and equations (2.22) for the web warping forces.

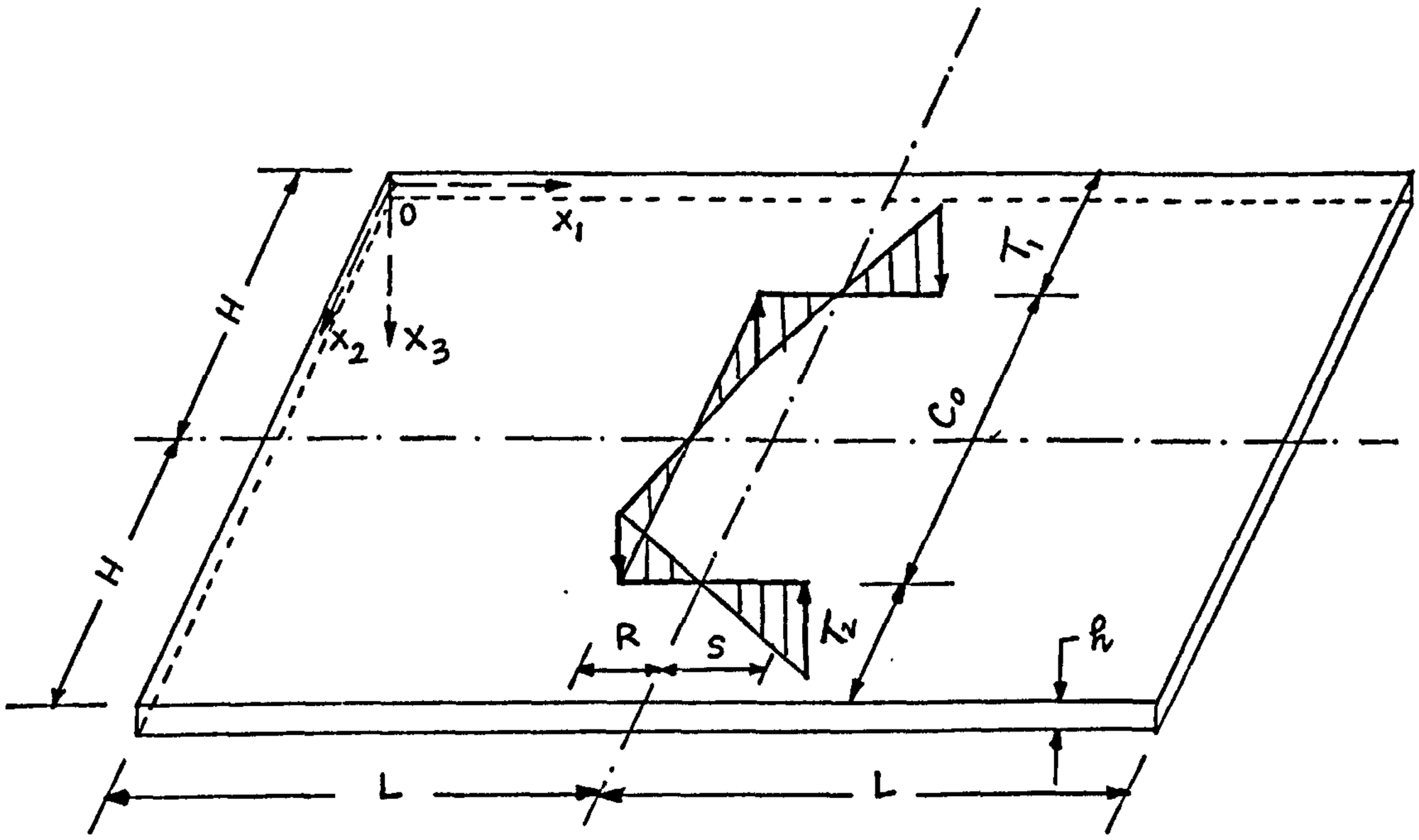

Fig.2.2a Side member web subject to the cross member end warping forces

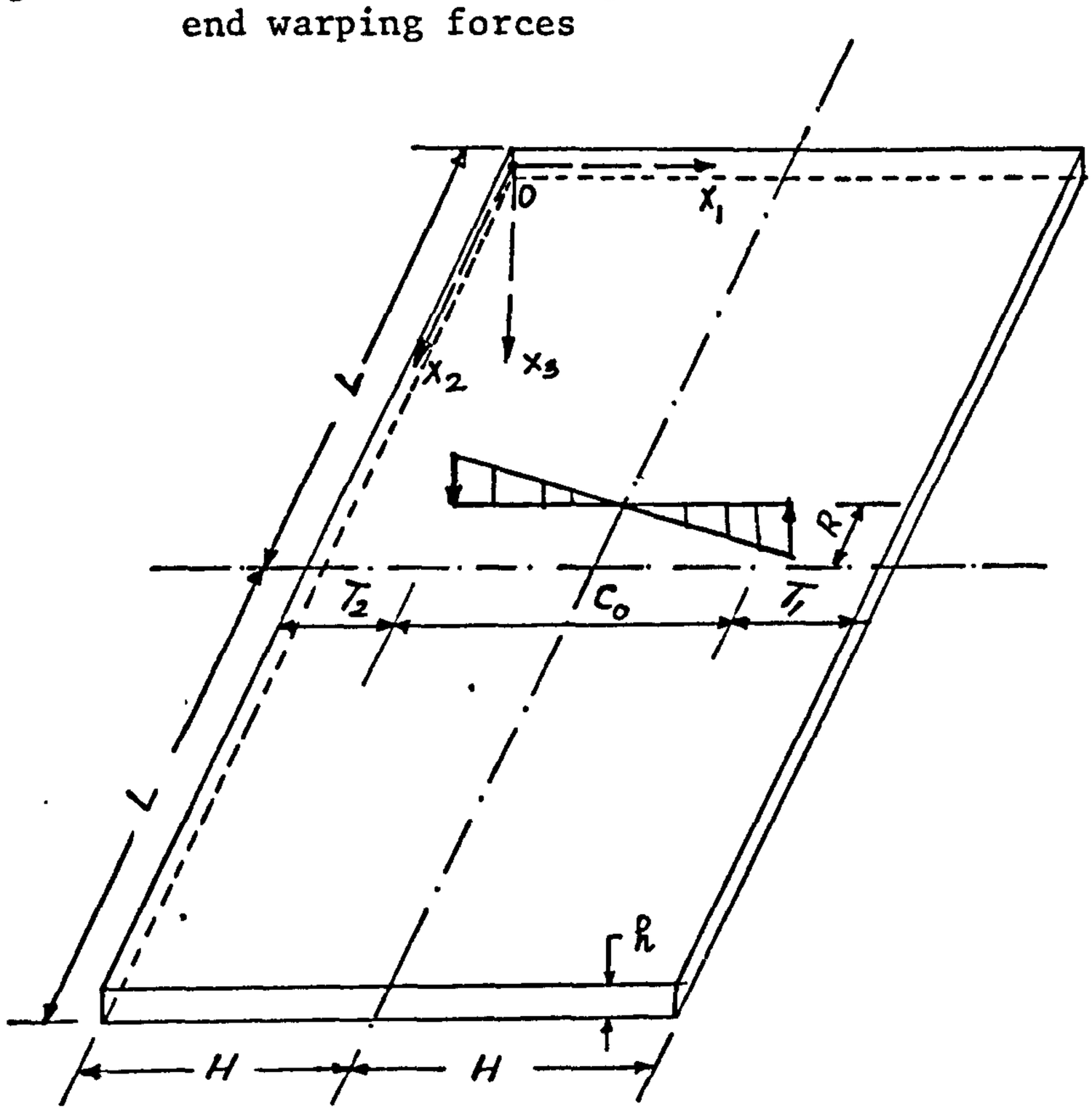

Fig.2.2b Side member web subject to the cross member web warping forces.

The unknown parameters are calculated from equations (2.9) and (2.22). Once these parameters are known then their values are used to calculate force/displacement/moment at any part of the side member web by equations (AI.23) and respective Fourier series. The combined effect of flange and web warping forces can be evaluated by super position.

iii) A channel section is treated as a joint between three rectangular flat plates in Section 2.3 as shown in fig.(2.3a).Since warping loads will not only produce bending but also stretching of the plate elements of a channel section side member, so this problem is analysed by combining the bending and stretching problems. Eight initial parameters are specified for each plate, four of which are used in the bending problem and the rest are used in stretching problem. So in general, there are twenty four parameters for a channel section. In fact, only eight of them are independent.

The relationships between the initial parameters of the web and the top flange are governed by boundary conditions along the common boundary AA as shown in fig(2.3a).Equations (2.27) represent these relations while equations (2.28) represent relations between the initial parameters of the bottom flange and the web of the channel section. Zaks [11] used identical relationships. By using these relations it is possible to express forces/displacements/moments etc. on any part of the channel section in terms of initial parameters of the top flange or bottom flange or web only. Therefore the whole problem of determining forces/displacements/moments etc. in a channel section side member is reduced to the determination of suitable values of these eight parameters from the boundary conditions.

iv) The effect of cross member warping loads on the side member is analysed in Section 2.5 for the joint shown in fig.(2.3b) The flange warping loads are considered in a similar way as described earlier in step(ii)whilethe web warping loads are replaced by various point loads which are applied to the side member web so that the total warping effect remains approximately unchanged. The number of point loads for each particular joint is determined by computing their effect on stresses and displacements in the side member and increasing the number of point loads until the difference between successive results is less than 1%.

Starting from stress free boundary conditions along the edge of the top flange, it is inevitable that some of its initial parameters will be zero as expressed by equations (2.33) through equations (2.32). If the joint is symmetrical i.e. $T_1 = T_2$ in fig.(2.4a).The rest of the unknown initial parameters can be determined from the boundary conditions along the horizontal axis of symmetry $\bar{x}\,\bar{x}$, as expressed by equations (2.30) and (2.31). These equations are expressed in terms of the unknown parameters of the top flange by equations (2.35) which include appropriate terms for external loading. Solution of these equations provides the values of the unknown parameters which are used in conjunction with the equations of Appendices I and II, to evaluate stresses/displacements at any point of the side member.

Section wall thickness = h

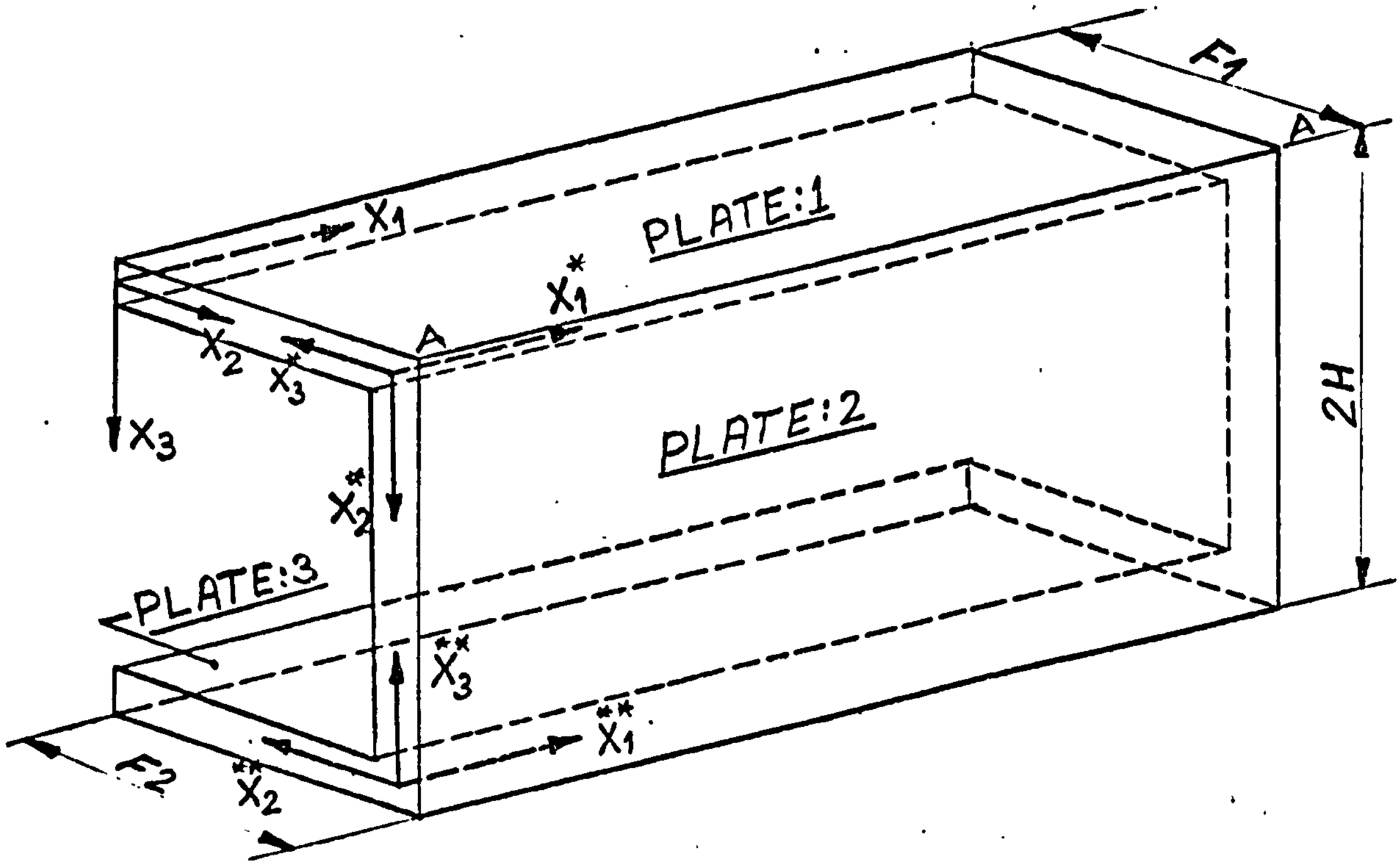

Fig.2.3a A channel section referred to the cartesian co-ordinate systems

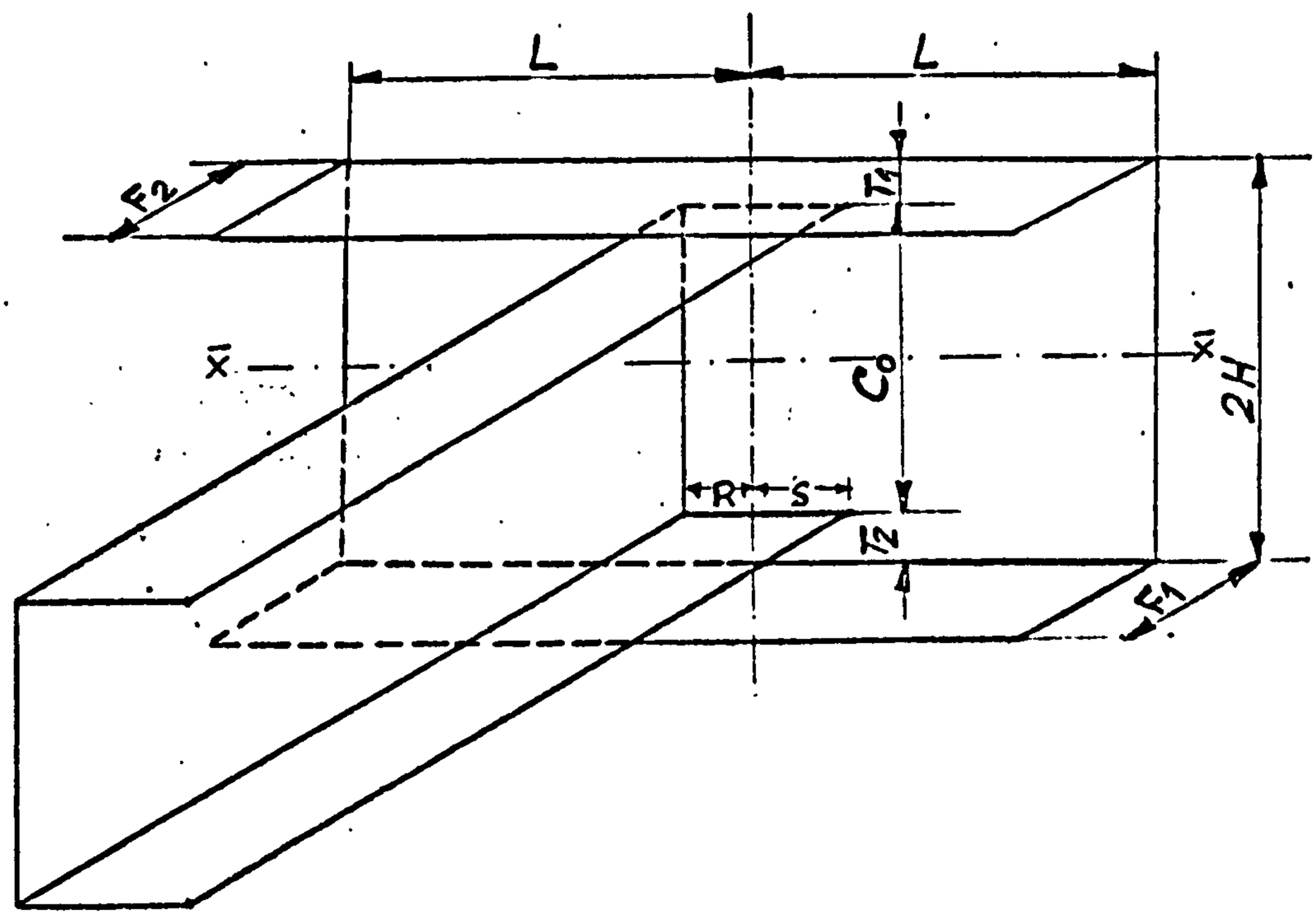

Fig 2.3b Joint under investigation

In the case of an asymmetrical joint i.e. $T_1 \neq T_2$ in fig.(2.4a) the unknown initial parameters of the top flange are determined from the boundary conditions along the free edge of the bottom flange which are given by equations (2.43), (2.44) and (2.45). These equations have to be written in terms of the initial parameters of the top flange by using relations given by equations (2.46). The resulting equations are solved for the unknown parameters. The values of these parameters are used in the equations of Appendices I and II to determine stress or displacement at any point of the side member.

v) Section 2.6 deals with the effect of the couple which is transmitted through the cross member end to the side member web, on the stress/displacement distribution in the side member. The magnitude of the couple forces is determined from the applied torque on the free end of the cross member as expressed by equation (2.48). This problem has been solved for a general case where $T_1 \neq T_2$ in fig.(2.4b) The unknown initial parameters of the top flange remain the same as in step(iv).They are determined from the boundary conditions along the free edge of the bottom flange in an identical manner as described in step(iv).Only the external loading terms change their values which are calculated by using equation (2.53).

2.2. BENDING OF A SIDE MEMBER WEB DUE TO CROSS MEMBER WARPING LOADS

Consider a joint of a channel section cross member attached to the web of a channel section side member. The cross member web is placed vertical to the longitudinal axis of the side member. In this case the warping of the cross member end is restrained by the side member web only. A simple theoretical solution can be developed by idealising the side member web as a flat plate simply supported along all the four edges. Such simplification has been used in the estimation of partial warping inhibition in joints [17,21].This problem can be reduced to the calculation of the deflection of such a plate subject to the cross member end warping loads.

The mid plane of a simply supported plate referred to $x_1x_2x_3$ cartesian axes is shown in fig.(2.2a). The distribution of the cross member end warping loads is assumed proportional to the free warping distribution (or law of sectorial areas). This assumption is logical and has been used directly in [11,17].

These external loads can be represented by distributed forces placed along the cross member end section.

A complete solution of this plate bending problem can be obtained by super position of two solutions obtained by solving separately for cross member flange warping loads and cross member web warping loads.

2.2.1. Cross member flange warping loads

The maximum force is acting at the flange end i.e. at

$$x_1 = L + S$$

$$p = \sigma_z t$$

$$= k_o S \qquad (2.1)$$

where k_o is the intensity of force.

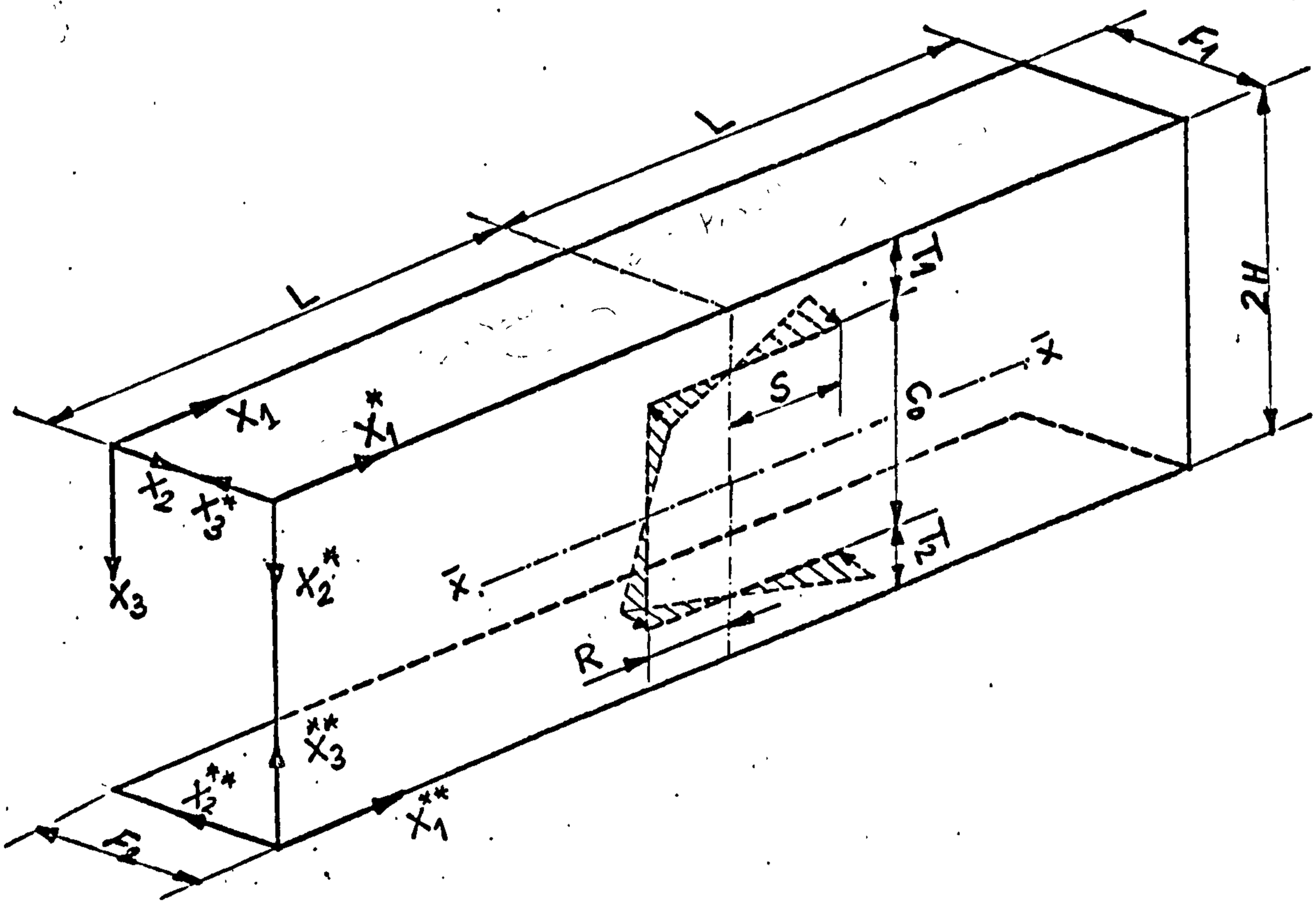

Fig.2.4a A channel section side member subject to a channel section cross member end warping forces.

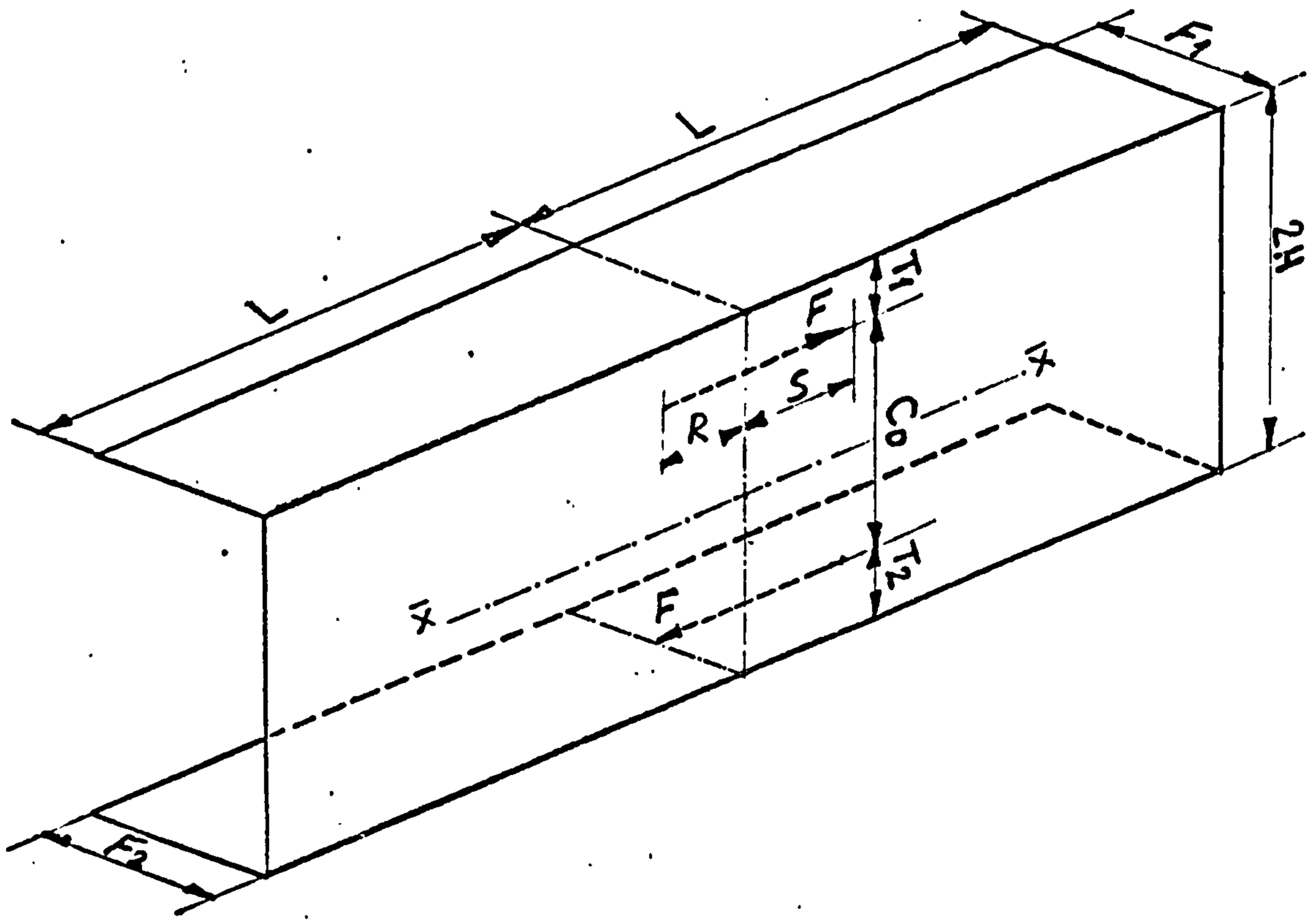

Fig 2.4b A channel section side member subject to a couple loading.

Distribution of the external forces is given by the following equation:

$$p(x_1) = \begin{cases} 0 & \text{for } 0 < x_1 < (L-R) \\ & \text{and } (L+S) < x_1 \leq 2L \\ k_o(x_1 - L) & \text{for } (L-R) < x_1 < (L+S) \end{cases} \qquad (2.2)$$

Let $p_I(x_1)$ and $p_{II}(x_1)$ be the forces/unit length in the top and bottom flanges of the cross member respectively.

Also $$p_I(x_1) = -p_{II}(x_1) \qquad (2.3)$$

Simply supported boundary conditions along the edges of the plate can be written in the following form.

At $x_1 = 0$ and $x_1 = 2L$

$$\left.\begin{aligned} u_3(x_1,x_2) &= 0 \\ m_{11}(x_1,x_2) &= 0 \end{aligned}\right\} \qquad (2.4)$$

At $x_2 = 0$ and $x_2 = 2H$

$$\left.\begin{aligned} u_3(x_1,x_2) &= 0 \\ m_{22}(x_1,x_2) &= 0 \end{aligned}\right\} \qquad (2.5)$$

Results developed in Appendix I can be directly applied to the problem under consideration. Equation (AI.10) satisfies the boundary conditions given by equation (2.4). Equations (AI.10) and (AI.15) should satisfy the conditions given in equations (2.5). On substitution in equations (2.5), the following conditions are obtained

At $x_2 = 0$ and $x_2 = 2H$

$$\left.\begin{aligned} W_m(x_2) &= 0 \\ M_{2m}(x_2) &= 0 \end{aligned}\right\} \qquad (2.6)$$

Equations (2.6) should include the respective loading terms for cross member flange warping forces. Conditions at $x_2 = 0$ imply that following initial parameters are zero.

$$\left.\begin{aligned} \overset{o}{W} &= 0 \\ \overset{o}{M}_2 &= 0 \end{aligned}\right\} \qquad (2.7)$$

The other two conditions at $x_2 = 2H$ give the following equations:

$$\left[\frac{bD_2}{\alpha_m}+ aD_3\right]\overset{o}{\theta} + \left[\xi\frac{D_2}{\alpha_m^3} - \xi\frac{D_3}{\alpha_m^2}\right]\overset{o}{V_2}+ P_{Im}\left[\xi\frac{\acute{D}_2}{\alpha_m^3} - \xi\frac{\acute{D}_3}{\alpha_m^2}\right]$$

$$+ P_{IIm}\left[\xi\frac{\overset{''}{D}_2}{\alpha_m^3} - \xi\frac{\overset{''}{D}_3}{\alpha_m^2}\right] = 0 \qquad (2.8)$$

$$-\left[\eta D_2 + \delta D_3\right]\overset{o}{\theta} + \left[\frac{bD_2}{\alpha_m} + aD_3\right]\overset{o}{V_2} + P_{Im}\left[\frac{\overset{''}{bD}_2}{\alpha_m} + \overset{''}{aD}_3\right]$$

$$+ P_{IIm}\left[\frac{\overset{''}{bD}_2}{\alpha} + \overset{''}{aD}_3\right] = 0 \qquad (2.9)$$

where

D_1, D_2, D_3 and D_4 are the values of the hyperbolic functions ϕ_1, ϕ_2, ϕ_3 and ϕ_4 determined at $x_2 = 2H$

D_1', D_2', D_3' and D_4 " " " " " " $x_2 = (2H - T_1)$

D_1'', D_2'', D_3'' and D_4'' " " " " " " $x_2 = T_1$

P_{Im} and P_{IIm} are Fourier coefficients of the external force expansions of the following form:

$$P_I = \sum_{m=1}^{\infty} P_{Im}(x_2) \sin \alpha_m x_1 \qquad (2.10)$$

$$P_{II} = \sum_{m=1}^{\infty} P_{IIm}(x_2) \sin \alpha_m x_1 \qquad (2.11)$$

Series expansions (2.10) and (2.11) are obtained from the fact that the external forces are acting parallel to the resultant shearing force v_2 and hence the expansion should have the same form. Coefficients P_{Im} and P_{IIm} can be evaluated in the following way:

$$P_{Im} = -P_{IIm} = \frac{1}{L}\int_{(L-R)}^{(L+S)} p \sin \alpha_m x_1 dx_1$$

$$= \frac{1}{L}\int_{(L-R)}^{(L+S)} k_o(L-x_1) \sin \alpha_m x_1 dx_1$$

$$= \frac{k_o}{L\alpha_m}\left[\frac{1}{\alpha_m}\left|\sin\alpha_m(L+S)-\sin\alpha_m(L-R)\right| - S\cos\alpha_m(L-R) - R\cos\alpha_m(L-R)\right] \qquad (2.12)$$

Equations (2.8) and (2.9) represent a system of two simultaneous equations involving the only two non zero unknown initial parameters of the problem which are $\overset{o}{\theta}$ and $\overset{o}{V}_2$. Once the values of $\overset{o}{\theta}$ and $\overset{o}{V}_2$ are found, it is easy to determine the deflection through equations (AI.23) and (AI.10) at any point of the plate. Equation (AI.10) has to include the external loading terms and is expressed in the following form:

(i) When the point lies between $o \leq x_2 \leq T_1$

$$u_3(x_1,x_2) = \sum_{m=1}^{\infty}\left(\left[\frac{b\phi_2}{\alpha_m}+a\phi_3\right]\overset{o}{\theta}+\xi\left[\frac{\phi_2}{\alpha_m^3}-\frac{\phi_3}{\alpha_m^2}\right]\overset{o}{V}_2\right)\sin\alpha_m x_1 \qquad (2.13)$$

(ii) When the point lies between $T_1 < x_2 \leq (T_1+c_o)$

$$u_3(x_1,x_2) = \sum_{m=1}^{\infty}\left(\left[\frac{b\phi_2}{\alpha_m}+a\phi_3\right]\overset{o}{\theta}+\xi\left[\frac{\phi_2}{\alpha_m^3}-\frac{\phi_3}{\alpha_m^2}\right]\overset{o}{V}_2+\xi\left[\frac{\overset{*}{\phi}_2}{\alpha_m^3}-\frac{\overset{*}{\phi}_3}{\alpha_m^2}\right]P_{Im}\right)\sin\alpha_m x_2 \qquad (2.14)$$

(iii) When the point lies between $(T_1+c_o) < x_1 \leq 2H$

$$u_3(x_1,x_2) = \sum_{m=1}^{\infty}\left(\left[\frac{b\phi_2}{\alpha_m}+a\phi_3\right]\overset{o}{\theta}+\xi\left[\frac{\phi_2}{\alpha_m^3}-\frac{\phi_3}{\alpha_m^2}\right]\overset{o}{V}_2+\xi\left[\left(\frac{\overset{*}{\phi}_2}{\alpha_m^3}-\frac{\overset{*}{\phi}_3}{\alpha_m^2}\right)-\left(\frac{\overset{**}{\phi}_2}{\alpha_m^3}-\frac{\overset{**}{\phi}_3}{\alpha_m^2}\right)\right]P_{Im}\right)\sin\alpha_m x_1 \qquad (2.15)$$

where

$\overset{*}{\phi}_2$ and $\overset{*}{\phi}_3$ are the values of the hyperbolic functions ϕ_2 and ϕ_3 respectively calculated at $x_2=(x_2-T_1)$

$\overset{**}{\phi}_2$ and $\overset{**}{\phi}_3$ " " " " " " " " " " $x_2=(x_2-T_1-c_o)$

2.2.2 Cross member web warping loads

Since all equations developed in Appendix I have been expressed in single trigonometric Fourier series along x_1 direction, so the results can be directly applied to such problems where the external forces can be expanded along x_1. The cross member web warping forces are varying along x_2 according to fig.(2.2a), hence it is necessary to interchange the direction of co-ordinate axes as shown in Fig.(2.2b). Now the results of Appendix I can be directly applied for this case.

The maximum force is exerted at the ends of the cross member web and is given by

$$p^*_{c_o} = \frac{1}{2} k^*_o c_o \tag{2.16}$$

where k^*_o is the intensity of force along the cross member web. Relationship between k_o and k^*_o can be expressed as follows:

$$\frac{1}{2} k^*_o c_o = k_o R$$

$$\text{or} \quad k^*_o = \frac{2R}{c_o} k_o \tag{2.17}$$

Distribution of warping forces on the plate is given by:

$$p^*(x_1) = \begin{cases} 0 \text{ for } 0 \leq x_1 \leq T_2 \text{ and } (T_2 + c_o) < x_1 \leq 2H \\ k^*_o (x_1 - T_2 - \frac{c_o}{2}) \text{ for } T_2 \leq x_1 \leq (T_2 + c_o) \end{cases} \tag{2.18}$$

Boundary conditions for the simply supported edges of the plate can be expressed in the following form:

At $x_1 = 0$ and $x_1 = 2H$

$$u_3(x_1, x_2) = m_{11}(x_1, x_2) = 0 \tag{2.19}$$

and at $x_2 = 0$ and $x_2 = 2L$

$$u_3(x_1, x_2) = m_{22}(x_1, x_2) = 0 \tag{2.20}$$

The solution of this problem can be obtained in a similar manner as already described for the cross member flange warping loads. Following resulting equations are obtained by satisfying the boundary conditions (2.20).

$$\left.\begin{aligned} \overset{o}{W} &= 0 \\ \overset{d}{M}_2 &= 0 \end{aligned}\right\} \tag{2.21}$$

$$\left[\frac{bF_1}{\alpha_m} + aF_3\right]\overset{o}{\Theta} + \xi\left[\frac{F_2}{\alpha_m^3} - \frac{F_3}{\alpha_m^2}\right]\overset{o}{V}_2 + P^*_m \xi \left[\frac{\acute{F}_2}{\alpha^3} - \frac{\acute{F}_3}{\alpha_m^2}\right] = 0 \tag{2.22a}$$

$$-\left[\eta F_2 + \delta F_3\right]\overset{o}{\Theta} + \left[\frac{bF_2}{\alpha_m} + aF_3\right]\overset{o}{V}_2 + P^*_m \left[\frac{b\acute{F}_2}{\alpha_m} + a\acute{F}_3\right] = 0 \tag{2.22b}$$

where

F_2 and F_3 are the values of the hyperbolic functions ϕ_2 and ϕ_3 respectively are determined at $x_2 = 2L$

$\acute{F}_2$ and $\acute{F}_3$ " " " " " " " " " " $x_2 = L+R$

P_m^* is the Fourier coefficient of the following equation:

$$p^* = \sum_{m=1}^{\alpha} P_m^* (x_2) \sin \alpha_m x_1 \qquad (2.23)$$

The value of $P_m^*(x_2)$ can be evaluated from equation (2.23) in the following way:

$$P_m^* = \frac{1}{H} \int_{T_2}^{(T_2+c_o)} p^* \sin \alpha_m x_1 dx_1$$

$$= \frac{1}{H} \int_{T_2}^{(T_2+c_o)} k_o^*(x_1 - T_2 - c_o) \sin \alpha_m x_1 dx_1$$

or

$$P_m^* = k_o \left[\frac{2R}{Hc_o \alpha_m}\right] \left(\frac{2}{\alpha_m} \sin \left(\frac{\alpha_m c_o}{2}\right) \cos \alpha_m \left(T_2 + \frac{c_o}{2}\right) - c_o \cos \left(\frac{\alpha_m c_o}{2}\right) \cos \alpha_m \left(T_2 + \frac{c_o}{2}\right) \right) \qquad (2.24)$$

Equations (2.22a and b) are solved for the unknown initial parameters $\overset{o}{\Theta}$ and $\overset{o}{V}$. Their values are substituted to obtain the following equations for the deflections of any point on the plate.

i) If the point lies between $0 \leq x_2 \leq (L-R)$

$$u_3(x_1,x_2) = \sum_{m=1}^{\alpha} \left(\left[\frac{b\phi_2}{\alpha_m} + a\phi_3\right] \overset{o}{\Theta} + \xi \left[\frac{\phi_2}{\alpha_m^3} - \frac{\phi_3}{\alpha_m^2}\right] \overset{o}{V_2} \right) \sin \alpha_m x_1 \qquad (2.25)$$

ii) If the point lies between $(L-R) < x_2 \leq 2L$

$$u_3(x_1,x_2) = \sum_{m=1}^{\alpha} \left(\left[\frac{b\phi_2}{\alpha_m} + a\phi_3\right] \overset{o}{\Theta} + \xi \left[\frac{\phi_2}{\alpha_m^3} - \frac{\phi_3}{\alpha_m^2}\right] \overset{o}{V} + \xi \left[\frac{F_2^*}{\alpha_m^3} - \frac{F_3^*}{\alpha_m^2}\right] P_m^* \right) \sin \alpha_m x_1 \qquad (2.26)$$

where

F_2^* and F_3^* are the values of hyperbolic functions ϕ_1 and ϕ_2 calculated at $x_2 = x_2-(L-R)$.

Deflection of the plate (i.e. side member web) can be determined at any point by simple algebraic addition of the two results of sections 2.2.1. and 2.2.2.This analysis does not calculate the stress distribution in the plate.

2.3. APPLICATION OF PLATE THEORY TO THIN WALLED BEAMS OF OPEN SECTION

It has been shown in section 2.2 that side member web deflections can be calculated when it is subjected to the cross member warping loads. Flanges of the side member were not considered in the previous analysis. Only bending of the side member web was considered, while in the actual case, the side member can deform in other planes as well. Deformation of the complete section can be estimated by employing the equations of plate bending and plate stretching problems together.

Stress, strain and displacement distributions of a side member of open section subject to warping loads can be analysed using the equations of plate theory. It should be possible to consider such an open section made by joining various plates along their edges.

Side members made of channel sections are very common in commercial vehicle chassis frames. So the analytical treatment is developed for a channel section side member. A channel section shown in fig. (2.3a) can be considered to be made from three flat plates of dimensions indicated. They are joined along their edges to form a channel section. Angle of inclination between two adjacent plates is taken as 90^{o}. Co-ordinate systems chosen for each plate are shown in fig.(2.3a). Mid plane of each plate provides the reference for the co-ordinate system.

Equations (AI.23) and (AII.19) can be applied to any plate for an arbitrary external loading. Stresses/displacements and moments of any plate can be determined if its eight initial parameters are known. These parameters are the same as used in Appendices I & II. Hence it can be seen that for each plate a system of eight simultaneous equations with eight unknowns (inital parameters) is obtained. It is possible to find out the relationships between the initial parameters of the adjoining plates by satisfying the conditions along the common boundary between them. In this way, the number of unknowns does not increase in the system and adequate number of equations are available to determine the unknowns.

Let $\overset{o}{U}$, $\overset{o}{V}$, $\overset{o}{N}_{22}$, $\overset{o}{N}_{12}$, $\overset{o}{W}$, $\overset{o}{\Theta}$, $\overset{o}{M}_2$ and $\overset{o}{V}_2$ be the initial parameters of Plate 1 which are defined at $x_2 = 0$. $\overset{*}{U}$, $\overset{*}{V}$, $\overset{*}{N}_{22}$, $\overset{*}{N}_{12}$, $\overset{*}{W}$, $\overset{*}{\Theta}$, $\overset{*}{M}_2$ and $\overset{*}{V}_2$ are the initial parameters of Plate 2 at $\overset{*}{x}_2 = 0$. Following relations are obtained from the common boundary conditions.

$$
\begin{aligned}
\overset{*}{U} &= U_m \quad (\text{at } x_2 = F_1) \\
\overset{*}{V} &= W_m \quad (\quad " \quad ") \\
\overset{*}{N}_{22} &= V_{2m} \quad (\quad " \quad ") \\
\overset{*}{N}_{12} &= N_{12m} \quad (\quad " \quad ") \\
\overset{*}{W} &= -V_m \quad (\quad " \quad ")
\end{aligned}
$$

$$
\left.\begin{aligned}
\overset{*}{\Theta} &= \Theta_m \quad (\text{at } x_2 = F_1)\\
\overset{*}{M_2} &= M_{2m} \quad (\text{ " " })\\
\overset{*}{V_2} &= -N_{22_m} \quad (\text{ " " })
\end{aligned}\right\} \quad (2.27)
$$

The right side of equations (2.27) can be determined from the equations (AI.23) and equations (AII.19)on substitution of the initial parameters of Plate 1. Hence equations (2.27) provide the relationships between the initial parameters of Plate 2 with the initial parameters of Plate 1.

Similarly relations between the initial parameters of Plate 3 and Plate 2 are obtained from the following equations.

$$
\left.\begin{aligned}
\overset{**}{U} &= U_m \quad (\text{at } \overset{*}{x}_2 = 2H)\\
\overset{**}{V} &= W_m \quad (\text{ " " })\\
\overset{**}{N_{22}} &= V_{2m} \quad (\text{ " " })\\
\overset{**}{N_{12}} &= N_{12m} \quad (\text{ " " })\\
\overset{**}{W} &= -V_m \quad (\text{ " " })\\
\overset{**}{\Theta} &= \Theta_m \quad (\text{ " " })\\
\overset{**}{M_2} &= M_{2m} \quad (\text{ " " })\\
\overset{**}{V_2} &= -N_{22m} \quad (\text{ " " })
\end{aligned}\right\} \quad (2.28)
$$

Where $\overset{**}{U}$, $\overset{**}{V}$, $\overset{**}{N_{22}}$, $\overset{**}{N_{12}}$, $\overset{**}{W}$, $\overset{**}{\Theta}$, $\overset{**}{M_2}$ and $\overset{**}{V_2}$ are the initial parameters of Plate 3 defined at $\overset{**}{x_2} = 0$.

Now on simple substitution of equations (2.27) in equations (2.28), relations between the parameters of Plate 3 and Plate 1 can be obtained. Hence the problem of a channel section can be analysed by determining the eight unknown parameters.

Beams of other open sections such as top hat and Z-sections can be treated in a similar way. It is necessary that the end boundary conditions of the beams are hinge type, otherwise the results of Appendices I and II are not applicable.

2.4. ANALYSIS OF A JOINT

The effect of a twisting moment applied on the free end of the cross member on the stress distribution in the side member of a joint shown in fig.(2.3b) has been analysed by using the approach suggested in section 2.3. The external load produces warping of the cross member section thus exerting warping forces on the side member web. It also produces a moment in the plane of the side member web. The stress/displacement

distributions in the side member will depend upon the following:

i) Cross member warping forces

ii) Moment acting in the plane of the side member web.
Separate analytical solutions are developed for these two loadings in the preceding sections and their combined effect on the side member is obtained by super-position of these solutions..

2.5. SIDE MEMBER SUBJECT TO CROSS MEMBER WARPING LOADS

Consider the case of a joint in which a channel section cross member is placed with its web vertical to the axis of a channel section side member. Also the cross member is attached to the inside of the side member web and the zero warping point on its flange is located symmetrically along the length of side member, as shown in fig 2.3b.The cross member has equal flanges.

When the axis passing through the shear centres of a side member and a cross member are intersecting each other, the joint will be referred to as a symmetric joint in the further work.

2.5.1. Analysis of a symmetric joint

According to fig 2.3b thecondition for intersection of axes through the shear centres of the respective members is fulfilled if:

$$T_1 = T_2 \qquad (2.29)$$

Equation (2.29) implies that cross member end warping forces are anti-symmetric about the centre line $\bar{x}\bar{x}$ of the side member web. Hence the resulting displacements of the side member will be also anti-symmetric about $\bar{x}\bar{x}$ which is an axis of symmetry. For this reason, analysis of the half portion of side member consisting of a flange and half of the web is sufficient. The top half of the side member is considered in this analysis.

Boundary conditions at the line $\bar{x}\bar{x}$ can be expressed in the following way from the conditions of anti-symmetry.

$$\text{At } x_2^* = H$$

$$\left.\begin{aligned} u_1 &= 0 \\ n_{22} &= 0 \\ u_3 &= 0 \\ m_{22} &= 0 \end{aligned}\right\} \qquad (2.30)$$

Equations (2.30) lead to the following conditions through equations (AII.9), (AII.16), (AI.10) and (AI.15).

$$\text{At } x_2^* = H$$

$$\left.\begin{aligned} U_m &= 0 \\ N_{2m} &= 0 \\ W_m &= 0 \\ M_{2m} &= 0 \end{aligned}\right\} \quad (2.31)$$

Boundary conditions at the free edge of the flange are expressed below.

$$\text{At } x_2 = 0$$

$$\left.\begin{aligned} n_{22} &= 0 \\ n_{12} &= 0 \\ m_{22} &= 0 \\ v_2 &= 0 \end{aligned}\right\} \quad (2.32)$$

Equations (2.32) lead to the following conditions.

$$\overset{o}{N}_{22} = \overset{o}{N}_{12} = \overset{o}{M}_2 = \overset{o}{V}_2 = 0 \quad (2.33)$$

Initial parameters of the web can be expressed by substituting equations (2.33), (AI.23) and (AII.19) in equations (2.27) by the following equations

$$\overset{*}{U} = [A_1 + b\alpha_m A_4]\overset{o}{U} - [aA_2 + b\alpha_m A_3]\overset{o}{V} \quad (2.34a)$$

$$\overset{*}{V} = [A_1 - a\alpha_m A_4]\overset{o}{W} + \left[\frac{bA_2}{\alpha_m} + aA_3\right]\overset{o}{\theta} \quad (2.34b)$$

$$\overset{*}{N}_{22} = \alpha_m^2 [\eta A_2 - \delta A_3]\overset{o}{W} + [\delta\alpha_m A_3]\overset{o}{\theta} \quad (2.34c)$$

$$\overset{*}{N}_{12} = [fA_2 + f\alpha_m A_3]\overset{o}{U} - [f\alpha_m A_4]\overset{o}{V} \quad (2.34d)$$

$$\overset{*}{W} = [aA_2 - b\alpha_m A_3]\overset{o}{U} - [A_1 - b\alpha_m A_4]\overset{o}{V} \quad (2.34e)$$

$$\overset{*}{\theta} = [b\alpha_m A_2 - a\alpha_m^2 A_3]\overset{o}{W} + [A_1 + a\alpha_m A_4]\overset{o}{\theta} \quad (2.34f)$$

$$\overset{*}{M}_2 = [\delta\alpha_m A_4]\overset{o}{W} - [\eta A_2 + \delta A_3]\overset{o}{\theta} \quad (2.34g)$$

$$\overset{*}{V}_2 = -[f\alpha_m A_4]\overset{o}{U} - [fA_2 - f\alpha_m A_3]\overset{o}{V} \quad (2.34h)$$

where

A_1, A_2, A_3 and A_4 are the values of hyperbolic functions ϕ_1, ϕ_2, ϕ_3 and ϕ_4 respectively, calculated at $x_2 = F_1 = F_2$. Equations (2.34),

(AI.23)and(AII.19) are then substituted in the boundary conditions given by equations (2.31) and the following equations result after rearranging the terms:

$$\left[(B_1 + b\alpha_m B_4)(A_1 + b\alpha_m A_4) + (\frac{dB_2}{\alpha_m} + cB_3)(fA_2 + f\alpha_m A_3)\right] \overset{o}{U}$$

$$- \left[(B_1 + b\alpha_m B_4)(aA_2 + b\alpha_m A_3) + (\frac{dB_2}{\alpha_m} + cB_3)(f\alpha_m A_4)\right] \overset{o}{V}$$

$$- \left[(aB_2 + b\alpha_m B_3)(A_1 - a\alpha_m A_4) + (cB_4)(\eta A_2 - \delta A_3)\alpha_m^2\right] \overset{o}{W}$$

$$- \left[(aB_2 + b\alpha_m B_3)(\frac{bA_2}{\alpha_m} + aA_3) + (cB_4)(\delta\alpha_m A_4)\right] \overset{o}{\Theta} = 0 \qquad (2.35a)$$

$$\left[(f\alpha_m B_4)(A_1 + b\alpha_m A_4) + (aB_2 + b\alpha_m B_3)(fA_2 + f\alpha_m A_3)\right] \overset{o}{U}$$

$$- \left[(f\alpha_m B_4)(aA_2 + b\alpha_m A_3) + (aB_2 + b\alpha_m B_3)(f\alpha_m A_4)\right] \overset{o}{V}$$

$$+ \left[(fB_2 - f\alpha_m B_3)(A_1 - a\alpha_m A_4) + (B_1 - b\alpha_m B_4)(\eta A_2 - \delta A_3)\alpha_m^2\right] \overset{o}{W}$$

$$+ \left[(fB_2 - f\alpha_m B_3)(\frac{bA}{\alpha_m} + aA_3) + (B_1 - b\alpha_m B_4)(\delta\alpha_m A_4)\right] \overset{o}{\Theta} = 0 \qquad (2.35b)$$

$$\left[(B_1 - a\alpha_m B_4)(aA_2 - b\alpha_m A_3) - \xi(\frac{B_2}{\alpha_m^3} - \frac{B_3}{\alpha_m^2})(f\alpha_m A_4)\right] \overset{o}{U} - \left[(B_1 - a\alpha_m B_4)\right.$$

$$\left.(A_1 - b\alpha_m A_4) + \xi(\frac{B_2}{\alpha_m^3} - \frac{B_3}{\alpha_m^2})(fA_2 - f\alpha_m A_3)\right] \overset{o}{V} + \left[(\frac{bB_2}{\alpha_m} + aB_3)\right.$$

$$\left.(B\alpha_m A_2 - a\alpha_m^2 A_3) - (\xi\frac{B_4}{\alpha_m})(\delta\alpha_m A_4)\right] \overset{o}{W} + \left[(\frac{bB_2}{\alpha_m} + aB_3)(A_1 + a\alpha_m A_4)\right.$$

$$\left. + (\xi\frac{B_4}{\alpha_m})(\eta A_2 + \delta A_3)\right] \overset{o}{\theta} + \xi\left[\frac{B_2^*}{\alpha_m^3} - \frac{B_3^*}{\alpha_m^2}\right] P_{Im} + \sum \xi\left[\frac{B_2'}{\alpha_m^3} - \frac{B_3'}{\alpha_m^2}\right] P_m' = 0 \quad (2.35c)$$

$$\left[(\delta\alpha_m B_4)(aA_2 - b\alpha_m A_3) - (\frac{bB_2}{\alpha_m} + aB_3)(f\alpha_m A_4)\right] \overset{o}{U} - \left[(\delta\alpha_m B_4)\right.$$

$$\left.(A_1 - b\alpha_m A_4) + (\frac{bB_2}{\alpha_m} + aB_3)(fA_2 - f\alpha_m A_3)\right] \overset{o}{V} - \left[(\eta B_2 + \delta B_3)\right.$$

$$\left.(b\alpha_m A_2 - a\alpha_m^2 A_3) - (B_1 + a\alpha_m B_4)(\delta\alpha_m A_4)\right] \overset{o}{W} - \left[(\eta B_2 + \delta B_3)\right.$$

$$\left.(A_1 + a\alpha_m A_4) + (B_1 + a\alpha_m B_4)(\eta A_2 + \delta A_3)\right] \overset{o}{\Theta} + \left[\frac{bB_2^*}{\alpha_m} + aB_3^*\right] P_{Im}$$

$$+ \sum\left[\frac{bB_2'}{\alpha_m} + aB_3'\right] P_m' = 0 \qquad (2.35d)$$

where
B_1, B_2, B_3 and B_4 are the values of hyperbolic functions ϕ_1, ϕ_2, ϕ_3 and ϕ_4 respectively are evaluated at $x_2^* = H$

B_2^* and B_3^* are the values of hyperbolic functions ϕ_2 and ϕ_3 respectively evaluated at $x_2^* = (H - T_1)$. Also B_2' and B_3 are evaluated w.r.t. the positions of point loads across the side member web such that x_2^* = the distance of point load from the centre line $\bar{x}\bar{x}$ of the web.

The Fourier coefficient P_{Im} of the cross member top flange warping force is evaluated by equation (2.12) and the Fourier coefficient P_m' of the cross member web warping force is evaluated as explained below.

Let the web warping effect of a cross member be represented by a suitable number of point loads. The magnitude of each point load equals the sum of distributed forces it has replaced on the portion of the end cross section. Each point load is located in the middle of the portion of end cross section upon which it has replaced the warping effect. If p' is a point load, it can be expanded in a Fourier series over the side member web as below

$$p' = \sum_{m=1}^{\infty} P_m' \sin\alpha_m x_1 \tag{2.36}$$

and

$$P_m' = \lim_{\gamma \to o} \frac{1}{L} \int_{(L-R-\gamma)}^{(L-R+\gamma)} \frac{p'}{2\gamma} \sin\alpha_m x_1 \tag{2.37}$$

where γ is a small dimension.

Deflection of a simply supported plate due to a point load has been evaluated in [30] in a similar way. Solution of the integral of equation (2.37) results in the following

$$P_m' = \frac{p' \sin\alpha_m (L-R)}{\alpha_m L} \left[\lim_{\gamma \to o} \frac{\sin\alpha_m \gamma}{\gamma} \right] \tag{2.38}$$

Limit within brackets of equation (2.38) can be evaluated by expanding $(\sin\alpha_m \gamma)$ in power series as:

$$\left[\lim_{\gamma \to o} \frac{\sin\alpha_m \gamma}{\gamma} \right] = \lim_{\gamma \to o} \frac{1}{\gamma} \left[(\gamma\alpha_m) - \frac{(\gamma\alpha_m)^3}{3!} + \frac{(\gamma\alpha_m)^5}{5!} - \ldots \right]$$

$$= \alpha_m \tag{2.39}$$

Hence equation (2.38) becomes

$$P_m' = \frac{p' \sin\alpha_m (L-R)}{L} \tag{2.40}$$

The magnitude of a point load $\acute{p}$ is evaluated by the following relation:

$$p' = \int_{a_1}^{a_2} k_o^* \, sds = \frac{k_o^*}{2} (a_2^2 - a_1^2). \qquad (2.41)$$

Where $a_1 a_2$ is the portion of end section of a cross member whose warping effect is replaced by a point load p'.

Equations (2.35) represent a system of four simultaneous linear equations involving four non zero unknowns which are $\overset{o}{\theta}$, $\overset{o}{V}$, $\overset{o}{W}$ and $\overset{o}{\Theta}$. Their values can be evaluated by solving equations (2.35). Then by substituting the values of these initial parameters in equations (AI.23) and (AII.19), Fourier coefficients W_m, θ_m, M_{2m}, V_{2m}, U_m, V_m, N_{22m} and N_{12m} are evaluated. The values of these Fourier coefficients are substituted in the respective series to obtain the values of various forces/displacements and moments etc. Values of W_m, θ_m, M_{2m} and V_{2m} for $T_1 < x_2^* \leq H$ of the side member web must include the external forces and are given by the following equations:

$$W_m = [\phi_1 - a\alpha_m\phi_4]\overset{*}{W} + [\frac{b\phi_2}{\alpha_m} + a\phi_3]\overset{*}{\theta} - [\xi \frac{\phi_4}{\alpha_m}]\overset{*}{M}_2$$

$$+ \xi[\frac{\phi_2}{\alpha_m^3} - \frac{\phi_3}{\alpha_m^2}]\overset{*}{V}_2 + \xi[\frac{\overset{*}{\phi}_2}{\alpha_m^3} \; \frac{\overset{*}{\phi}_3}{\alpha_m^2}]P_{Im} + \sum \xi[\frac{\acute{\phi}_2}{\alpha_m^3} - \frac{\acute{\phi}_3}{\alpha_m^2}]P'_m \qquad (2.42a)$$

$$\theta_m = [b\alpha_m\phi_2 - a\alpha^2{}_m\phi_3]\overset{*}{W} + [\phi_1 + a\alpha_m\phi_4]\overset{*}{\theta} + \xi[\frac{\phi_2}{\alpha_m} + \phi_3]\overset{*}{M}_2$$

$$- [\xi \frac{\phi_4}{\alpha_m}m]\overset{*}{V}_2 - [\xi\frac{\overset{*}{\phi}_4}{\alpha_m}]P_{Im} - \sum[\xi \frac{\acute{\phi}_4}{\alpha_m}]P'_m \qquad (2.42b)$$

$$M_{2m} = [\delta\alpha_m\phi_4]\overset{*}{W} - [\eta\phi_2 + \delta\phi_3]\overset{*}{\theta} + [\phi_1 + a\alpha_m\phi_4]\overset{*}{M}_2$$

$$+ [\frac{b\phi_2}{\alpha_m} + a\phi_3]\overset{*}{V}_2 + [\frac{b\phi_2}{\alpha_m} + a\phi_3]P_{Im} + \sum [\frac{b\acute{\phi}_2}{\alpha_m} + a\acute{\phi}_3] P'_m \qquad (2.42c)$$

$$V_{2m} = [\eta\alpha^2{}_m\phi_2 - \delta\alpha^2{}_m\phi_3]\overset{*}{W} + [\delta\alpha_m\phi_4]\overset{*}{\theta} + [b\alpha_m\phi_2 - a\alpha_m{}^2\phi_3]\overset{*}{M}_2$$

$$+ [\phi_1 - a\alpha_m\phi_4]\overset{*}{V}_2 + [\overset{*}{\phi}_1 - a\alpha_m\overset{*}{\phi}_4]P_{Im} + \sum[\acute{\phi}_1 - a\alpha_m\acute{\phi}_4]P'_m \qquad (2.42d)$$

Where
$\overset{*}{\phi}_1, \overset{*}{\phi}_2, \overset{*}{\phi}_3$ and $\overset{*}{\phi}_4$ are the values of hyperbolic functions ϕ_1, ϕ_2, ϕ_3 and ϕ_4 respectively evaluated at $x_2 = (x_2^* - T_1)$ and $\phi_1', \phi_2', \phi_3'$ and ϕ_4' are evaluated for point loads at $x_2 = d_i$ (distance of the point load from the centre of the side member web).

Evaluation of forces/stresses/moments or displacements on any part of the side member is done by using the values of initial parameters which are valid for that particular part, i.e. $\overset{o}{U}, \overset{o}{V}, \overset{o}{N}_{22}, \overset{o}{N}_{12}, \overset{o}{W}, \overset{o}{\theta}, \overset{o}{M}_2$ and $\overset{o}{V}_2$ for the flange and $\overset{*}{U}, \overset{*}{V}, \overset{*}{N}_{22}, \overset{*}{N}_{12}, \overset{*}{W}, \overset{*}{\Theta}, \overset{*}{M}_2$ and $\overset{*}{V}_2$ for the web.

2.5.2. Analysis of an asymmetric joint

Fig (2.4a) represents an asymmetric joint as the cross member web is not located symmetrically on the side member web i.e. $T_1 \neq T_2$. In this case the entire side member section has to be considered in the analysis.

Boundary conditions at the free edge of the top flange are the same as those used in a symmetric joint and are given by equations (2.32) and (2.33). Four non zero initial parameters of the top flange are $\overset{o}{U}$, $\overset{o}{V}$, $\overset{o}{W}$ and $\overset{o}{\theta}$. They have to be determined from boundary conditions at the free edge of the bottom flange which are expressed below:

$$\left.\begin{aligned} \text{At } \overset{**}{x}_2 &= F_2 \\ n_{22} &= 0 \\ n_{12} &= 0 \\ m_{22} &= 0 \\ v_2 &= 0 \end{aligned}\right\} \quad (2.43)$$

Equations (2.43) result in the following equations through equations (AII.16), (AI.15) and (AI.17)

$$\text{At } \overset{**}{x}_2 = F_2$$

$$N_{22m} = N_{12m} = M_{2m} = V_{2m} = 0 \quad (2.44)$$

Boundary conditions (2.44) can be written in extended form by substituting equations (AI.23) and (AII.19) in them. They become

$$[f\alpha_m J_4]\overset{**}{U} + [fJ_2 - f\alpha_m J_3]\overset{**}{V} + [J_1 - b\alpha_m J_4]N_{21} + [aJ_2 + b\alpha_m J_3]\overset{**}{N}_{12} = 0 \quad (2.45a)$$

$$[fJ_2 + f\alpha_m J_3]\overset{**}{U} - [f\alpha_m J_4]\overset{**}{V} + [aJ_2 - b\alpha_m J_3]\overset{**}{N}_{22} + [J_1 + b\alpha_m J_4]\overset{**}{N}_{12} = 0 \quad (2.45b)$$

$$[\delta\alpha_m J_4]\overset{**}{W} - [\eta J_2 + \delta J_3]\overset{**}{\theta} + [J_1 + a\alpha_m J_4]\overset{**}{M}_2 + \left[\frac{bJ_2}{\alpha_m} + aJ_3\right]\overset{**}{V}_2 = 0 \quad (2.45c)$$

$$[\eta\alpha_m^2 J_2 - \delta\alpha_m^2 J_3]\overset{**}{W} + [\delta\alpha_m J_4]\overset{**}{\Theta} + [b\alpha_m J_2 - a\alpha_m^2 J_3]\overset{**}{M}_2$$

$$+ [J_1 - a\alpha_m J_4]\overset{**}{V}_2 = 0 \quad (2.45d)$$

Where

J_1, J_2, J_3 and J_4 are the values of hyperbolic functions ϕ_1, ϕ_2, ϕ_3 and ϕ_4 respectively evaluated at $\overset{**}{x}_2 = F_2$.

Equations (2.45) represent a system of four simultaneous linear equations involving eight unknown parameters which cannot be evaluated directly from this system. However, the number of unknowns can be reduced to four of these parameters which are expressed in terms of non zero initial parameters of the top flange. These relations can be obtained by substituting equations (2.34) in (2.28) and allowing for the contribution of external warping forces on the side member web. The final form of such relations after some rearrangement is expressed below:

$$\begin{aligned}
\overset{**}{U} &= \left[(G_1 + b\alpha_m G_4)(A_1 + b\alpha_m A_4) + \left(\frac{dG_2}{\alpha_m} + cG_3\right)(fA_2 + f\alpha_m A_3)\right] \overset{o}{U} \\
&\quad - \left[(G_1 + b\alpha_m G_4)(aA_2 + b\alpha_m A_3) + \left(\frac{dG_2}{\alpha_m} + cG_3\right)(f\alpha_m A_4)\right] \overset{o}{V} \\
&\quad - \left[(aG_2 + b\alpha_m G_3)(A_1 - a\alpha_m A_4) + (cG_4)(\eta A_2 - \delta A_3)\alpha_m^2\right] \overset{o}{W} \\
&\quad - \left[(aG_2 + b\alpha_m G_3)\left(\frac{bA_2}{\alpha_m} + aA_3\right) + (cG_4)(\delta\alpha_m A_4)\right] \overset{o}{\Theta} \qquad (2.46a)
\end{aligned}$$

$$\begin{aligned}
\overset{**}{V} &= \left[(G_1 - a\alpha_m G_4)(aA_2 - b\alpha_m A_3) - \xi\left(\frac{G_2}{\alpha_m^3} - \frac{G_3}{\alpha_m^2}\right)(f\alpha_m A_4)\right] \overset{o}{U} \\
&\quad - \left[(G_1 - a\alpha_m G_4)(A_1 - b\alpha_m A_4) + \xi\left(\frac{G_2}{\alpha_m^3} - \frac{G}{\alpha_m^2}\right)(fA_2 - f\alpha_m A_3)\right] \overset{o}{V} \\
&\quad + \left[\left(\frac{bG_2}{\alpha_m} + aG_3\right)(b\alpha_m A_2 - a\alpha_m^2 A_3) - \left(\xi\frac{G_4}{\alpha_m}\right)(\delta\alpha_m A_4)\right] \overset{o}{W} \\
&\quad + \left[\left(\frac{bG_2}{\alpha_m} + aG_3\right)(A_1 + a\alpha_m A_4) + \left(\xi\frac{G_4}{\alpha_m}\right)(\eta A_2 + \delta A_3)\right] \overset{o}{\theta} \\
&\quad + \sum \xi \left[\frac{G_2'}{\alpha_m^3} - \frac{G_3'}{\alpha_m^2}\right] P_m' + \xi\left[\left(\frac{\overset{*}{G}_2}{\alpha_m^3} - \frac{\overset{*}{G}_3}{\alpha_m^2}\right) - \left(\frac{\overset{**}{G}_2}{\alpha_m^3} - \frac{\overset{**}{G}_3}{\alpha_m^2}\right)\right] P_{Im} \qquad (2.46b)
\end{aligned}$$

$$\begin{aligned}
\overset{**}{N} &= \left[\alpha_m^2(\eta G_3 - \delta G_3)(aA_2 - b\alpha_m A_3) - (G_1 - a\alpha_m G_4)(f\alpha_m A_4)\right] \overset{o}{U} \\
&\quad - \left[\alpha_m^2(\eta G_2 - \delta G_3)(A_1 - b\alpha_m A_4) + (G_1 - a\alpha_m G_4)(fA_2 - f\alpha_m A_3)\right] \overset{o}{V} \\
&\quad + \left[(\delta\alpha_m G_4)(b\alpha_m A_2 - a\alpha_m^2 A_3) + (b\alpha_m G_2 - a\alpha_m^2 G_3)(\delta\alpha_m A_4)\right] \overset{o}{W} \\
&\quad + \left[(\delta\alpha_m G_4)(A_1 + a\alpha_m A_4) - (b\alpha_m G_2 - a\alpha_m^2 G_3)(\eta A_2 + \delta A_3)\right] \overset{o}{\theta} \\
&\quad + \left[(\overset{*}{G}_1 - a\alpha_m \overset{*}{G}_4) - (\overset{**}{G}_1 - a\alpha_m \overset{**}{G}_4)\right] P_{Im} \\
&\quad + \sum \left[G_1' - a\alpha_m G_4'\right] P_m' \qquad (2.46c)
\end{aligned}$$

$$\overset{**}{N}_{12} = \left[(fG_2+ f\alpha_m G_3)(A_1 + b\alpha_m A_4)+(G_1+ b\alpha_m G_4)(fA_2 + f\alpha_m A_3)\right] \overset{o}{U}$$

$$-\left[(fG_2+ f\alpha_m G_3)(aA_2+ b\alpha_m A_3)+ (G_1+ b\alpha_m G_4)(f\alpha_m A_4)\right] \overset{o}{V}$$

$$-\left[f\alpha_m G_4)(A_1- a\alpha_m A_4)- (aG_2 - b\alpha_m G_3)(\eta A_2-\delta A_3)\alpha_m^2\right] \overset{o}{W}$$

$$-\left[(f\alpha_m G_4)(\frac{bA_2}{\alpha_m}+ aA_3)- (aG_2- b\alpha_m G_3)(\delta\alpha_m A_4)\right]\overset{o}{\theta} \qquad (2.46d)$$

$$\overset{**}{W} = -\left[(b\alpha_m G_3-aG_2)(A_1+ b\alpha_m A_4)+(cG_4)(fA_2+ f\alpha_m A_3)\right] \overset{o}{U}$$

$$+\left[(b\alpha_m G_3- aG_2)(aA_2 + b\alpha_m A_3)+(cG_4)(f\alpha_m A_4)\right] \overset{o}{V}$$

$$-\left[(G_1 -b\alpha_m G_4)(A_1-a\alpha_m A_4)+ (\frac{dG_2}{\alpha_m}- cG_3)(\eta A_2- \delta A_3)\alpha_m^2\right] \overset{o}{W}$$

$$-\left[(G_1 - b\alpha_m G_4)(\frac{bA_2}{\alpha_m}+ aA_3)+ (\frac{dG_2}{\alpha_m}- cG_3)(\delta\alpha_m A_4)\right]\overset{o}{\theta} \qquad (2.46e)$$

$$\overset{**}{\theta} = \left[(b\alpha_m G_2 - a\alpha_m^2 G_3)(aA_2 -b\alpha_m A_3)+(\xi\frac{G_4}{\alpha_m})(f\alpha_m A_4)\right] \overset{o}{U}$$

$$-\left[(b\alpha_m G_2-a\alpha_m^2 G_3)(A_1 -b\alpha_m A_4)- (\xi \frac{G_4}{\alpha_m})(fA_2- f\alpha_m A_3)\right] \overset{o}{V}$$

$$+\left[(G_1+ a\alpha_m G_4)(b\alpha_m A_2 -a\alpha_m^2 A_3) - \xi(\frac{G_2}{\alpha_m}+ G_3)(\delta\alpha_m A_4)\right] \overset{o}{W}$$

$$+\left[(G_1+ a\alpha_m G_4)(A_1+ a\alpha_m A_4)+ \xi(\frac{G_2}{\alpha_m}+ G_3)(\eta A_2 + \delta A_3)\right]\overset{o}{\theta}$$

$$-\xi\left[\frac{\overset{*}{G}_4}{\alpha_m}- \frac{\overset{**}{G}_4}{\alpha_m}\right] P_{Im} -\sum\left[\xi\frac{G'_4}{\alpha_m}\right]P'_m \qquad (2.46f)$$

$$\overset{**}{M}_2 = \left[(\delta\alpha_m G_4)(aA_2- b\alpha_m A_3)-(\frac{bG_2}{\alpha_m}+ aG_3)(f\alpha_m A_4)\right] \overset{o}{U}$$

$$-\left[(\delta\alpha_m G_4)(A_1 - b\alpha_m A_4)+(\frac{bG_2}{\alpha}+ aG_3)(fA_2 -f\alpha_m A_3)\right] \overset{o}{V}$$

$$-\left[\eta G_2 +\delta G_3)(b\alpha_m A_2-a\alpha_m A_3)-(G_1+a\alpha_m G_4)(\delta\alpha_m A_4)\right] \overset{o}{W}$$

$$-\left[(\eta G_2+ \delta G_2)(A_1 + a\alpha_m A_4) + (G_1+ a\alpha_m G_4)(\eta A_2+\delta A_3)\right]\overset{o}{\theta}$$

$$-\left[(\frac{bG_2}{\alpha_m}+ \overset{*}{a}G_3) - (\frac{bG_2}{\alpha_m}+ \overset{**}{a}G_3)\right] P_{Im}$$

$$+\sum\left[\frac{bG_2'}{\alpha_m}+ aG_3'\right]P'_m \qquad (2.46g)$$

$$V_2^{**} = -\left[(f\alpha_m G_4)(A_1 + b\alpha_m A_4) + (aG_2 + b\alpha_m G_3)(fA_3 + f\alpha_m A_3)\right] \overset{o}{U}$$

$$+ \left[(f\alpha_m G_4)(aA_2 + b\alpha_m A_3) + (aG_2 + b\alpha_m G_3)(f\alpha_m A_4)\right] \overset{o}{V}$$

$$- \left[(fG_2 - f\alpha_m G_3)(A_1 - a\alpha_m A_4) + (G_1 - b\alpha_m G_4)(\eta A_2 - \delta A_3)\alpha_m^2\right] \overset{o}{W}$$

$$- \left[(fG_2 - f\alpha_m G_3)\left(\frac{bA_2}{\alpha_m} + aA_3\right) + (G_1 - b\alpha_m G_4)(\delta\alpha_m A_4)\right] \overset{o}{\Theta} \qquad (2.46h)$$

Where
G_1, G_2, G_3 and G_4 are values of hyperbolic functions ϕ_1, ϕ_2, ϕ_3 and ϕ_4 respectively calculated at $x_2^{**} = F_2$.

Also
$\overset{*}{G}_1, \overset{*}{G}_2, \overset{*}{G}_3$, and $\overset{*}{G}_4$ are evaluated at $x_2 = 2H - T_1$

$\overset{**}{G}_1, \overset{**}{G}_2, \overset{**}{G}_3$ and $\overset{**}{G}_4$ " " " $x_2 = T_2$

While

G_1', G_2', G_3' and G_4' are evaluated for each particular point load at x_2= distance of the point load from the corner of bottom flange and web.

Equations (2.45) after substituting equations (2.46) in them, are solved for four non zero initial parameters of the top flange, which are $\overset{o}{U}$, $\overset{o}{V}$, $\overset{o}{W}$ and $\overset{o}{\Theta}$. Their values are substituted in the relevant equations of Appendices I and II to obtain any particular distribution on the top flange. For the web, initial parameters are evaluated from equations (2.34) and they are used in equations of Appendices I and II to determine a required value at any point on the web. Values of W_m, θ_m M_{2m} and V_{2m} are modified to include the effect of external warping forces on the web, and are to be calculated from the following equations:

$$W_m = \left[\phi_1 - a\alpha_m\phi_4\right] \overset{*}{W} + \left[\frac{b\phi_2}{\alpha_m} + a\phi_3\right] \overset{*}{\Theta} - \left[\xi\,\frac{\phi_4}{\alpha_m}\right] \overset{*}{M}_2 + \xi\left[\frac{\phi_2}{\alpha_m^3} - \frac{\phi_3}{\alpha_m^2}\right] \overset{*}{V}_2$$

$$+ \xi\left[\left(\frac{\overset{*}{\phi}_2}{\alpha_m^3} - \frac{\overset{*}{\phi}_3}{\alpha_m^2}\right) - \left(\frac{\overset{**}{\phi}_2}{\alpha_m^3} - \frac{\overset{**}{\phi}_3}{\alpha_m^2}\right)\right] P_{Im} + \sum \xi\left[\frac{\phi_2'}{\alpha_m^3} \quad \frac{\phi_3'}{\alpha_m^2}\right] P_m' \qquad (2.47a)$$

$$\theta_m = \left[b\alpha_m\phi_2 - a\alpha_m^2\phi_3\right] \overset{*}{W} + \left[\phi_1 + a\alpha_m\phi_4\right] \overset{*}{\Theta} - \left[\frac{\xi\phi_2}{\alpha_m} + \xi\phi_3\right] \overset{*}{M}_2$$

$$- \left[\xi\,\frac{\phi_4}{\alpha_m}\right] \overset{*}{V}_2 - \xi\left[\frac{\overset{*}{\phi}_4}{\alpha_m} - \frac{\overset{**}{\phi}_4}{\alpha_m}\right] P_{Im} - \sum \left[\xi\,\frac{\phi_4'}{\alpha_m}\right] P_m' \qquad (2.47b)$$

$$M_{2m} = \left[\delta\alpha_m\phi_4\right] \overset{*}{W} - \left[\eta\phi_2 + \delta\phi_3\right] \overset{*}{\Theta} + \left[\phi_1 + a\alpha_m\phi_4\right] \overset{*}{M}_2$$

$$+ \left[\frac{b\phi_2}{\alpha_m} + a\phi_3\right] \overset{*}{V}_2 + \left[\left(\frac{b\overset{*}{\phi}_2}{\alpha_m} + a\overset{*}{\phi}_3\right) - \left(\frac{b\overset{**}{\phi}_2}{\alpha_m} + a\overset{**}{\phi}_3\right)\right] P_{Im}$$

$$+ \sum \left[\frac{b\phi_2'}{\alpha_m} + \phi_3'\right] P_m' \qquad (2.47c)$$

$$V_{2m} = [\eta\alpha_m^2 \phi_2 - \delta\alpha_m^2 \phi_3]\overset{*}{W} + [\delta\alpha_m\phi_4]\overset{*}{\theta} + [b\alpha_m\phi_2 - a\alpha_m^2 \phi_3]\overset{*}{M}_2$$
$$+[\phi_1 - a\alpha_m\phi_4]\overset{*}{V}_2 + [(\overset{*}{\phi}_1 - a\alpha_m\overset{*}{\phi}_4) - (\overset{**}{\phi}_1 - a\alpha_m\overset{**}{\phi}_4)]P_{Im}$$
$$+ \sum [\phi' \quad \alpha \phi_4']\acute{P}_m \qquad (2.47d)$$

Where

$\overset{*}{\phi}_1, \overset{*}{\phi}_2, \overset{*}{\phi}_3$ and $\overset{*}{\phi}_4$ are values of hyperbolic functions ϕ_1, ϕ_2, ϕ_3 and ϕ_4 respectively, evaluated at $x_2 = x_2 - T_1$.

$\overset{**}{\phi}_1, \overset{**}{\phi}_2, \overset{**}{\phi}_3$ and $\overset{**}{\phi}_4$ are evaluated at $x_2 = x_2 - (T_1 + c_o)$

and

$\phi_1', \phi_2', \phi_3'$ and ϕ_4' are evaluated for every individual point load at x_2 = (x_2 - distance of the point load from the top flange and web corner) such that the difference on the right side is always a positive quantity.

Equations (2.47) are to be used for evaluation of u_3, θ, m_{22} and v_2 on any part of the web subject to the following conditions:

1. For $o \leq x_2 \leq T_1$

$$\overset{*}{\phi}_1 = \overset{*}{\phi}_2 = \overset{*}{\phi}_3 = \overset{*}{\phi}_4 = 0$$

$$\overset{**}{\phi}_1 = \overset{**}{\phi}_2 = \overset{**}{\phi}_3 = \overset{**}{\phi}_4 = 0$$

$$\phi_1' = \phi_2' = \phi_3' = \phi_4' = 0$$

2. For $T_1 < x_2 \leq (T_1 + c_o)$

$$\overset{**}{\phi}_1 = \overset{**}{\phi}_2 = \overset{**}{\phi}_3 = \overset{**}{\phi}_4 = 0$$

Equations (2.46) are used for evaluating the values of the initial parameters of bottom flange and subsequently they are used in equations of Appendices I and II to determine different distributions on the bottom flange.

2.6 SIDE MEMBER SUBJECT TO A COUPLE LOADING

Torque applied on the free end of a cross member in an isolated joint will produce a moment loading which acts in the plane of side member web. The effect of this moment is considered by applying a couple in the plane of side member web as shown in fig. (2.4b). It is assumed that the couple forces are acting in the flanges of the cross member end only and their magnitude is given by the following relation

$$F \times c_o = T \qquad (2.48)$$

where T is the applied torque and F is a force acting over a

length (R + S) of the side member web. The force per unit length corresponding to this force is given by:

$$F'(x_1) = \frac{F}{(R+S)} \tag{2.49a}$$

or

$$F'(x_1) = \frac{T}{c_o(R+S)} \tag{2.49b}$$

Any force which acts in the plane of the web will result in stretching of the web. Hence the effect of such an external loading can be included in equations derived in Appendix II.

It is considered that the cross member is not located symmetrically on the side member web, i.e. $T_1 \neq T_2$ in general. A complete section of the side member has to be considered in this analysis.

Boundary conditions on the free edge of the top flange are given by equations (2.32) and (2.33) while equations (2.43) and (2.44) give the boundary conditions at the free edge of the bottom flange. The former conditions are expressed by equations (2.45) in an extended form through the use of equations (AII.19c and d) and (AI.23c and d). Initial parameters of the bottom flange depend upon the initial parameters of the web and the external loading. These relations are expressed by the following equations.

$$\overset{**}{U} = [G_1 + b\alpha_m G_4]\overset{*}{U} - [aG_2 + b\alpha_m G_3]\overset{*}{V} - [cG_4]\overset{*}{N}_{22} + \left[\frac{dG_2}{\alpha_m} + cG_3\right]\overset{*}{N}_{12} - \left[\left(\frac{d\overset{*}{G}_2}{\alpha_m} + c\overset{*}{G}_3\right) - \left(\frac{d\overset{**}{G}_2}{\alpha_m} + c\overset{**}{G}_3\right)\right] F_m \tag{2.50a}$$

$$\overset{**}{V} = [G_1 - a\alpha_m G_4]\overset{*}{W} + \left[\frac{bG_2}{\alpha_m} + aG_3\right]\overset{*}{\theta} - \left[\xi\frac{G_4}{\alpha_m}\right]\overset{*}{M}_2 + \xi\left[\frac{G_2}{\alpha_m^3} - \frac{G_3}{\alpha_m^2}\right]\overset{*}{V}_2 \tag{2.50b}$$

$$\overset{**}{N}_{22} = [\eta\alpha_m^2 G_2 \quad \delta\alpha_m^2 G_3]\overset{*}{W} + [\delta\alpha_m G_4]\overset{*}{\theta} + [b\alpha_m G_2 - a\alpha_m^2 G_3]\overset{*}{M}_2 + [G_1 - a\alpha_m G_4]\overset{*}{V}_2 \tag{2.50c}$$

$$\overset{**}{N}_{12} = [fG_2 + f\alpha_m G_3]\overset{*}{U} - [f\alpha_m G_4]\overset{*}{V} + [aG_2 - b\alpha_m G_3]\overset{*}{N}_{22} + [G_1 + b\alpha_m G_4]\overset{*}{N}_{12} - [(G_1 + b\alpha_m \overset{*}{G}_4) - (\overset{**}{G}_1 + b\alpha_m \overset{**}{G}_4)] F_m \tag{2.50d}$$

$$\overset{**}{W} = -\Big\{[b\alpha_m G_3 - aG_2]\overset{*}{U} + [G_1 - b\alpha_m G_4]\overset{*}{V} + \left[\frac{dG_2}{\alpha_m} - cG_3\right]\overset{*}{N}_{22} + [cG_4]\overset{*}{N}_{12} - [(c\overset{*}{G}_4) - (c\overset{**}{G}_4)] F_m\Big\} \tag{2.50e}$$

$$\overset{**}{\theta} = \left[b\alpha_m G_2 - a\alpha_m^2 G_3\right]\overset{*}{W} + \left[G_1 + a\alpha_m G_4\right]\overset{*}{\theta} - \xi\left[\frac{G_2}{\alpha_m} + G_3\right]\overset{*}{M}_2 - \left[\xi\frac{G_4}{\alpha_m}\right]\overset{*}{V}_2 \qquad (2.50f)$$

$$\overset{**}{M}_{22} = \left[\delta\alpha_m G_4\right]\overset{*}{W} - \left[\eta G_2 + \delta G_3\right]\overset{*}{\theta} + \left[G_1 + a\alpha_m G_4\right]\overset{*}{M}_2 + \left[\frac{bG_2}{\alpha_m} + aG_3\right]\overset{*}{V}_2 \qquad (2.50g)$$

$$\overset{**}{V}_2 = -\left(\left[f\alpha_m G_4\right]\overset{*}{U} + \left[fG_2 - f\alpha_m G_3\right]\overset{*}{V} + \left[G_1 - b\alpha_m G_4\right]\overset{*}{N}_{22} + \left[aG_2 + b\alpha_m G_3\right]\overset{*}{N}_{12} - \left[(a\overset{*}{G}_2 + b\alpha_m\overset{*}{G}_3) - (a\overset{**}{G}_2 + b\alpha_m\overset{**}{G}_3)\right] F_m\right) \qquad (2.50h)$$

where

F_m is the Fourier coefficient of the following series:

$$F'(x_1) = \sum_{m=1}^{\infty} F_m \cos\alpha_m x_1 \qquad (2.51)$$

F_m is evaluated from the following relation:

$$F_m = \frac{1}{L}\int_{(L-R)}^{(L+S)} F'(x_1)\cos\alpha_m x_1 dx_1 \qquad (2.52)$$

The final form of equation (2.52) after its solution becomes:

$$F_m = \left[\frac{2T}{c_o\alpha_m L(R+S)}\right]\cos\alpha_m\left(L + \frac{S-R}{2}\right)\sin\alpha_m\left(\frac{R+S}{2}\right) \qquad (2.53)$$

Relationships between the initial parameters of bottom flange and top flange are obtained by substituting equations (2.34) in equations (2.50). The resulting equations are substituted in boundary conditions (2.45) to obtain a system of four simultaneous linear equations involving four non zero initial parameters of the top flange. This system is solved for these unknowns which are then used in equations of Appendices I and II to determine stress/displacement or other distributions on the top flange of the side member. Similar distributions are obtained on any part of the web by using the initial parameters of the web which are evaluated from equations (2.34). Since external forces are acting on the web, so some of the Fourier coefficients of equations (AI.23) and equations (AI.19) are modified to include their effects. These modified relations are given below:

$$U_m = \left[\phi_1 + b\alpha_m\phi_4\right]\overset{*}{U} - \left[a\phi_2 + b\alpha_m\phi_3\right]\overset{*}{V} - \left[c\phi_4\right]\overset{*}{N}_{22} + \left[\frac{d\phi_2}{\alpha_m} + c\phi_3\right]\overset{*}{N}_{12}$$

$$- \left[\left(\frac{d\overset{*}{\phi}_2}{\alpha_m} + c\overset{*}{\phi}_3\right) - \left(\frac{d\overset{**}{\phi}_2}{\alpha_m} + c\overset{**}{\phi}_3\right)\right] F_m \qquad (2.54a)$$

$$\underline{V}_m = \left[b\alpha_m\phi_3 - a\phi_2\right]\overset{*}{U} + \left[\phi_1 - b\alpha_m\phi_4\right]\overset{*}{V} + \left[\frac{d\phi_2}{\alpha_m} - c\phi_3\right]\overset{*}{N}_{22}$$

$$+ \left[c\phi_4\right]\overset{*}{N}_{12} - \left[\left(c\overset{*}{\phi}_4\right) - \left(c\overset{**}{\phi}_4\right)\right] F_m \qquad (2.54b)$$

$$N_{22m} = \left[f\alpha_m\phi_4\right]\overset{*}{U} + \left[f\phi_2 - f\alpha_m\phi_3\right]\overset{*}{V} + \left[\phi_1 - b\alpha_m\phi_4\right]\overset{*}{N}_{22}$$

$$+ \left[a\phi_2 + b\alpha_m\phi_3\right]\overset{*}{N}_{12} - \left[\left(a\overset{*}{\phi}_2 + b\alpha_m\overset{*}{\phi}_3\right) - \left(a\overset{**}{\phi}_2 + b\alpha_m\overset{**}{\phi}_3\right)\right] F_m \qquad (2.54c)$$

$$N_{12m} = \left[f\phi_2 + f\alpha_m\phi_3\right]\overset{*}{U} - \left[f\alpha_m\phi_4\right]\overset{*}{V} + \left[a\phi_2 - b\alpha_m\phi_3\right]\overset{*}{N}_{22}$$

$$+ \left[\phi_1 + b\alpha_m\phi_4\right]\overset{*}{N}_{12} - \left[\left(\overset{*}{\phi}_1 + b\alpha_m\overset{*}{\phi}_4\right) - \left(\overset{**}{\phi}_2 + b\alpha_m\overset{**}{\phi}_4\right)\right] F_m \qquad (2.54d)$$

Equations (2.54) are to be used subject to the following conditions:

1. For $0 \leq x_2 \leq T_1$

$$\overset{*}{\phi}_1 = \overset{*}{\phi}_2 = \overset{*}{\phi}_3 = \overset{*}{\phi}_4 = 0$$

$$\overset{**}{\phi}_1 = \overset{**}{\phi}_2 = \overset{**}{\phi}_3 = \overset{**}{\phi}_4 = 0$$

2. For $T_1 < x_2 \leq (T_1 + c_o)$

$$\overset{**}{\phi}_1 = \overset{**}{\phi}_2 = \overset{**}{\phi}_3 = \overset{**}{\phi}_4 = 0$$

Distributions of various quantities on the bottom flange can be obtained by using the values of initial parameters of the bottom flange in the relevant equations of Appendices I and II. Initial parameters of the bottom flange can be evaluated from equations (2.50).

2.7 COMPUTATION OF ANALYTICAL SOLUTIONS

The analytical approach developed in the previous sections was applied on the analysis of isolated joints and ladder frame subjected to torsion. Since the approach involved the solution of simultaneous equations to determine the initial parameters of the problem under consideration, so it was necessary to use a computer to facilitate calculation work. The nature of the calculation work involved did not require a large computer or even sophisticated subroutines. A small desk model computer H.P.9830A was available in the School and was used for the calculation work. It only accepted programs in Basic language.

Two separate programs based on the following methods were written:

(a) Plate bending solution derived in section (2.2), to calculate deflection of the side member web treated as a rectangular plate simply supported along all its edges.

(b) Application of the plate theory on a channel section side member subjected to (i) A channel section cross member warping forces (Section 2.5) and (ii) cross member couple loading (Section 2.6).

The main program was based on (b) and was developed to analyse the following joint configurations.

i) A channel section cross member attached to a channel section side member with the cross member web vertical to the longitudinal axis of the side member. This included symmetric or asymmetric location of the cross member in the joint.

ii) An I-section cross member attached to a channel section side member with the same restrictions as described in (i).

Flow charts of both programs are included in Appendix III. Output obtained from these programs was in terms of the intensity factor of the cross member warping forces. All the values outputted were for a unit torque applied to the free end of the beam representing a part of the cross member in a joint. The displacements associated with any point of the side member were multiplied by Young's Modulus of the material before being outputted so that the values could be directly used in the calculation of the cross member warping restraint constants. Theoretical distributions of stress/displacements of all the isolated joints and the ladder frame were obtained using the main program up to the first 16 terms of the respective Fourier series. In some cases where the numbers became very large during the execution of the main program a lesser number of terms of the series were evaluated.

The values of the side member web normal displacements U_3 and bending moments M_{22} at a section below the cross member web were computed from both of the programs for Joint No.III. Their distributions along that section are shown in Figs (2.5a) and (2.5b). These distributions were plotted to compare the approximation of the side member web as a simply supported rectangular plate.

2.8 THEORETICAL ESTIMATION OF CROSS MEMBER WARPING RESTRAINT FACTORS

The magnitude of stress/displacement at any point of the side member was dependent on the value of the cross member warping force intensity factor in the analytical solution. So it was necessary to determine it either experimentally or from theoretical considerations. It has been mentioned in Chapter I that most of the research workers relied on experimental measurements while only Tidbury, Marshall and Roach [17] and Megson and Alade [21] employed analytical approaches to assess the degree of warping inhibition in a joint. Once its value is obtained then it is easy to estimate the magnitude of cross member

warping force intensity factor.

The author wanted to make the analytical method developed in the present work a self sufficient one for the estimation of stresses in the joints. This could only be achieved if the cross member warping restraint factor for a joint configuration under consideration was estimated from the present analytical work. The relationship between the strip beam constant "C"[17] and the cross member warping constant "K" [21] was derived as follows:

$$K = \frac{1}{1 + \left[\frac{1}{\overset{*}{C}\ \mu \tanh(\mu \ell)}\right]} \qquad (2.55)$$

The average value of $\overset{*}{C}$ for a particular joint configuration was defined from the cross member end displacements and the stresses in the follwoing way:

$$\overset{*}{C}_{av} = \frac{E \int w ds}{\int \sigma_z ds} \qquad (2.56)$$

$\overset{*}{C}_{av}$ was evaluated from the values of bending displacements of the side member web under the cross member end profile by the following relation:

$$\overset{*}{C}_{av} = \left[E\ k_o \int u_3 ds\right] \Big/ \left[\frac{k_o}{t} \int p ds\right] \qquad (2.57)$$

The values of the integral terms of equation (2.57) were estimated by measuring areas under the respective curves. The value of $\overset{*}{C}_{av}$ obtained from equation (2.57) was used in equation (2.55) to estimate K. Then the value of the cross member end warping force intensity factor per unit applied torque "$\frac{k_o}{T}$"was evaluated from the following equations.

$$\sigma_p = (1-K)\sigma_\Gamma \quad \text{(of Ref. [21] with original notation)}$$

$$\sigma_\Gamma = -\sqrt{\left(\frac{E}{GJ\Gamma_E}\right)}\ T2A_E\ \frac{\sinh \mu(L-z)}{\cosh \mu L} \quad \text{(of Ref. [31] with original notation)}$$

The bending displacements of the side member web along the upper half of the cross member profile (as the joints were symmetrical) was plotted for each of the joints. These distributions are shown in Figs. (2.6),(2.7),(2.8) and (2.9). The values of $\overset{*}{C}_{av}$,K and ko/T were found using the strip beam theory [17],finite element analysis [21], plate bending solution and plate theory as used in the present work. The values of the constants obtained from each method are given in Table I.

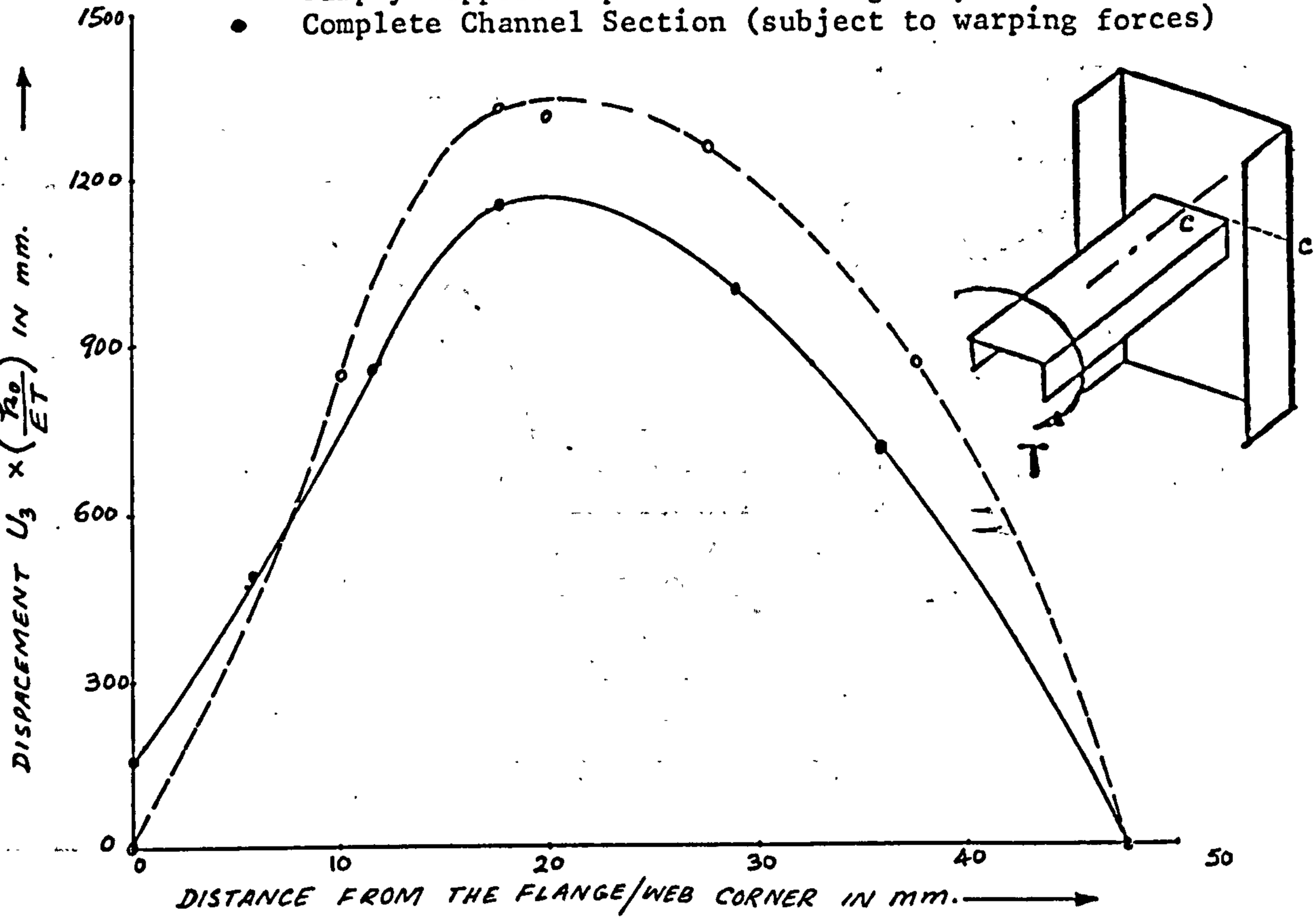

Fig.2.5a Theoretical distribution of normal displacements on section CC of the side member web. (Joint III)

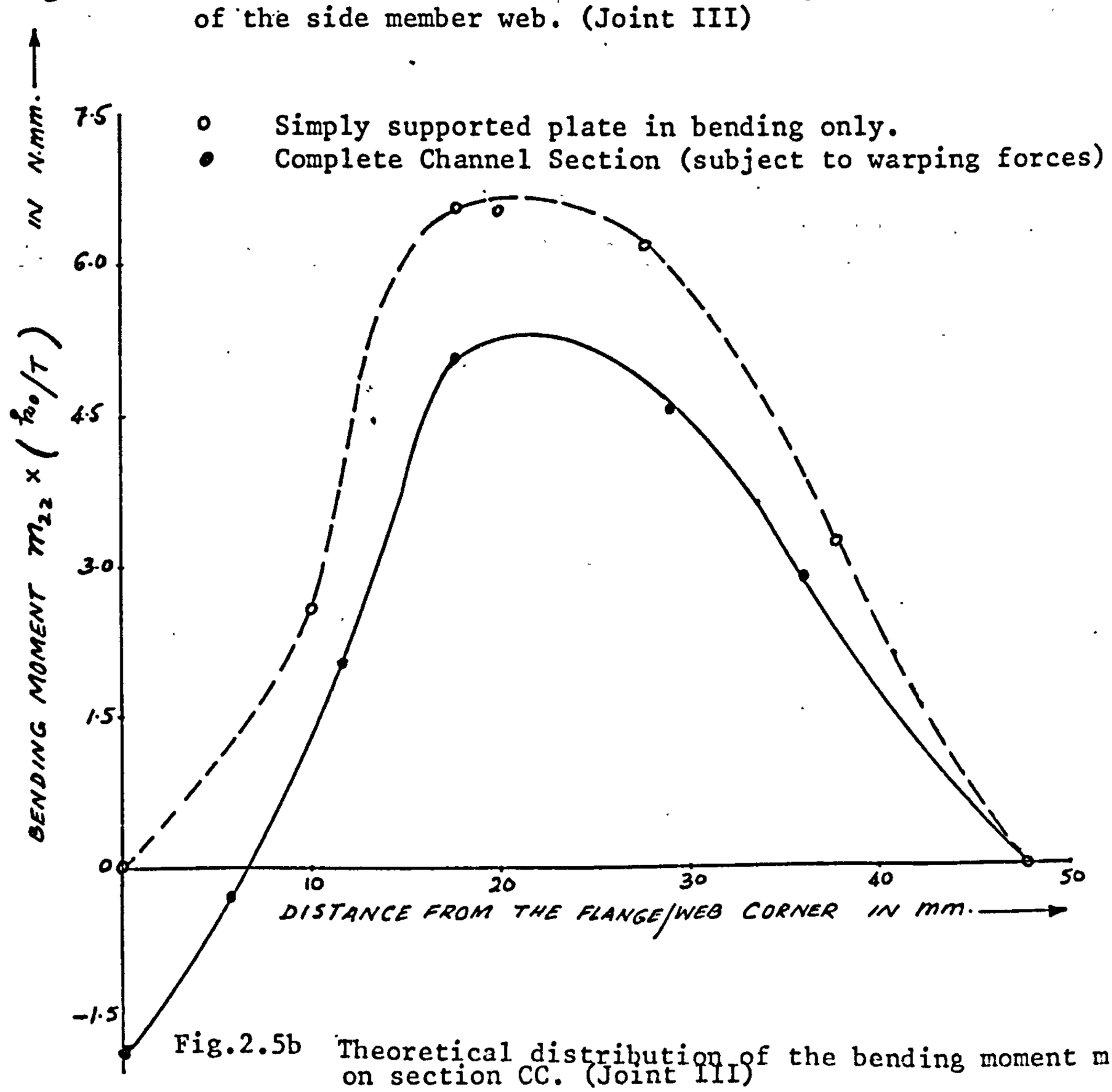

Fig.2.5b Theoretical distribution of the bending moment m_{22} on section CC. (Joint III)

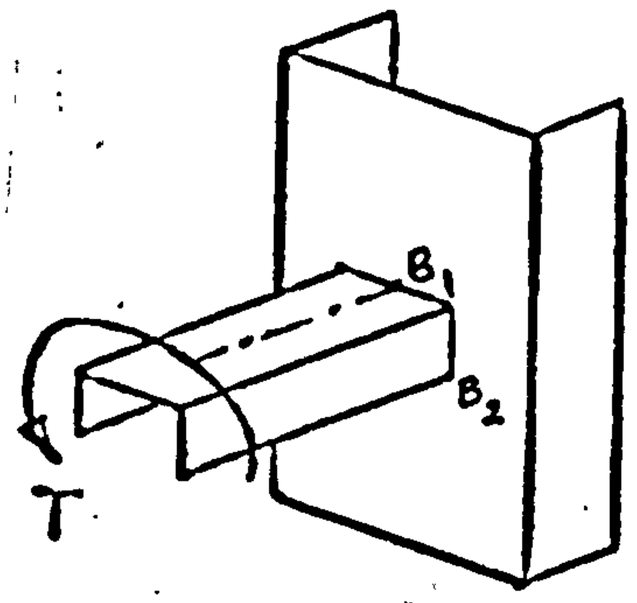

o— Simply supported plate in bending only.
•— Complete channel section (subject to warping forces)
×— Complete channel section (subject to warping forces and couple)

DISPLACEMENT $U_3 \times \left(\frac{h_0}{ET}\right)$ IN mm.

DISTANCE FROM B_1 IN mm. →

Fig.2.6 Theoretical distribution of the side member web normal displacement along cross member end profile (Joint I)

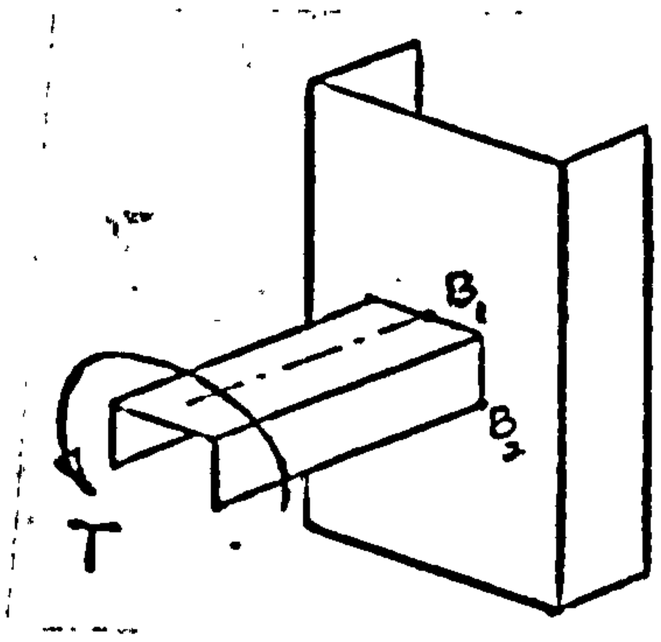

Fig 2.7a Theoretical distribution of tne side member web normal displacement along cross member end profile (Joint II)

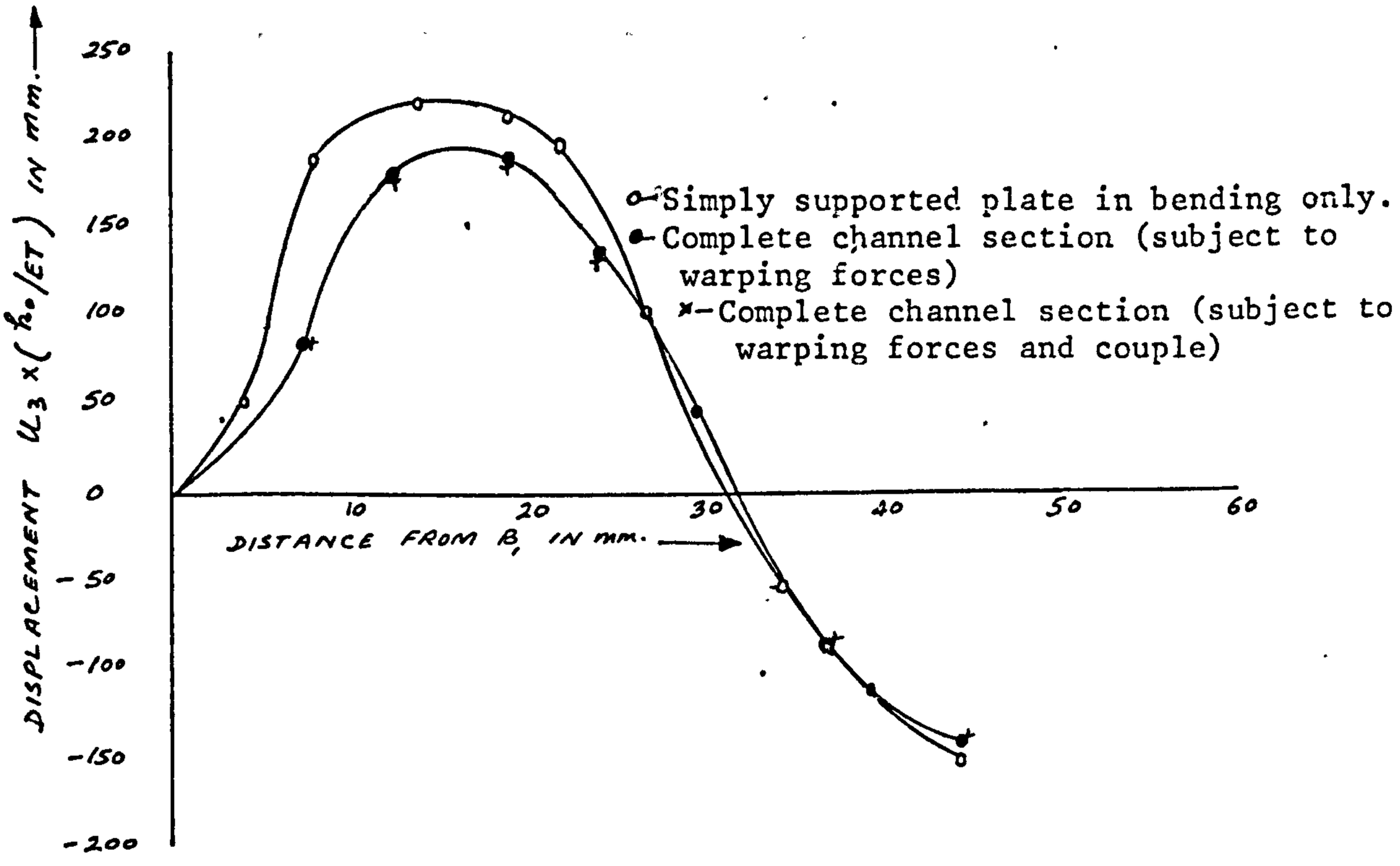

Fig.2.7b Theoretical distribution of the side member web normal displacement along cross member end profile (Joint IV)

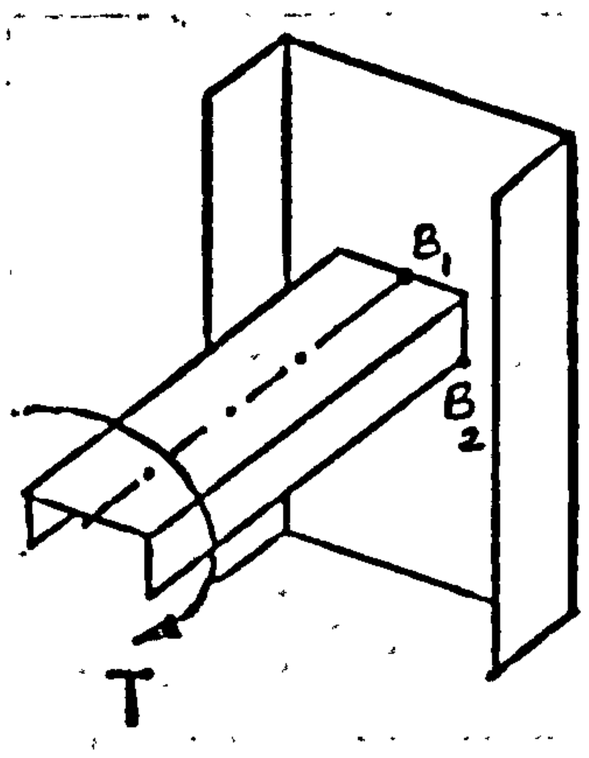

Fig.2.8 Theoretical distribution of the side member web normal displacement along cross member end profile (Joint III)

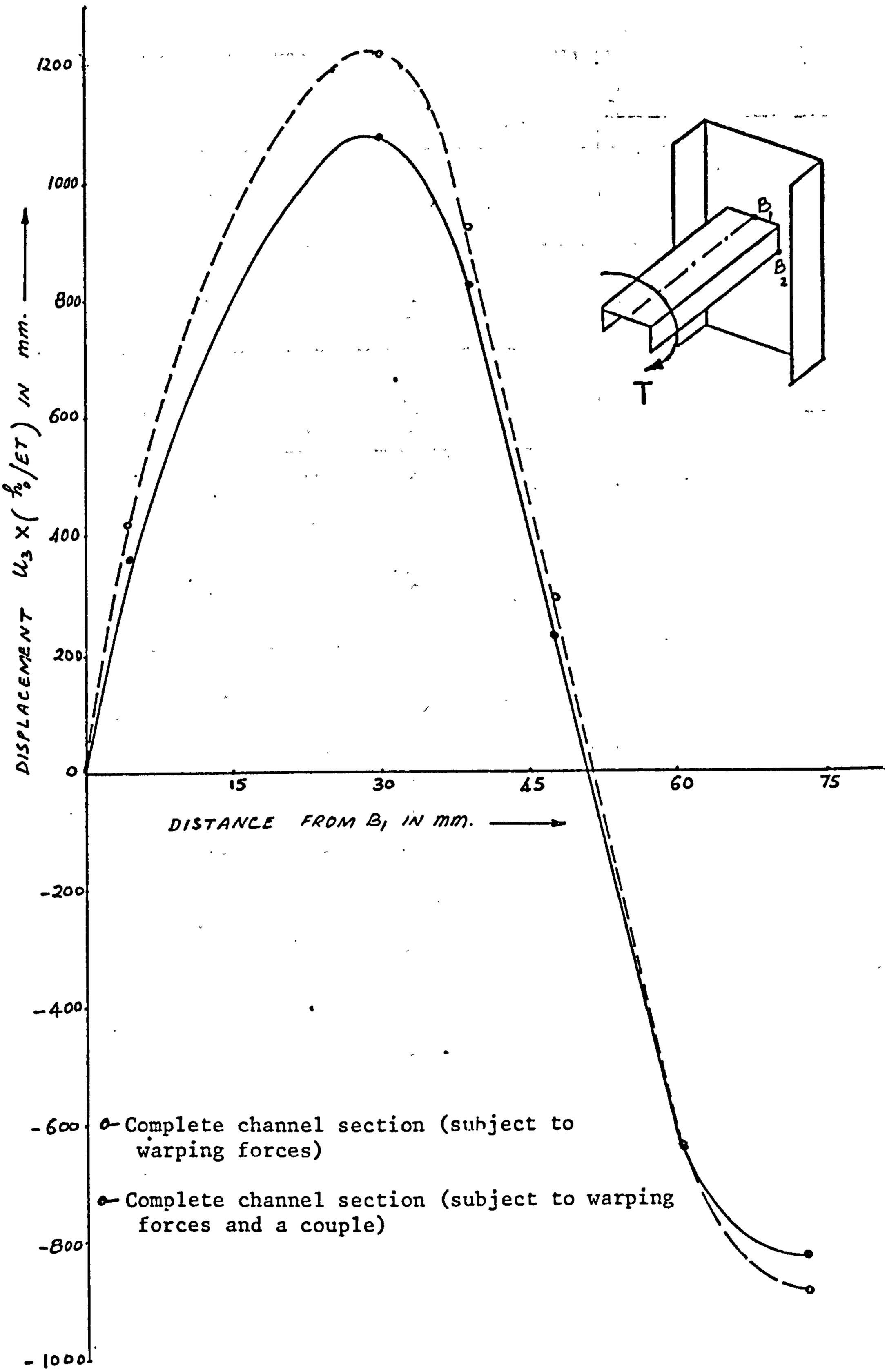

Fig.2.9 Theoretical distribution of the side member web normal displacement along cross member end profile (Ladder frame inner joint).

TABLE I. CROSS MEMBER PARTIAL WARPING CONSTANTS

Joint No	Strip Beam Theory			Finite Element Method			Simply supported plate in Bending only			Plate Theory Applied to a Complete Section		
	C*	K	$\frac{ko}{T}$	$\overset{*}{C}_{av}$	K	$\frac{ko}{T}$	$\overset{*}{C}_{av}$	K	$\frac{ko}{T}$	$\overset{*}{C}_{av}$	K	$\frac{ko}{T}$
I	40.72	0.756	0.206	-	0.42	0.492	9.32	0.415	0.494	7.66	0.37	0.534
II	36.1	0.729	0.354	-	0.36	0.834	6.53	0.328	0.88	5.8	0.302	0.91
III	137.2	0.825	0.072	-	0.42	0.24	27.33	0.483	0.214	22.5	0.43	0.236
IV	40.72	0.796	0.244	-	0.42	0.696	7.89	0.43	0.68	7.09	0.40	0.72
Ladder frame inner joint	137.2	0.786	0.069	-	0.42	0.187	-	-	-	24.52	0.40	0.193

CHAPTER 3 EXPERIMENTAL INVESTIGATIONS

3.1 INTRODUCTION

The main purpose of the present experimental investigation was to determine stress distributions in the joints of chassis frames. Joints made of channel section members with cross members attached to the web of the side member, were to be used in this investigation so that results could be compared with theoretical analysis.

A general survey of the experimental methods available for stress/strain measurements showed that electrical strain gauging was a commonly used technique. Many researchers investigating in the area of vehicle chassis frames had employed dial gauges for displacement measurements and electrical strain gauges for stress/strain measurements. Takahashi [13] employed a "vibration method" using a hand held extensometer for measuring strains on a truck chassis frame. He obtained very good results by this technique.

Since it was expected that localised stresses could develop in the region of a joint, an experimental method which could detect such regions easily was considered more useful in the present case. It was also intended to measure the magnitude of localised stresses accurately. Various methods of stress/strain measurements could only measure average values of these quantities over a certain gauge length. This results in measuring lower than the actual values of localised stresses. These inaccuracies depend upon the gauge length of the gauge used and gradient of stress/strain. Electrical strain gauges and other methods employing the use of an extensometer were not considered suitable in the present experimental work. The photoelastic technique was chosen as it would be suitable for qualitative and quantitative analysis very effectively.

Some simple photoelastic models were made and investigated to justify the usefulness of the photoelastic technique in analysing thin walled beams of open section. Once the initial experiments demonstrated good results, channel sections were cast in aluminium moulds and various isolated joints and a model of a simple chassis frame were constructed. Preparation of reliable photoelastic models by casting requires a specialised technique and the details are given in Appendix IV for future guidance. Photoelastic investigation of all the models was carried out by using a reflection polariscope with a white light source. Coloured and black and white photographs were taken of some of the models to show distribution of fringes.

3.2. METHOD OF PHOTOELASTIC ANALYSIS EMPLOYED

Photoelastic analysis of a thin walled structure such as a joint between a side member and a cross member by a transmission polariscope is not feasible. This is because the light transmitted through any plane surface of a photoelastic model could be obstructed by some other surface

of the same model, e.g. both of the flanges of a channel section would lie in the way of a light ray. By mounting birefringement coatings on the surface of a structure and analysing the photo-elastic effect by a reflection polariscope, one could solve the above-mentioned difficulty. Use of birefringent coatings is quite common in the analysis of complicated structures and the effect of bracket holes in a side member of a truck frame was studied [32] by using this method.

The birefringent coating technique has some limitations which effect the quantitative analysis although qualitative results could be obtained easily. These limitations are:

(a) A birefringent coating tends to reinforce the strength of the actual structure. The reinforcing effect depends on the coating thickness [33].

(b) The coating material should be optically very sensitive so that comparatively small surface strains in a metallic structure could produce reasonable amount of birefringence in the coatings.

(c) Residual birefrigence could result during the cementing of coatings on a structure.

(d) Strain distortions could result due to difference of the elastic properties of plastic, structural material and adhesive [34].

The second limitation was the most important because of the experience of many other researchers and in particular of the author's own [35]. These considerations led to the choice of using the method successfully employed in [35]. This involved the use of a reflection polariscope for analysing photoelastic models after putting a thin reflective layer on one surface. The advantages are twofold. Firstly, the amount of bi-refringence is increased by directly loading a photoelastic model and secondly the loading rig becomes light and simple to construct. The use of reflection techniques also doubles the birefringence effect. The present experimental work confirmed this choice.

3.3. PHOTOELASTIC MODELS

Photoelastic models used in the present work were developed systematically in stages. The details of photoelastic model preparations are described in Appendix IV. The sequence of development is described below.

(a) Channel sections of dimensions shown in Table II were fabricated from CT200 plastic sheets. Three pieces were cut to size and were joined by Araldite adhesive to form a channel section of the required dimensions. They proved successful in simple experiments but the joints were not very reliable and it was not possible to obtain sections of relatively large dimensions, specially lengths, as explained in Appendix IV. So this technique of making channel sections was abandoned.

TABLE II. FABRICATED CHANNEL SECTIONS

Section	Section Dimension (mm)	Length (mm)
FI	68 x 32 x 3	305
FII	36 x 38 x 3	323
FIII	37 x 30 x 3	297

(b) It was decided to cast channel sections. They were cast in aluminium moulds by pouring a mixture of CT200 Araldite and HY905 Hardener in them, under temperature controlled conditions. Curing and annealing of the cast sections were carried out in an electric oven as described in Appendix IV. Dimensions of the cast channel sections are given in Table III. The aluminium moulds are shown in Plate 3.1 along with some of the cast sections. The sections produced by this method were almost free from residual birefringence which is a necessary requirement for an accurate photoelastic analysis.

TABLE III DIMENSIONS OF CAST CHANNEL SECTIONS

Section	Section Dimension (mm)	Length (mm)
CI	42 x 40(max.)x 3.8	320
CII	64 x 60(max.)x 3.8	545
CIII	99 x 52(max.)x 3.8	495

(c) An aluminium mould was designed to cast an Araldite model of a complete joint between two channel sections. Plate 3.3 shows various parts of this mould and its assembled view is shown in Plate 3.4. Castings could be made in the mould but the cast model could not be released easily from the mould surface. The mould release agent which was used in casting individual channel sections did not give satisfactory results. Even a small force employed in releasing the model resulted in its breakage as Araldite is a brittle material. This method of casting complete joints was abandoned as a suitable mould release agent could not be found. A broken model is shown in Plate 3.4.

(d) Photoelastic models of four isolated joints, in which the channel section representing a part of a cross member was directly attached to the web of a channel section representing a part of a side member, were made by using a special temperature cured Araldite adhesive. Its constituents were AY105 Epoxy Resin and HY951 Hardener. Joints of sufficient strength were obtained by this adhesive. One model of a joint in which the cross member was attached to the side member web with Araldite brackets and bolts was made. Bracket holes at sections of zero warping were drilled at the cross member flanges and web. The cross member

end was free to warp because of a clearance left between it and the side member web. All the joints investigated experimentally in the present work are shown in Plate 3.2 and the dimensions are given in Table IV.

(e) A model of a three bay ladder type chassis frame was made by joining cast sections with the same adhesive as used for making isolated joints. Residual stresses developed in the frame during its assembly had to be reduced by subjecting the whole frame to a heat curing cycle in a large oven. Usually it is not possible to remove residual birefringence completely. By this method residual stresses on the side members were removed but small permanent deformations were obtained in cross members due to sagging. This produced residual birefringence in the middle portion of the cross members but their ends and side members were suitable for photoelastic investigation. Dimensions of the frame are shown in Fig. (3.1).

TABLE IV DIMENSIONS OF ISOLATED JOINTS

Joint	Description	Side member		Cross member	
		Section Dimension (mm)	Length (mm)	Section Dimension (mm)	Length (mm)
I	Adhesive Joint	64 x 59 x 3.8	382	42 x 33 x 3.8	255
II	"	64 x 51 x 3.8	266	37 x 30 x 3	297
III	"	99 x 39 x 4	482	64 x 45 x 3.8	500
IV	"	64 x 51 x 3.8	266	42 x 27.5 x 3.8	281
V	Bolted Assembly	99 x 42 x 4	445	64 x 39 x 3.8	455

3.4. CALIBRATION OF CT200 ARALDITE PLASTIC

It was essential to determine the values of Elastic constants of the photoelastic material used for making models as the values were not obtainable for the material used in the present work. Quantitative results from photoelastic measurements can be obtained if the stress-optic or strain-optic characteristics of the photoelastic material are known.

3.4.1. Determination of Elastic Constants

A tension specimen of dimensions shown in Fig.3.2 was cut from one of the cast sections of CT200 Araldite. One electrical strain gauge was stuck on each surface at the middle part of the specimen. These gauges were mounted in such a way that one would indicate longitudinal strain while the other would measure transverse strain in the specimen. Dummy gauges were also mounted for temperature compensation on another CT200 Araldite piece.

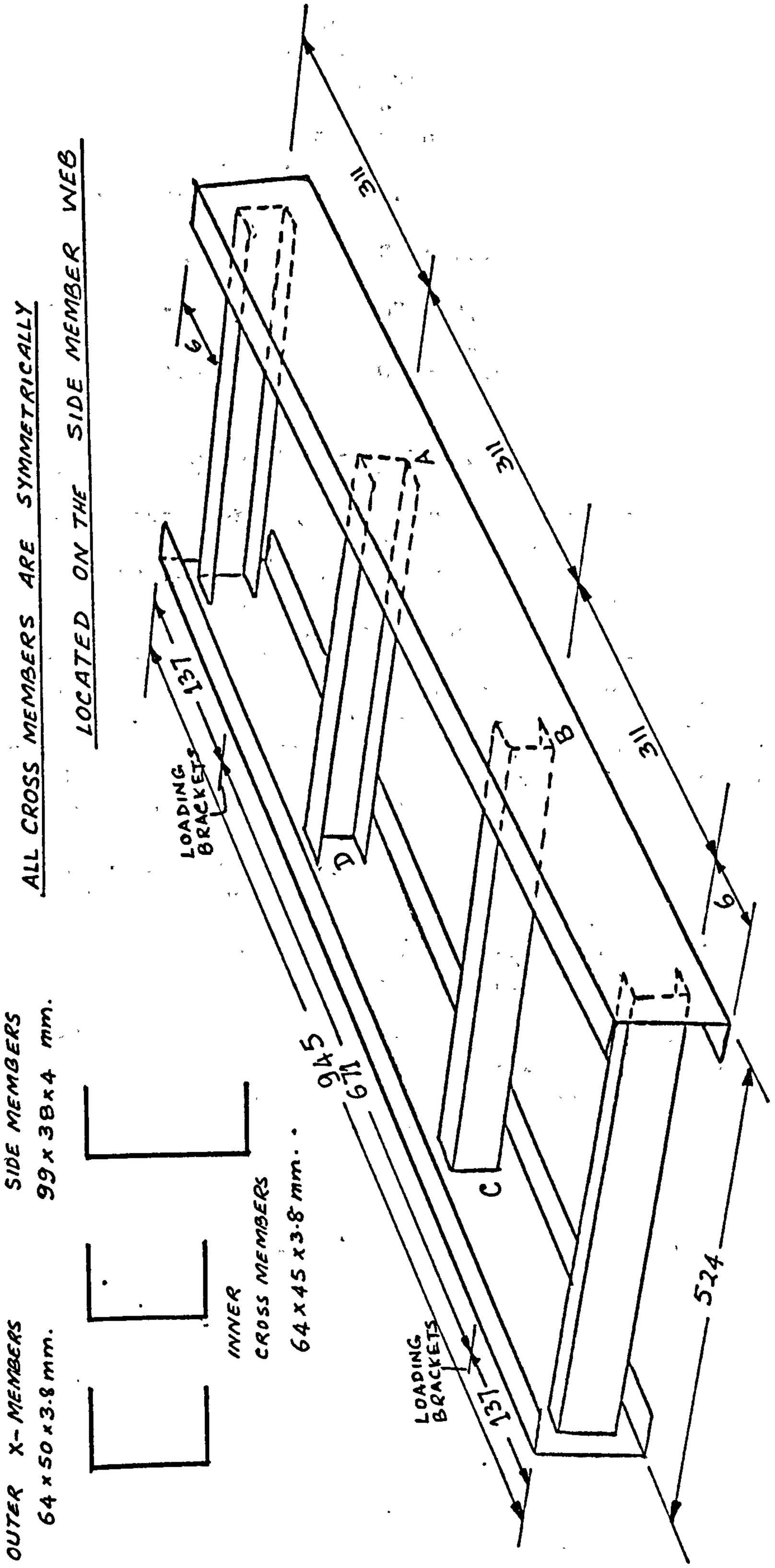

Fig. 3.1. Dimensions of the ladder frame

Loads were applied to the specimen and strain readings were recorded at different values of loads. Measurements were also made when the specimen was unloaded. Average values of both sets of readings were used in the calculation of the elastic constants.Fig.(3.2) shows variation of load and strains in the longitudinal and transverse directionsof the test specimen. The following values of the various material constants were calculated.

a) Young's Modulus "E" = $22.15 \times 10^6 N/m^2$

b) Poisson Ratio "ν" = 0.405

c) Shear Modulus of elsticity "G" = $\frac{E}{2(1+\nu)} = 7.882 \times 10^6 N/m^2$

3.4.2. Determination of Material Fringe Value "f_σ"

Stress-optic characteristics of CT200 model material were investigated from two types of calibration models. Hendry [36] suggested the use of a circular disc loaded in axial compression instead of a tension or compression test piece as true axial load cannot be easily obtained. The author preferred to use both, a circular disc and a tension piece, to obtain a comparatively reliable value of the material fringe value. One surface of each specimen was made reflective by spraying silver paint. They were loaded accordingly and fringe order measurements were made by a reflection polariscope at different values of load. The fringe order was measured at the centre of the disc and at the middle of the tension piece. The separation line between red and blue colours was taken as a reference for counting the order of fringes at a particular point on the calibration models. Fractional fringe orders were recorded by the Tardy Compensation technique [37]. These measurements were recorded for increasing values of load and when the load was decreasing. Average values of the two sets were considered in the calculation of the material fringe value.

A calibration curve between the applied load and the fringe order was drawn in each case. The value of the material fringe constant was obtained from the curve and it was used to calculate the material fringe value from the following relations.

a) For a tension piece:

Material fringe value "f_σ" = $\frac{2P}{w_o N}$

(b) For a circular disc in axial compression:

Material fringe value obtained from fringe order at the centre of calibration disc

$$"f_\sigma" = \frac{16P}{\pi D N}$$

Figs (3.3),(3.4) show the dimensions of the circular disc and tension specimen along with calibration curves respectively. The values of f_σ

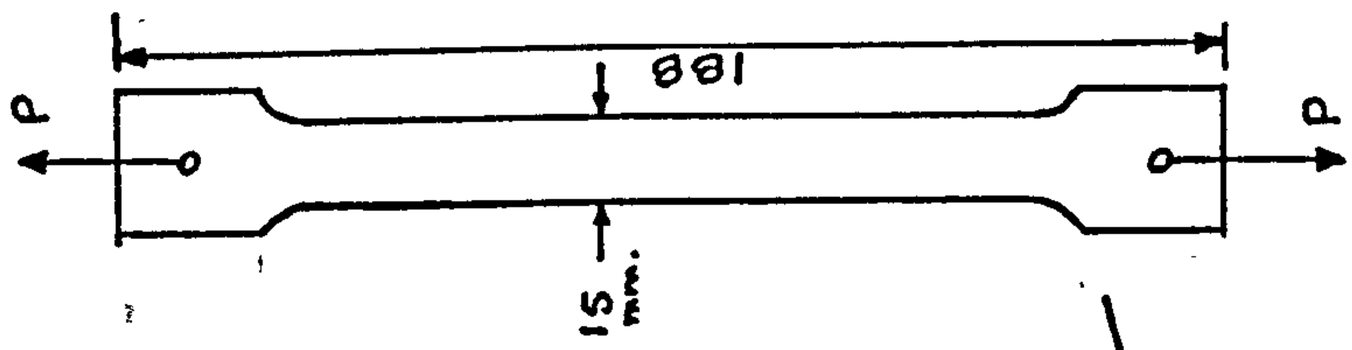

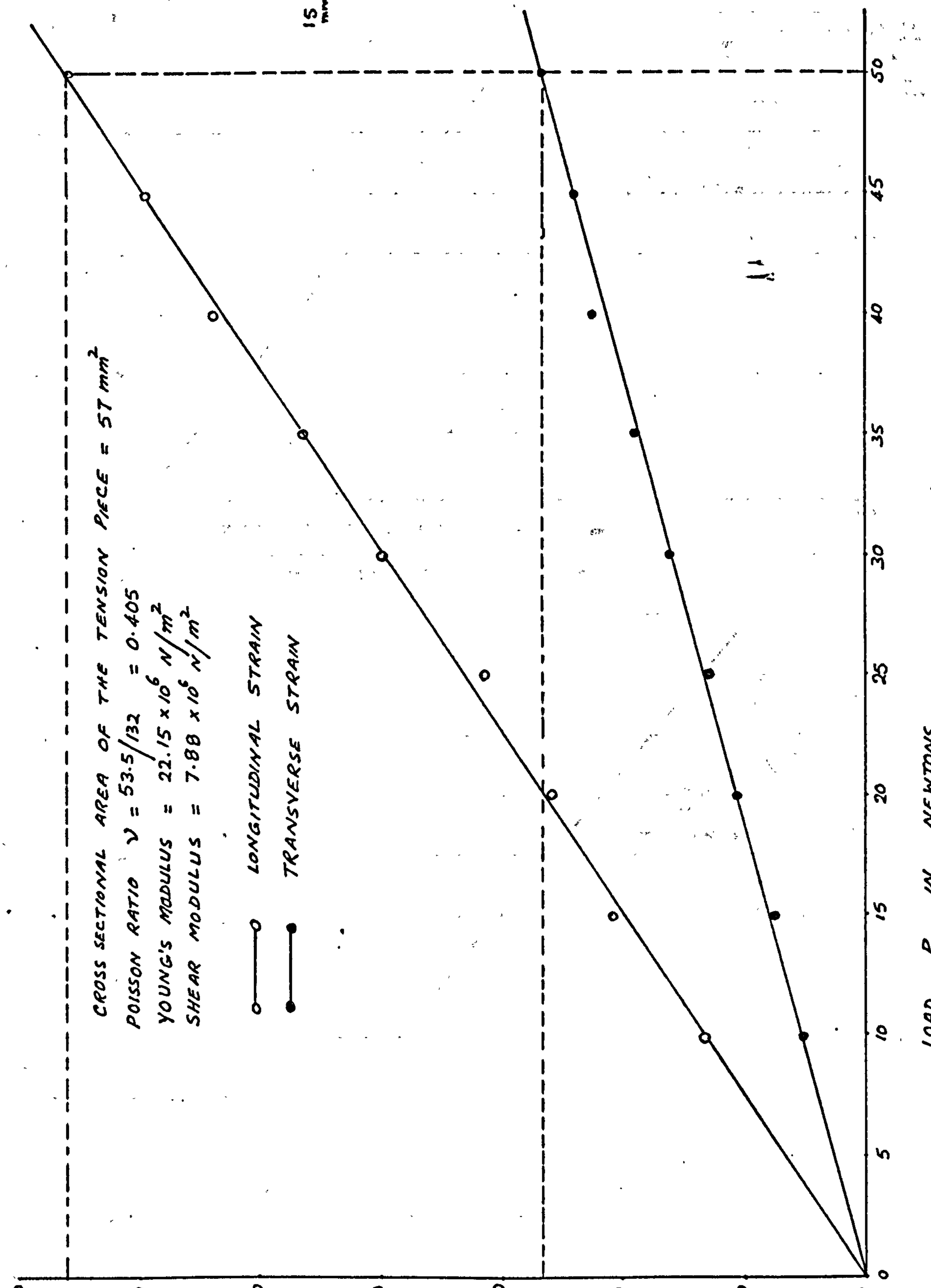

Fig 3.2 Calibration of CT200 Araldite for the determination of Elastic constants.

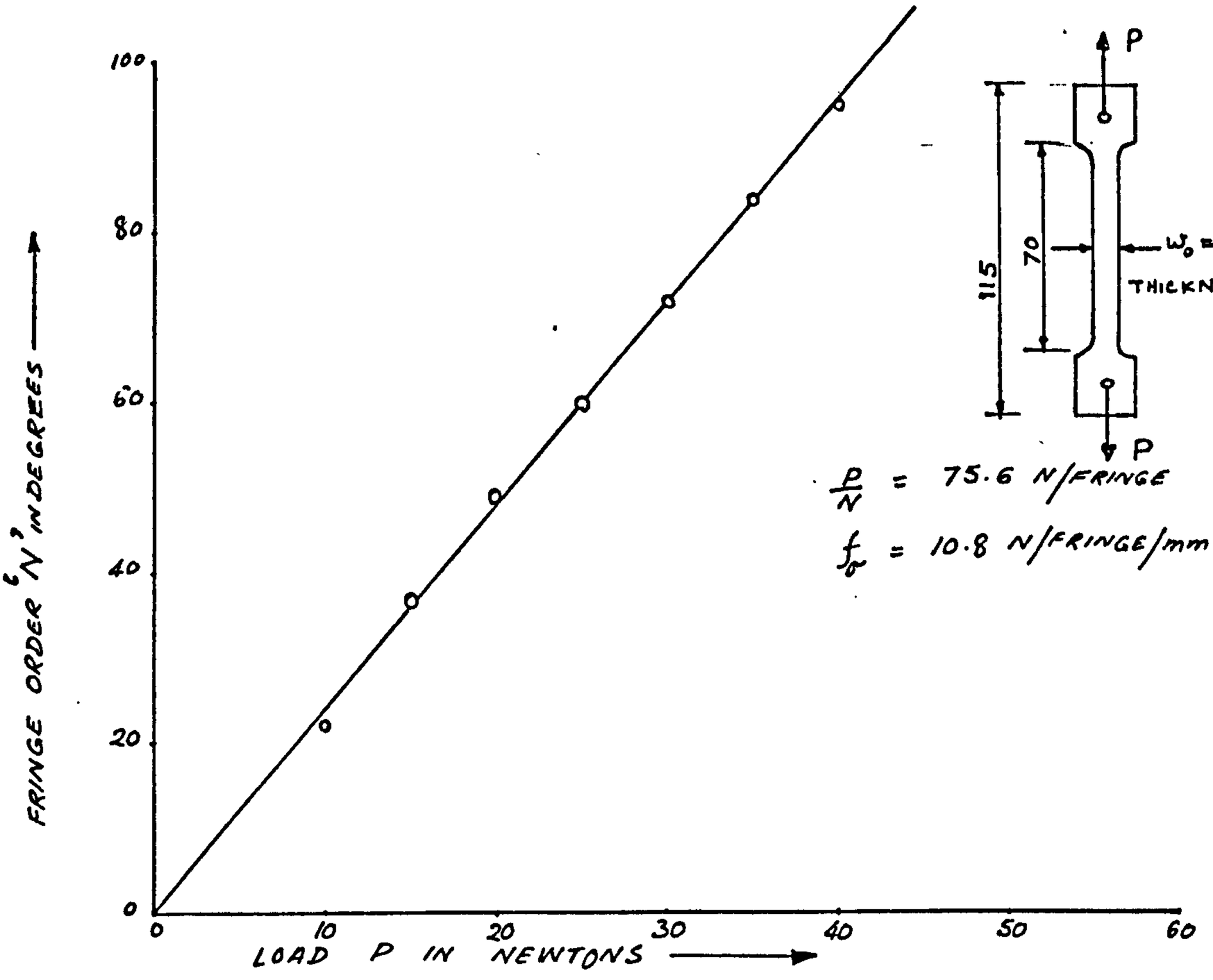

Fig 3.3 Calibration using a tension piece.

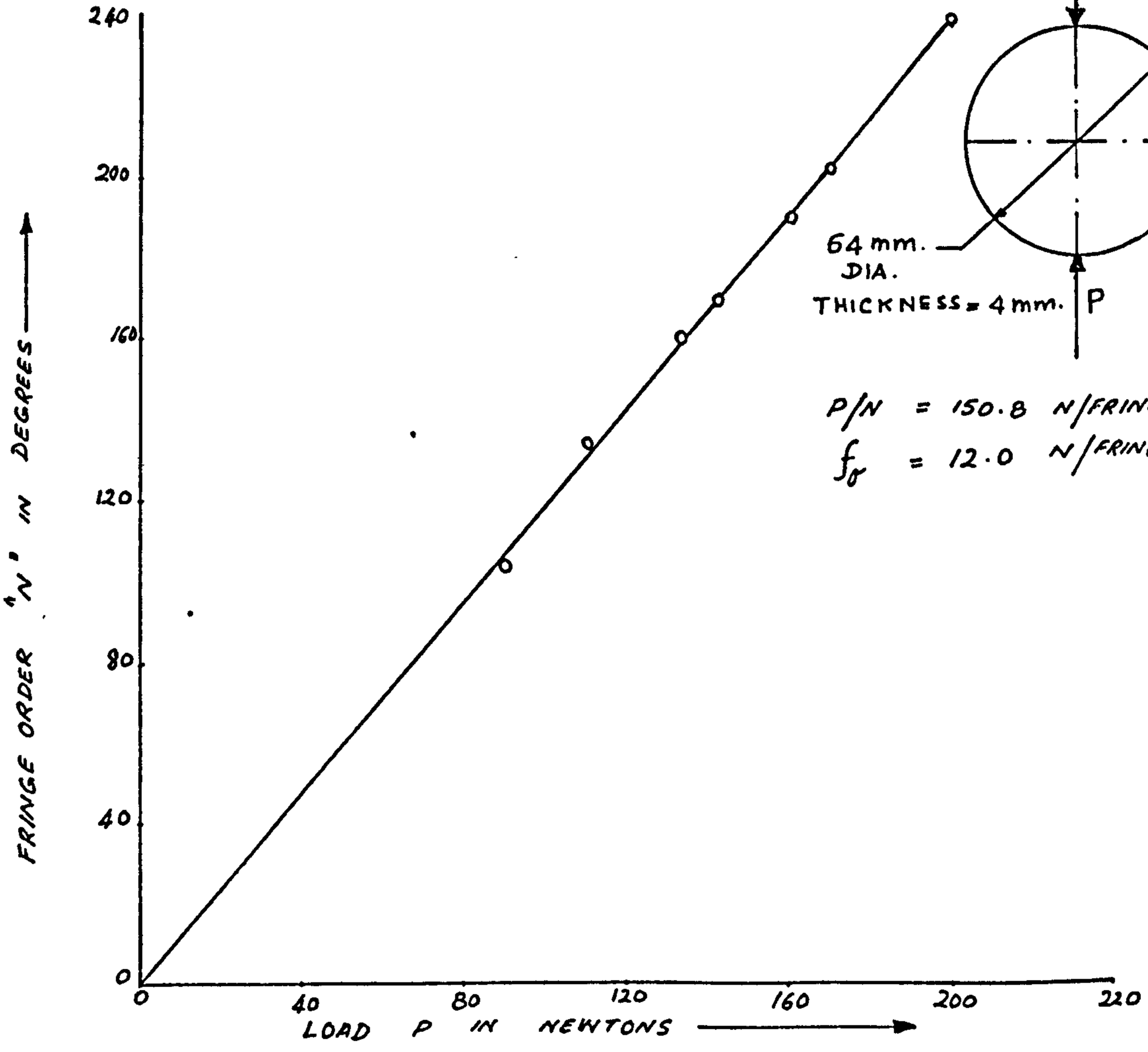

Fig.3.4 Calibration using a compression disc.

obtained from the two calibration models agreed well with each other and the following material fringe value was used in all further calculations.

f_σ = 11.4 N/mm/fringe.

3.5 PHOTOELASTIC INVESTIGATION OF A COMPLETE WARPING INHIBITION CASE

Fabricated channel section F.II was used to observe the photoelastic effect of stresses produced by warping inhibition. One end of section F.II was bonded to a thick mild steel plate with Araldite adhesive to obtain a cantilever model of a channel section. A reflective layer, made up by joining a silvered paper on a piece of transparent double sided adhesive tape, was bonded to the inside surface of the section.

The problem of application of a pure torque at the free end of a cantilever was carefully studied. The drilling of holes in a photoelastic model usually results in residual stress patterns which distort the stress patterns produced by external loads. The holes also act as stress raisers thus changing stress patterns in the surrounding regions. It was decided to avoid any method of load application which would require drilling of holes in the model. Fork ended mild steel pins shown in Plate 3.2. were made and the gap between two legs was kept slightly more than the wall thickness of the channel section. The pins were attached to the flanges and web of the section at the points of theoretical zero warping.

A light aluminium circular disc was mounted on these pins at the free end of the section. A couple was applied on the disc by applying equal and opposite forces through a dead weight, pulley and string arrangement.

The coloured stress pattern was observed through a reflection polariscope. Fringes due to warping inhibition stresses were very dominant on the flanges at the built-in end and their number reduced sharply as the distance from this end increased. A black zero order fringe appeared on the flange along the line of zero warping. The fringe distribution on the model seemed to be in good agreement with theoretical stress distribution along the edge. This model was kept as a demonstration model and actual measurements were not made on it.

Another model of a built-in beam was made by using a cast channel section and was loaded as described above. Fringe orders were measured along the free edge of the flange. The distribution of fringes and dimensions of the beam are shown in Fig. (3.5).

3.6 TESTING OF ISOLATED JOINTS

All the five joints described in section 3.3 were analysed photoelastically in the following manner:

3.6.1. Method of support and loading

The three point method of support at two ends was employed to support

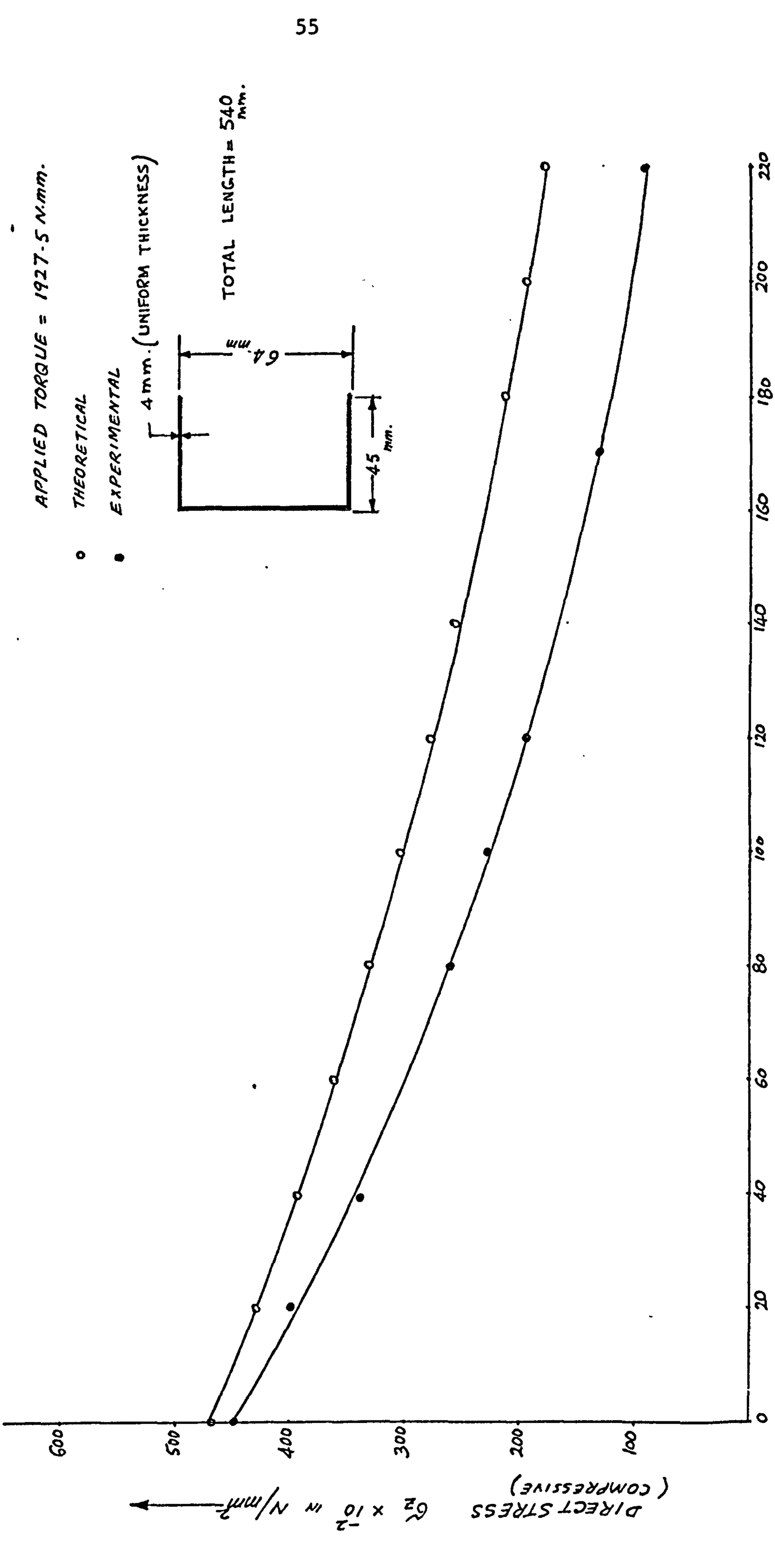

Fig.3.5 Distribution of direct stress along the free edge of the channel section.

the part of each joint representing the side member. Fork-ended pins were mounted with temperature cured Araldite at the two ends of a side member. These pins were located at the points of zero warping on the flanges and web of the section. The part representing the side member was supported in two end plates vertically through the pins. The pins could move freely in the holes provided in the end plates thus providing practically no warping inhibition to the side member section of a joint.

Torque at the free end of the cross member section was applied through a wooden bar which was supported on three pins as described in Section 3.5. A wooden bar was used instead of a circular disc to obtain a longer moment arm without increasing the overall weight of the arrangement.

3.6.2. Photoelastic investigation

The method of obtaining a reflective surface described in Section 3.5 showed that the fringe pattern was affected by the orientation of the double sided adhesive tape. Spraying aluminium paint on the surface of a model provided a more uniform and better reflective surface than the adhesive tape.

A fine square grid of 5mm spacing was drawn on the portion of side member section in the region of the joint. Measurements of isochromatic fringe order and isoclinic parameters were made at various points of the grid by a reflection polariscope.[38]. The presence of residual birefringence affected the stress patterns on the flanges. The position of isochromatic and isoclinic fringes was also sketched on squared paper separately so as to have a check on the accuracy of direct measurements made at individual points on the model. Isochromatic fringes of the whole order and half order, and isoclinic fringes of 0^{o}, 15^{o}, 30^{o}, 45^{o}, 60^{o}, and 75^{o} were sketched. Measurements were made at various values of clockwise and anti-clockwise torques applied to the cross member free end. Fringe orders were also recorded at the free end of the cross member flanges.

Since a white light source was employed in the whole analysis, all isochromatic fringes were coloured except for the zero order fringe which was black. All isoclinics were black. Some pictures were taken of the stress patterns on the joints and are presented in this work.

Attempts were made to obtain another set of isochromatic fringe measurements by using an oblique incidence attachment with the reflection polariscope. They proved unsuccessful because scattered reflection of light from the top surface of the photoelastic model made colour distinction almost impossible. Oblique incidence measurements were required for the calculation of individual principal stress values at any point. Plate 3.5 shows the method of support and loading of a photoelastic model of an isolated joint employed in the present experimental work.

3.7 TESTING OF A LADDER FRAME MODEL

ACT200 Araldite photoelastic model of a ladder frame was subjected to

torsion to investigate stress distribution in the region of its joints. The loading and testing of the frame is described below.

3.7.1. Method of support and loading

As the frame had two axes of symmetry it was decided to support the frame at four theoretical points of contraflexure as shown in Fig. (3.6). Two brackets were specially designed to support the frame at sections lying in the middle of the side members. The brackets provided a three point support at these sections as shown in Fig. (3.7). Drilling of holes in the side members was avoided by this arrangement. The whole frame was suspended by long rods attached to the support brackets at approximately the shear centre of the section. The frame was supported on a cylindrical bar lying along its longitudinal axis of symmetry.

Four brackets were designed similar to the support brackets for loading the frame in torsion. They provided a method of applying loads through the shear centre of the side member section without producing local twisting of the section. They were attached to the side member section at three points of zero warping without drilling holes in the section. This design of bracket provided more flexibility in regard to the choice of distance between two brackets on the same side member. A twisted view of the frame is shown in Plate 3.6. A similar method of loading was used in [22].

3.7.2. Photoelastic investigation

Square grids of 5 mm spacing were drawn in black pencil on the flanges and webs of the side members of the frame in the region of the joints. Some residual birefringence was present on the free edges of the side member flanges. It was due to cutting of the flange edges with a band saw. The nature of residual birefringence was studied with a reflection polariscope. It was noticed that the compressive stresses produced as a result of cutting had produced this effect. The measurement of fringe order was made to estimate the magnitude of residual birefringence at various points on the model.

The stress pattern in the region of the joints was observed through the reflection polariscope after twisting the frame by the application of shear loads in the brackets. Due to the presence of residual birefringence on the side member flanges, the resulting stress patterns were affected. The portion on which compressive stresses due to the applied loads were produced, the combined fringe order increased due to the presence of the compressive residual birefringence. But at other parts where the loading and the residual effects were of opposite nature, the combined fringe order reduced. The loading effect was much more dominant on the side member flanges well away from their free edges as residual birefringence was negligible in those regions. The part of the side member web in the region of any joint did not show fringes of significant order due to the applied loading. The fringe pattern in that region was not a regular one and was largely affected by the irregular flow of adhesive used in the construction of the frame. The stress patterns on the side member flanges provided a better information of stress distribution. The measurement of isochromatic and

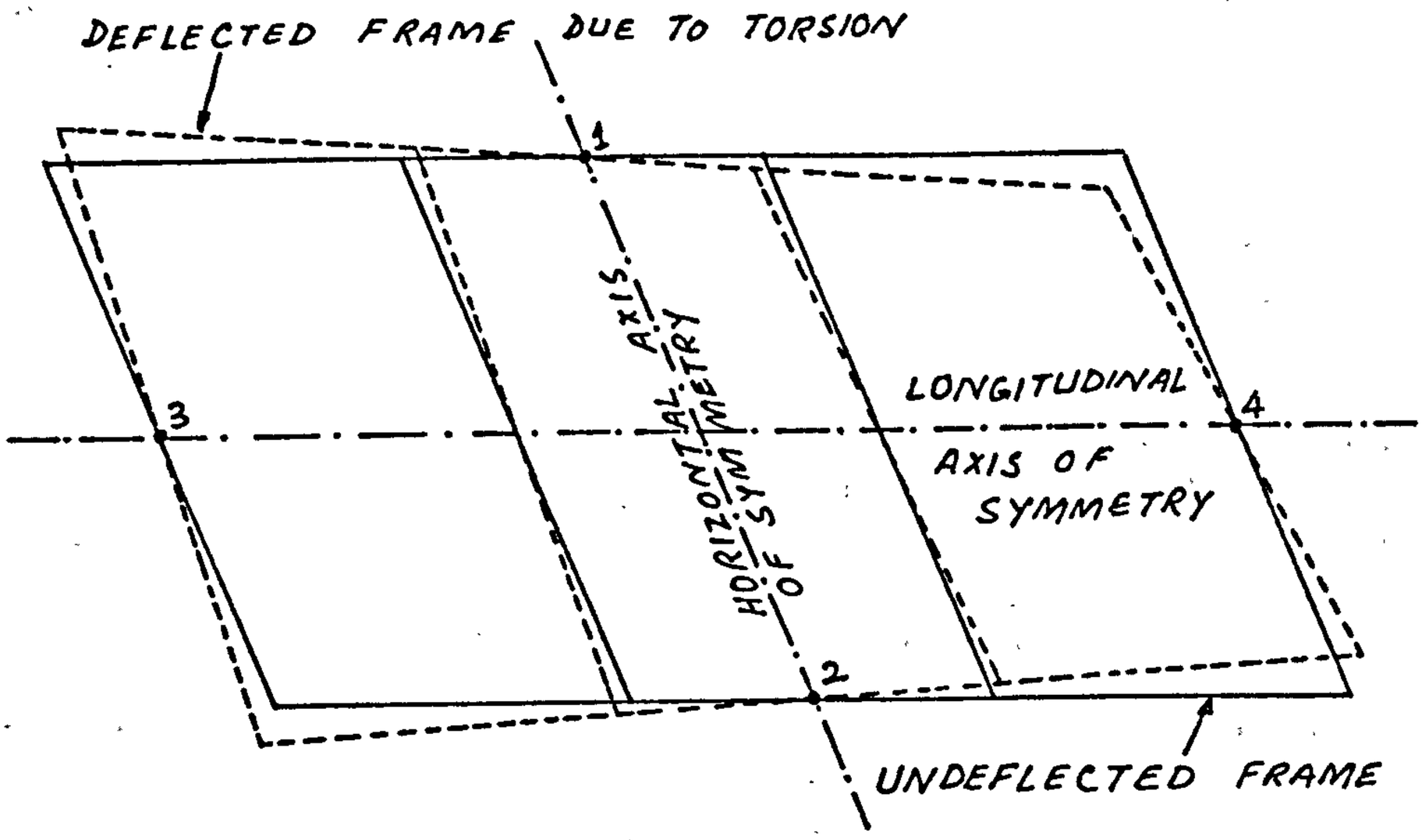

1, 2, 3 AND 4 ARE THE POINTS OF SUPPORT

Fig.3.6 Support points on the ladder frame.

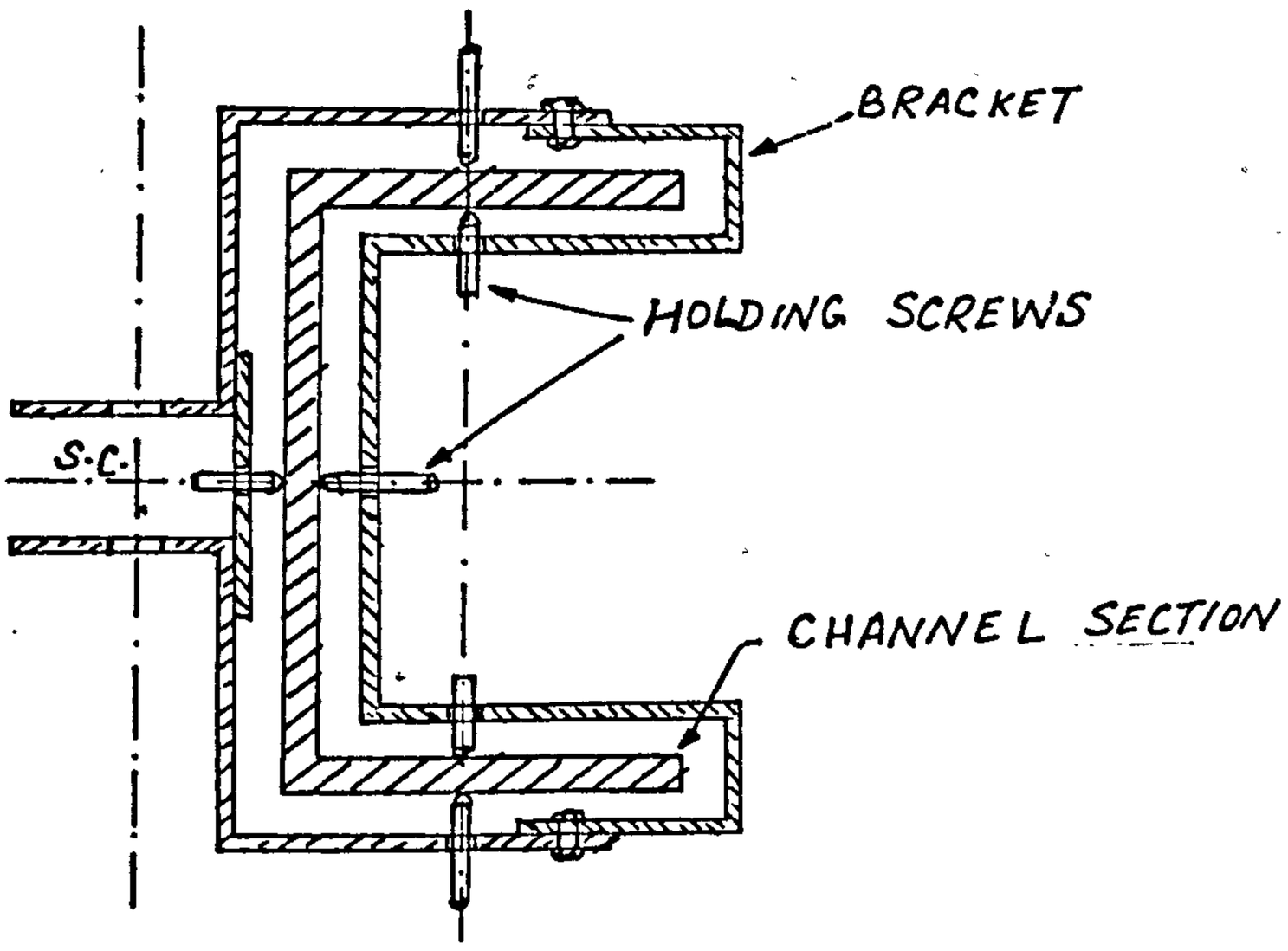

Fig.3.7 Method of attachment of brackets.

isoclinic fringes was made when the frame was subjected to a torque of 17.28 x 10^3N.mm. Similar measurements were made on the portions of the cross member flanges near the joints. The fringe patterns were also observed when the direction of the applied torque was reversed.

3.8. PHOTOGRAPHIC RECORD OF FRINGE PATTERNS

One of the main advantages of the photoelastic method lies in its ability to provide a visual representation of the stress/strain distributions in a model. Isochromatic and isoclinic fringe patterns of a stressed photoelastic model provide such information. It is easy to keep a permanent record of fringe patterns using the photographic technique.

The fringe patterns obtained by a transmission polariscope are easy to photograph as enough light is transmitted through the photoelastic models during their photoelastic analysis. But the use of a reflection polariscope for such analysis does not provide light of sufficient intensity after being reflected from the reflective surface of the photoelastic model. Most of the incident light is lost due to scattering after reflection. This complicates the photographic procedure. This difficulty was experienced in the photography of fringe patterns in the present work. It was also experienced that the reflection of the incident light from the top surface of every photoelastic model proved a major problem in obtaining good photographic results.

The entire photoelastic analysis was done using a white light projection lamp fitted in the reflection polariscope producing coloured fringe patterns. A few colour slides of these fringe patterns were made. Plate Nos. (3.7) to (3.14) show colour prints made from these slides and show isochromatic fringe patterns (i.e. magnitude fringes) and combined fringe patterns (isochromatics and isoclinics) as labelled on the photographs. Plate Nos. (3.9), (3.10), (3.13) and (3.14) were taken with the lamp source provided in the reflection polariscope while Plate Nos (3.7), (3.8), (3.11) and (3.12) were taken with an electronic flash gun used as a light source.

Black and white photographs of various fringe patterns were taken using a red filter with the camera. They are included in the next chapter.

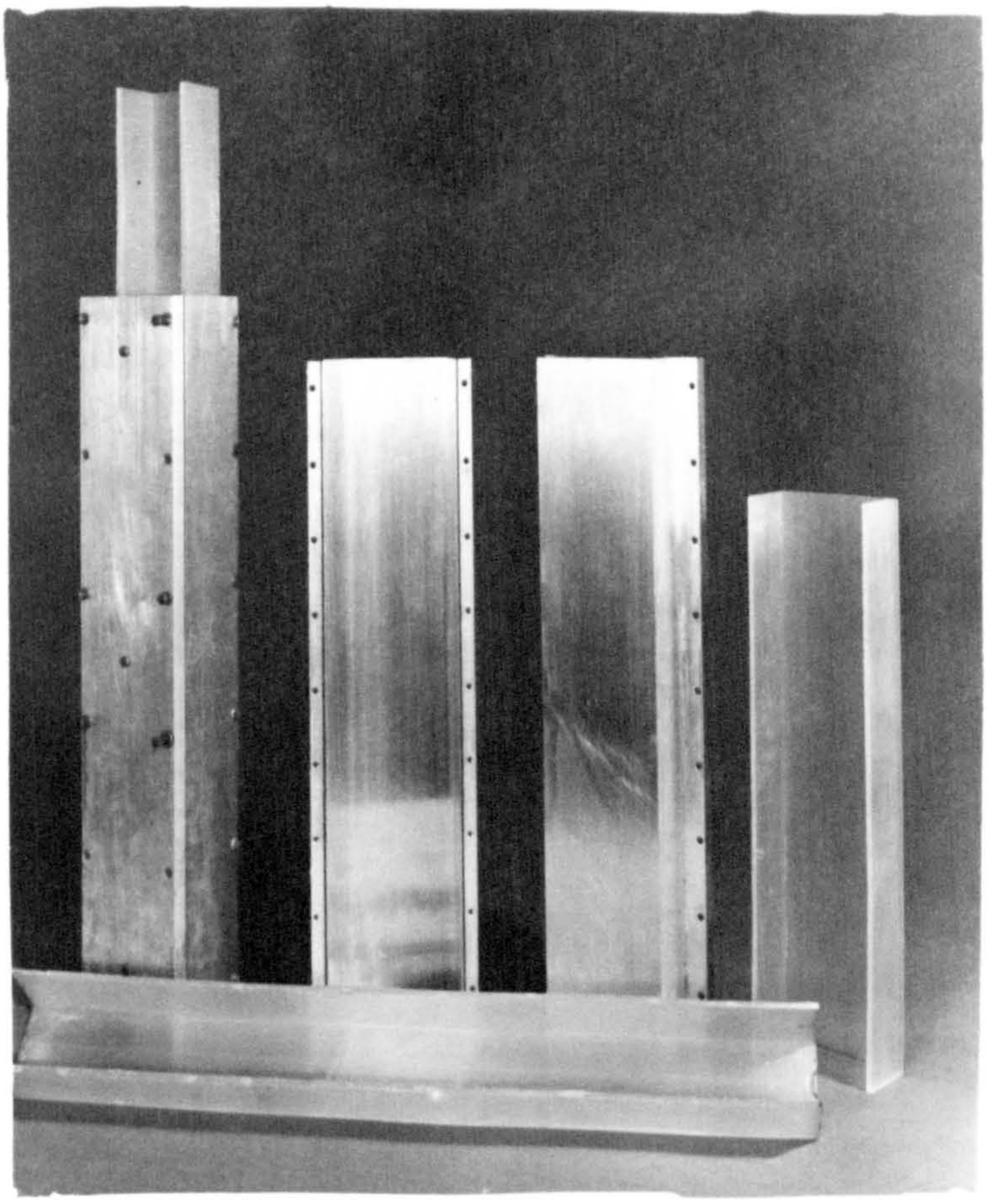

Plate 3.1. Aluminium Moulds and cast channel sections

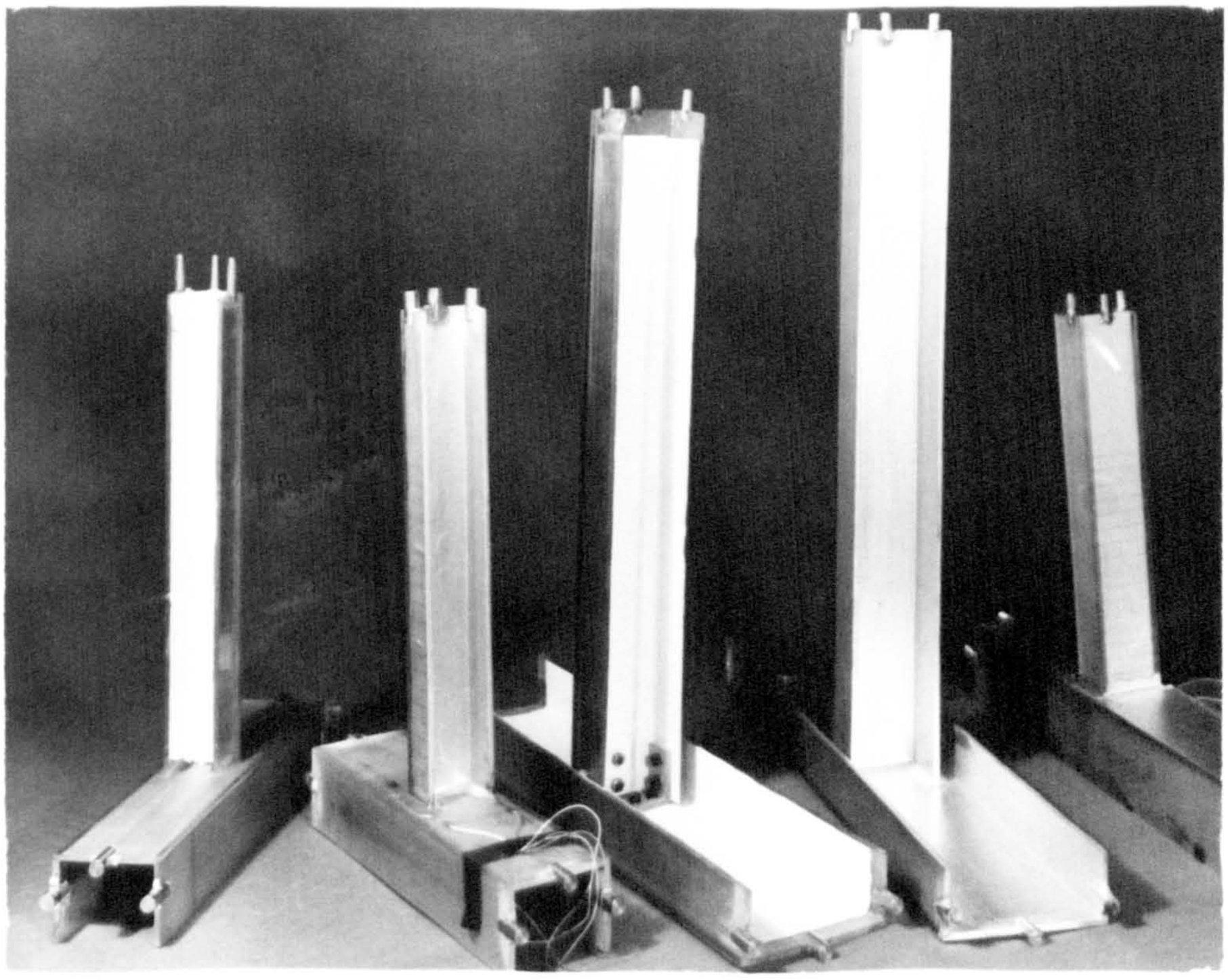

Plate 3.2. Photoelastic Models of the Isolated Joints

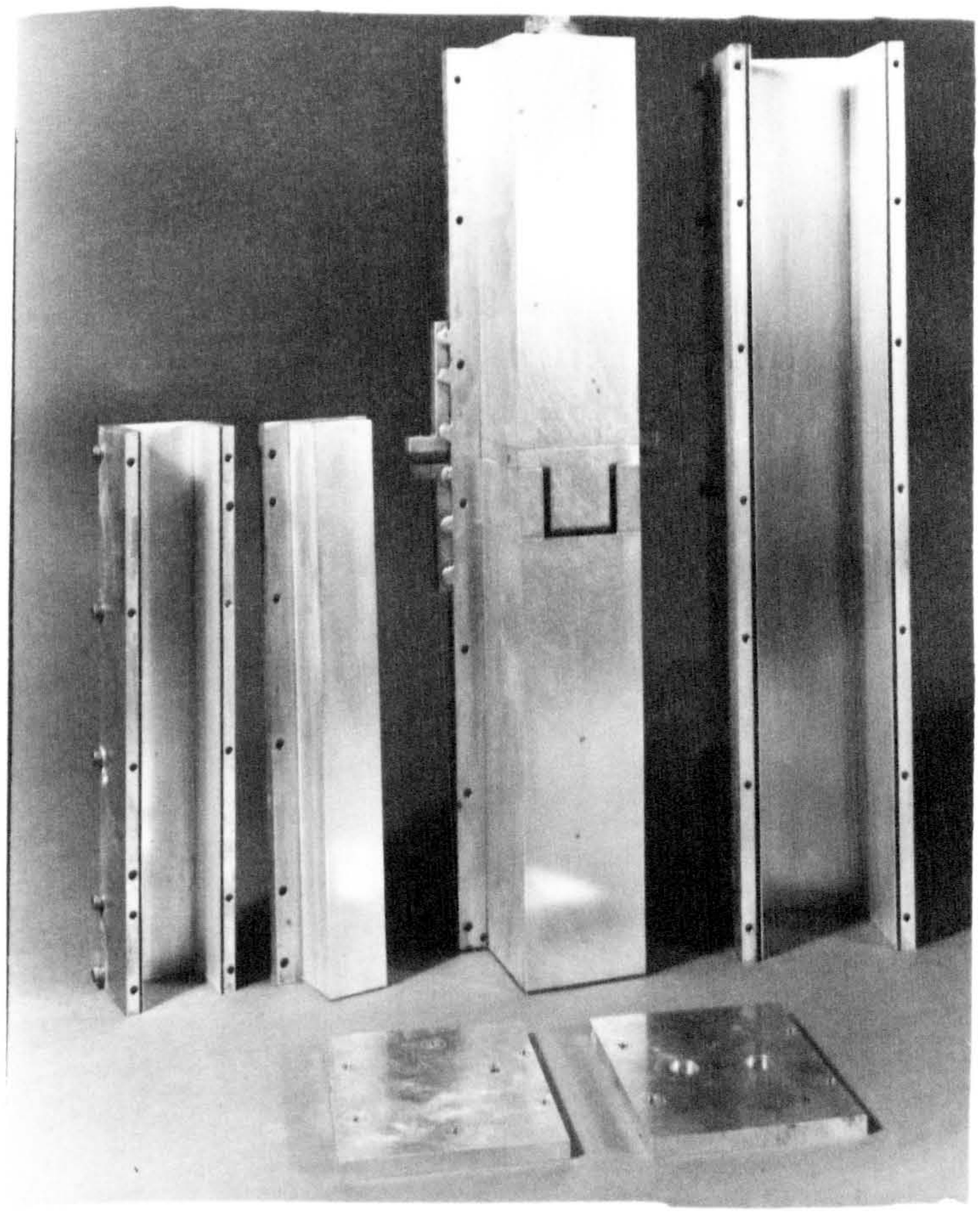

Plate 3.3. Parts of the Joint Casting Mould

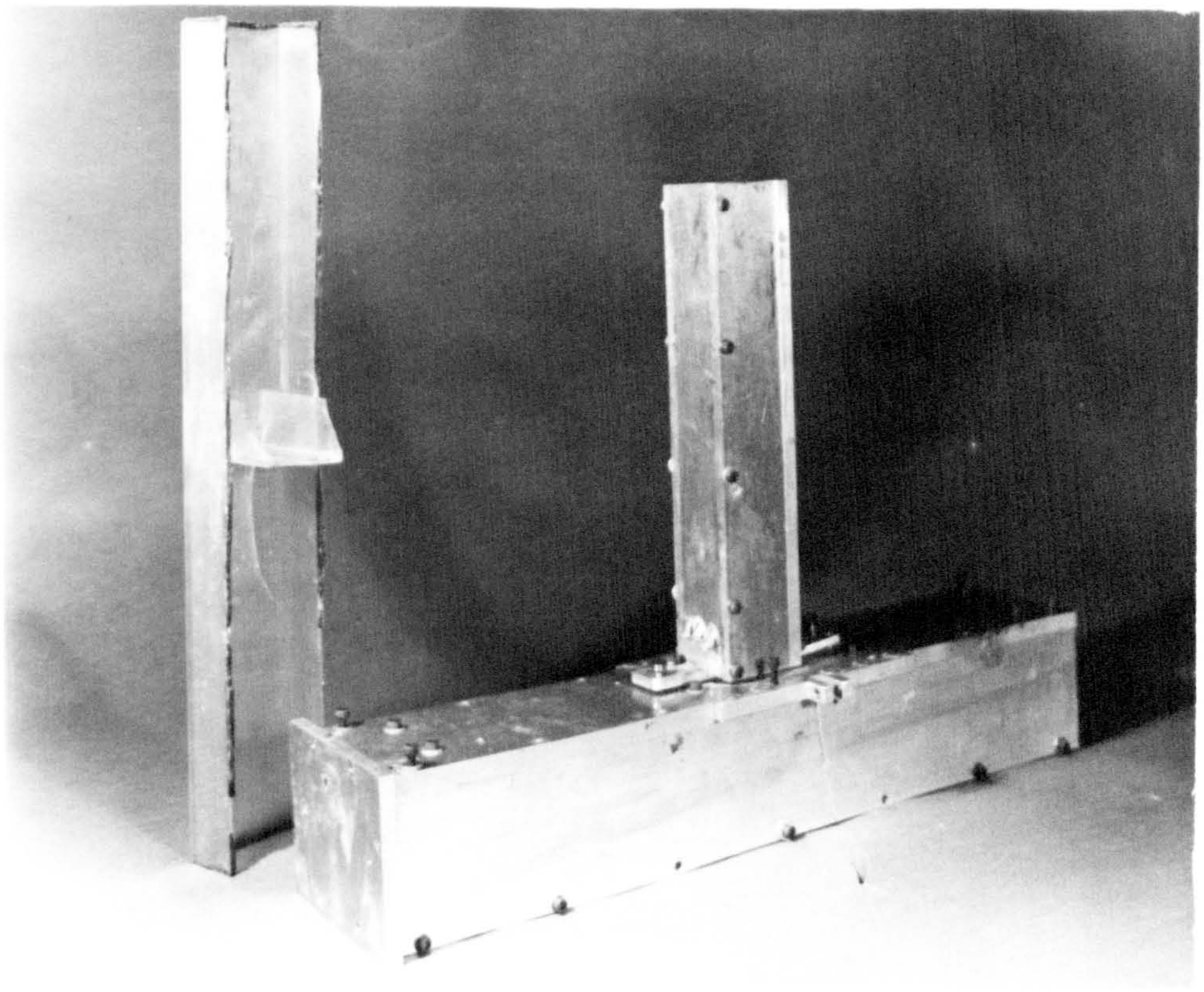

Plate 3.4. Aluminium mould and model of the cast joint

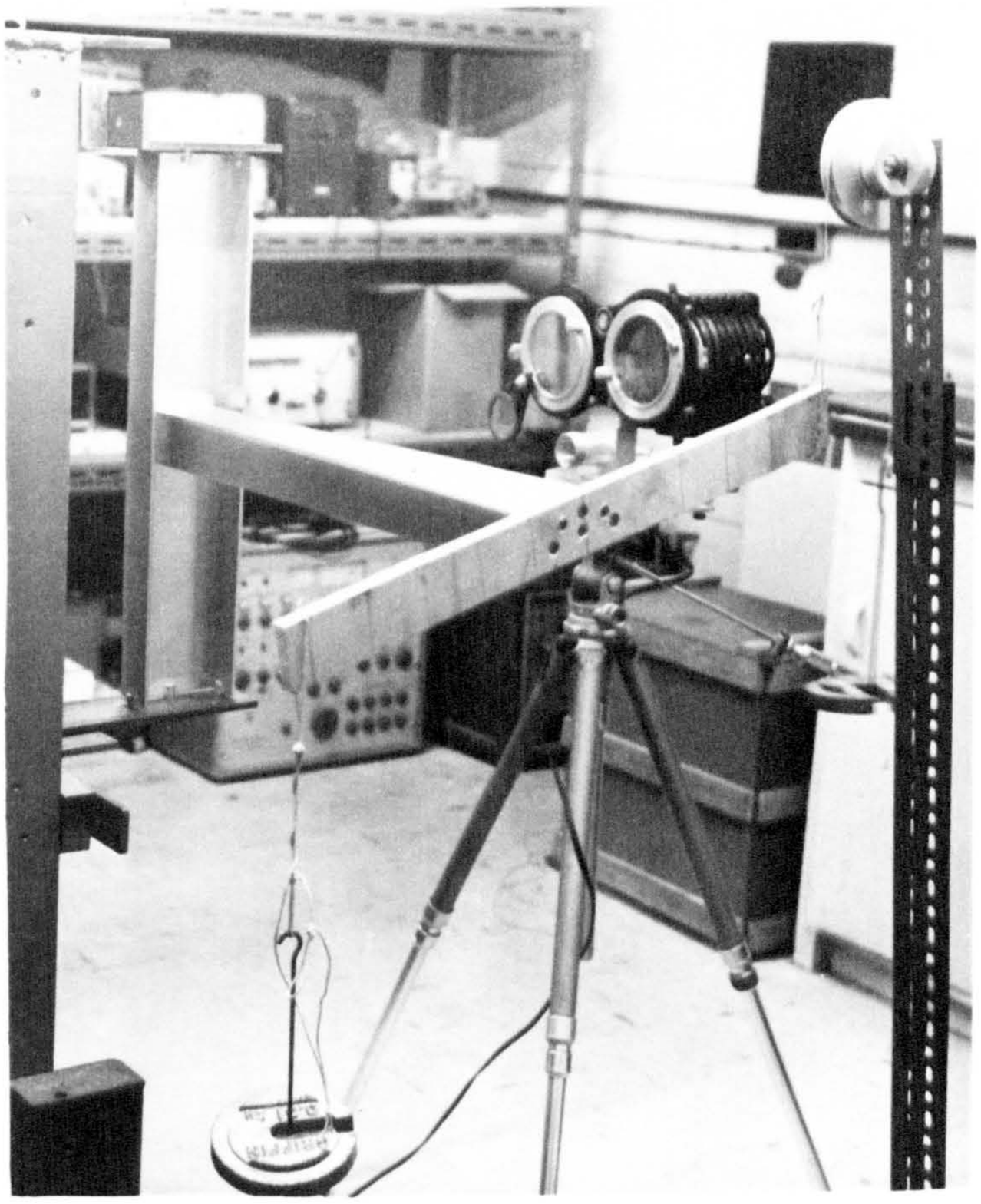

Plate 3.5 Testing of an isolated joint

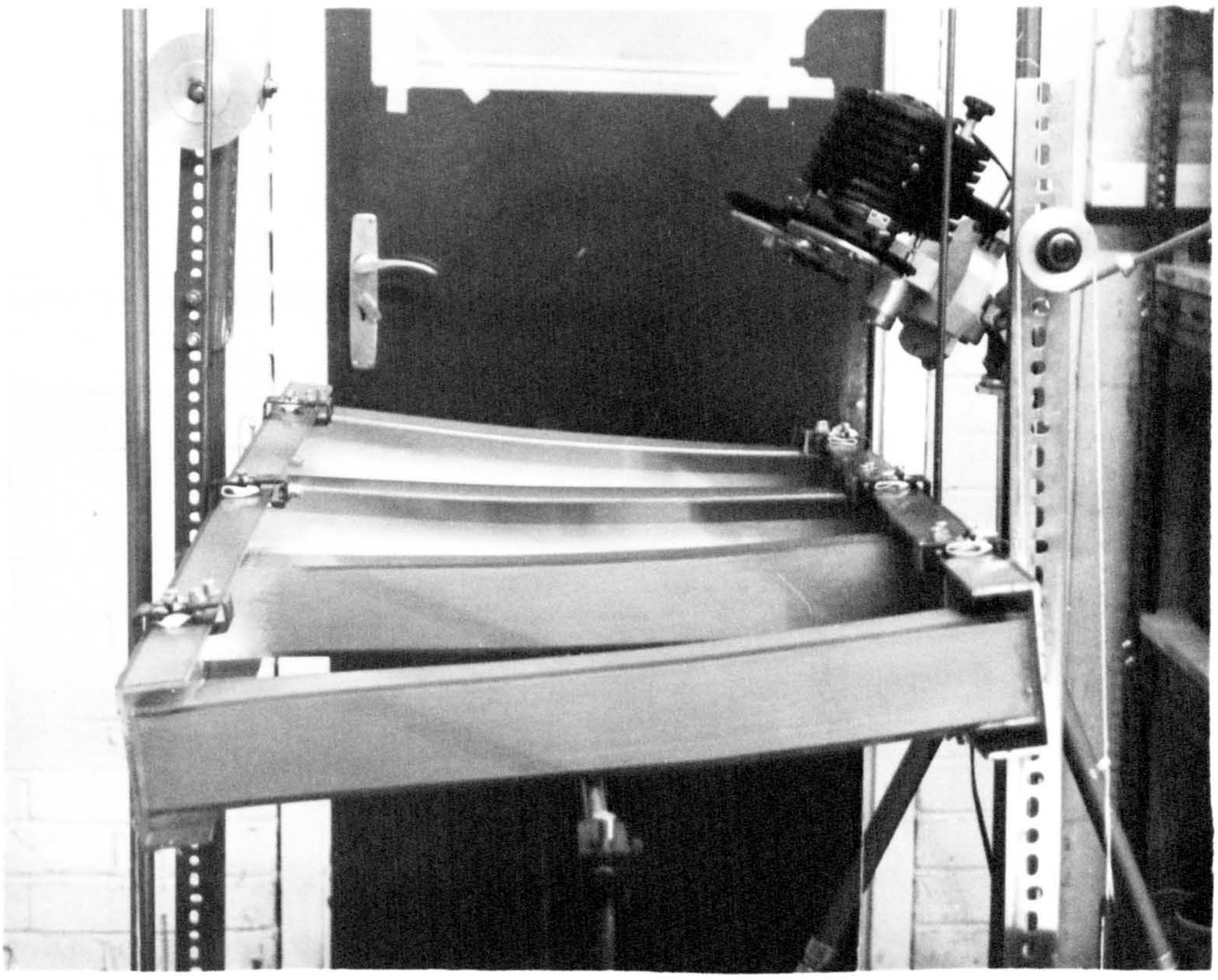

Plate 3.6 The ladder frame subject to twisting

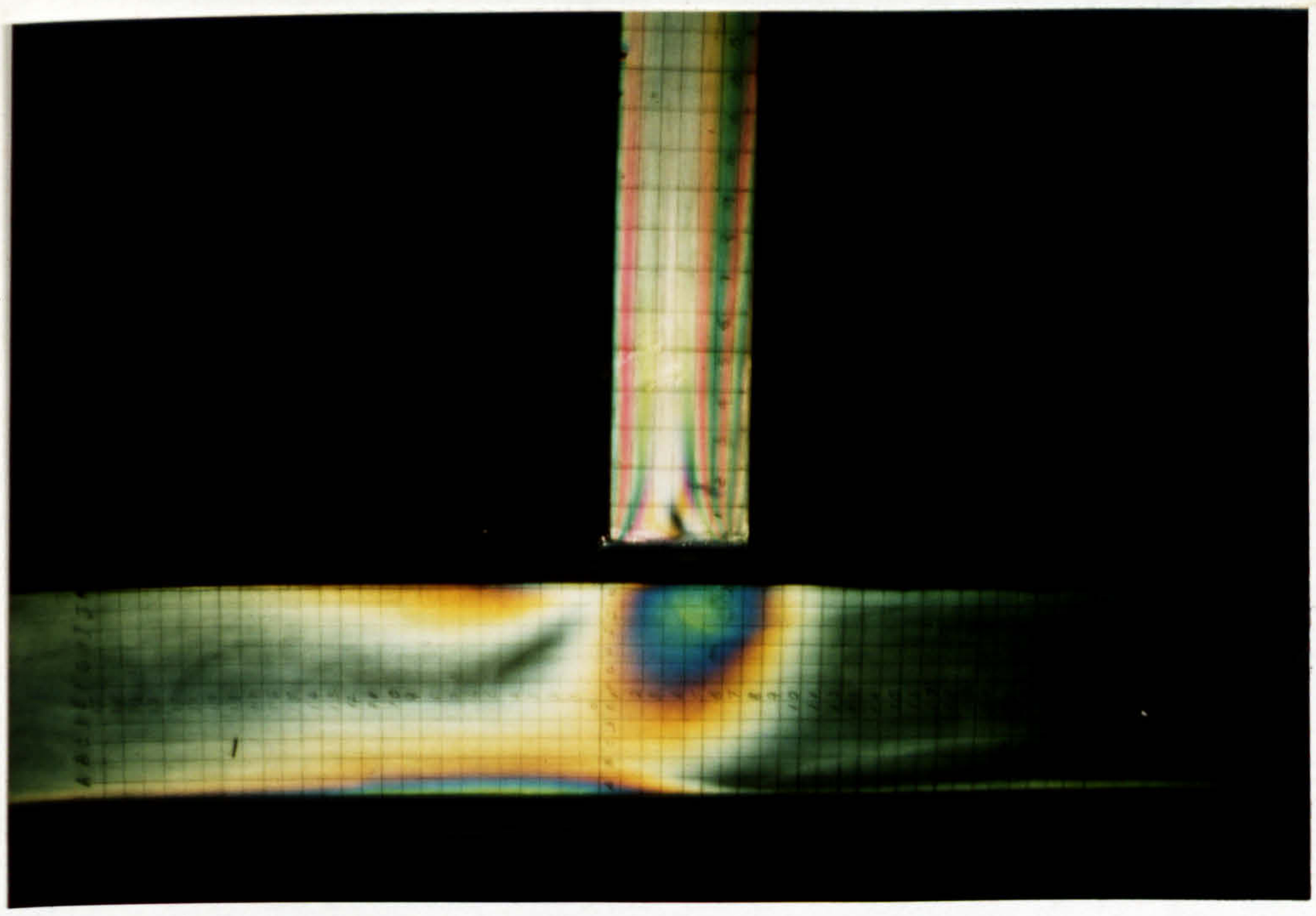

Plate 3.7 Whole order isochromatic fringe pattern on the flanges (Joint I)

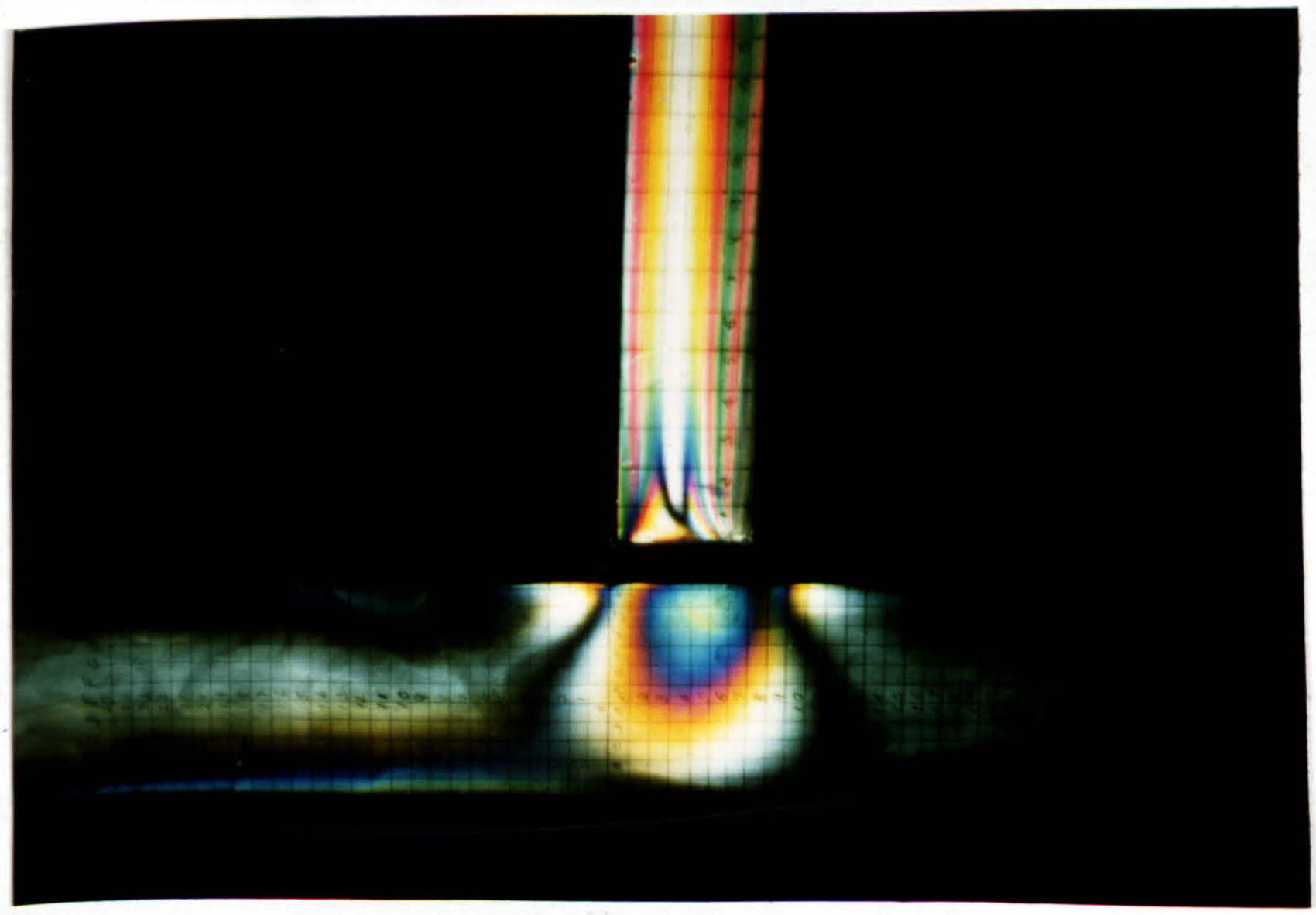

Plate 3.8 Mixed pattern containing 0^{o} isoclinics on the flanges (Joint I)

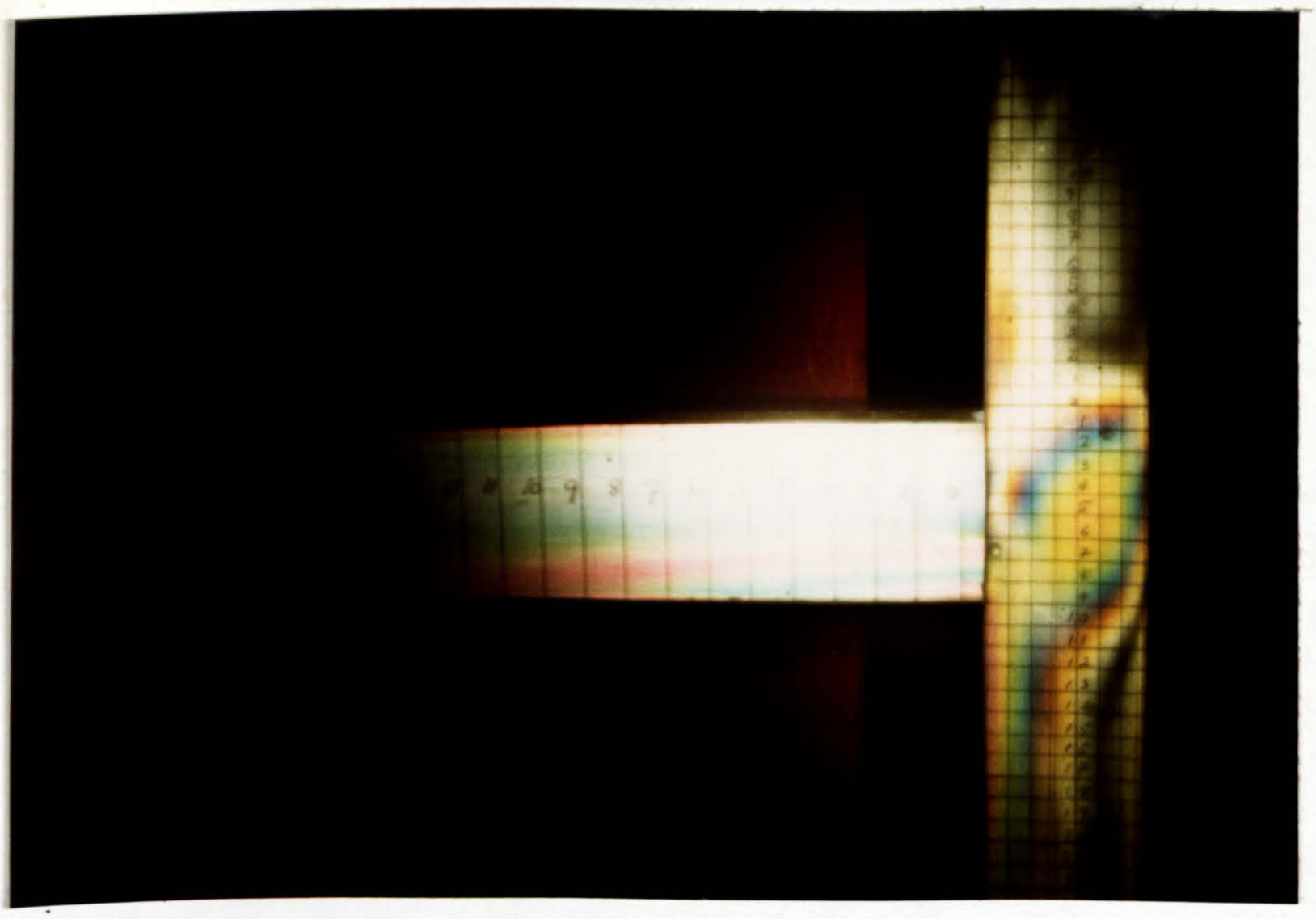

Plate 3.9 Whole order isochromatic fringe pattern on the flanges (Joint III)

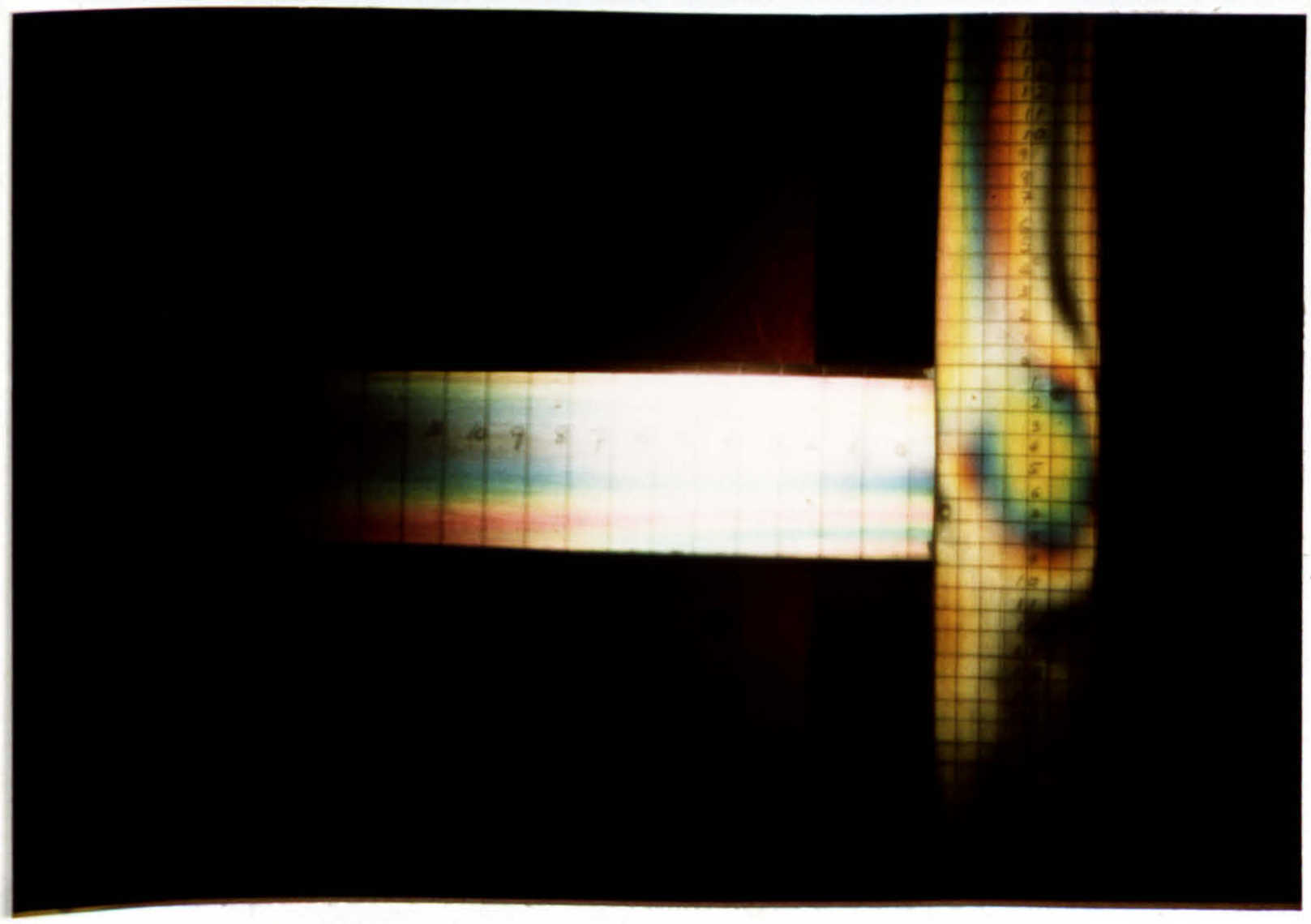

Plate 3.10 Whole order isochromatic fringe pattern on the flanges (Joint III)

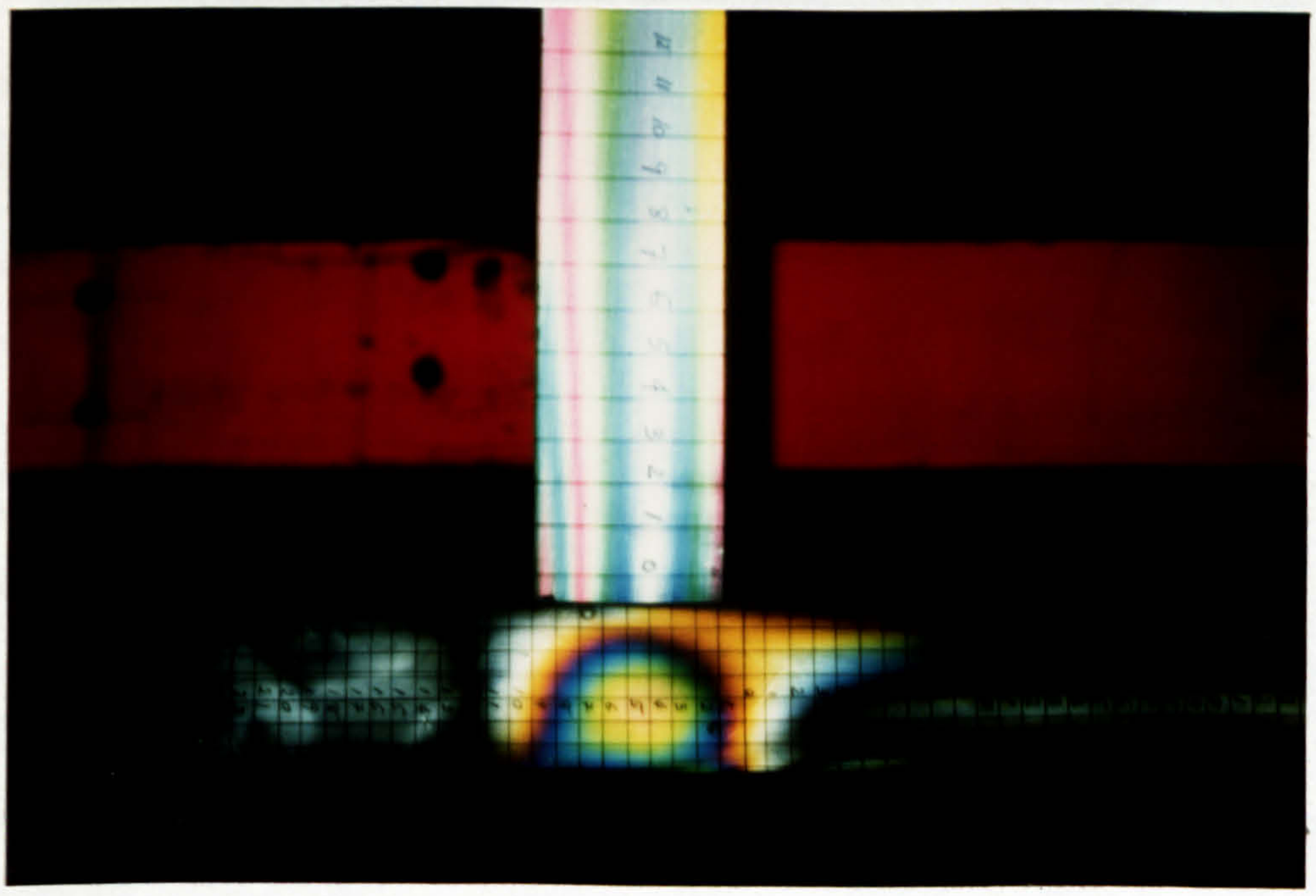

Plate 3.11 Mixed fringe pattern on the flanges (Joint III)

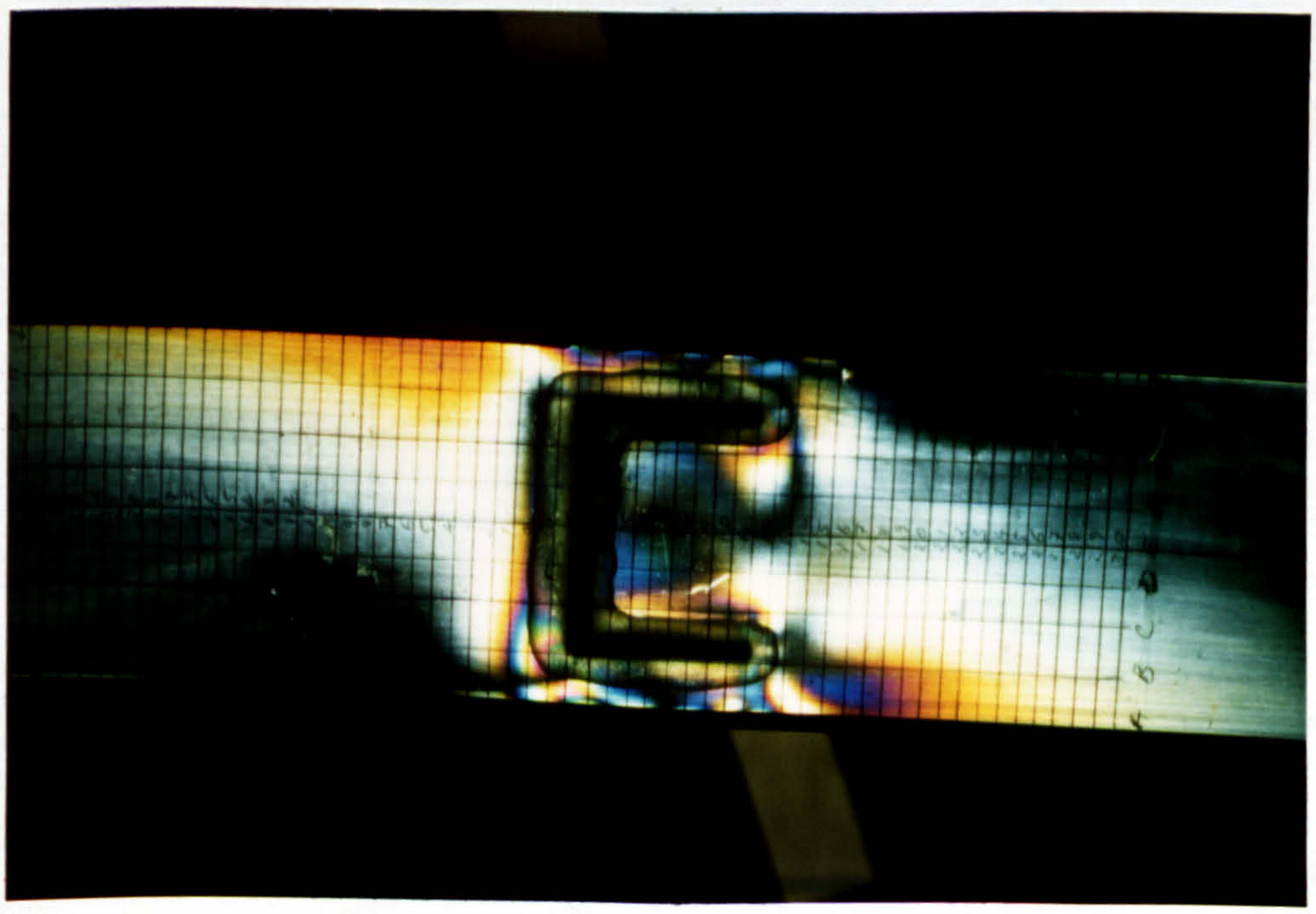

Plate 3.12 Mixed fringe pattern on the web (Joint III)

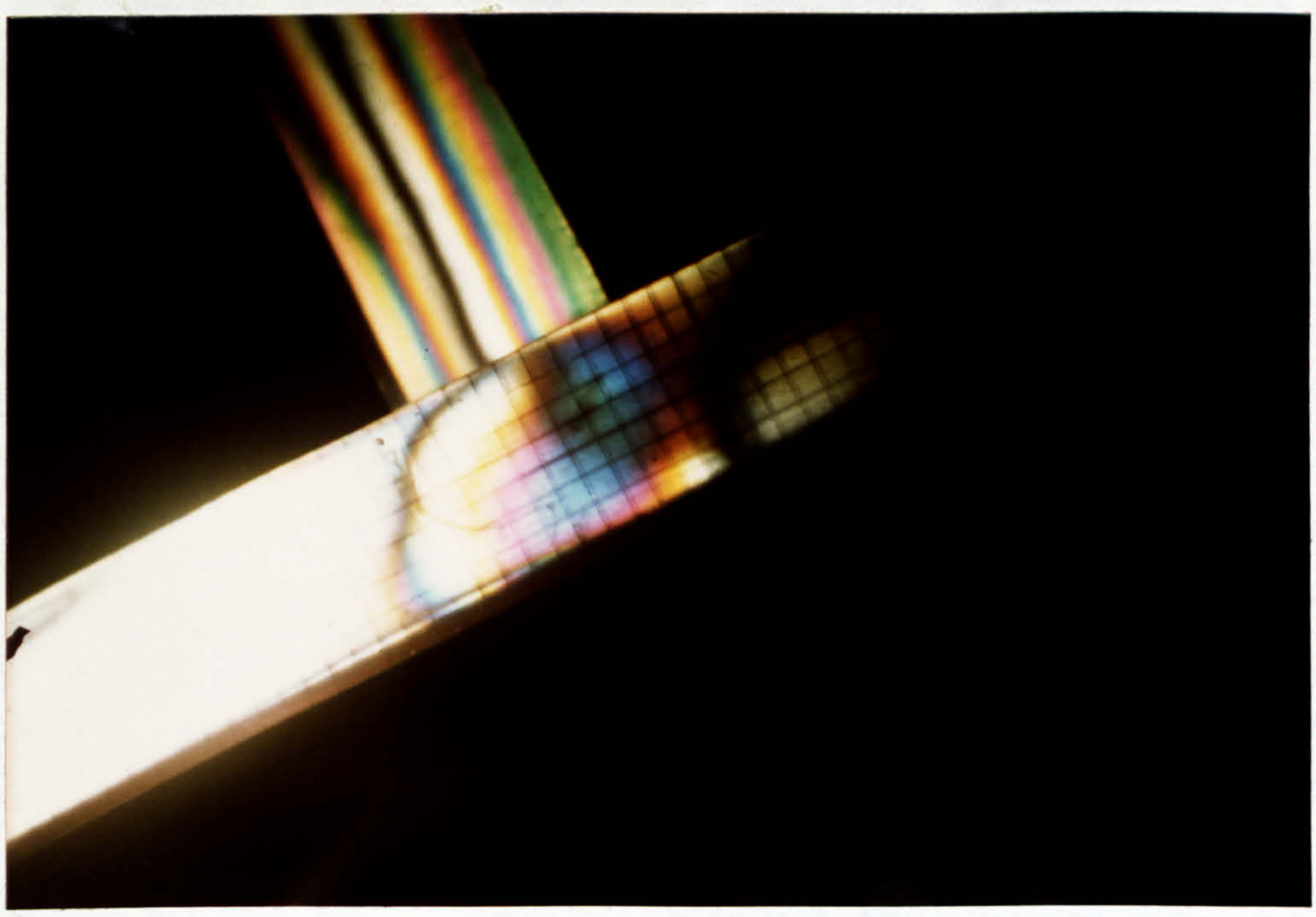

Plate 3.13 Whole order isochromatic pattern on the flanges (Ladder frame joint)

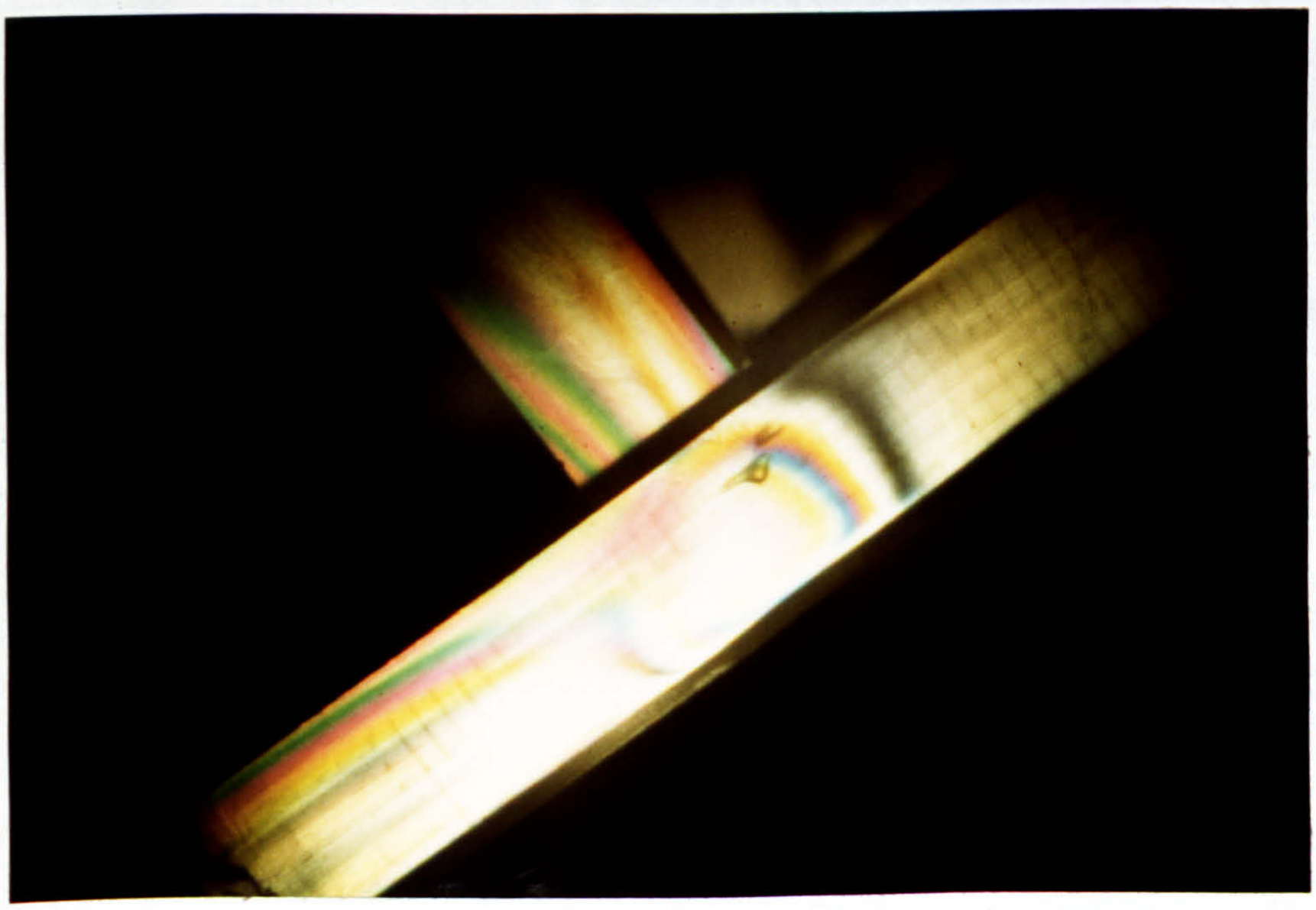

Plate 3.14 Fringe pattern on the flanges (Ladder frame joint).

CHAPTER 4 DISCUSSION OF RESULTS

4.1 BEHAVIOUR OF CT200 MODEL MATERIAL

CT200 Araldite was used as a photoelastic model material in the present work and showed linear and elastic behaviour for the maximum load requirements on various models. This trend is shown in Fig (3.2) which indicates this material is suitable as a model material for the analysis of stresses and strains in structures in the elastic range. Fig (3.3) shows its linear optical-stress property but its material fringe value is high which indicates its low sensitivity. The number of fringes at the highly stressed regions on the side member of the joint remained less than two. This can be seen from all the photographs presented in this work. However on the cross member flange near the joint, fringe orders of three were obtained.

4.2. INTERPRETATION OF FRINGE PATTERNS

It is important to identify isochromatics (magnitude fringes representing lines of constant maximum shear stress/strain) and isoclinics (directional fringes identifying lines of constant inclination of principle stress/strain) in a fringe pattern. Isochromatic fringe patterns are obtained with circularly polarised light and usually contain a zero order isochromatic fringe of black colour in coloured as well as black and white fringe patterns. Isoclinic fringes (always of black colour) superimposed by isochromatic fringes appear in a fringe pattern obtained with plane polarised light. If the stresses induced in the model are small then the pattern can contain only isoclinics otherwise both types of fringes appear. Various fringe patterns obtained during the present work are described in the light of the above-mentioned introduction as follows.

4.2.1. Coloured fringe patterns

The distribution of isochromatic fringes on the flanges of the side member and the cross member in the Joint I is shown in Plate (3.7). The region of maximum fringe order on the side member flange is clearly identified by a blue fringe next to the flange/web corner. The blue fringe is also present on the free edge of the flange in the upper half portion only. The presence of the residual birefringence of compressive nature on the free edge has caused an increase of the fringe order in the upper portion while it has reduced the fringe order in the lower portion. This effect was observed on all the models near the edges. The presence of a black fringe in the middle portion of the upper half indicates that the maximum shear stress becomes zero but attains maximum values on the edges. The fringe pattern shows that warping inhibition causes only localised effects on the side member. The isochromatic fringes are distributed along the cross member length and their maxmimum concentration is visible in

the joint near the free edge of the flange which shows that the maximum stress occurs there. It has been noticed from the various photographs taken with flash gun that the zero order black isochromatics on the cross member flanges have not appeard distinctly as were observed with the actual light source during analysis. A white band has appeared in its place because of their inadequate contrast in the coloured pattern, which approximately coincides with the zero warping line on the flange. It is also seen that the fringes go on disappearing rapidly along the free edge of the flange as the distance increases from the joint. This clearly indicates that the warping inhibition stresses along the cross member decrease rapidly as the distance from the joint increases. Some distortion of the fringe pattern is visible near the joint. It was observed that irregular fringe patterns were produced along the boundaries of the joints due to curing of the Araldite adhesive. This local effect produced residual birefringence in the joint. Isochromatic fringes with a better colour contrast are visible for Joint I in a mixed fringe pattern shown in Plate (3.8). The black fringes surrounding the coloured fringes on the side member identify the position of $0^{o}/90^{o}$ isoclinics depending on the orientation of the polarising axes of the reflection polariscope. The region of the maximum fringe order on the side member flange can be clearly identified which occurs near the flange/web corner in line approximately with the white band on the cross member flange. The white band as described above is the position of the zero order fringe identifying the position of the theoretical zero warping section.

The distribution of the isochromatic fringes on the members of Joint III is shown in Plates (3.9) and (3.10)for equal clockwise and anti-clockwise torques applied respectively at the end of the cross member . The anti-symmetry of the two fringe patterns with respect to the joint agrees with the theoretical considerations observed for a symmetric joint. The region of the maximum fringe order is again near the flange/web corner on the side member flange. The black fringes are visible on the side member and the cross member showing regions of zero maximum shear stress. The reflection of the light source from the outer surface of the model has affected the visibility of the fringes on the cross member. The region of the maximum fringe order on the side member flange of this joint is better identified in Plate (3.11)which represents a mixed fringe pattern of the joint. This region is in line with the white band on the cross member as for joint I but is slightly away from the flange/web corner. This shows that the location of the maximum fringe order region on the side member flange is affected by the dimensions of the members meeting in a joint.

A photograph of the mixed fringe pattern on the side member web in Joint III is shown in Plate (3.12). An irregular fringe pattern exists which is difficult to interpret. The main reason for this irregular pattern is due to the presence of the residual birefringence as a result of adhesive curing. It was observed by varying applied torque on the joint that a very small birefringence affect was produced on the side member web as compared to the side member flanges. This indicated that the flanges experienced more stresses than the web of the side member. Roach has also reported [39] that by far the

greatest number of failures which occurred on frame side members took place in the top or compression flange. The distortion of the fringe pattern in the side member web occurred in every joint as the fringes, due to load, were small so the photoelastic analysis was carried on the flanges only.

The isochromatic fringe patterns obtained on the inner joint of the ladder frame are shown in Plates (3.13), (3.14). The zero order black fringe on the cross member flange coinciding with the line of theoretical zero warping is clearly shown in Plate (3.13). The fringes are regularly distributed on the cross member as observed in the fringe patterns of isolated joints which indicates that warping inhibition is the main factor. This is also demonstrated from the fringe patterns on the side member flanges. Some distortion of the pattern is attributed to the residual birefringence caused in the frame during assembly which was later partially relieved by annealing. The region of the maximum fringe order on the side member flanges as seen in Plate (3.9) shows a fair agreement with that in Plate (3.14). The distribution of fringes on the side member flange towards the left end was affected by the support bracket. It was observed that fringes appeared in the sections near the loading and support brackets because of the tightening of the clamping screws. It was difficult to adjust the tightening force on the various screws uniformly but care was taken not to exert more force on the plastic model. The effect of using these special brackets was certainly better than attaching brackets through bolt holes as was experienced with Joint V.

4.2.2. Black and white fringe patterns

The development of the isochromatic fringe pattern in the Joint I due to applied torque is shown in Plates (4.1a) and (4.1b). The latter pattern was photographed at a higher torque than the former. A comparison of the two shows that the fringe encircling the maximum stressed area near the side member flange/web corner has expanded slightly while an additional fringe has appeared on the free edge of the cross member flange. This demonstrates that the warping inhibition stresses increase very rapidly in the cross member flange as compared to the side member flange. Plates (4.2a) and (4.2b) represent the mixed fringe patterns on the Joint I showing the position of $0^{o}/90^{o}$ and 45^{o} isoclinic fringes on the side member flange. A comparison of the two indicates that the principal stresses change their directions very rapidly near the flange/web corner on the side member flange. The direction of the principal stresses has changed through 45^{o} in a distance of less than 10 mm. near the corner but this effect decreases towards the middle of the flange. The inner black fringe of order one in Plate (4.2a) encloses the region of maximum fringe order.

The positions of the whole order and half order fringes on Joint II are shown in Plates (4.3a) and (4.3b) respectively. The region of the maximum fringe order on the side member flange is shown in the mixed pattern Plate (4.3c). The channel section used to represent a portion of the cross member in the Joint I was made from a CT200 plate. During cementing of the strips to form a channel section, one of the flange strips moved to distort the section. The effect of this distortion has slightly distorted the isoclinic patterns obtained on

the two flanges of the side member shown in Plates (4.4), (4.5) and (4.6). A comparison of Plates (4.5) and (4.6) shows the anti-symmetry of the respective isoclinic fringe patterns on the side member flanges as expected in a symmetric joint between two channel sections. These patterns do not show isochromatic fringes on the side member flanges as they were recorded at a small applied torque. The small movement of the isoclinic fringes of various parameters near the flange/web corner of the side member clearly indicate the transitional state of principal stresses in this region.

The mixed fringe patterns on the side member web in the joints of the ladder frame shown in Plates (4.8a) and (4.8b) indicate irregular patterns as experienced in the isolated Joint III. It appears if the additional amount of adhesive is somehow removed during its curing stage then a better fringe pattern representation may result. This would affect the joint strength considerably. However, the effect of the residual birefringence caused by the curing of the adhesive would still distort the fringe pattern in the region of the joint. Plates (4.9a), (4.9b) and (4.9c) show the patterns of whole order and half order isochromatic fringes on the joints of the ladder frame during testing at various loads. It is clear from these patterns that the region of the maximum fringe order on the side member flange exists nearer to the flange/web corner than the free edge of the flange. The distribution of the fringes around the region of the maximum fringe order on these joints resembles the corresponding distribution on the isolated joints. The cross member flanges also show identical fringe distribution to the cross member flange of an isolated joint.

Small distortions present in the fringe patterns were largely due to the presence of residual birefringence mostly along the free edges of the flanges which were taken into consideration during actual measurements. Because of the presence of the residual birefringence it was not possible to obtain direct measurements from the photographic record. An irregular residual birefringence in a model can further complicate the photoelastic analysis [38]. The photographic record of the fringe patterns on the various joints clearly identify the regions of maximum fringe order qualitatively. It has been shown that on a side member this region is present on the flanges near the flange/web corner. Its position is also identified to coincide approximately with the line of theoretical zero warping on the cross member flange. A comparison between the experimental stress values and the theoretical ones is made at the end of this chapter.

Joint V which represented a bolted joint did not show enough birefringence on the side member or cross member for the applied torque. This shows that when the cross member end in the joint is not restrained to warp then very small stresses develop in the joint. It was observed that high birefringence resulted around bracket holes because of bolt tightening force. Such effects must be occurring in the actual joints but are ignored.

4.3 CROSS MEMBER PARTIAL WARPING RESTRAINT FACTORS

Since the degree of warping inhibition plays an important role in the theoretical estimation of stresses in various members of a joint, an approximate method for its calculation was used in the present work. This calculation was based on the assumption that the values of $\overset{*}{C}$ and K remain constant around the cross member end profile in a joint. The values of these constants were calculated for comparison purposes from various available methods and are shown in Table. I.

The comparison indicates that the strip beam theory estimates the values of these constants near the free warping condition of the cross member in these joints. If these values are used in the estimation of stresses in the side member or cross member of a joint then the resulting stresses will be very small as compared to the practical case. This can be readily checked for any joint by multiplying the computed stress value with a ratio of

$$\left[\ \left|{}^{ko}/_{T}\right| \text{ by strip beam}\right] \Big/ \left[\left|\frac{ko}{T}\right| \text{ by plate theory}\right]$$

However, the values of K and $\frac{ko}{T}$ obtained by the other three methods show a good agreement between them. In most cases the values computed by the Plate theory estimates stresses up to 9% higher than estimated by the finite element method [21] which shows a good comparison.

4.4. COMPARISON OF EXPERIMENTAL AND THEORETICAL STRESS VALUES

The isochromatic fringes directly give the values of the maximum shear stress while the isoclinic fringes determine the direction of the principal stresses in a photoelastic model. In order to determine the individual values of the principal stresses at a point, an experimental method known as "Oblique Incidence Method" is usually employed to obtain another set of measurements involving principal stresses. Then individual principal stresses are found from the two measurements. The oblique incidence technique could not be used successfully in the present work as reflections from the model surface made the distinction of colours unreliable. The analytical method known as "Shear Difference Method" which is based on the numerical integration of the stress equilibrium equations was tried to separate the principal stresses. It is a very cumbersome method and can lead to incorrect results if the input data is not estimated accurately. The isoclinic fringes being thick black bands could not be estimated with a fair accuracy on small models without a photometer. The presence of residual birefringence on the edges further made this estimation difficult and so this approach was abandoned.

The failure criteria of a material subject to a biaxial state of stress depends on the value of the maximum shear stress rather than the maximum direct stress in the material. The stresses occurring in the joints, consisting of thin walled beams, are not uniaxial but combined and so maximum shear stress becomes the most important stress regarding their failure. Considering the importance of the maximum shear stresses in the joints it was decided to make a comparison between their theoretical and experimental values at the critical sections.

The isochromatic fringes provided their values directly. The fringe order at a point lying on a stress free boundary directly determines the value of the tangential principal stress as the normal stress is zero. The edges of the side member and cross member flanges being free from stresses made it easy to compare direct stresses along free edges. The values of the cartesian shear stress component τ_{12} along the critical section on the side member flanges were also compared with theoretical values.

The maximum direct stress for the complete warping inhibition condition at the built-in end of a channel section beam shows a good agreement with theory as shown in Fig (3.5). The experimental value is smaller than the theoretical value by less than 5%. The experimental stress decreases more rapidly than the theoretical stress as the distance from the fixed end increases.

Figs. (2.5a) and (2.5b) show that the flange/web corners do not behave as simply supported edges but they transmit moment m_{22} and also undergo bending displacement u_3.

It was found that the couple loading produced stresses/displacements of the opposite nature than the cross member warping forces in the side member thus reducing the combined effect. But the magnitude of stress/displacements produced due to the couple loading was found to be very small in all the joints analysed in this work. Their contribution was less than 2% on the Joints I, II and IV, but up to 10% on Joint III. It was also found that the affect of the couple loading on the distribution of stresses/displacements in the side member was larger on the web than the flanges of the side member in a joint. The effect of the couple loading was considered in the evaluation of $\overset{*}{C}_{av}$ and K in Joint III and the ladder frame joints but was ignored in the comparison of stresses on the flanges of the side members.

4.4.1. Isolated joints

i) The comparison of the maximum shear stress values on the side member flange shows that the experimental values lie between the estimated partial warping and zero warping values in the critical region as shown in Figs (4.1) to (4.4), they do not indicate a regular trend near the free edge of the flange. The experimental fringe values in this region were very small and were affected by the presence of residual birefringence. The location of the critical area predicted by theory agrees very well with the experimental results and the maximum estimated stress value is within 6% to 13% of the experimental value except for Joint II.

ii) Figures (4.5) to (4.8) show that the comparison of the shear stress τ_{12} on the side member flange also follow the same pattern as observed for the maximum shear stress on the same section.

iii) The experimental distribution of the direct stress on the free edge of the side member flange indicates the same trend as

as predicted by the plate theory. This is shown in Fig. (4.9) to (4.12). The experimental values lie close to the partial warping curve for joints III and IV while Joint II does not compare well. The Joint I also shows closer comparison with partial warping values than zero warping values. The theoretical estimation of the maximum stress region agrees very well with the experimental one. The length of the side member portion influenced by local effects of a joint can be approximately determined with reference to the position of the cross member flange zero warping line. This length extends on both sides of this reference line equal to the distance of the sum of the widths of the cross member and the side member flanges.

iv) The direct stress along the free edge of the cross member flange in Joints I and III shows a better correlation with the partially warping case near the joint than with free warping or zero warping conditions as shown in Figs. (4.13) and (4.15) But Fig. (4.14) indicates that the values of direct stress in Joint II are closer to the zero warping curve.

The comparison of the distribution of various experimental stresses on the side member and the cross member portions of the joints I, III and IV described above clearly indicates that the plate theory can estimate their theoretical distributions very accurately. However, the values of the stresses can be determined within close approximations by considering the partial warping of the cross member. The regions of the maximum stress on the side member are accurately determined by the plate theory. Joint II has not shown a good agreement with theoretical values. It seems that the permanent distortion of the section caused during assembly of the section is responsible for these errors. Also the joint has a small value of K so the actual stresses approach zero warping condition as reported in [22]. But the other joints do not confirm this trend although their K values are slightly higher than Joint II.

4.4.2. Ladder frame joints

The values of stresses measured by the photoelastic method in the joints of the ladder frame required some comparison with the estimated values. It has been shown in the isolated joints that for known values of the applied torque on the free end of the channel section representing a portion of the cross member in a joint, it was possible to estimate values of stresses analytically.

In the case of the ladder frame testing, the total torque applied to the whole frame was known but the distribution of the external torque in individual members of the frame was not known. It is difficult to assess the share of the external torque in every member of the frame. As the cross members were attached to the side member web, so the cross member offers a very small restraint to the warping of the side member. In such joints, the warping inhibition of the cross member mainly contributes to the stresses in a joint [11]. As a first approximation in solving the underlying problem of torque distribution, it was assumed that the external torque applied to the ladder frame was distributed entirely in the cross members of the frame. It was further

assumed that the torque was shared by all the cross members of the frame proportional to their flange widths as their web heights were equal. The resulting values of torque were used to estimate stresses in the inner joints of the frame.

It was interesting to see that the experimental values of the maximum shear stress on the critical section of the side member flanges in two identically loaded joints of the frame showed a good comparison with the theoretical values. The agreement for the location of the maximum stress region was even better which confirmed the assumption that the cross member warping inhibition forces were the main contributing factor. Regarding the assumption about the distribution of the external torque in various members of the frame, it proved satisfactory for the joints in which the cross members were only attached to the side member webs and the ratio of their web heights being 0.65.

The comparison of the tangential stress on the free edge of the cross members showed that the estimation of partial warping inhibition in the joint predicted stress values which compared better than the zero warping or the free warping conditions. Small differences in the measured values of stresses on the two identically loaded joints in the frame were observed. These could be due to the minor difference in the end conditions in the support brackets.

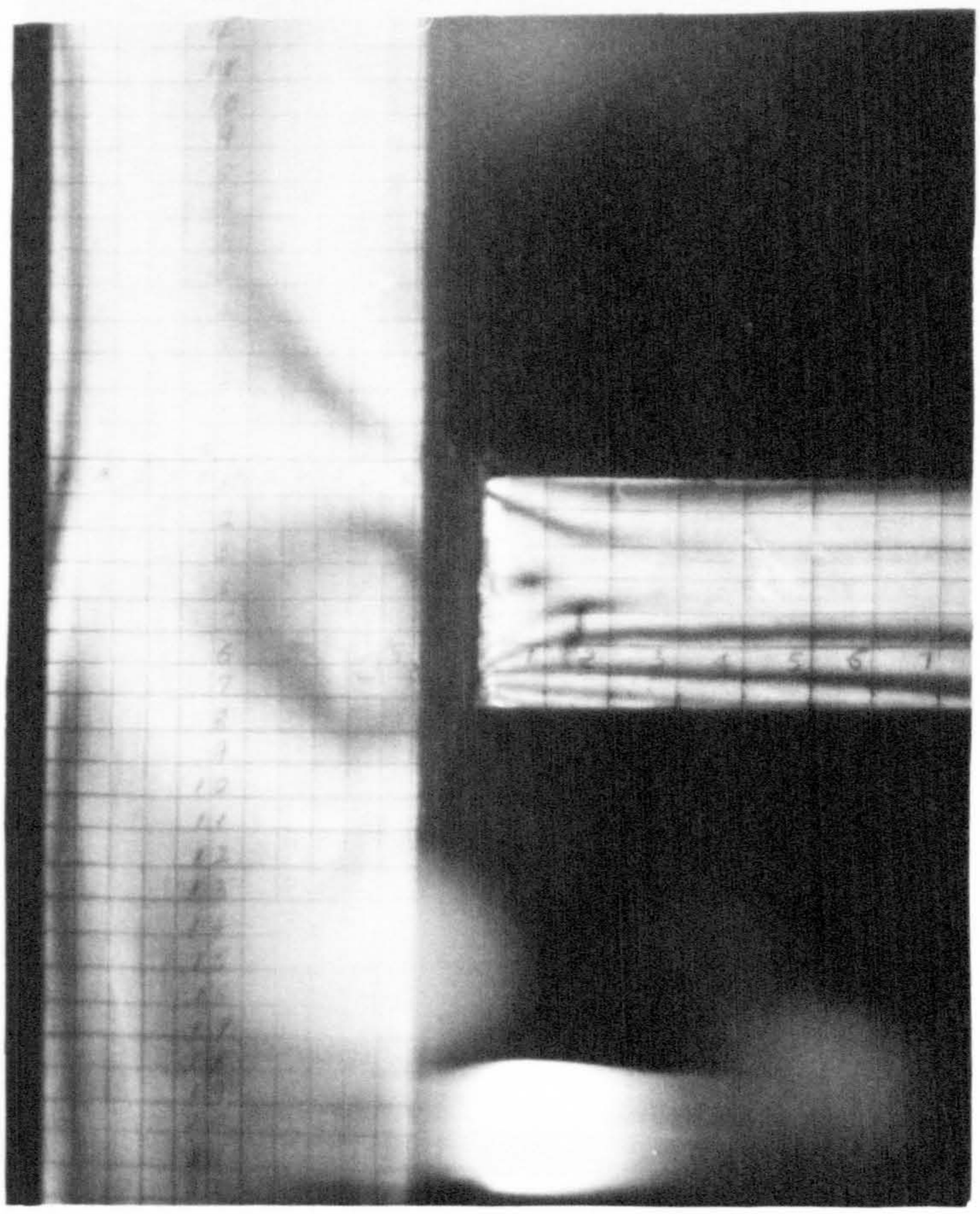

(a) Applied torque = 2560 N.mm

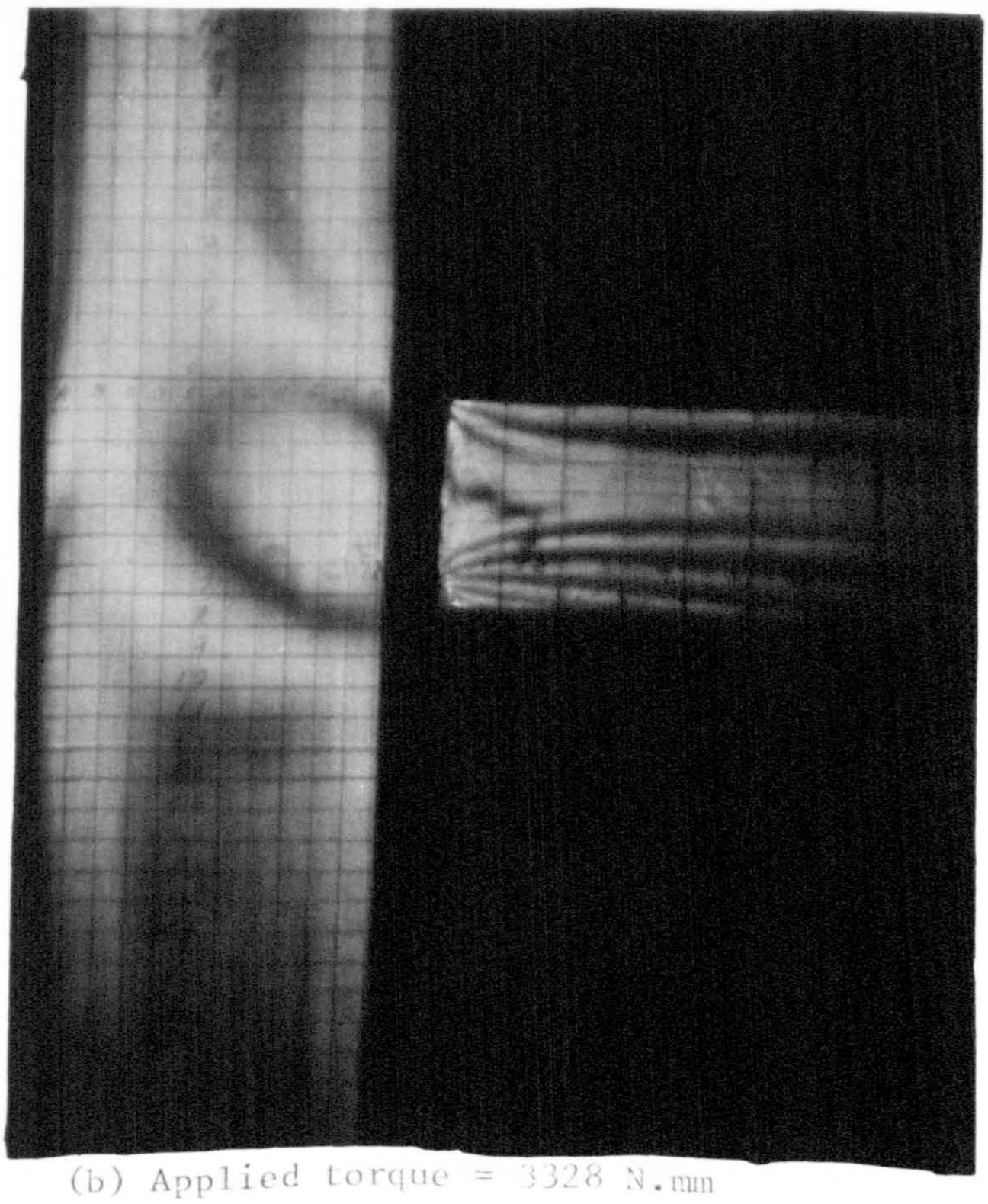

(b) Applied torque = 3328 N.mm

Plate 4.1 Whole order isochromatic fringe patterns on flanges (Joint F)

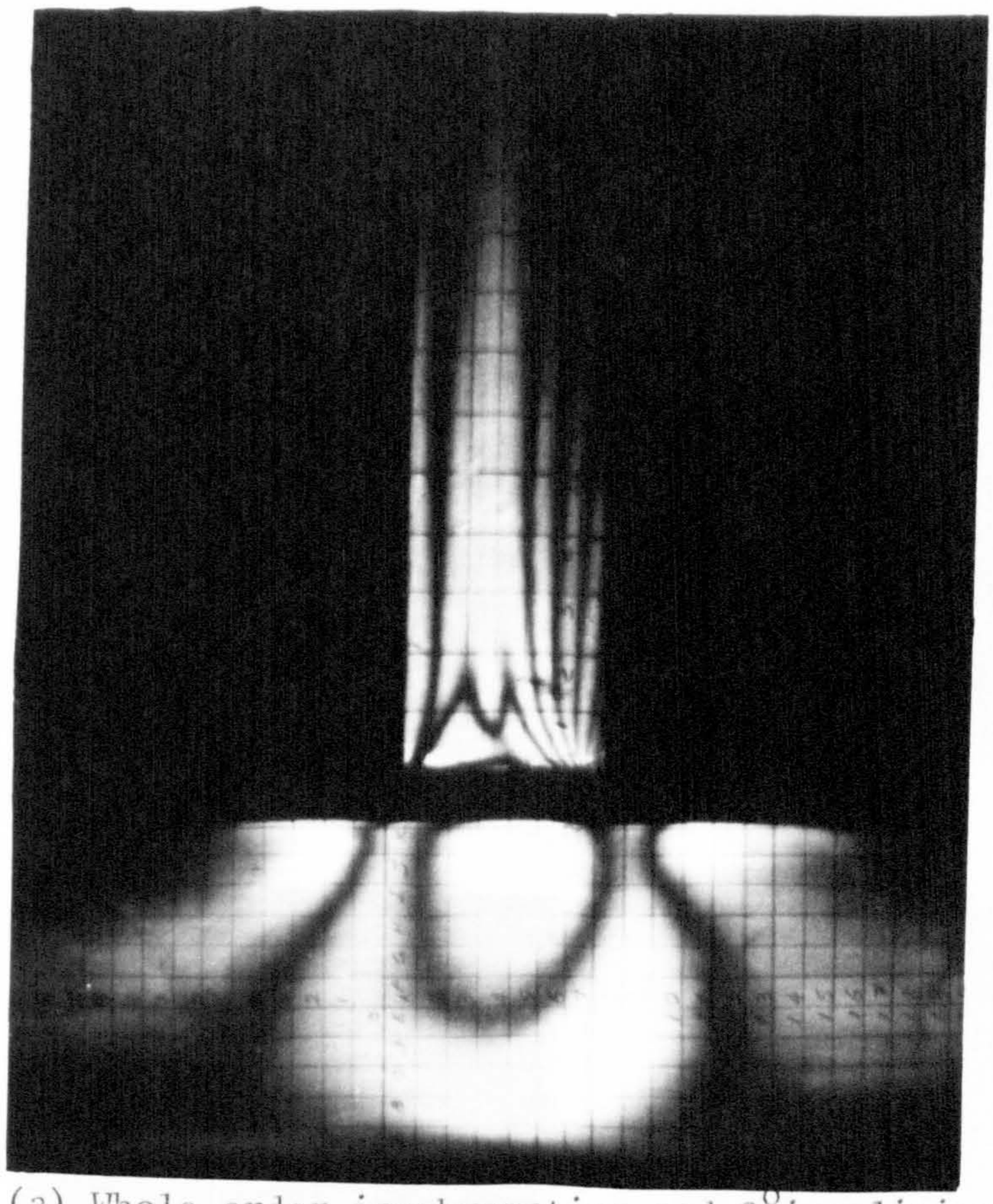

(a) Whole order isochromatics and 0^{0} isoclinics

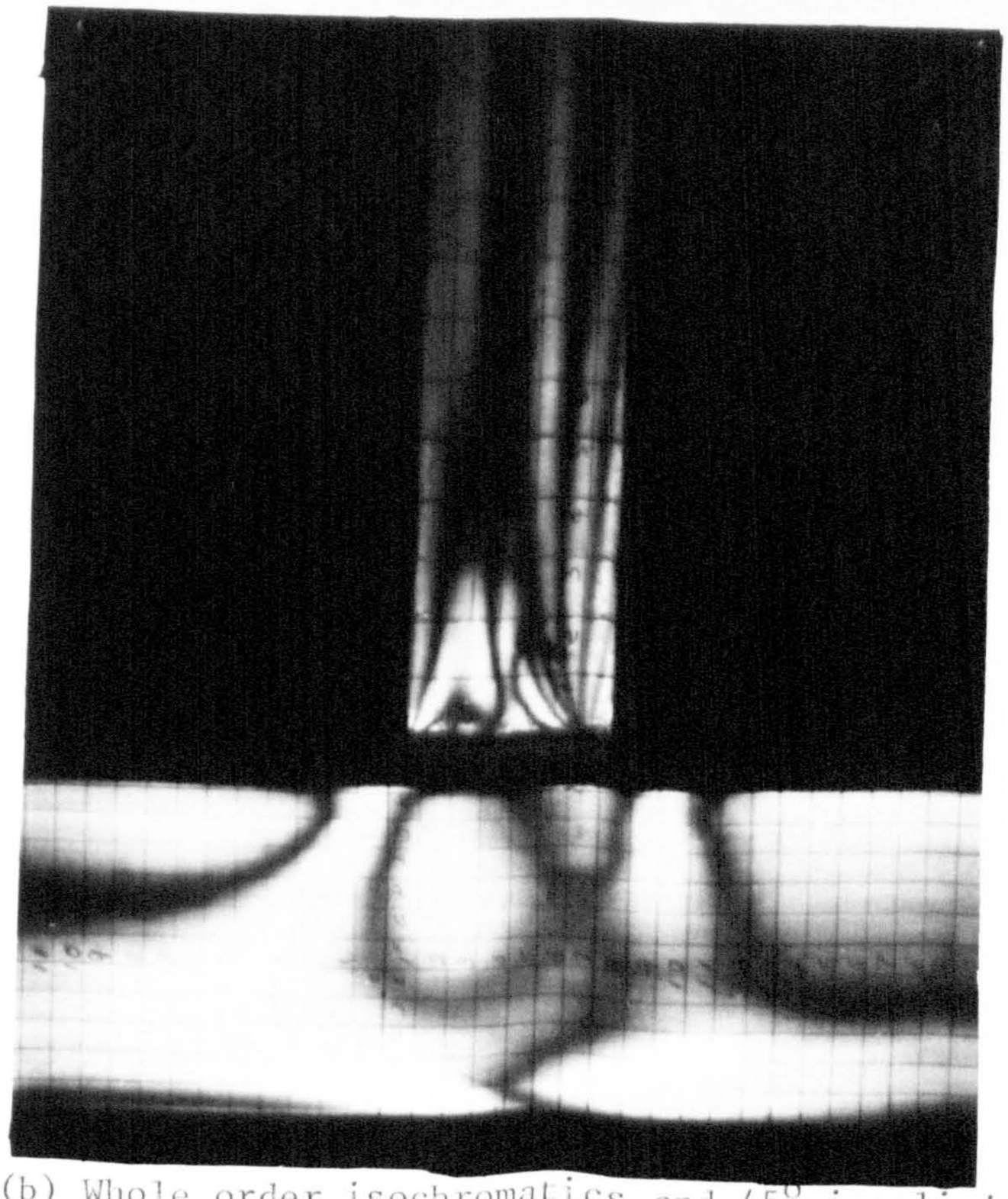

(b) Whole order isochromatics and 45^{0} isoclinic

Plate 4.2. Mixed fringe patterns on the flanges (Joint I)

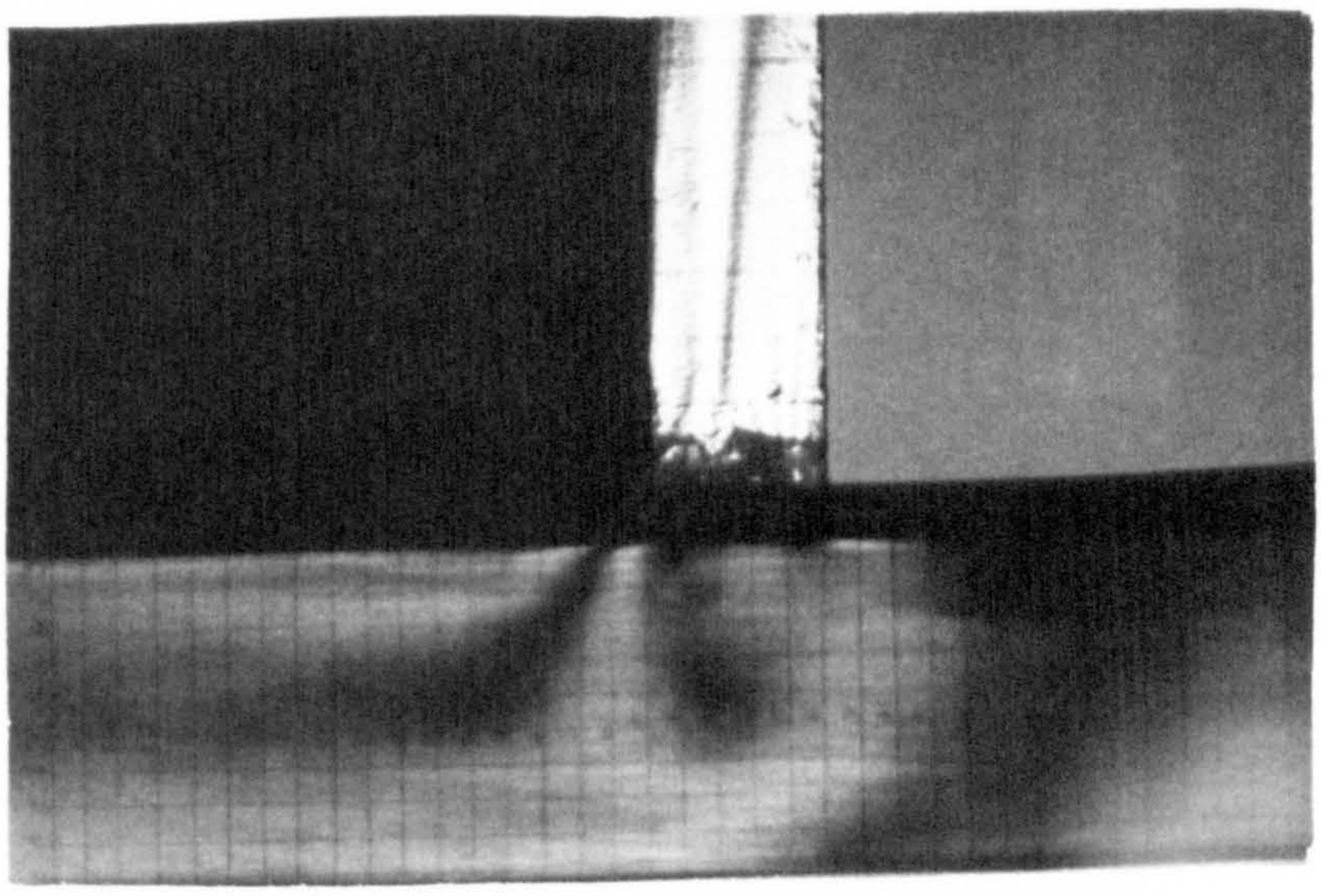

(a) Whole order fringes

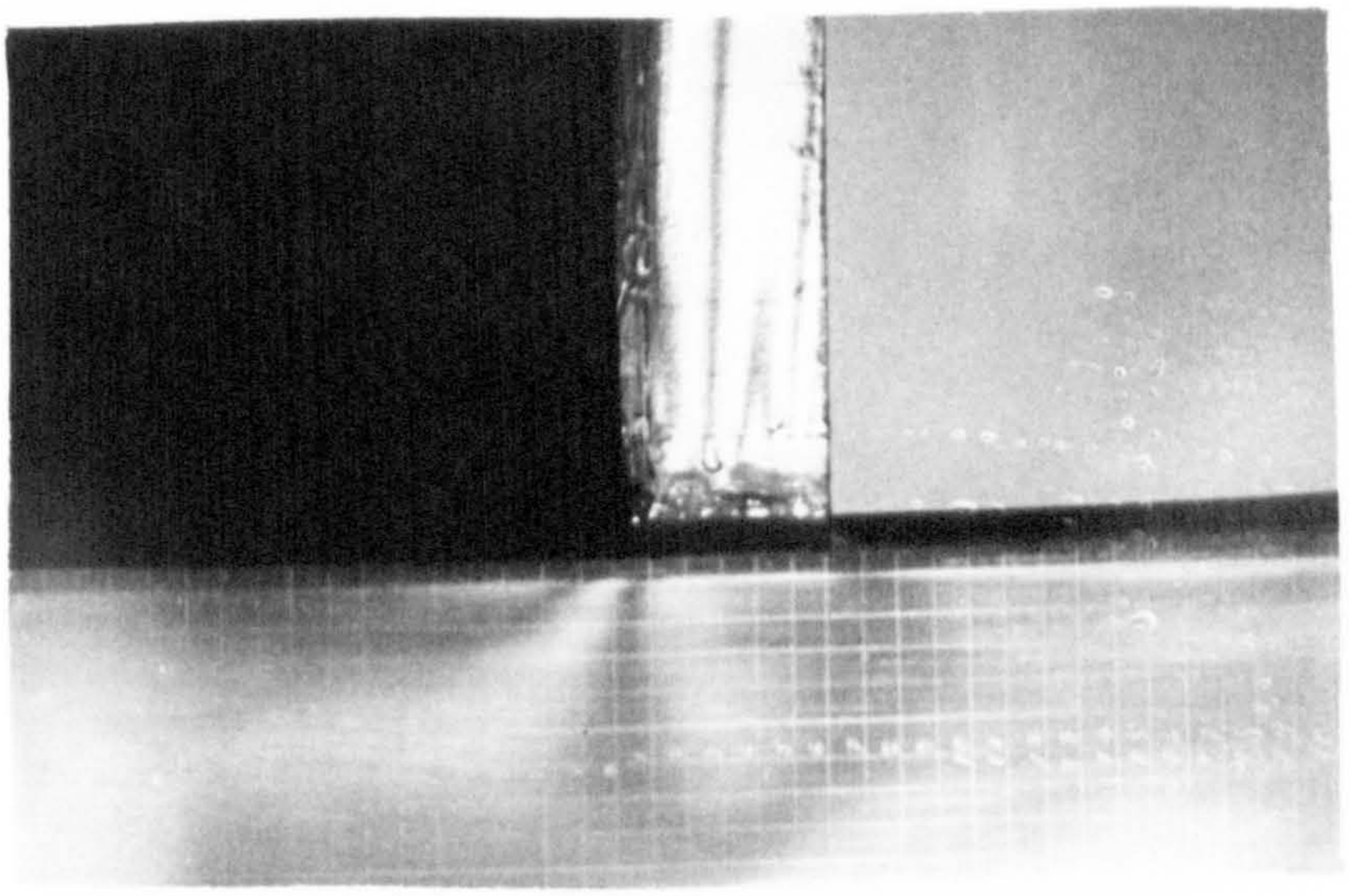

(b) Half order fringes

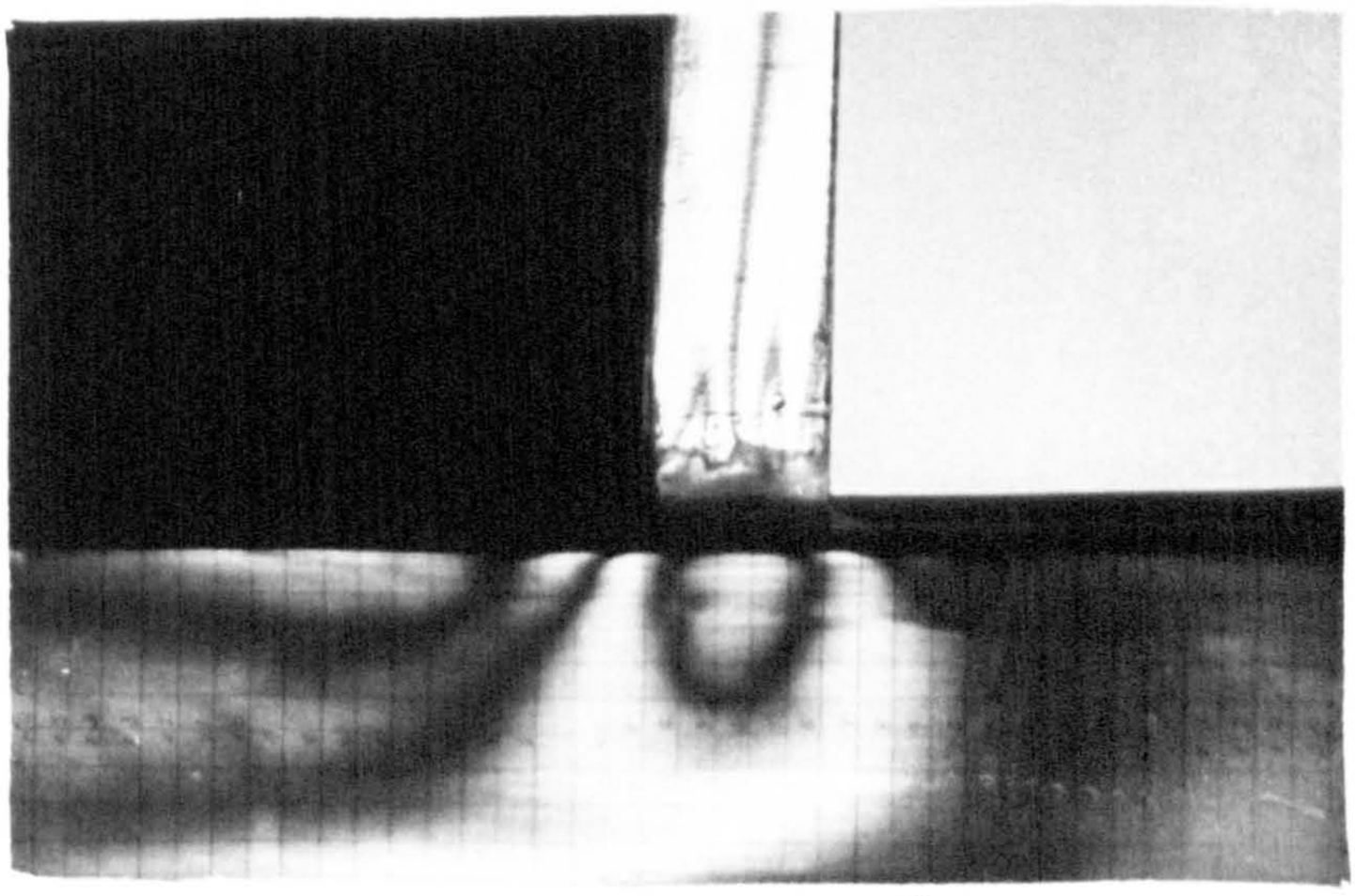

(c) Whole order fringes with 0^{o} isoclinics

Plate 4.3. Fringe Patterns on the flanges (Joint II)

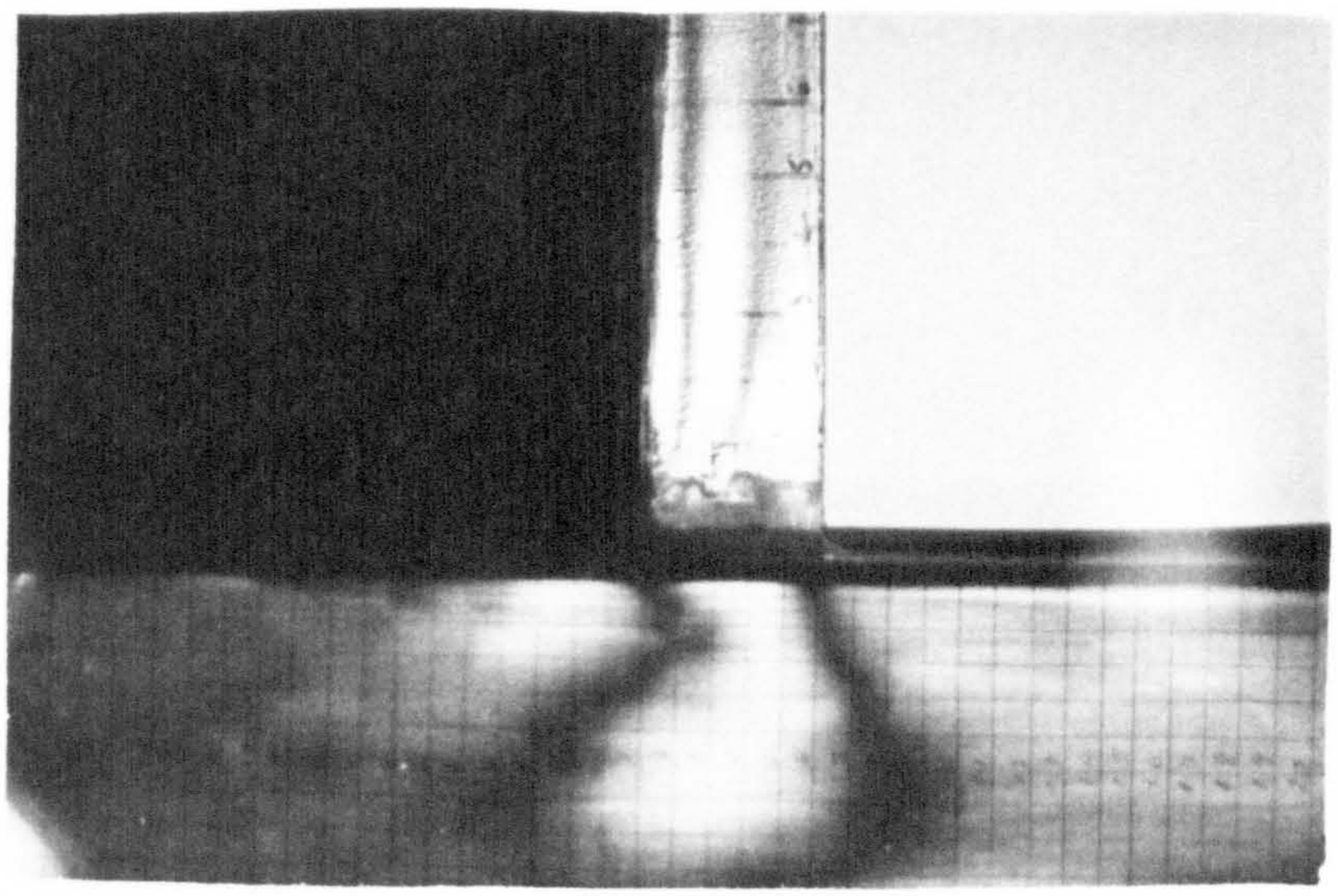

(a) 0^{o} isoclinics

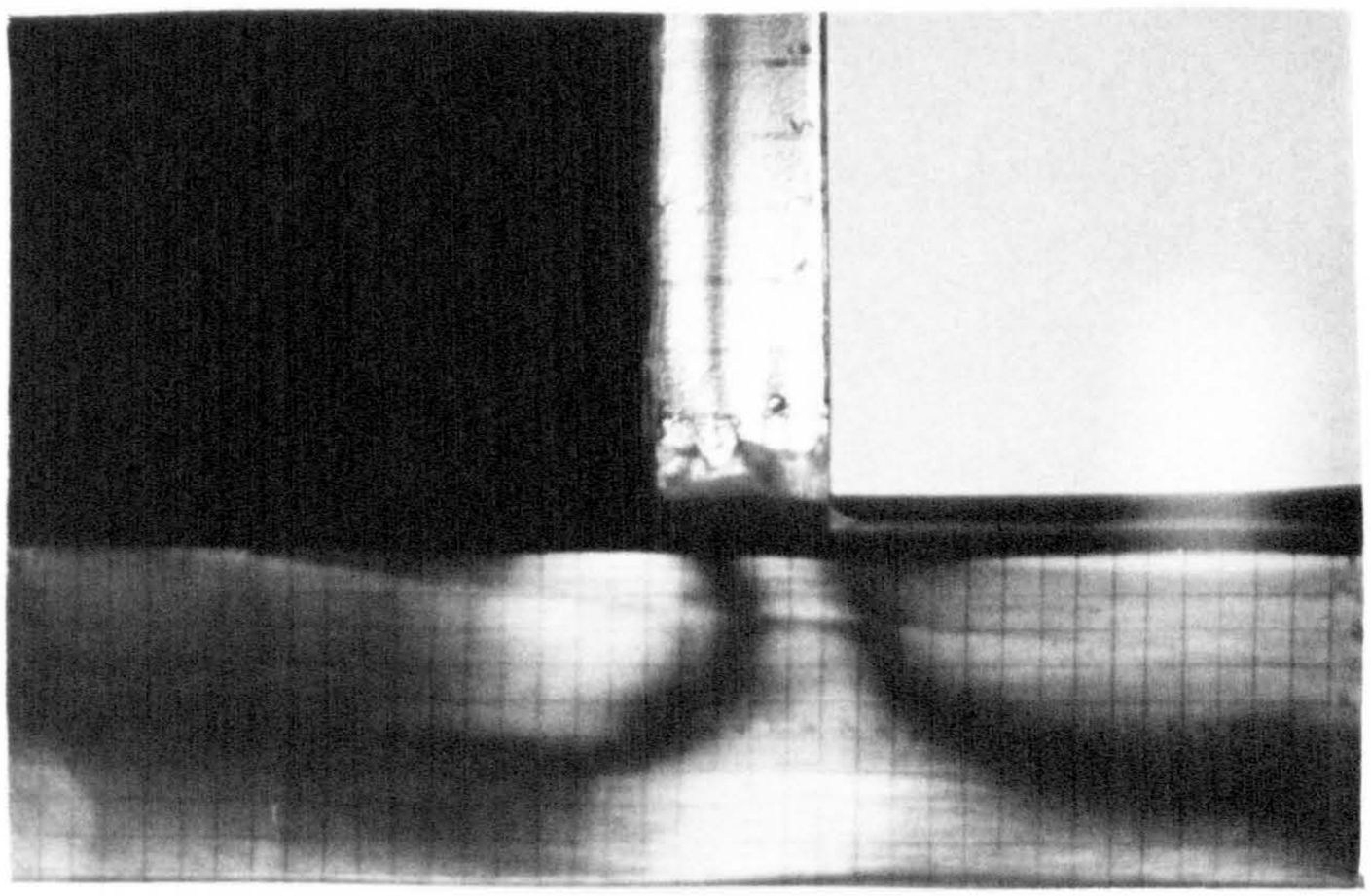

(b) 30^{o} isoclinics

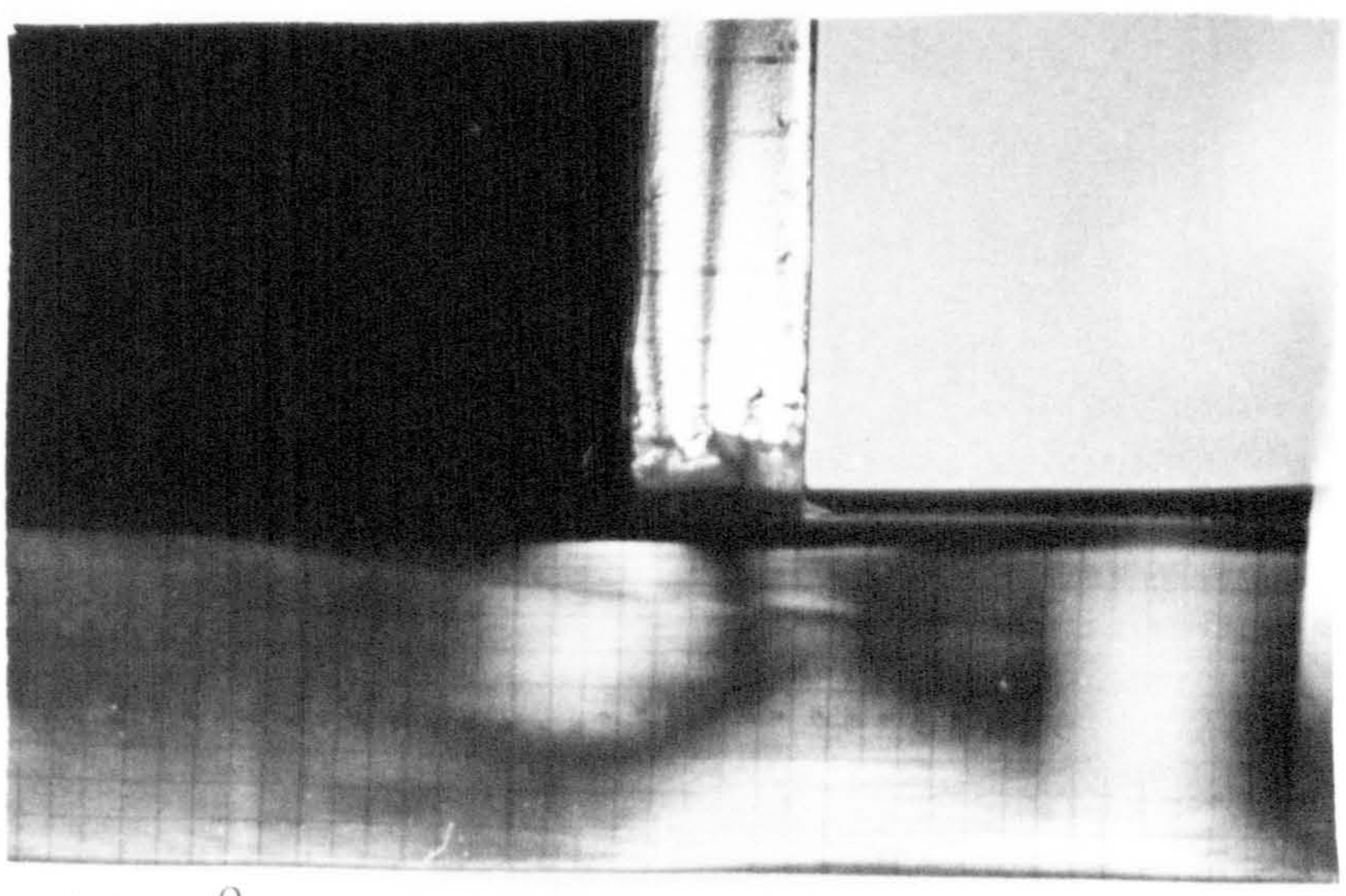

(c) 45^{o} isoclinics

Plate 4.4. Isoclinic fringe patterns on the left flange (Joint II)

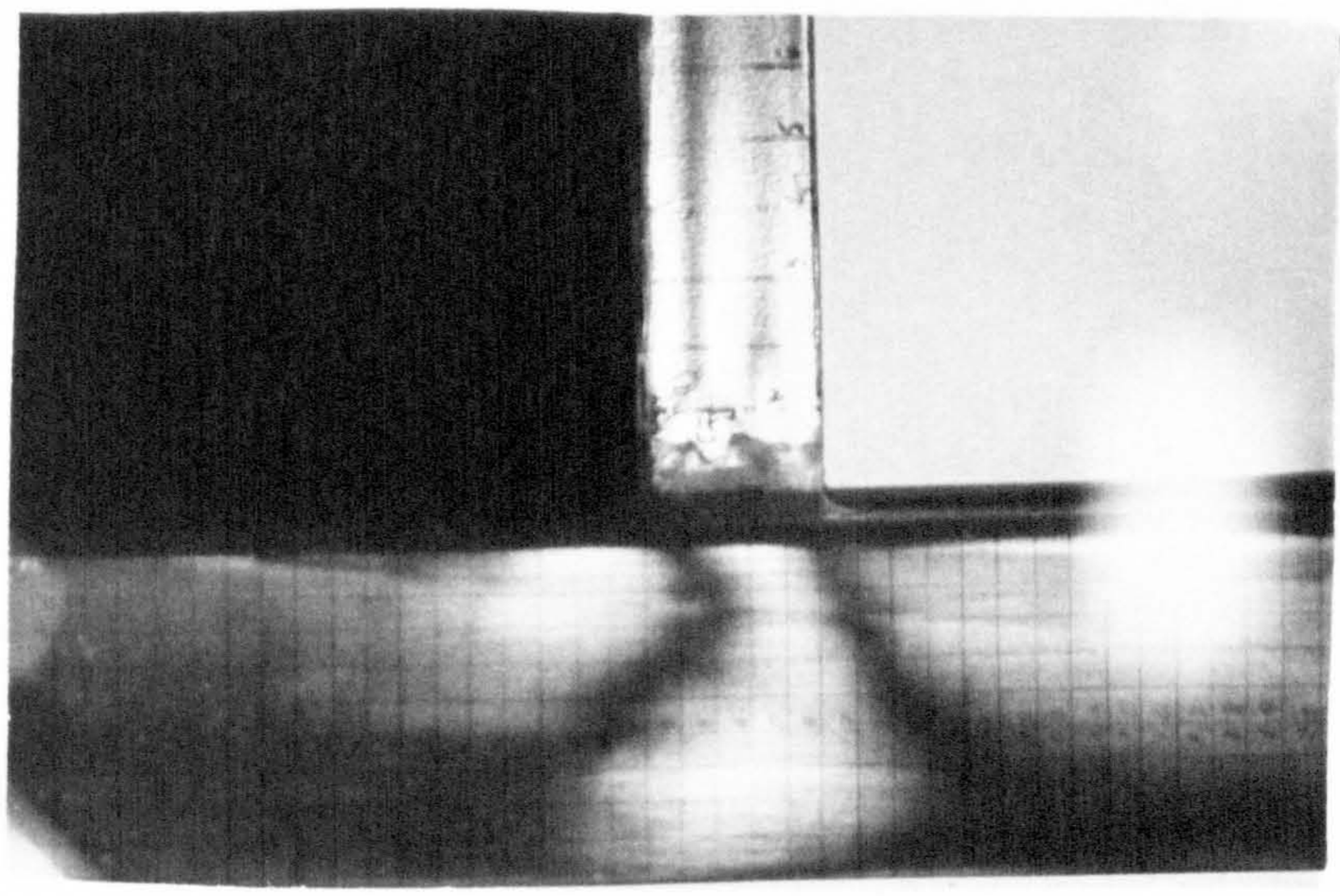

(a) 15^{o} isoclinics

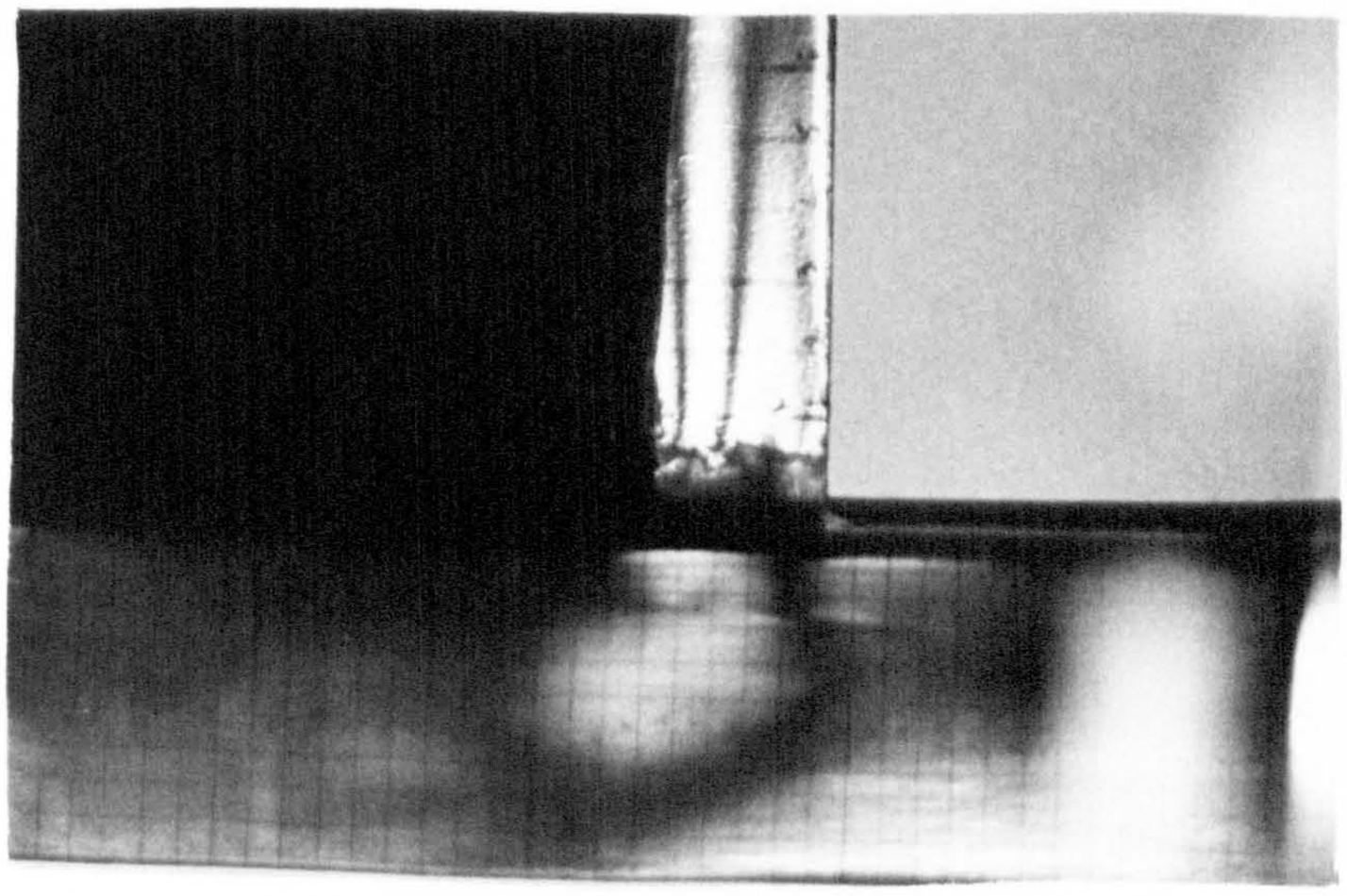

(b) 60^{o} isoclinics

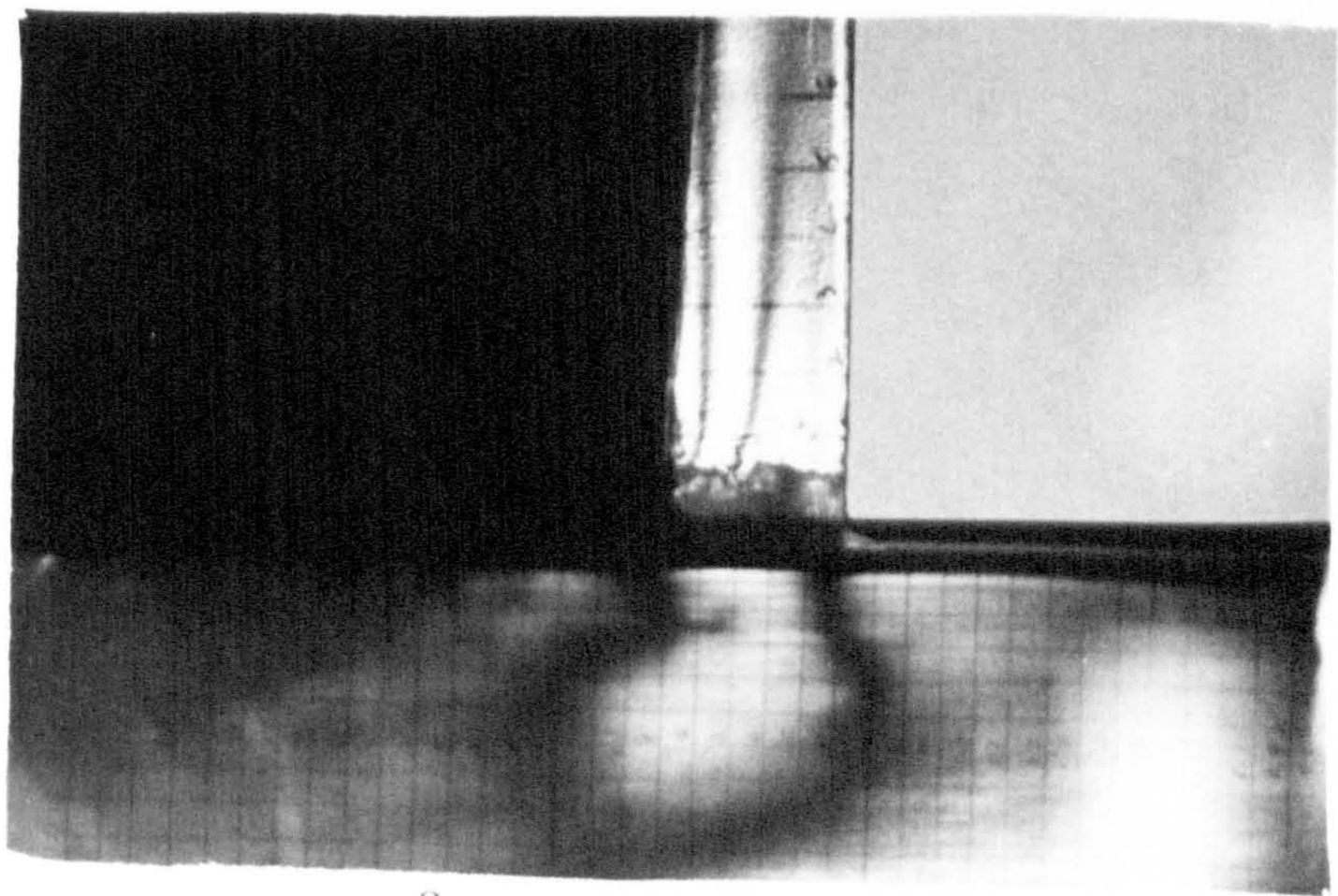

(c) 75^{o} isoclinics

Plate 4.5. Isoclinic fringe patterns on the left flange (Joint II)

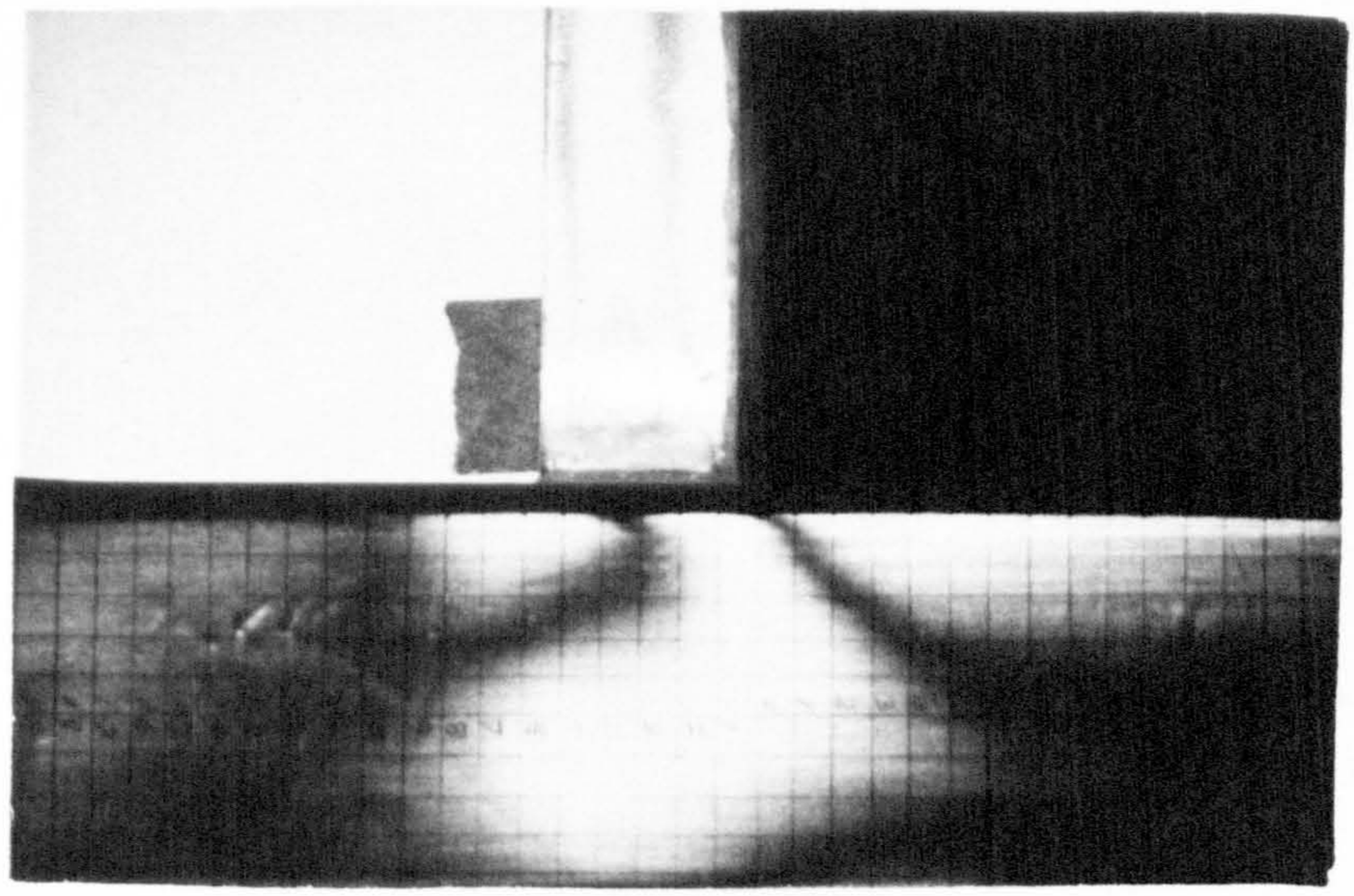

(a) 15^{o} isoclinics

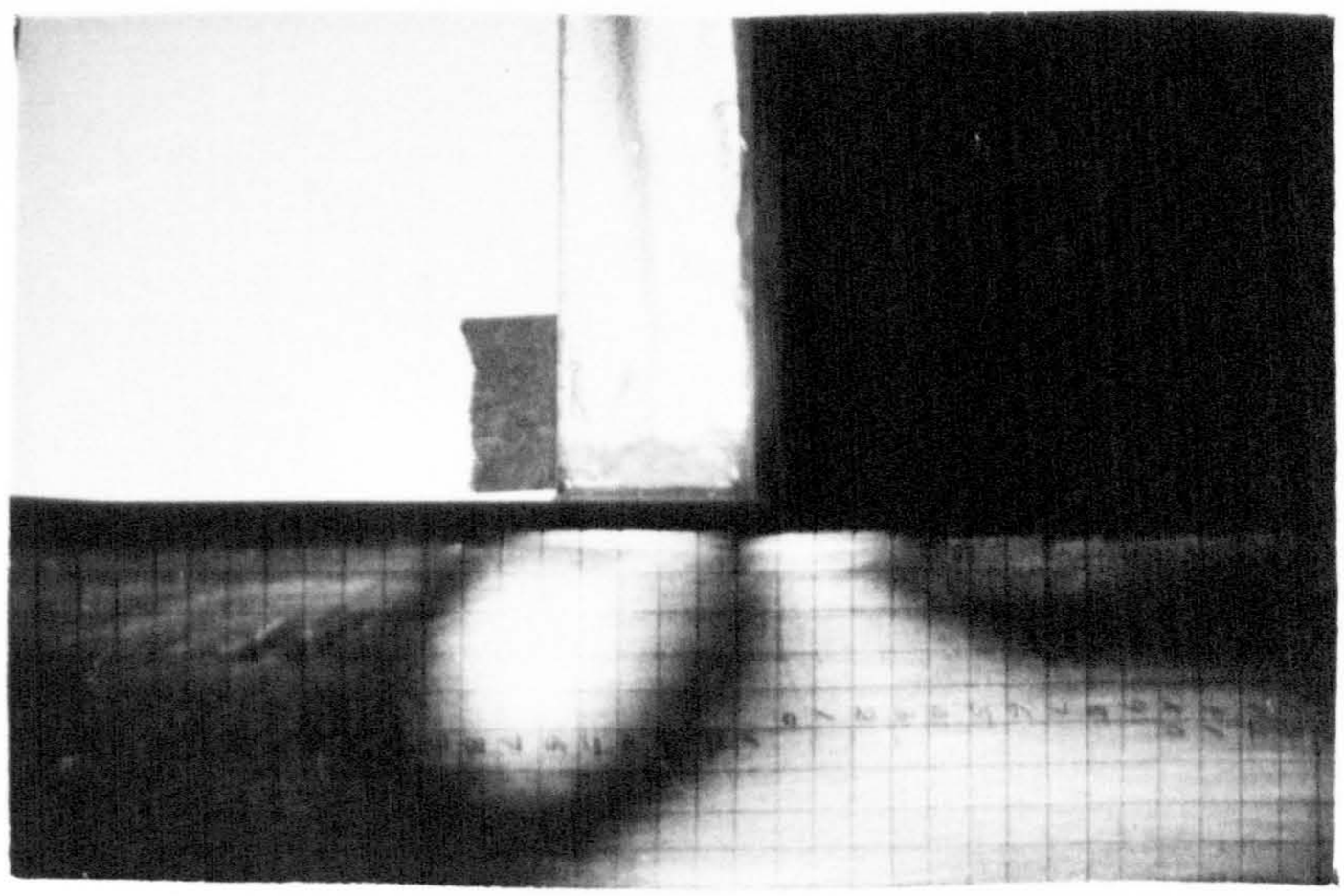

(b) 60^{o} isoclinics

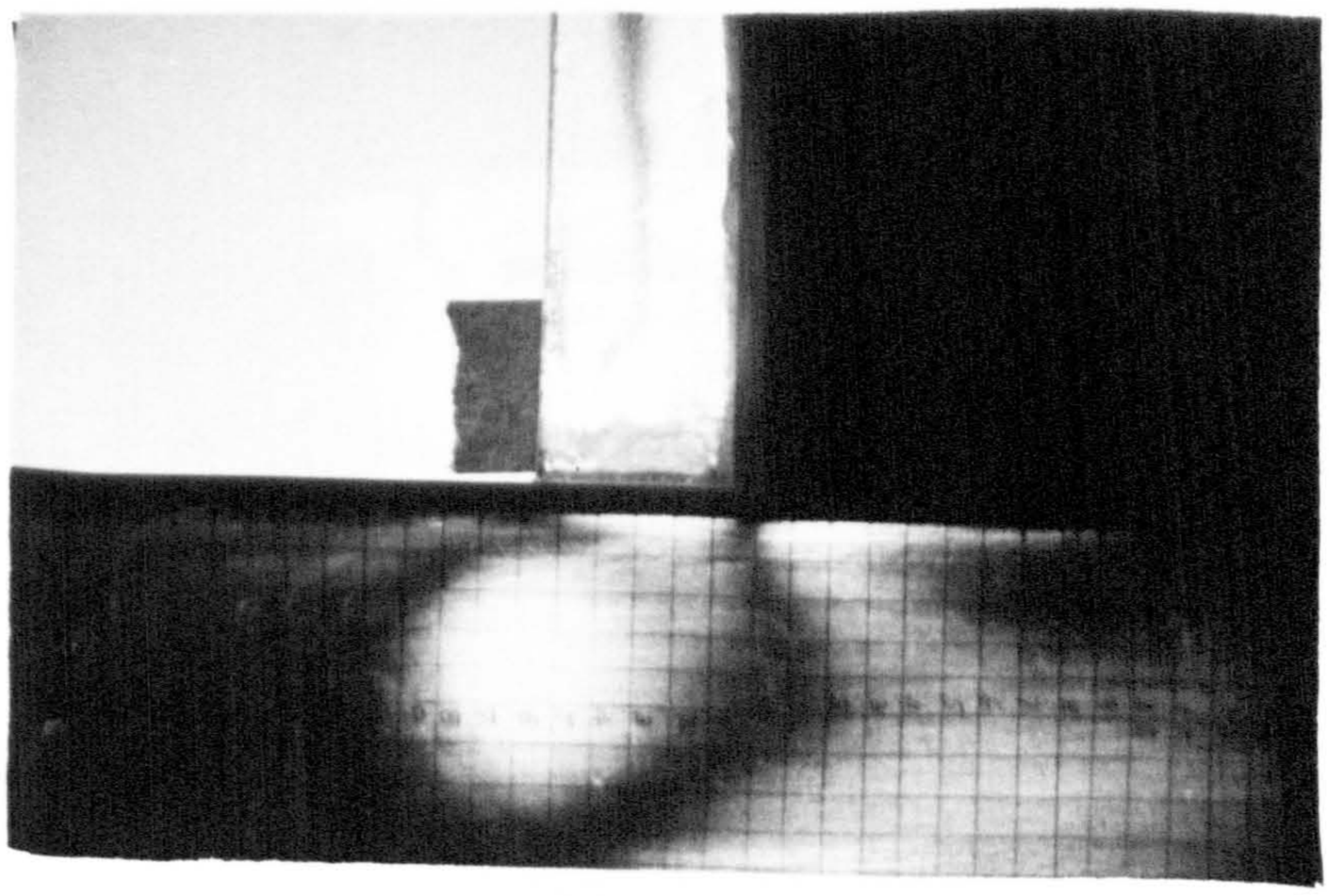

(c) 75^{o} isoclinics

Plate 4.6 Isoclinic fringe patterns on the right flange (Joint II)

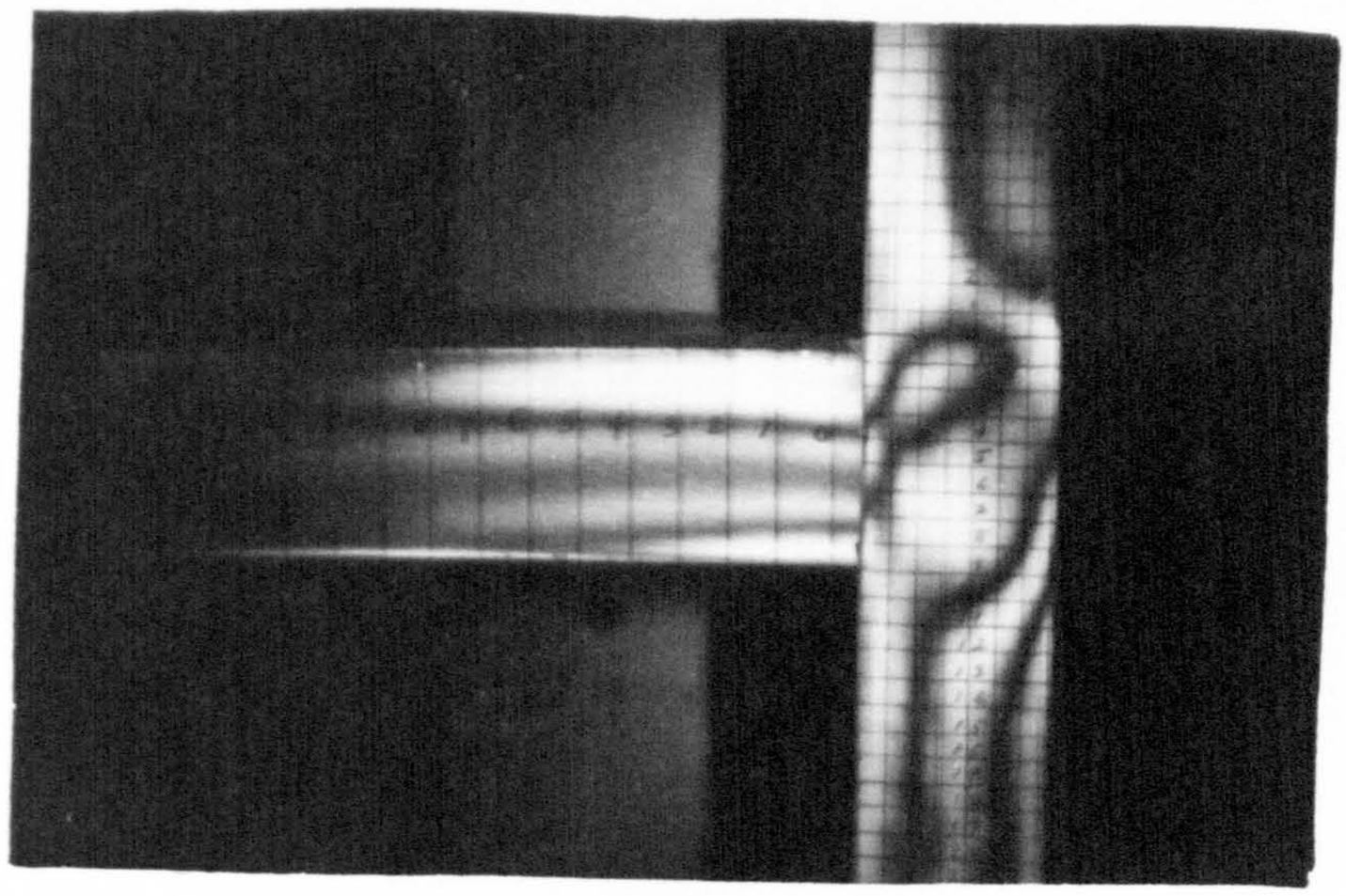

Plate 4.7 A mixed fringe pattern on the flanges (Joint III)

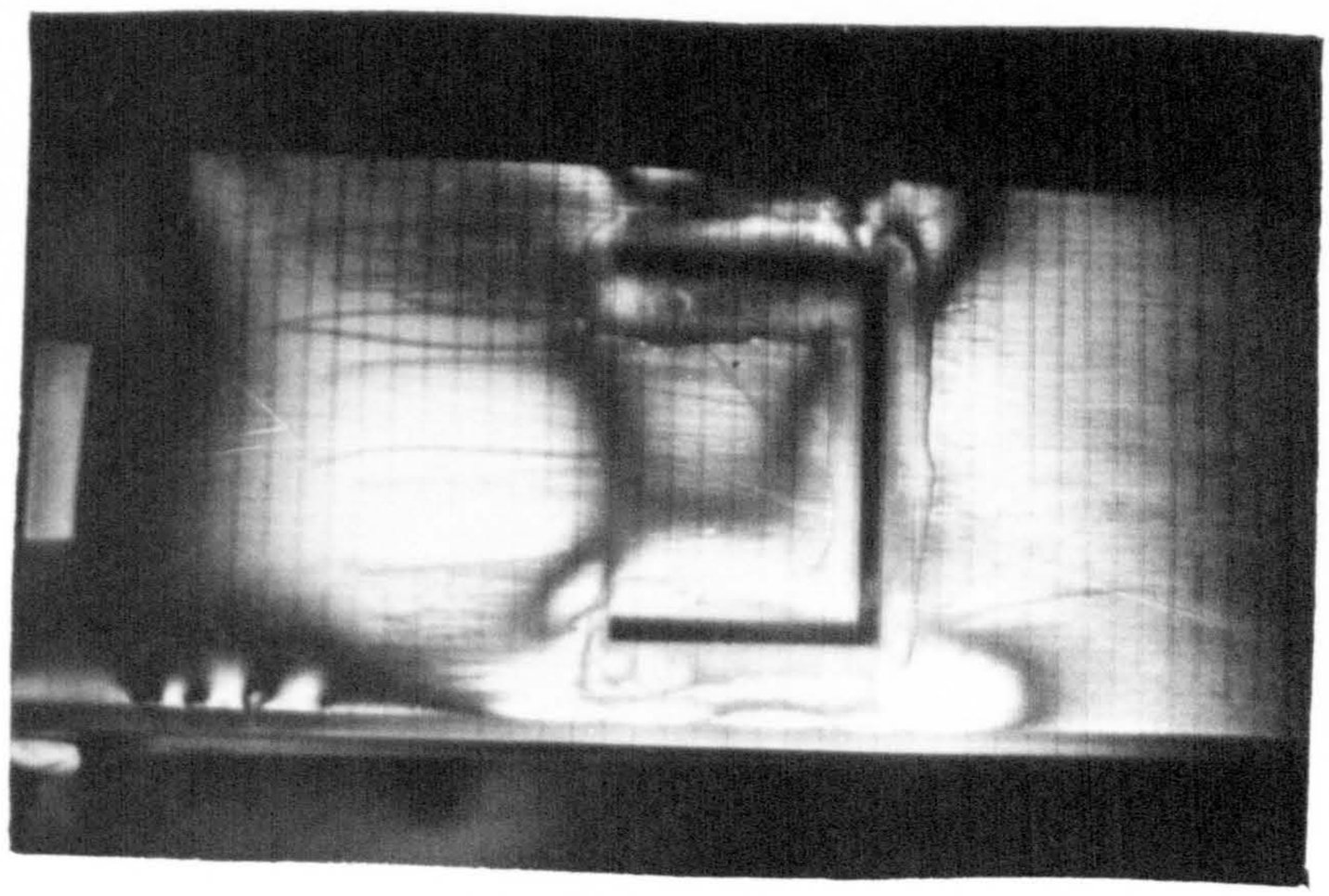

(a) Mixed fringe pattern

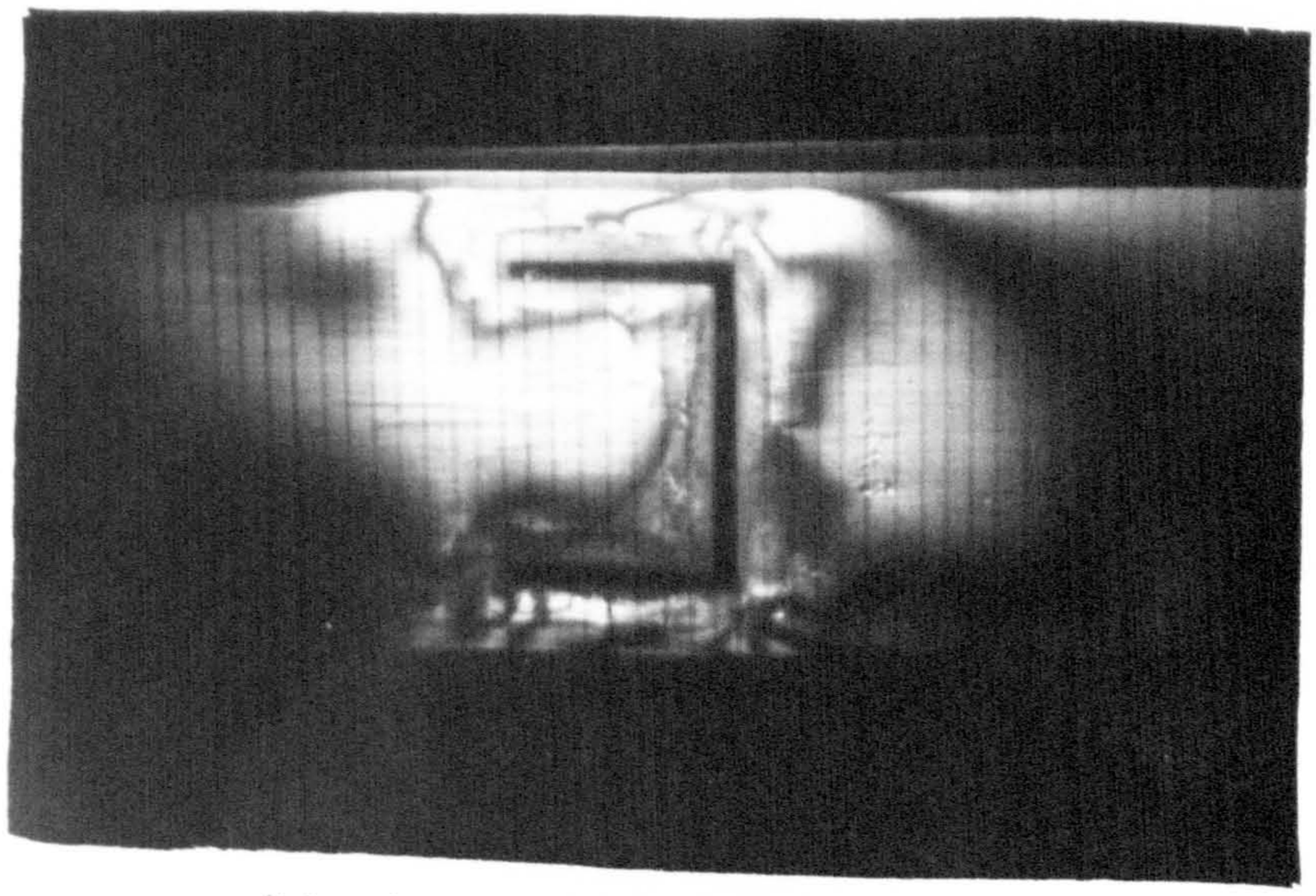

(b) Mixed fringe pattern

Plate 4.8 Mixed fringe patterns on the side member web (Ladder Frame Joints)

(a) Whole order fringes

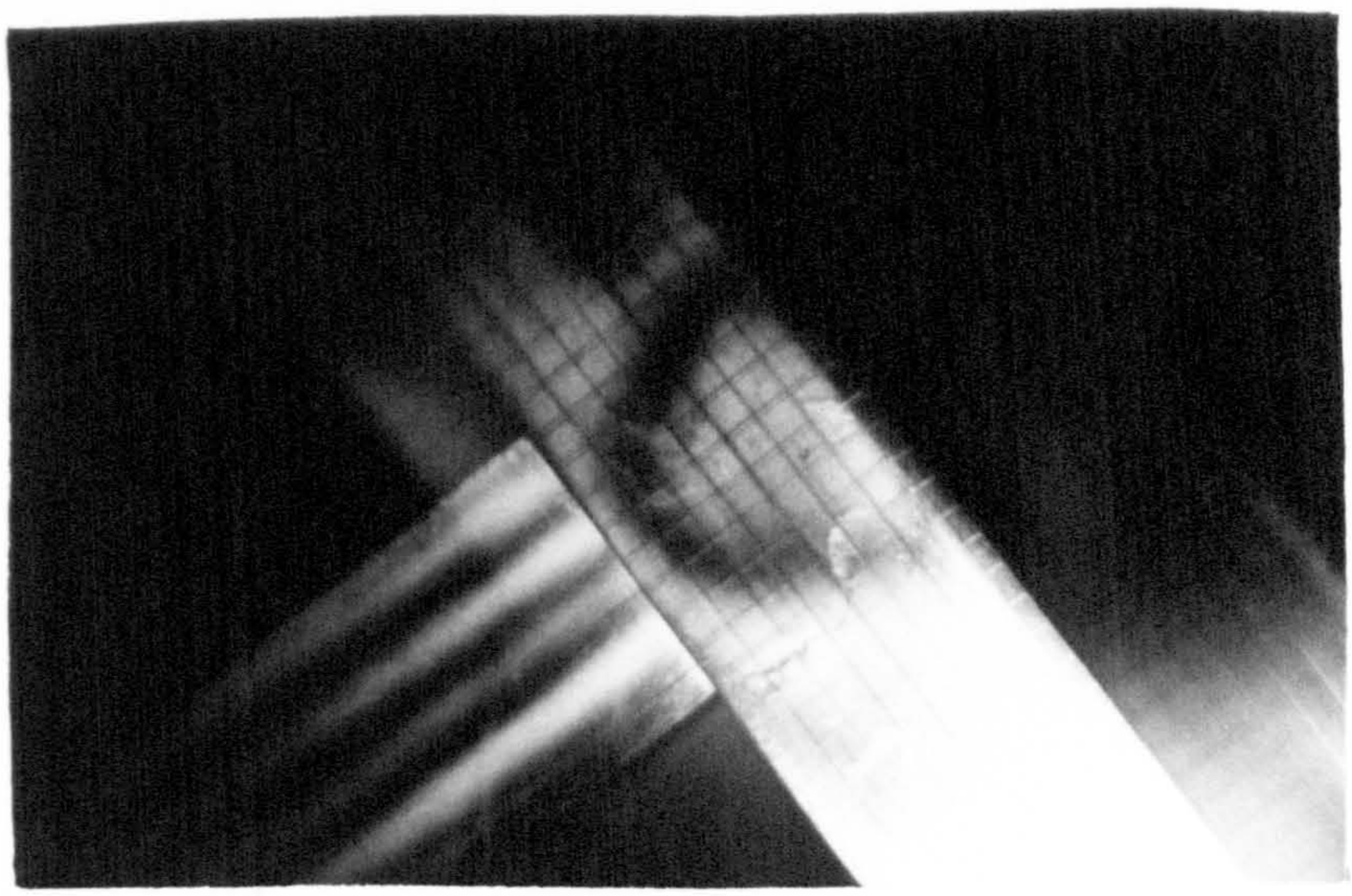

(b) Half order fringes

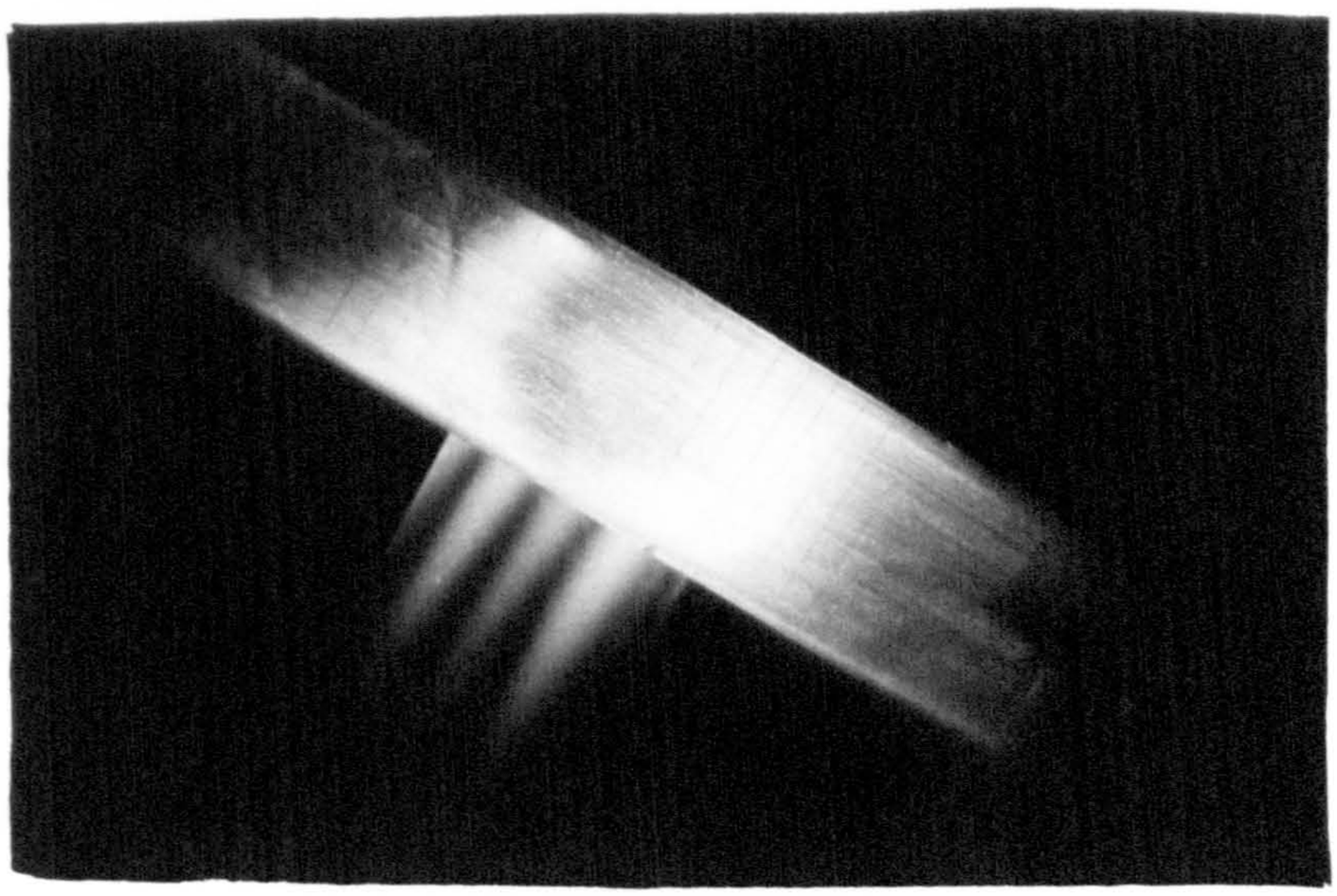

(c) Whole order fringes

Plate 4.9 Isochromatic fringe patterns on the ladder frame joints

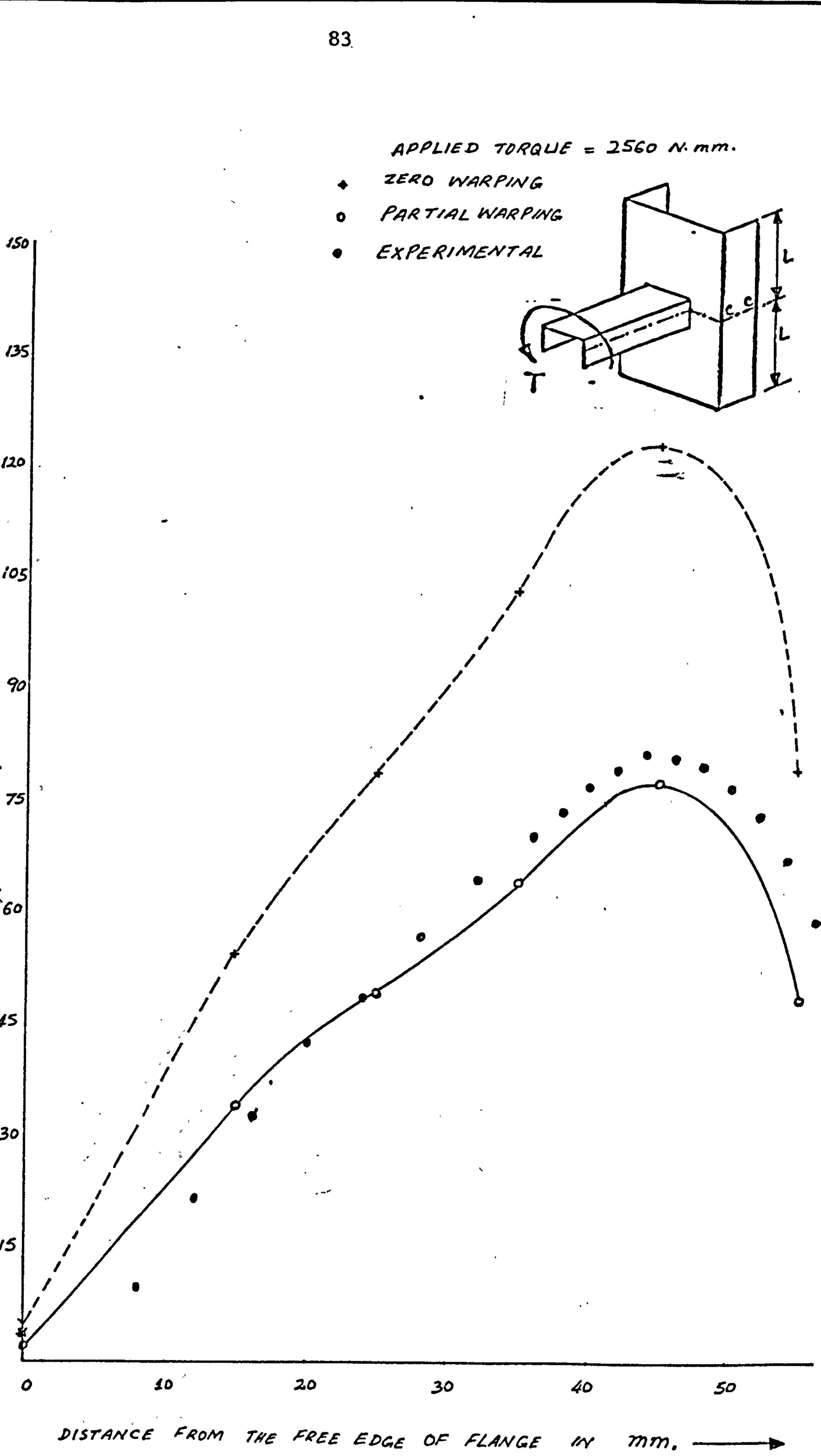

Fig.4.1 The distribution of maximum shear stress on the side member flange at Section CC. (Joint I)

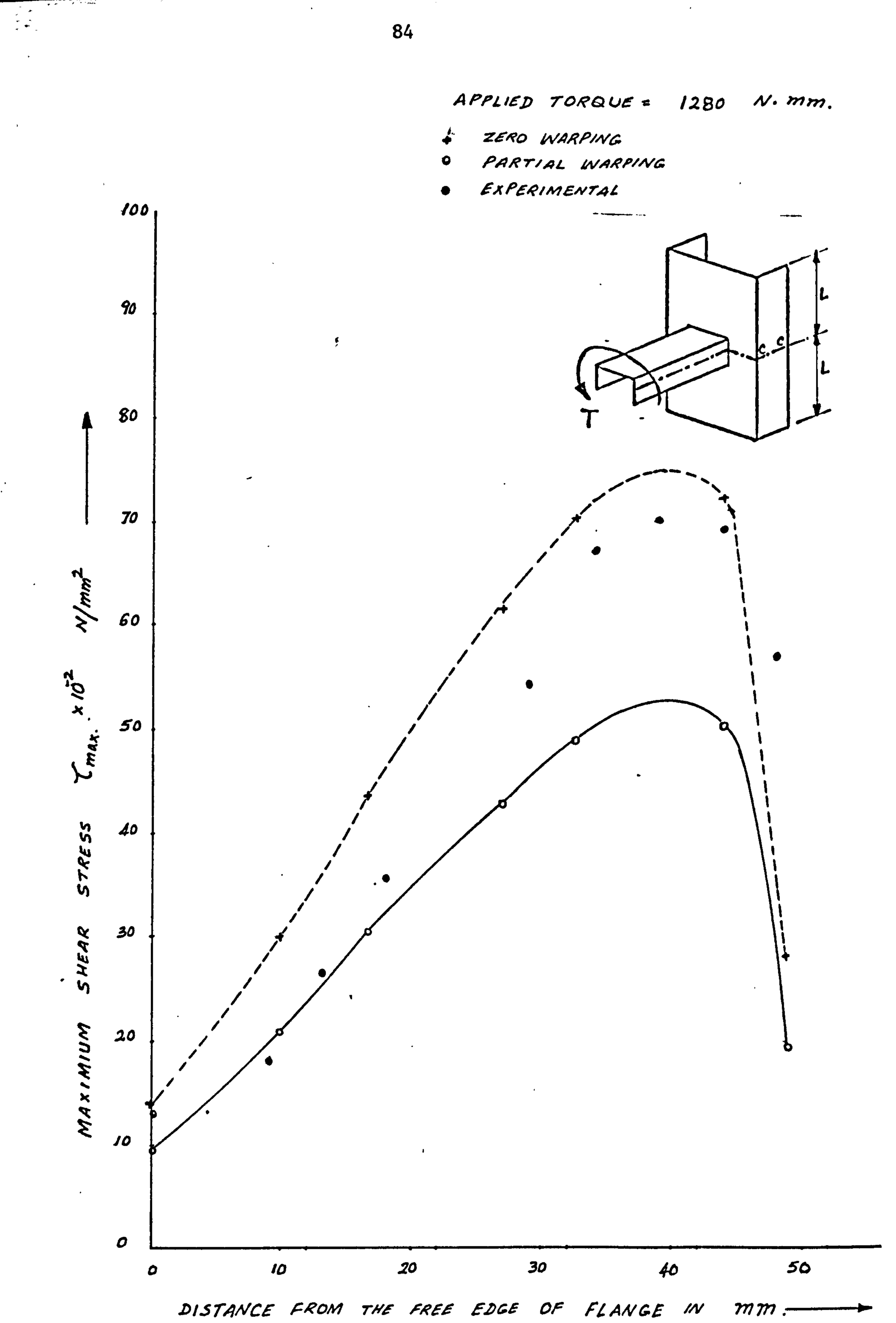

Fig.4.2. The distribution of maximum shear stress on the side member flange at Section CC. (Joint II)

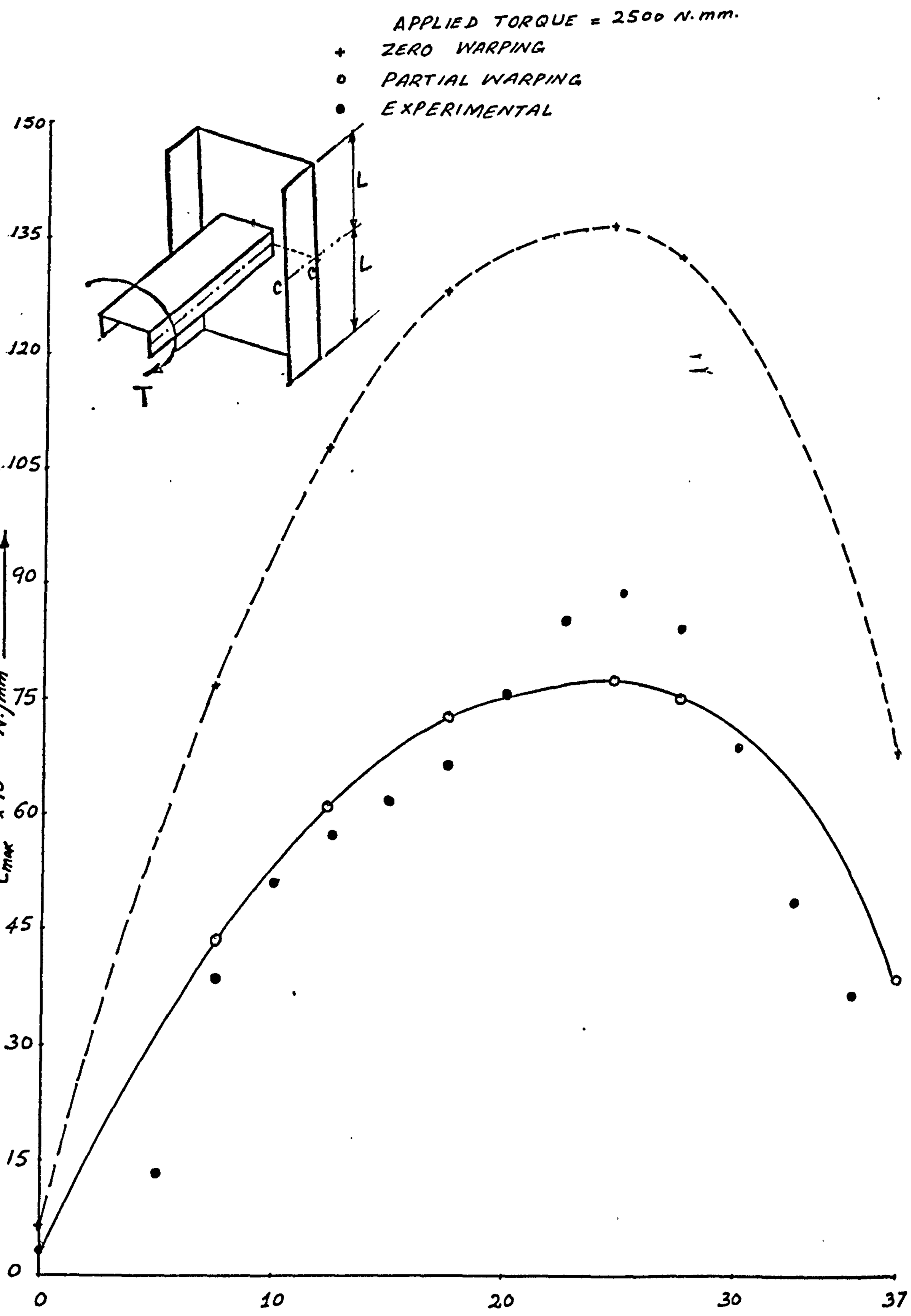

Fig.4.3. The distribution of maximum shear stress on the side member flange at Section CC. (Joint III)

APPLIED TORQUE = 2500 N.mm.

- ◆ ZERO WARPING
- o PARTIAL WARPING
- ● EXPERIMENTAL

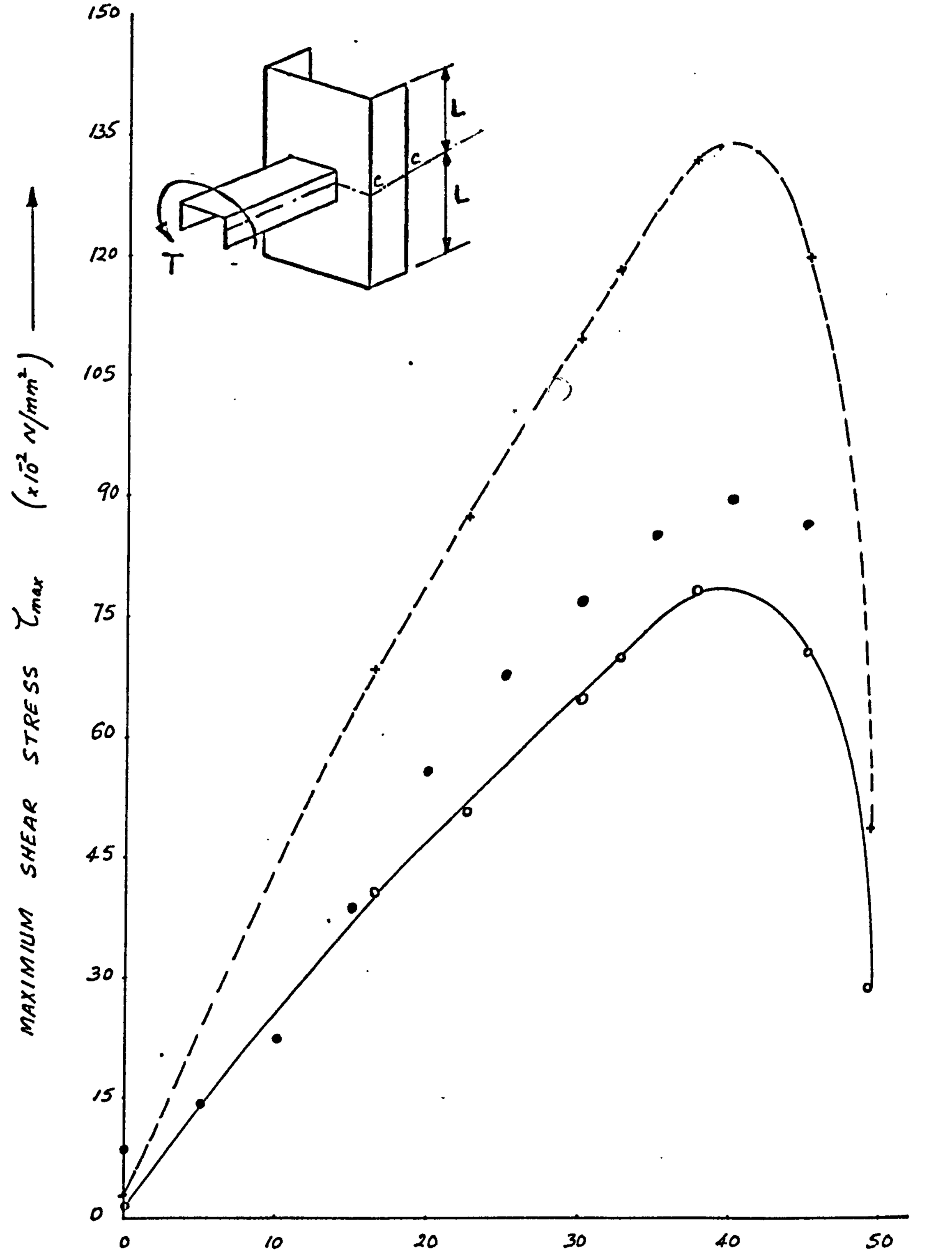

Fig.4.4. The distribution of maximum shear stress on the side member flange at Section CC. (Joint IV)

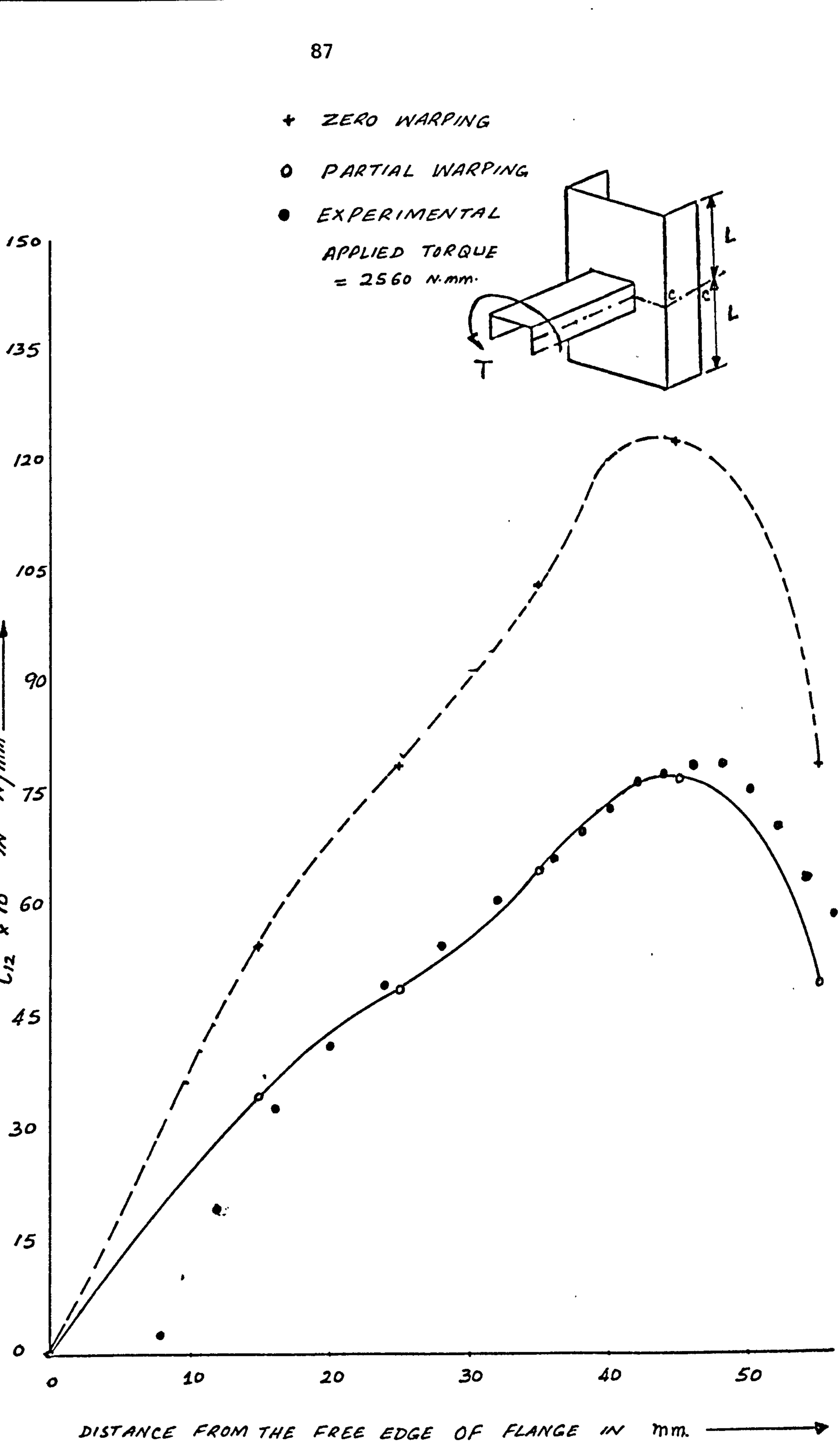

Fig.4.5 The distribution of the shear stress on the side member flange at Section CC. (Joint I)

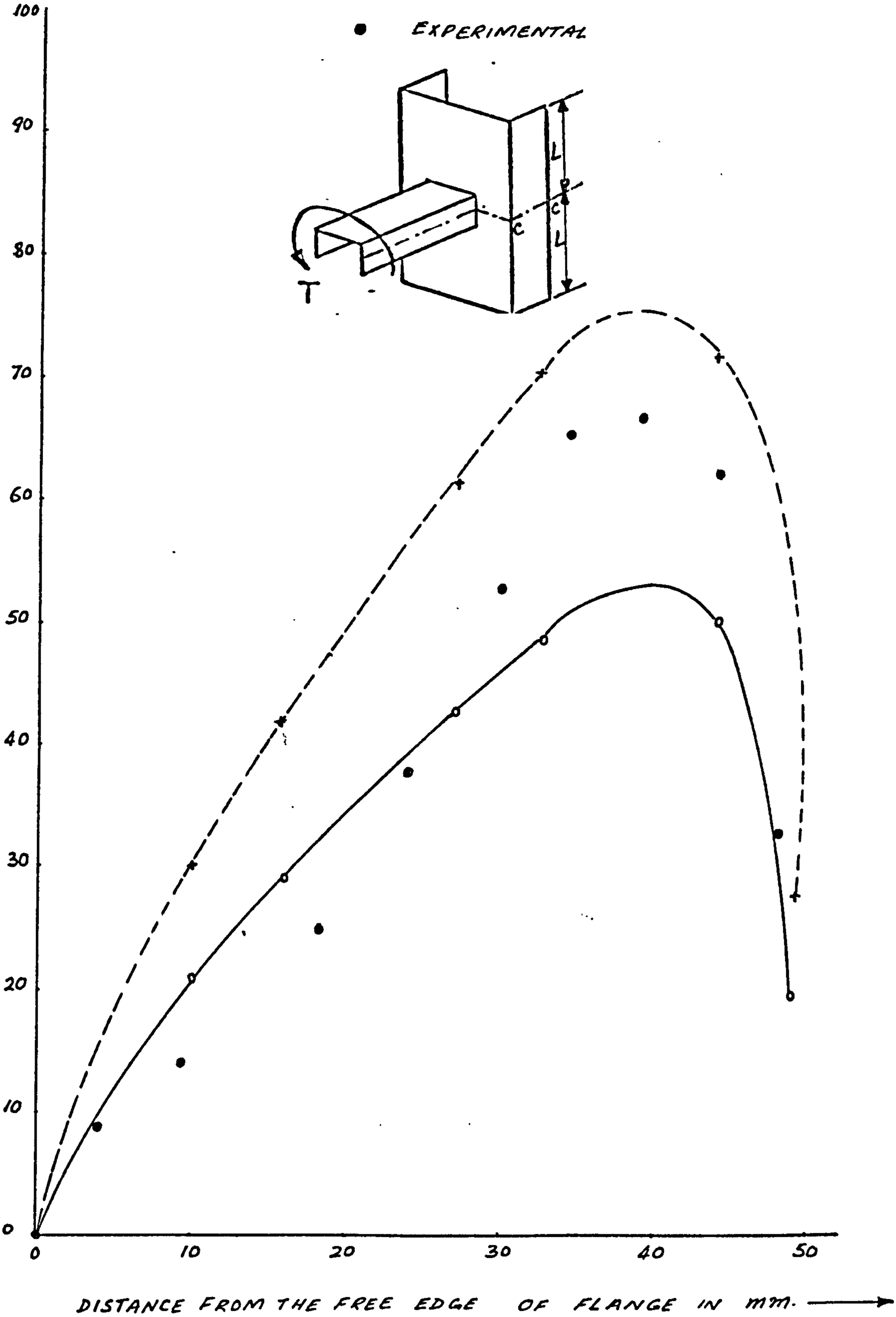

Fig.4.6 The distribution of the shear stress on the side member flange at Section CC. (Joint II)

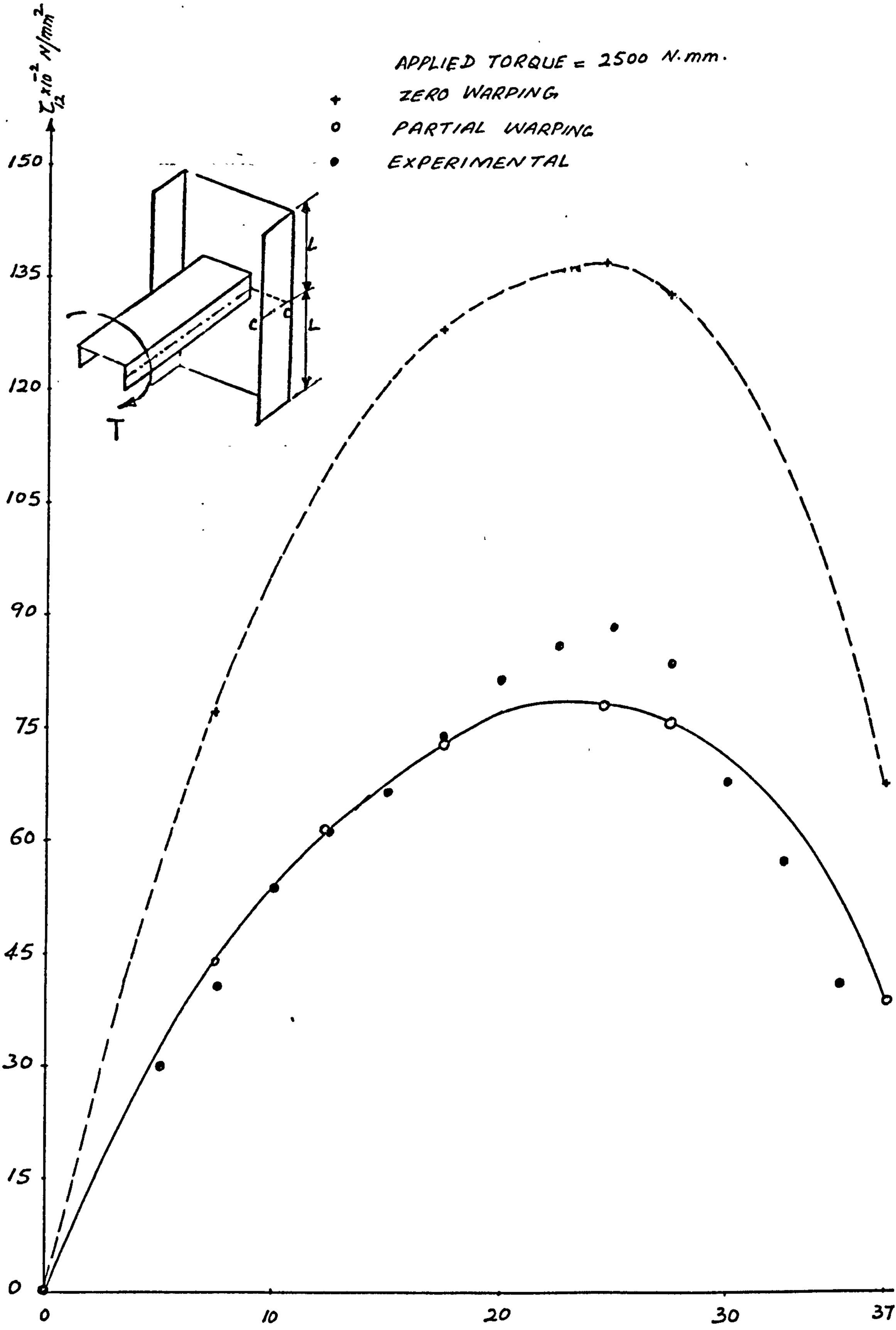

Fig.4.7 The distribution of the shear stress on the side member flange at Section CC. (Joint III)

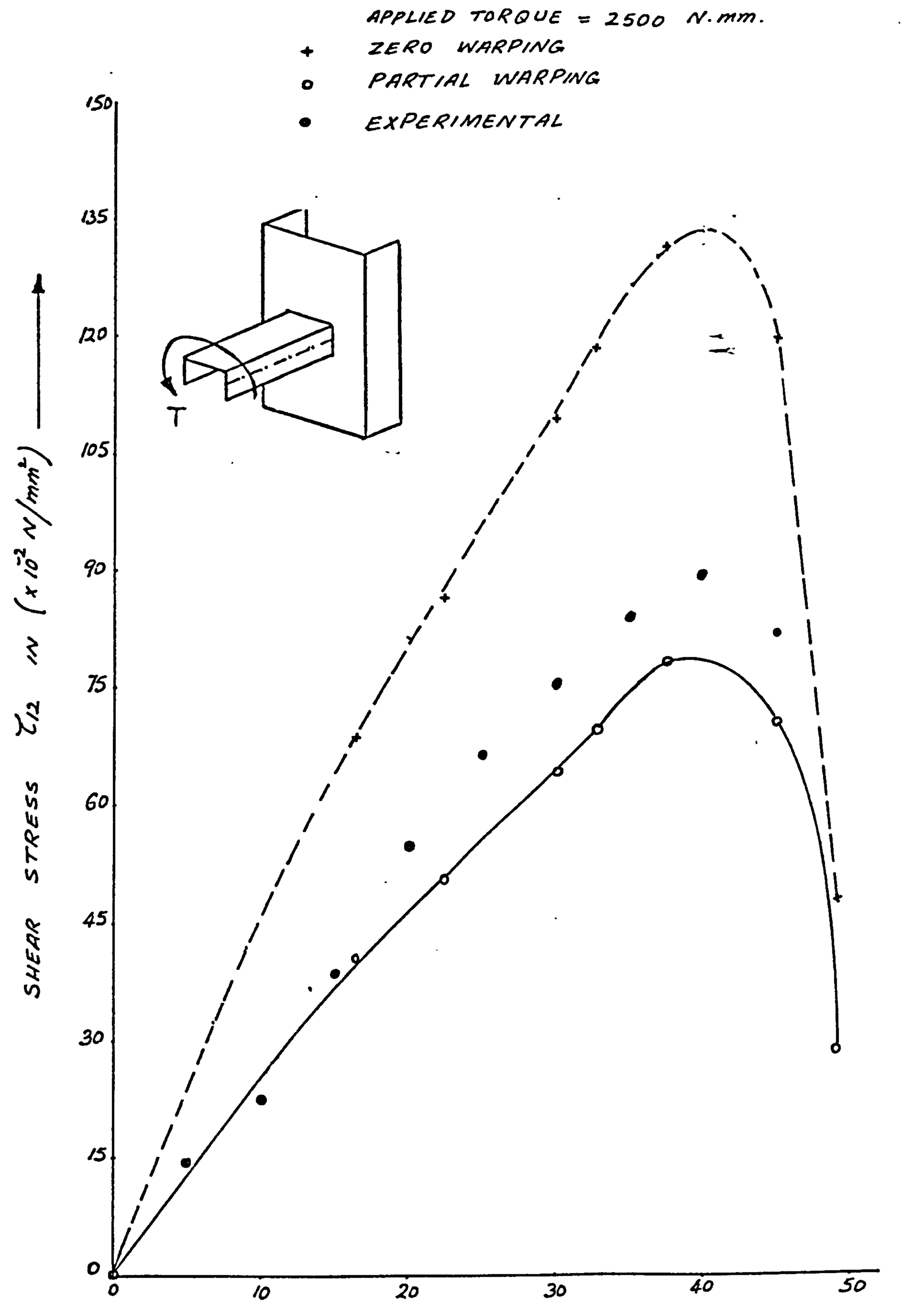

Fig.4.8 The distribution of the shear stress on the side member flange at Section CC. (Joint IV)

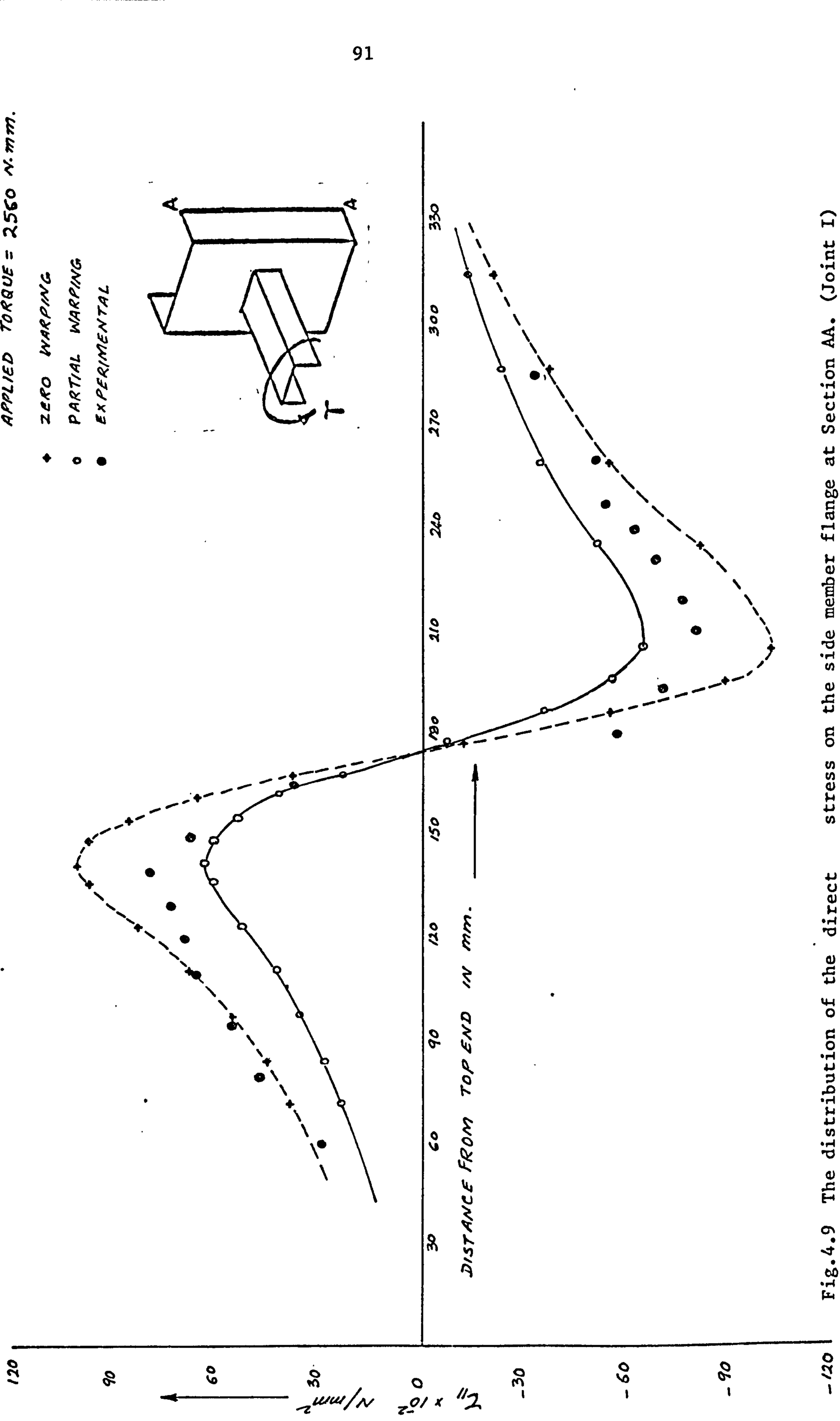

Fig.4.9 The distribution of the direct stress on the side member flange at Section AA. (Joint I)

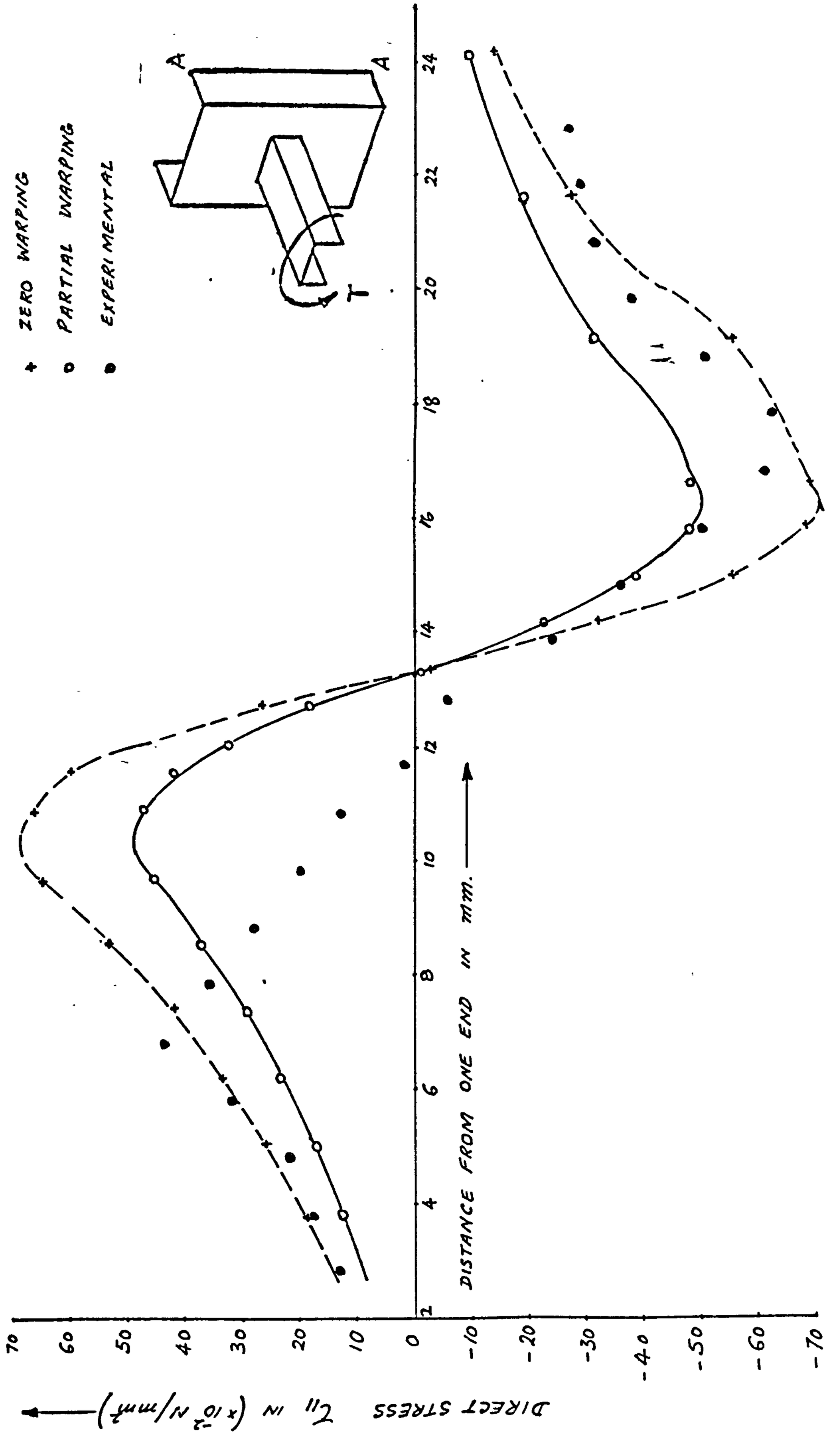

Fig.4.10. The distribution of the direct stress on the side member flange at Section AA. (Joint II)

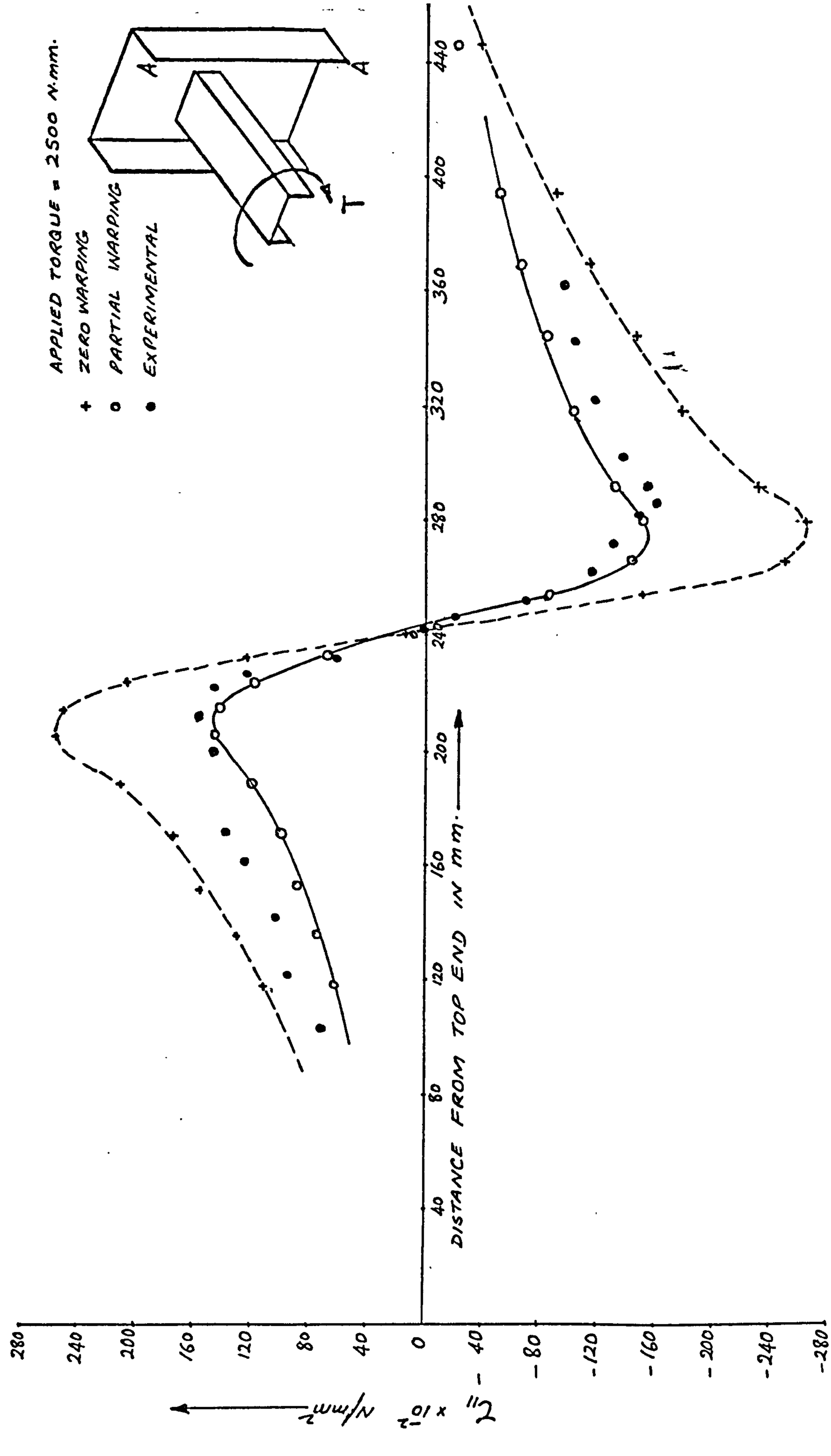

Fig.4.11 The distribution of the direct stress on the side member flange at Section AA. (Joint III)

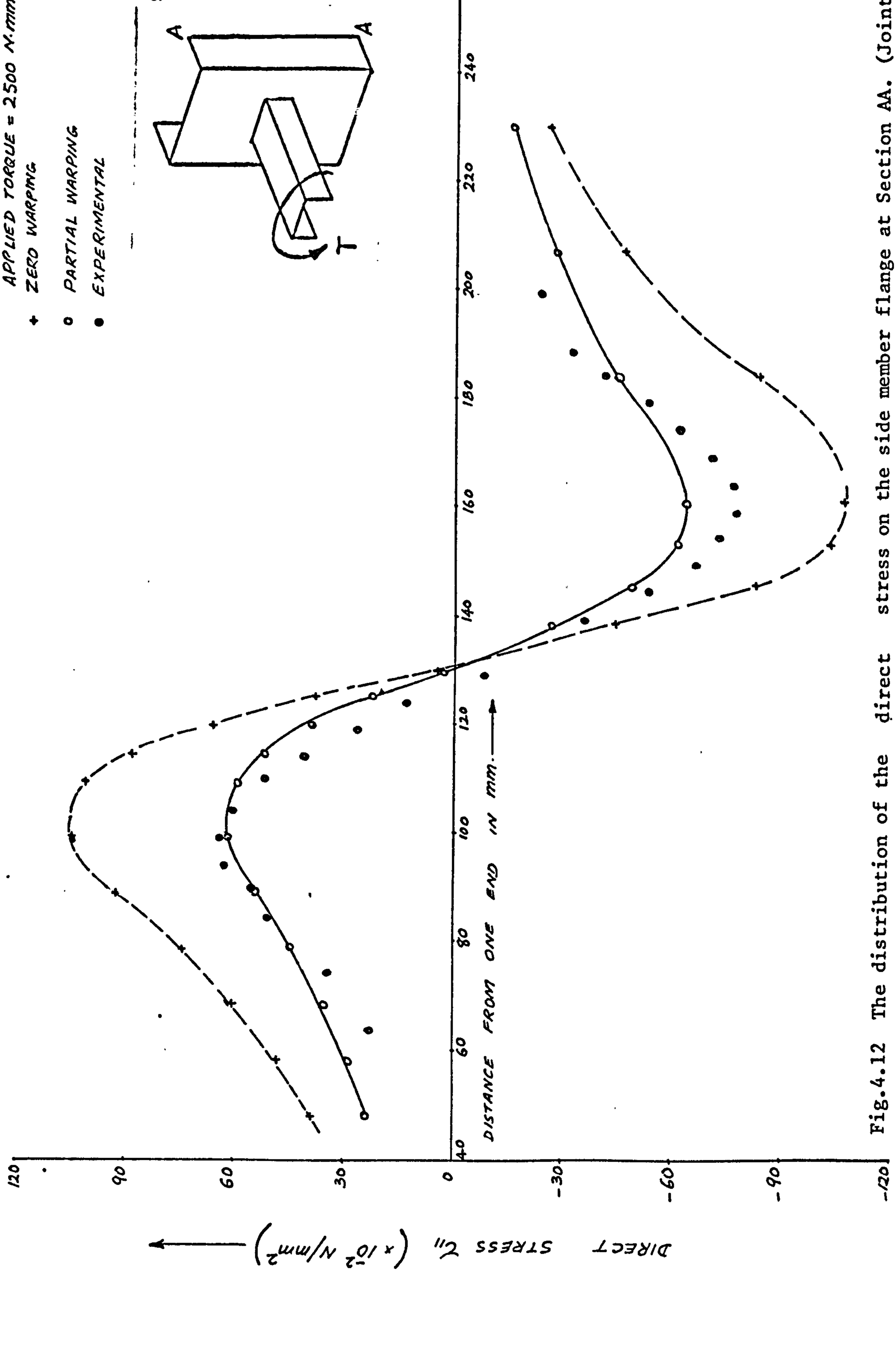

Fig.4.12 The distribution of the direct stress on the side member flange at Section AA. (Joint IV)

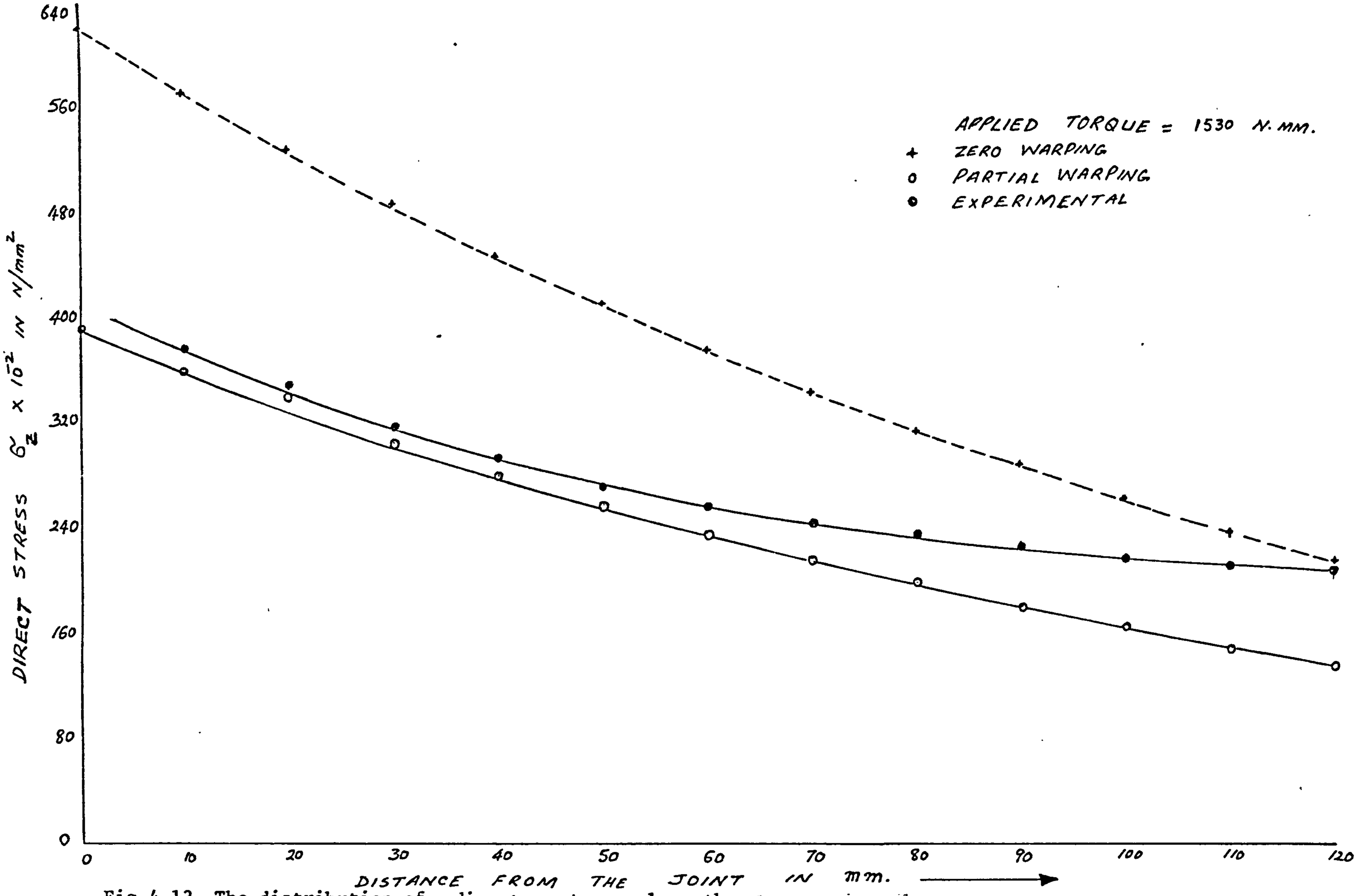

Fig.4.13 The distribution of direct stress along the free edge of the cross member flange (Joint I)

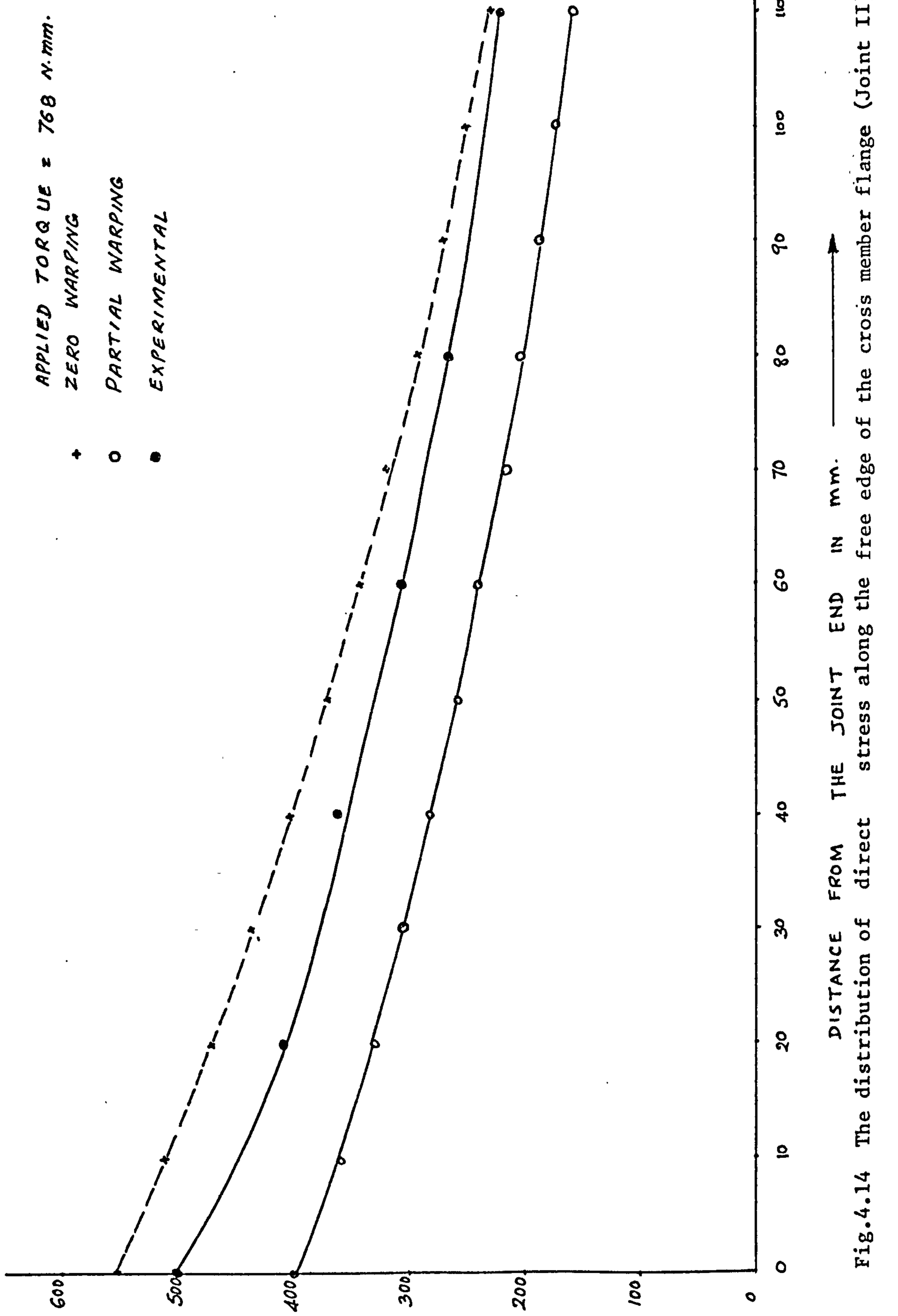

Fig.4.14 The distribution of direct stress along the free edge of the cross member flange (Joint II)

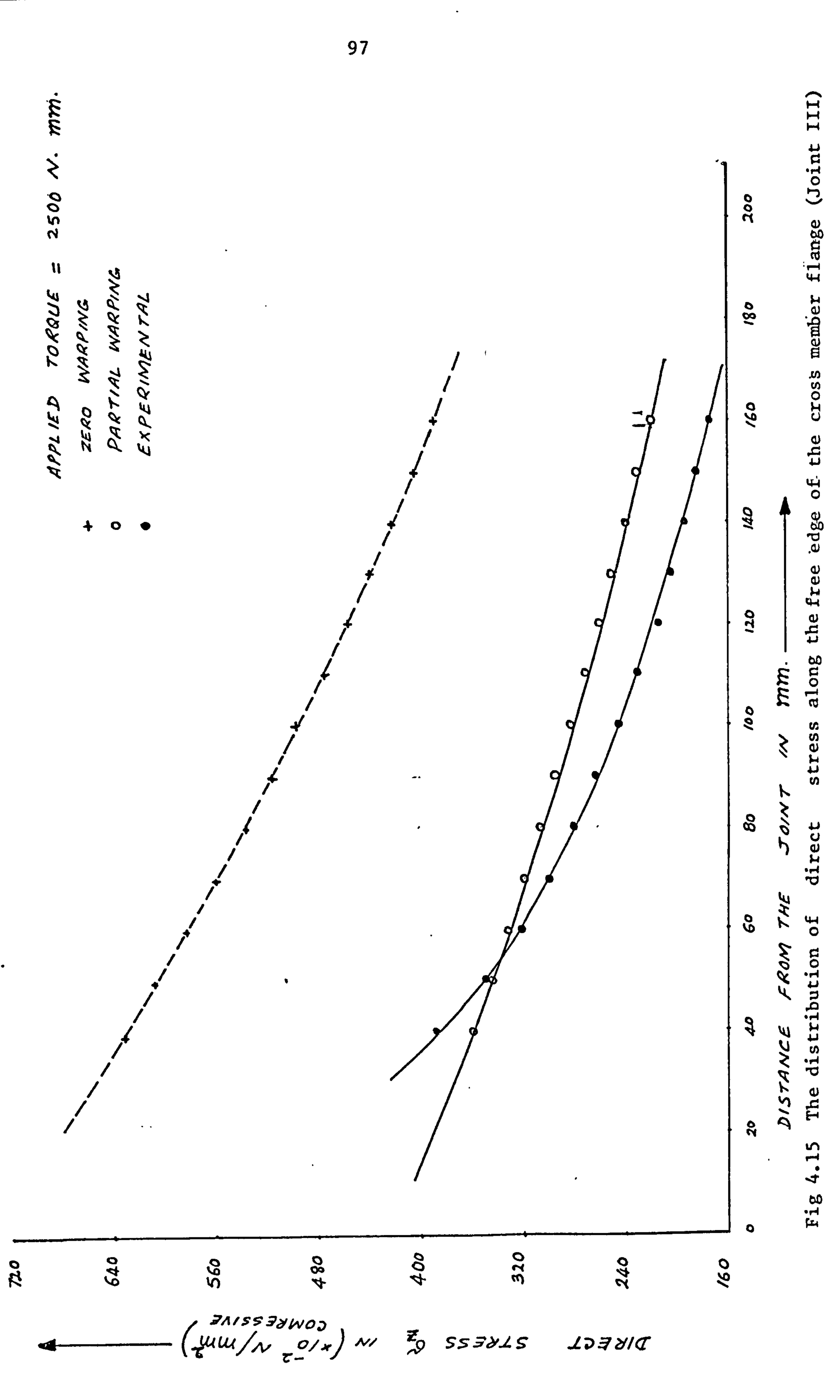

Fig 4.15 The distribution of direct stress along the free edge of the cross member flange (Joint III)

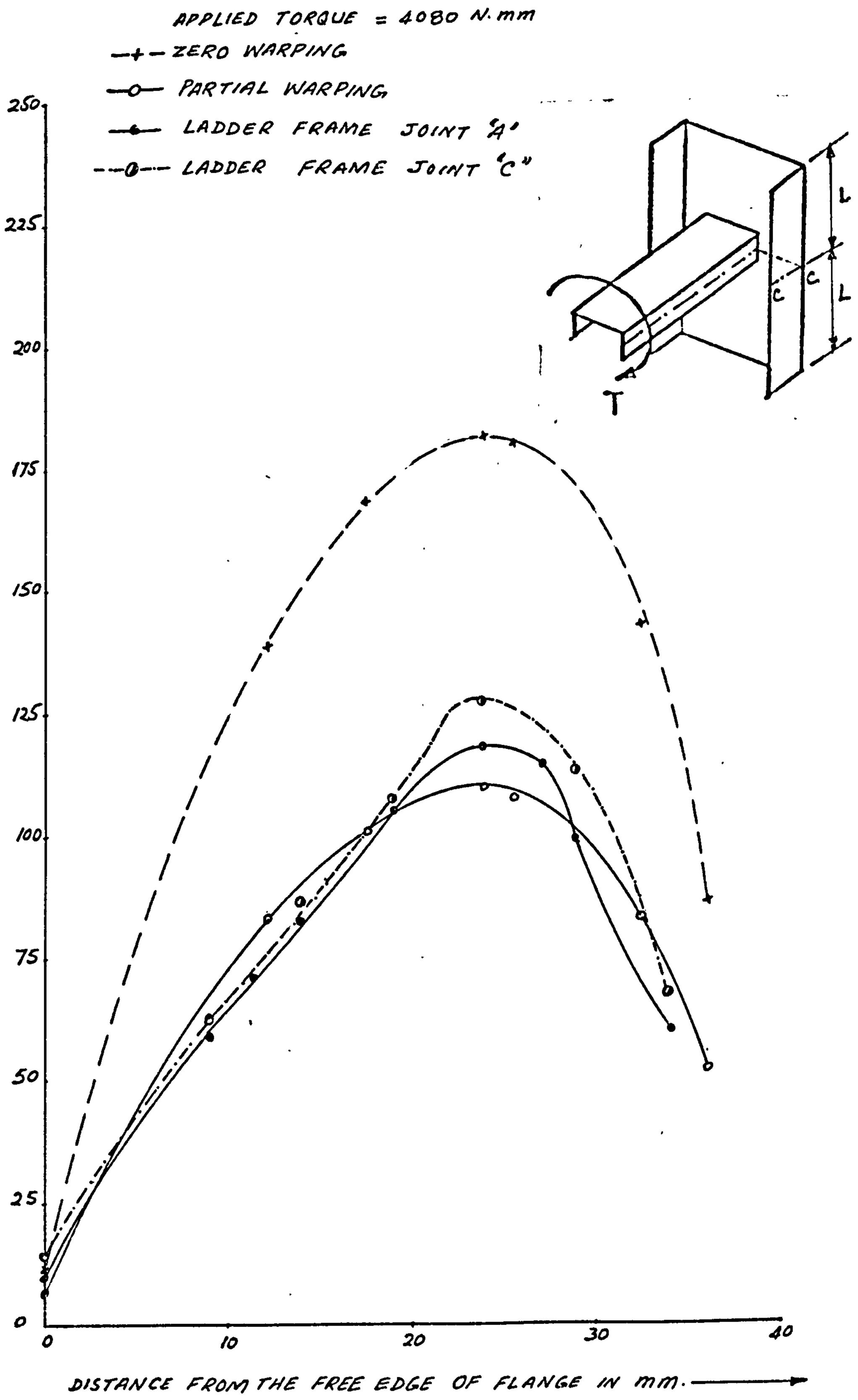

Fig.4.16 The distribution of maximum shear stress on the side member flange at Section CC. (Ladder frame joints)

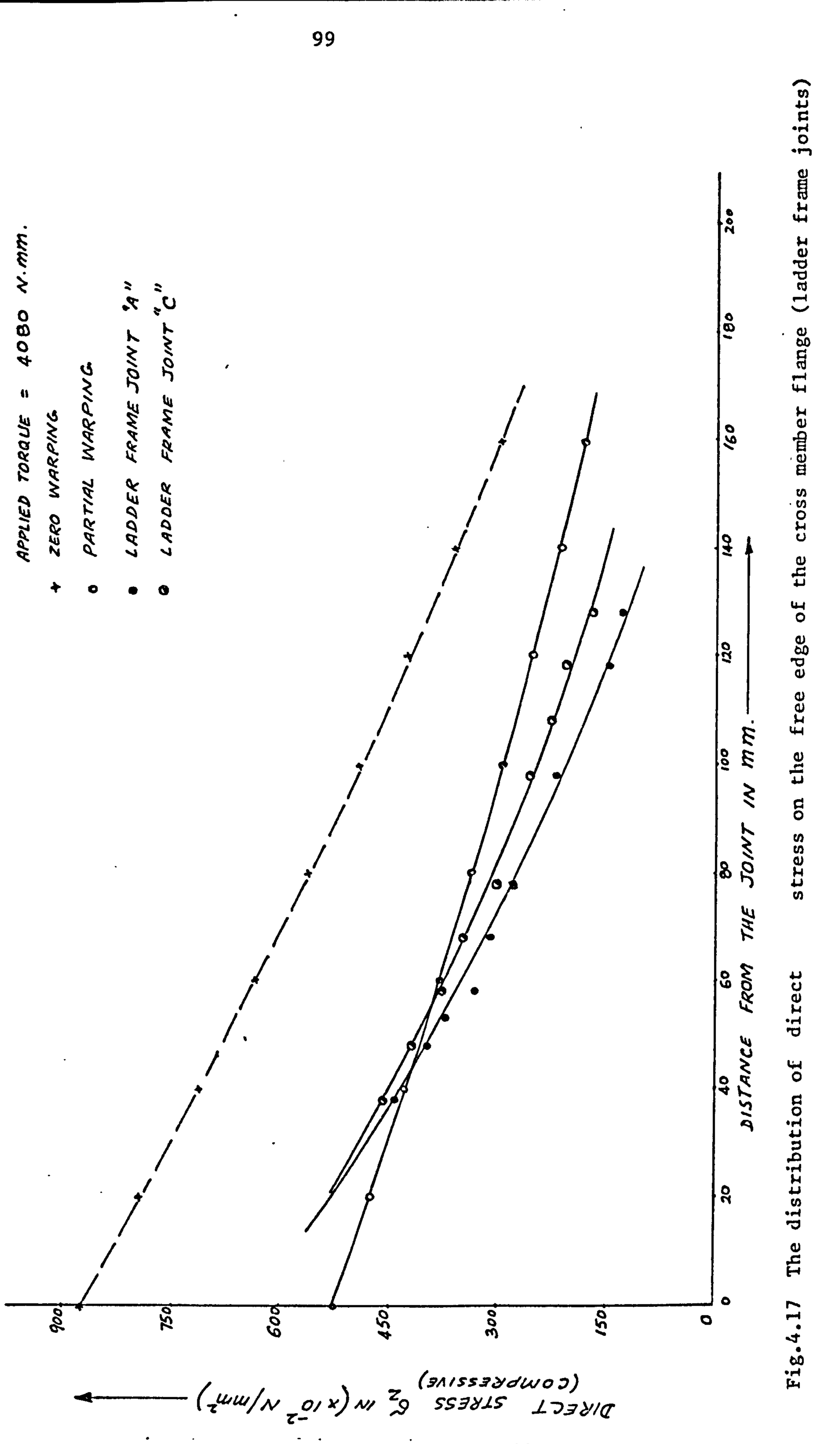

Fig.4.17 The distribution of direct stress on the free edge of the cross member flange (ladder frame joints)

CHAPTER 5 CONCLUSIONS AND FUTURE APPROACH

5.1. CONCLUSIONS

The present work has mainly shown that the plate theory can be successfully applied to analyse the state of stress in a chassis frame joint of a channel section cross member directly attached to the web of a channel section side member. Previously the application of the plate theory was restricted to the analysis of joints consisting of only symmetric I-section cross members attached to the web of the channel section side members. But now joints consisting of asymmetric I-section or channel section cross members can be effectively analysed. The contribution of the channel section cross member web warping forces on the side member in a joint has been included in the present analysis.

A close comparison between the experimental and the analytical estimated values of the maximum shear stress at the critical section of the side member flange clearly indicates that the consideration of partial warping inhibition in welded joints is justified. The degree of partial warping inhibition of the cross member in welded joints can be estimated with a fair accuracy by the proposed analytical approach. It has been shown that the average bending displacement of the side member web can be related to the partial warping of the cross member end in the joint. The relationship between the partial warping constants of the strip beam theory [17] and the finite element method [21] can be used to estimate the cross member warping force exerted to the side member web in a joint. The results have shown in most cases that the prediction of stresses in various members of the joint on the basis of the present approach gave better estimation than other methods.

The effect of the cross member torque on the stress distribution in a side member has been analysed by considering the warping forces and the shear couple forces of the cross member separately by using the plate theory. It was found that the contribution of the couple loading on the stresses in the side member was very small as compared to the cross member warping forces.

The other information provided by the present work can be described as follows:

i) The photoelastic models as employed in this investigation can be used to determine stresses in thin walled open section beams. For problems in which a combined state of stress is expected, photoelastic analysis will lead to the accurate location and measurement of the critical stress.

ii) The critical section where the maximum shear stress attains its peak value in the side member portion of a welded joint lies on the flange in line with the zero warping line on the cross

member flange. The critical region lies on this section near the flange/web corner. The point at which the maximum stress occurs can be located by the present analysis. The distributions of other stress/displacement components on the channel section side member can also be determined by the present analysis.

iii) The length of the side member portion affected by the localised effects of the joint extends on both sides of the joint approximately equal to the sum of the widths of flanges of the cross member and side member.

5.2 SUGGESTIONS FOR FUTURE APPROACH

i) A more sensitive photoelastic model material should be used in future work to obtain better fringe patterns.

ii) The present mathematical model of the joint can be modified to include the effect of other forces acting on the side member, e.g. the longitudinal forces described in [19]. The photoelastic model of the ladder frame used in the present investigation can be used to determine the effect of such forces on the frame.

iii) The present analysis assumes that the cross member is attached with its web vertical to the longitudinal axis of the side member. It is possible to modify it to consider any orientation of the cross member web. It should be modified to include top hat section cross members. This can be achieved by adding terms in the present analysis to represent the warping effect of a top hat section. The warping effect of each part of the section can be represented in a similar manner as shown for a channel section in the present analysis.

REFERENCES

1. VLASOV, V.S. "Thin walled elastic beams"
Israel Programme for Scientific translations, Jerusalem 1961.

2. DOICH, I. "An approach to the calculation of an automobile frame in torsion"
Avtom.Prom. No.6, 1961 (in Ruessian)

3. GELF'GAT,D.B. and OSHOKOV,V.A. "Commercial Vehicle hassis frames"
MASGIZ, 1959 (in Russian)

4. HANKE, M. "Theory of the Monoplane joint (from Thin-walled beams in vehicles")
Part II, Automobile No. 8, 1959 (English translation of Czech original).

5. ZAKS, M. "Calculation of torsional stiffness of commercial vehicle frames with flexible joints"
Autmobile Industry, No.4, 1964 (English translation of Russian original).

6. ZAKS,M. N. and BELOKUROV, V.N. "Investigation of the soft joint layout in a twisted automobile frame"
Avtom. Prom. No.5, 1971 (in Russian)

7. ZAKS,M.N. and BELOKUROV,V. "Control of torsional stiffness of the automobile frame"
Avtom.Prom No.4, 1972 (in Russian)

8. ZAKS,M.N. and BELOKUROV,V. "Bimoment equation in a soft joint of an automobile frame"
Avtom. Prom. No.5, 1973 (in Russian)

9. ZAKS,M.N. and SAHAROV,A.A. and BELOKUROV,V. "Calculation of short open section thin walled beams in Automobile frames"
Avtom.Prom. No.6, 1974 (in Russian)

10. ZAKS,M.N. and ZAHAROV,A.A. "Investigation of the deformation of the chassis frame members".
Avtom. Prom. No.5, 1975 (in Russian)

11. ZAKS,M.N. "Stress state in joints of a twisted automobile frame"
NAMI Proceedings, No.61, 1963 (English translation of Russian original)

12. KOBRIN,M.N. KILIMNIK, L.Sh and TITOV,A.A. "Investigation of the stress state and durability of (vehicle)frame side member walls at the point of load transfer" Avtom.Prom No.11, 1969. (English translation of Russian original).

13. TAKAHASHI,K. "A torsion strength analysis of truck frame using open section members"
SAE No. 710595, 1971.

14. ALI, R. HEDGES.J.L and MILLS,B. "The application of finite element techniques to the analysis of an automobile structure. Static analysis of an automobile chassis frame." Proc. Inst.Mech.E. Vol 185, 1970-1971.

15. HEDGES,J.L., NORVILLE, C.C. & GURDOGAN, O. "The application of finite element to the analysis of an automobile structure. Stress analysis of an automobile chassis frame." Proc. Inst.Mech.E. Vol 185, 1970-1971.

16. ALI, R., HEDGES, J.L. & MILLS, B. "Dynamic analysis of an automobile chassis frame", Proc. I.Mech.E., Vol.185, 1970-71.

17. MARSHALL, P.H., ROACH A.A. and TIDBURY, G.H. "Torsional stiffness of commercial vehicle chassis frames." F.I.S.I.T.A. XII Congress,Barcelona, 1968.

18. AWUDU, G. "Warping inhibitions in the joints of vehicle chassis frames." A.S.A.E. Thesis, Cranfield 1968.

19. TIDBURY, G.H. i) "The torsional stiffness of an open section thin walled beam in terms of bimoments and the generalisation of partial warping inhibition boundary conditions." Motor & Veh.Conf.Belgrade, 1974. ii) Thin walled beam theory in commercial vehicle design. Unpublished report of School of Automotive Studies, Cranfield, 1975.

20. AZODI, K.D. "Effects of longitudinal loads on the stress distribution of open sections." M.Sc. Thesis, Cranfield Institute of Technology, 1977.

21. MEGSON, T.H.G. and ALADE,G.A. "Structural analysis of ladder frames under torsion" Proc. Inst.Mech.E. Vol 190, 1976.

22. ALADE, G.A. "Structural analysis of ladder frames under torsion". Ph.D. Thesis, University of Leeds, 1974.

23. MEGSON,T.H.G. "Extension of the Wagner Torsion Bending Theory to allow for several systems of loading." The Aeronautical Quarterly, Vol XXVI, August, 1975.

24. IVANOV, A.A. "Calculation of automobile frames using finite element methods" Avtom. Prom. No.4, 1973, (in Russian)

25. IVANOV, A.A. "Application of finite element method in the calculation of semi-trailer frames." Avtom. Prom. No.8, 1974 (in Russian)

26. ROMANOW, F., SLOMKA,A and ZABLOCKI, W. — "Calculation of lorry frames, taking into consideration the theory of restrained torsion." Politech. Wrochawskia, IKEM 1976 (in German)

27. BEERMANN, J. — "Calculation of torsion of weak commercial vehicle frames taking into consideration twist-restraint nodes" Automobile Industry, 1976 (in German)

28. KOBRIN, M and GORBONOS, M. — "Determination of Optimum parameter values of truck frames by analysis of the existing designs" Israel Institute of Tech. Haifa, May 1976.

29. LASEVICH, L.G. SKOLNIKOV, M.B. and PODLEGAEVA, T.D. — "Selection of optimum sections of commercial vehicle chassis frames" Avtom. Prom No.2, 1975 (in Russian)

30. TIMOSHENKO, S. WOINOWSKY-KRIEGER, S. — "Theory of Plates and Shells" Edition 2, McGraw-Hill Book Co Inc., 1959.

31. MEGSON,T.G.H. — "Linear analysis of thin walled elastic structurs" Surrey University Press, 1974.

32. CARVER, G.C. — "Truck chassis frame considerations in equipment mounting" S.A.E. No. 760291, 1976

33. ZANDMAN, F., RENDER, S. S. & RIEGNER, E.I. — "Reinforcing effect of birefringent coatings." Exptl.Mech., Vol.2., No.2, 1962.

34. DUFFY, J., and LEE, T.C. — "Measurement of surface strain by means of Bonded Birefringent Strips". Exptl.Mech. Vol.1, No.9, 1961.

35. ALVI, M.S.I. — "Photoelastic analysis of perforated (circular holes) tubes under axial compression" M.A.Sc. Thesis, University of Toronto, 1967.

36. HENDRY, A.W. — "Photoelastic Analysis" st.Edition, Pergamon Press 1966.

37. DALLY, J.W. and RILEY, W.F. — "Experimental stress analysis" McGraw-Hill Book Co, 1965.

38. Instruction manual for large field universal meter. Bulletin PS-3043, BUDD, S.A. Comp. U.S.A.

39. ROACH, A.H. — "Warping inhibition in commercial vehicle frames." A.S.A.E. Cranfield, 1966.

40. "Process for Casting Araldite CT200 Sheets for Photoelastic Purposes." Instruction Sheet. Sharples Ltd.

41. "Materials for Photoelastic Coatings and Photoeslastic Midels." Bulletin P-1120-1 Photolastic Inc. Pa. U.S.A.

42. "Notes on a technique for fabricating Araldite Models constructed from Araldite CT200 Sheets." Instruction Sheet, Sharples Ltd.

APPENDIX I

GENERAL BENDING PROBLEM OF A RECTANGULAR PLATE

Consider a rectangular flat plate of uniform thickness h referred to a cartesian co-ordinate system as shown in fig. (2.1a). The x_1x_2-plane coincides with the mid plane of the plate. The plate is subjected to some forces which are perpendicular to its mid plane only. The plate will bend due to the action of these forces.

The deflection of the middle surface of this plate can be determined by taking into account Kirchhoff's assumptions [30].

The expressions for moments "m_{ij}" and vertical shearing forces "q_i" are given below in indicial notation.

Moments

$$m_{ij} = \int_{-h/2}^{+h/2} \tau_{ij}\, x_3 dx_3 \qquad \begin{matrix}(i = 1,2)\\(j = 1,2)\end{matrix} \qquad \text{(AI.1)}$$

Vertical Shearing forces

$$q_i = \int_{-h/2}^{+h/2} \tau_{i3}\, dx_3 \qquad \text{(AI.2)}$$

Displacement, strain and stress fields can be expressed by the following equations

$$\left.\begin{aligned} u_i\ (x_1,x_2,x_3) &= u_i^o(x_1,x_2) - x_3\frac{\partial u_3}{\partial x_i}(x_1, x_2) \\ u_3\ (x_1,x_2,x_3) &= u_3(x_1,x_2) \end{aligned}\right\} \qquad \text{(AI.3)}$$

$$\varepsilon_{ij} = \varepsilon^o_{ij} - x_3 K_{ij} \qquad \text{(AI.4)}$$

where

$$\overset{o}{\varepsilon}_{ij} = \tfrac{1}{2}(u^o_{i,j} + u^o_{j,i})$$

$$K_{ij} = u_{3,ij}$$

$$\tau_{ij} = \frac{E}{(1-\nu^2)}\left[\{(1-\nu)\varepsilon^o_{ij} + \nu\delta_{ij}\varepsilon^o_{kk}\} - \{(1-\nu)K_{ij} + \nu\delta_{ij}K_{kk}\}x_3\right] \qquad \text{(AI.5)}$$

Substitution of equation (AI.5) in equations (AI.1) gives the following expression for moments:

$$\begin{aligned} m_{ij} &= -D\left[(1-\nu)K_{ij} + \nu\delta_{ij}K_{kk}\right] \\ &= -D\left[(1-\nu)u_{3,ij} + \nu\delta_{ij}u_{3,kk}\right] \end{aligned} \qquad \text{(AI.6)}$$

It is easy to obtain the following expression for q_i after integrating the equilibrium equations in the absence of body forces.

$$q_i = -D \frac{\partial}{\partial x_i} (\nabla^2 u_3) \qquad \text{(AI.7)}$$

where $D = \frac{Eh^3}{12(1-\nu^2)}$ is called the Bending Rigidity of the plate.

The resultant vertical shearing forces become

$$\left.\begin{aligned} v_1 &= q_1 - m_{12,2} \\ v_2 &= q_2 - m_{12,1} \end{aligned}\right\} \qquad \text{(AI.8)}$$

The positive signs for moments and vertical shearing forces are taken according to fig. (2.1b).

The governing equation of the bending problem of a plate in the absence of the external forces can be expressed as

$$\nabla^4 u_3 = 0 \qquad \text{(AI.9)}$$

This equation has to be solved for any particular problem and the boundary conditions have to be satisfied. The external forces have to be accounted for while satisfying the boundary conditions of the problem.

RECTANGULAR PLATE WITH TWO SIMPLY SUPPORTED EDGES

The bending problem of a rectangular plate with two simply supported parallel edges can be solved by assuming a solution of the governing equation (AI.9) in the form of a single trigonometric Fourier series as

$$u_3(x_1,x_2) = \sum_{m=1}^{\infty} W_m(x_2) \sin \alpha_m x_1 \quad (\text{where } \alpha_m = \frac{m\pi}{2L}) \qquad \text{(AI.10)}$$

Equation (AI.10) satisfies the boundary conditions along the two simply supported edges of the plate as shown in fig.(2.1a). The boundary conditions along the two edges can be written as below:

$$\left.\begin{aligned} &1 \quad \text{Along the edge } x_1 = 0 \\ &\qquad m_{11} = 0 \\ &\qquad u_3 = 0 \\ &2 \quad \text{Along the edge } x_1 = 2L \\ &\qquad m_{11} = 0 \\ &\qquad u_3 = 0 \end{aligned}\right\} \qquad \text{(AI.11)}$$

Equation (AI.10) should now satisfy the governing equation (AI.9), which takes the following form on substitution of equation (AI.10).

$$\frac{\partial^4 W_m}{\partial x_2^4} - 2\alpha_m^2 \frac{\partial^2 W_m}{\partial x_2^2} + \alpha_m^4 W_m = 0 \qquad \text{(AI.12)}$$

Equation (AI.12) is a fourth order ordinary homogeneous differential equation whose general solution can be written in the following form.

$$W_m(x_2) = c_1 \cosh\alpha_m x_2 + c_2 x_2 \cosh\alpha_m x_2 + c_3 \sinh\alpha_m x_2 + c_4 x_2 \sinh\alpha_m x_2$$

$$\text{or} \quad W_m(x_2) = c_1\phi_1 + c_2\phi_3 + c_3\phi_2 + c_4\phi_4 \qquad \text{(AI.13)}$$

$$\left.\begin{aligned} \text{where} \quad \phi_1 &= \cosh \alpha_m x_2 \qquad \phi_3 = x_2 \cosh \alpha_m x_2 \\ \phi_2 &= \sinh \alpha_m x_2 \qquad \phi_4 = x_2 \sinh \alpha_m x_2 \end{aligned}\right\} \qquad \text{(AI.14)}$$

c_1, c_2, c_3 and c_4 are constants which have to be determined from the four boundary conditions along the edges $x_2 = 0$ and $x_2 = 2H$ of the plate.

Once W_m is known, its value can be substituted in the relevant formulae to obtain the values of plate deflection, moments, vertical shearing forces and resultant vertical shearing forces. If the bending moment m_{22}, the angle of twist along x_2 i.e. $\theta = \partial u_3/\partial x_2$ and the resultant vertical shearing force v_2 are assumed as single trigonometric Fourier series of the following forms:

$$m_{22}(x_1,x_2) = \sum_{m=1}^{\infty} M_{2m}(x_2) \sin \alpha_m x_1 \qquad \text{(AI.15)}$$

$$\theta(x_1,x_2) = \sum_{m=1}^{\infty} \Theta_m(x_2) \sin\alpha_m x_1 \qquad \text{(AI.16)}$$

$$v_2(x_1,x_2) = \sum_{m=1}^{\infty} V_{2m}(x_2) \sin\alpha_m x_1 \qquad \text{(AI.17)}$$

The corresponding expressions for m_{22}, θ and v_2 can be obtained in the following form on substitution of equation (AI.13) in the relevant formulae

$$m_{22}(x_1,x_2) = \sum_{m=1}^{\infty} -D\Big[\big[2\alpha_m c_4 + \alpha_m^2(1-\nu)c_1\big]\phi_1 + \alpha_m^2(1-\nu)c_2\phi_3 + \big[2\alpha_m c_2 + \alpha_m^2(1-\nu)c_3\big]\phi_2 + \alpha_m^2(1-\nu)c_4\phi_4\Big] \sin \alpha_m x_1 \qquad \text{(AI.18)}$$

$$\theta(x_1,x_2) = \sum_{m=1}^{\infty} \big[(c_2 + \alpha_m c_3)\phi_1 + \alpha_m c_4\phi_3 + (c_4+\alpha_m c_1)\phi_2 + \alpha_m c_2\phi_4\big]\sin\alpha_m x_1$$

(AI.19)

$$v_2(x_1,x_2) = \sum_{m=1}^{\alpha} -\alpha_m^2 D \{[(1+\nu)c_2 - \alpha_m(1-\nu)c_3]\phi_1 - \alpha_m(1-\nu)c_4\phi_3$$

$$[(1+\nu)c_4 - \alpha_m(1-\nu)c_1]\phi_2 - \alpha_m(1-\nu)c_2\phi_4\}\sin(\alpha_m x_1) \qquad \text{(AI.20)}$$

The values of the Fourier coefficients $M_{2m}(x_2)$, $\Theta_m(x_2)$ and $V_{2m}(x_2)$ can be determined by equating equations (AI.15) and (AI.18), equations (AI.16) and (AI.19) and equations (AI.17) and (AI.20) respectively.

The equations for deflection, moments, resultant shearing forces and angle of twist can be represented in terms of four initial parameters of the plate defined along the edge $x_2 = 0$.

The initial parameters chosen are $\overset{o}{W}$, $\overset{o}{M}_2$, $\overset{o}{\Theta}$ and $\overset{o}{V}_2$, and their values can be obtained in the following form by substituting $x_2 = 0$ in in the expressions for $W_m(x_2)$, $M_{2m}(x_2)$, $\Theta_m(x_2)$ and $V_{2m}(x_2)$

$$\left.\begin{aligned} \overset{o}{W} &= c_1 \\ \overset{o}{M}_2 &= -D[\alpha_m(1-\nu)c_1 + 2\alpha_m c_4] \\ \overset{o}{\Theta} &= c_2 + \alpha_m c_3 \\ \overset{o}{V}_2 &= -D[\alpha_m^2(1+\nu)c_2 - \alpha_m^3(1-\nu)c_3] \end{aligned}\right\} \qquad \text{(AI.21)}$$

Equations (AI.21) can be solved for c_1, c_2, c_3 and c_4 in terms of the initial parameters giving the following relations:

$$\left.\begin{aligned} c_1 &= \overset{o}{W} \\ c_2 &= \frac{(1-\nu)}{2}\overset{o}{\Theta} - \frac{1}{2\alpha_m^2 D}\overset{o}{V}_2 \\ c_3 &= \frac{(1+\nu)}{2\alpha_m}\overset{o}{\Theta} + \frac{1}{2\alpha_m^3 D}\overset{o}{V}_2 \\ c_4 &= -\frac{1}{2\alpha_m D}\overset{o}{M}_2 - \frac{\alpha_m(1-\nu)}{2}\overset{o}{W} \end{aligned}\right\} \qquad \text{(AI.22)}$$

Now the Fourier coefficients $W_m(x_2)$, $\Theta_m(x_2)$, $M_{2m}(x_2)$ and $V_{2m}(x_2)$ can be expressed in terms of the initial parameters by the following equations after substituting the values of the constants c_1, c_2, c_3 and c_4 from equations (AI.22).

$$W_m(x_2) = [\phi_1 - a\alpha_m\phi_4]\overset{o}{W} + \left[\frac{b\phi_2}{\alpha_m} + a\phi_3\right]\overset{o}{\Theta}$$

$$- \left[\xi\frac{\phi_4}{\alpha_m}\right]\overset{o}{M}_2 + \left[\xi\frac{\phi_2}{\alpha_m^3} - \xi\frac{\phi_3}{\alpha_m^2}\right]\overset{o}{V}_2 \qquad \text{(AI.23a)}$$

$$\theta_m(x_2) = [b\alpha_m\phi_2 - a\alpha_m^2\phi_3]\overset{o}{W} + [\phi_1 + a\alpha_m\phi_4]\overset{o}{\theta}$$

$$- [\xi\frac{\phi_2}{\alpha_m} + \xi\phi_3]\overset{o}{M}_2 - [\xi\frac{\phi_4}{\alpha_m}]\overset{o}{V}_2 \qquad \text{(AI.23b)}$$

$$M_{2m}(x_2) = [\delta\alpha_m\phi_4]\overset{o}{W} - [\eta\phi_2 + \delta\phi_3]\overset{o}{\theta}$$

$$+ [\phi_1 + a\alpha_m\phi_4]\overset{o}{M}_2 + [\frac{b\phi_2}{\alpha_m} + a\phi_3]\overset{o}{V}_2 \qquad \text{(AI.23c)}$$

$$V_{2m}(x_2) = [\eta\alpha_m^2\phi_2 - \alpha_m^2\phi_3]\overset{o}{W} + [\delta\alpha_m\phi_4]\overset{o}{\theta}$$

$$+ [b\alpha_m\phi_2 - a\alpha_m^2\phi_3]\overset{o}{M}_2 + [\phi_1 - a\alpha_m\phi_4]\overset{o}{V}_2 \qquad \text{(AI.23d)}$$

where

$$\left.\begin{aligned} a &= \frac{1+\nu}{2} \\ b &= \frac{1-\nu}{2} \\ \xi &= \frac{6(1-\nu^2)}{Eh^3} \\ \eta &= \frac{Eh^3\alpha_m(3+\nu)}{24(1+\nu)} \\ \delta &= \frac{Eh^3\alpha_m^2(1-\nu)}{24(1+\nu)} \end{aligned}\right\} \qquad \text{(AI.24)}$$

are constants.

APPENDIX II

GENERAL STRETCHING PROBLEM OF A RECTANGULAR PLATE

Consider a rectangular plate as shown in fig. 2.1a being subjected to forces which are acting in the plane of the plate. The plate will deform in its own plane. This problem is known as a stretching problem.

This problem can be formulated in terms of displacements from the basic equations of theory of plates which are summarised below in indicial notation.

1 Equilibrium equations in X_i direction:

$$n_{ij,j} + s_i + g_i = 0 \qquad \text{For } i = 1,2;\ j = 1,2 \qquad \text{(AII.1)}$$

where

$$s_i = \tau_{33} \Big|_{\text{at}-\frac{h}{2}}^{\text{at}\ \frac{h}{2}}$$

$$g_i = \int_{-\frac{h}{2}}^{+\frac{h}{2}} F_i dx_3$$

Fig (2.1c) shows the sign convention for in-plane forces on the plate.

2 Constitutive equations:

$$n_{ij} = B\left[\varepsilon^o_{ij}(1-\nu) + \delta_{ij}\,\varepsilon^o_{kk}\right] \qquad \text{(AII.2)}$$

where

$B = \frac{Eh}{(1-\nu^2)}$ is known as Plate Stretching Rigidity.

3 Strain displacement relations:

$$\varepsilon^o_{ij} = \tfrac{1}{2}\left[u^o_{i,j} + u^o_{j,i}\right] \qquad \text{(AII.3)}$$

where u^o_i and ε^o_{ij} are displacements and strains of the mid plane of the plate respectively.

4 Compatibility equations:

$$\varepsilon^o_{11,22} + \varepsilon^o_{22,11} - 2\varepsilon^o_{12,12} = 0 \qquad \text{(AII.4)}$$

Substituting equation (AII.3) in equation (AII.2) and then the resulting equation in equation (AII.1), the following system of coupled equations is obtained:

$$u^o_{1,11} + \frac{(1-\nu)}{2} u^o_{1,22} + \frac{(1+\nu)}{2} u^o_{2,12} = 0 \qquad \text{(AII.5)}$$

$$\frac{(1-\nu)}{2} u^o_{2,11} + u^o_{2,22} + \frac{(1+\nu)}{2} u^o_{1,12} = 0 \qquad \text{(AII.6)}$$

These coupled equations have to be solved for any particular problem subject to the prescribed boundary conditions. The external forces have to be considered while satisfying the boundary conditions.

RECTANGULAR PLATE WITH HINGED SUPPORTS

For a rectangular plate with hinged supports at the two ends and defined by the following conditions

$$\left.\begin{array}{l} \text{At } x_1 = 0 \text{ and } x_1 = 2L \\ \tau_{11} = 0 \quad \text{(i.e. no axial force at the ends)} \\ \phi = 0 \quad \text{(i.e. twist angle is zero)} \end{array}\right\} \qquad \text{(AII.7)}$$

These conditions lead to the following boundary conditions at the two ends:

$$\left.\begin{array}{l} \text{At } x_1 = 0 \text{ and } x_1 = 2L \\ \dfrac{\partial u_1}{\partial x_1} = 0 \quad \text{and} \quad u_2 = 0 \end{array}\right\} \qquad \text{(AII.8)}$$

The boundary conditions (AII.8) are satisfied if the displacement components u_1 and u_2 are assumed of the following forms:

$$\left.\begin{array}{l} u_1(x_1, x_2) = \sum_{m=1}^{\infty} U_m(x_2) \cos\alpha_m x_1 \\ u_2(x_1, x_2) = \sum_{m=1}^{\infty} V_m(x_2) \sin\alpha_m x_1 \end{array}\right\} \qquad \text{(AII.9)}$$

where $\alpha_m = \dfrac{m\pi}{2L}$

On substitution of equations (AII.9) in equations (AII.5) and (AII.6) following equations are obtained.

$$\left.\begin{array}{l} -2\alpha_m^2 U_m + (1-\nu)\dfrac{\partial^2 U_m}{\partial x_2^2} + (1+\nu)\alpha_m \dfrac{\partial V_m}{\partial x_2} = 0 \\ 2\dfrac{\partial^2 V_m}{\partial x_2^2} - (1-\nu)\alpha_m^2 V_m - (1+\nu)\alpha_m \dfrac{\partial U_m}{\partial x_2} = 0 \end{array}\right\} \qquad \text{(AII.10)}$$

Solving the two equations (AII.7) for U_m results in the following single equation.

$$\frac{\partial^4 U_m}{\partial x_2^4} - 2\alpha_m^2 \frac{\partial^2 U_m}{\partial x_2^2} + \alpha_m^4 U_m = 0 \qquad \text{(AII.11)}$$

Equation (AII.8) is an ordinary homogeneous differential equation of fourth order and its solution is given below:

$$U_m(x_2) = c_1 \cosh\alpha_m x_2 + c_2 x_2 \cosh\alpha_m x_2 + c_3 \sinh\alpha_m x_2 + c_4 x_2 \sinh\alpha_m x_2$$

This solution can be written in the following form by substituting relations (AI.14).

$$U_m(x_2) = c_1\phi_1 + c_2\phi_3 + c_3\phi_2 + c_4\phi_4 \qquad \text{(AII.12)}$$

The constants c_1, c_2, c_3 and c_4 are to be determined from the boundary conditions along the other two edges of the plate. Then the displacements/stresses/forces can be evaluated on the plate by substitution of equations (AII.9) in the relevant formulae.

It becomes easy to evaluate various results if the initial parameters of the plate are specified along the edge $x_2 = 0$. It is necessary to express all the resulting equations in terms of the initial parameters. Fourier coefficient $V_m(x_2)$ can be expressed as

$$V_m(x_2) = \left[\frac{(\nu-3)}{(1+\nu)\alpha_m} c_2 + c_3\right]\phi_1 + \left[c_1 + \frac{(\nu-3)}{(1+\nu)\alpha_m} c_4\right]\phi_2 + c_4\phi_3 + c_2\phi_4 \qquad \text{(AII.13)}$$

Force components n_{22} and n_{12} can be determined by substituting equations (AII.9, 11 and 13) in equations (AII.1) and the following results are obtained:

$$n_{22}(x_1,x_2) = B\sum_{m=1}^{\infty}\Big(\left[\alpha_m(1-\nu)c_1 - \frac{2(1-\nu)}{(1+\nu)} c_4\right]\phi_1 + \alpha_m(1-\nu)c_2\phi_3 + \left[\alpha_m(1-\nu)c_3 - \frac{2(1-\nu)}{(1+\nu)}c_2\right]\phi_2 + \alpha_m(1-\nu)c_4\phi_4\Big) \sin\alpha_m x_1 \qquad \text{(AII.14)}$$

$$n_{12}(x_1,x_2) = B(1-\nu)\sum_{m=1}^{\infty}\Big(\left[\alpha_m c_3 - \frac{(1-\nu)}{(1+\nu)}c_2\right]\phi_1 + \left[\alpha_m c_1 - \frac{(1-\nu)}{(1+\nu)}c_4\right]\phi_2 + \alpha_m c_4\phi_3 + \alpha_m c_2\phi_4\Big)\cos\alpha_m x_1 \qquad \text{(AII.15)}$$

Equations (AII.14) and (AII.15) can be expressed in simple forms as

$$n_{22}(x_1,x_2) = \sum_{m=1}^{\infty} N_{22m}(x_2) \sin\alpha_m x_1$$

and

$$n_{12}(x_1,x_2) = \sum_{m=1}^{\infty} N_{12m}(x_2) \cos\alpha_m x_1 \qquad \text{(AII.16)}$$

The Fourier coefficients N_{22m} and N_{12m} can be evaluated by comparing the coefficients of equations (AII.16) and equations (AII.14,15) for N_{22} and N_{12} respectively. Four initial parameters are prescribed at $x = 0$ which are $\overset{o}{U}$, $\overset{o}{V}$, $\overset{o}{N}_{22}$ and $\overset{o}{N}_{12}$. Their values can be obtained as follows by substituting $x_2 = 0$ in the respective Fourier coefficients:

$$\left.\begin{aligned}
\overset{o}{U} &= c_1 \\
\overset{o}{V} &= \left[\frac{(\nu-3)}{\alpha_m(1+\nu)} c_2 + c_3\right] \\
\overset{o}{N}_{22} &= B\left[\alpha_m(1-\nu)\, c_1 - \frac{2(1-\nu)}{(1+\nu)} c_4\right] \\
\overset{o}{N}_{12} &= B(1-\nu)\left[\alpha_m c_3 - \frac{(1-\nu)}{(1+\nu)} c_2\right]
\end{aligned}\right\} \quad \text{(AII.17)}$$

Constants c_1, c_2, c_3 and c_4 can be expressed in terms of initial parameters as follows:

$$\left.\begin{aligned}
c_1 &= \overset{o}{U} \\
c_2 &= \frac{(1+\nu)^2}{2Eh} \overset{o}{N}_{12} - \frac{\alpha_m(1+\nu)}{2} \overset{o}{V} \\
c_3 &= \frac{(1+\nu)(3-\nu)}{2Eh\alpha_m} \overset{o}{N}_{12} - \frac{(1-\nu)}{2} \overset{o}{V} \\
c_4 &= \frac{\alpha_m(1+\nu)}{2} \overset{o}{U} - \frac{(1+\nu)}{2Eh} \overset{o}{N}_{22}
\end{aligned}\right\} \quad \text{(AII.18)}$$

Now Fourier coefficients $U_m(x_2)$, $V_m(x_2)$, $N_{22m}(x_2)$ and $N_{12m}(x_2)$ can be expressed in terms of the initial parameters through equations (AII.18) in the following forms:

$$U_m(x_2) = \left[\phi_1 + b\alpha_m\phi_4\right]\overset{o}{U} - \left[a\phi_2 + b\alpha_m\phi_3\right]\overset{o}{V} - \left[c\phi_4\right]\overset{o}{N}_{22} + \left[\frac{d\phi_2}{\alpha_m} + c\,\phi_3\right]\overset{o}{N}_{12} \quad \text{(AII.19a)}$$

$$V_m(x_2) = \left[-a\phi_2 + b\alpha_m\phi_3\right]\overset{o}{U} + \left[\phi_1 - b\alpha_m\phi_4\right]\overset{o}{V} + \left[\frac{d\phi_2}{\alpha_m} - c\phi_3\right]\overset{o}{N}_{22} + \left[c\phi_4\right]\overset{o}{N}_{12} \quad \text{(AII.19b)}$$

$$N_{22m}(x_2) = \left[f\alpha_m\phi_4\right]\overset{o}{U} + \left[f\phi_2 - f\alpha_m\phi_3\right]\overset{o}{V} + \left[\phi_1 - b\alpha_m\phi_4\right]\overset{o}{N}_{22} + \left[a\phi_2 + b\alpha_m\phi_3\right]\overset{o}{N}_{12} \quad \text{(AII.19c)}$$

$$N_{12m}(x_2) = \left[f\phi_2 + f\alpha_m\phi_3\right]\overset{o}{U} - \left[f\alpha_m\phi_4\right]\overset{o}{V} + \left[a\phi_2 - b\alpha_m\phi_3\right]\overset{o}{N}_{22} + \left[\phi_1 + b\alpha_m\phi_4\right]\overset{o}{N}_{12} \qquad \text{(AII.19d)}$$

where

$$\left.\begin{aligned} a &= \frac{1-\nu}{2} \\ b &= \frac{1+\nu}{2} \\ c &= \frac{(1+\nu)^2}{2Eh} \\ d &= \frac{(1+\nu)(3-\nu)}{2Eh} \\ f &= \frac{Eh\alpha_m}{2} \end{aligned}\right\} \qquad \text{(AII.20)}$$

$n_{11}(x_1,x_2)$ can be expressed in the following form:

$$n_{11}(x_1,x_2) = \sum_{m=1}^{\infty} N_{11m}(x_2)\sin\alpha_m x \qquad \text{(AII.21)}$$

where Fourier coefficient $N_{11m}(x_2)$ can be evaluated in terms of the initial parameters as given below:

$$N_{11m}(x_2) = Eh\left(-\left[\alpha_m\overset{o}{U} + \frac{\nu}{Eh}\overset{o}{N}_{22}\right]\phi_1 + \left[\frac{\alpha_m}{2}\overset{o}{V} - \frac{(3+\nu)}{2Eh}\overset{o}{N}_{12}\right]\phi_2 + \left[\frac{\alpha_m^2}{2}\overset{o}{V} - \frac{b\alpha_m}{Eh}\overset{o}{N}_{12}\right]\phi_3 + \left[-\frac{\alpha_m^2}{2}\overset{o}{U} + \frac{b\alpha_m}{Eh}\overset{o}{N}_{22}\right]\phi_4\right) \qquad \text{(AII.22)}$$

APPENDIX III

FLOW CHARTS

PLATE BENDING SOLUTION

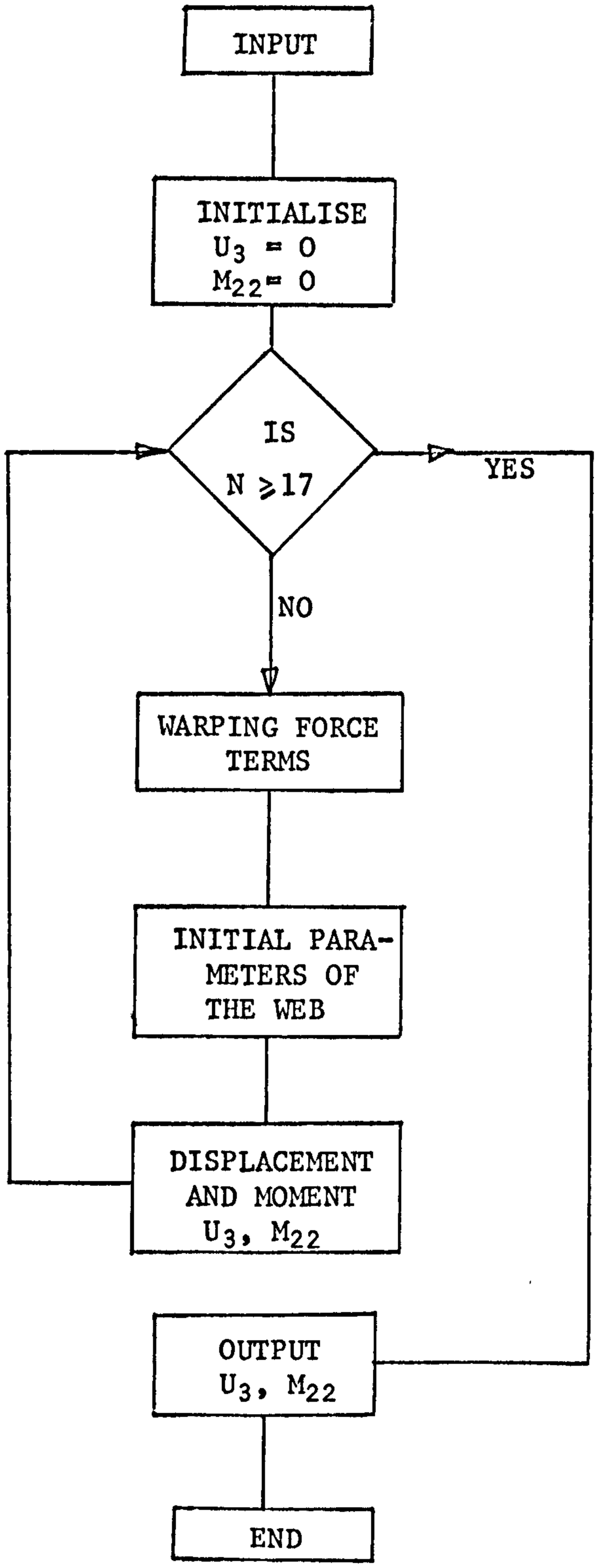

PLATE THEORY SOLUTION

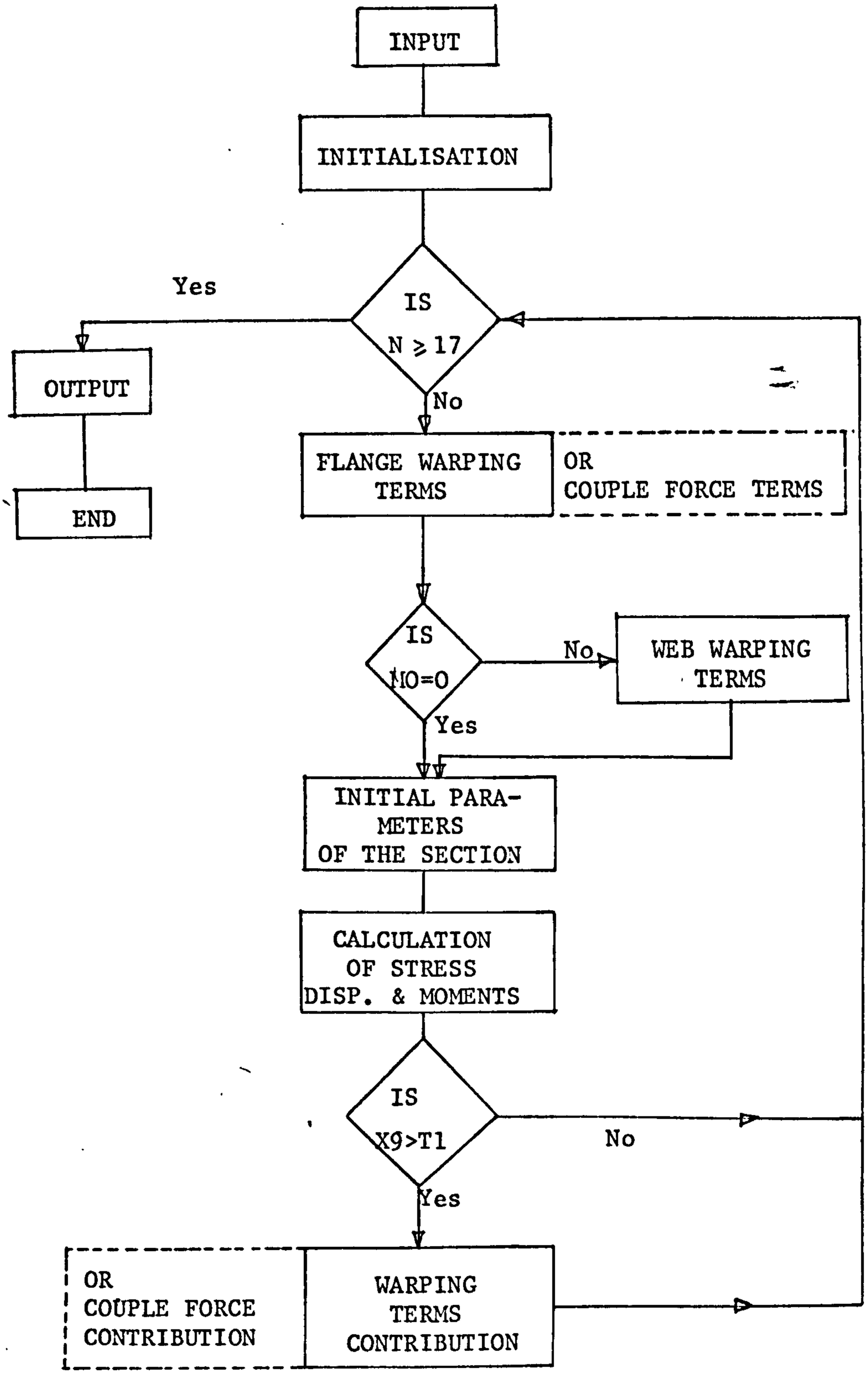

APPENDIX IV

PREPARATION OF PHOTOELASTIC MODELS

Photoelastic models of channel sections were made from CT 200 Araldite by two different methods which are described below.

i) FABRICATED PHOTOELASTIC MODELS

Sheets of CT 200 Araldite were obtained from Sharples Photomechanic Ltd. They were available in $\frac{1}{8}$inch thickness or more as desired. The maximum size of the sheet obtainable from the above source was approximately 16" x 12".

A chamel section was made by cutting three strips (two for the flanges and one for the web of a channel section) which were bonded together with Araldite adhesive to form the required section. Later two similarly fabricated channel sections were bonded together to obtain a model of a joint in which a channel section representing a part of a cross member is attached to the web of another channel section representing a part of a side member. The purpose of this exercise was to study the feasibility of the method of fabricating photoelastic models needed in the present experimental work.

It was considered that the photoelastic models fabricated in this way would save time and labour. But the experience showed that finishing and smoothing of the straight edges of strips cut from a large sheet was a laborious job. The dimensional accuracy of a section could only be maintained if the edges of the strips were perfectly straight and smooth before bonding with Araldite adhesive. Strips were cut by jig saw and the edges were later smoothed by filing. During the bonding process it was noticed that it was difficult to ensure a uniform layer of adhesive in a joint of such a long length (approximately 16in. Some portion of the joint could be starved of adhesive thus resulting in an unreliable joint.

The models made by this fabrication method did not prove very reliable as joints were broken during testing. Fabrication of channel sections of lengths larger than 16 inches was not possible as the supplied sheet size did not permit this. These limitations led to the decision to casting channel sections.

ii) CAST PHOTOELASTIC MODELS

The major portion of the experimental work was conducted on photo-elastic models made from cast channel sections. The success of a photo-elastic investigation mainly depends on the proper manufacture of good photoelastic models which are free from residual birefringence. The process of casting photoelastic models of even simple shapes requires adequate facilities and sufficient experience in the field. It is often preferred to use commercially available photoelastic sheets, blocks or circular bars rather than casting the desired sections. Sharples Ltd (U.K.) and Photolastic Inc (U.S.A.) have specialised interests in the photoelastic field and they provide consultancy, design and manufacturing facilities in this field. Unfortunately like all other commercially orientated business concerns, the cost of such

service is extremely high for academic institutions to bear. Because of this consideration, the bare necessary facilities were created in the laboratory to undertake the casting of photoelastic models. After a series of tests and modifications it became possible to cast photoelastic models of channel section beams with little residual birefringence.

This exercise took more than a year before giving adequate results.The various steps involved in the casting process are described below.

ii.a) Choice of photoelastic model material

The choice of a proper model material is very important in photoelastic work and the necessary characteristics for its selection depend on the type of owork. These characteristics are described in [37].

A channel section fabricated from CT 200 Araldite sheet showed good results in terms of isochromatic fringe distribution when stresses due to complete warping inhibiton were studied with it. This material was basically recommended for stress freezing technique. The available facilities in The School of Automotive Studies laboratory were not adequate for stress freezing. CT 200 exhibited a low stress optical sensitivity in normal photoelastic work and fringe orders between one and two were obtained by a reflection polariscope without distorting the shape of a model. This material is quite brittle and all machining operations require careful handling. Small residual birefringence was noticed on machined edges of the models made from CT 200. Time edge effect was practically very small over a period of six months and can easily be ignored. It did not exhibit appreciable creeping effects under load over a period of 24 hours. The casting procedure requires annealing in carefully controlled temperature conditions i.e. the temperature drop should not be more than $2^{o}C$/hour |40|.

Some other photoelastic materials with high stress optical sensitivity and requiring simple casting methods are available from Photolastic Inc.(U.S.A.)[41]. These materials were considered very expensive for use in the present work. CT 200 was the least expensive model material for casting purposes and its constituents were available from Ciba Geigy (U.K.) in bulk quantities. The commercial names of these constituents of CT 200 are:

(i) Araldite CT 200
(ii) Hardener HT 901

The choice of CT 200 as a model material in the present experimental work was mainly made because of its low cost and quick procurement.

ii.b) Design of the moulds

A major requirement of the experimental work was to cast channel section models of uniform wall thickness and this was considered in the design of suitable moulds.

A very simple mould consisting of an outer U-shaped aluminium shell

with a solid aluminium block was designed and manufactured. The block when placed in the outer shell provided a uniform gap in which a channel section of uniform thickness can be cast. The casting surfaces of the mould were polished so as not to produce scratches in the casting. One end of the mould was closed by an aluminium end plate and two aluminium spacers were inserted along the mould flanges. Molten Araldite and Hardener mixture was poured in the cavity and the mould was kept in vertical position. The leakage of the mixture from the mould posed a serious problem. A large variety of sealing agents such as Hermatite, Pyroma, clay, plaster of Paris and high melting point grease etc. were tried to stop this leakage but in vain. At a casting temperature of 130°C, the leakage was not be controlled. Whatever mixture was left in the mould solidified as desired, but releasing this casting from the mould posed another difficulty. Draught angles were not used on the flange mould surfaces as a uniform wall thickness was a main requirement. The photo-elastic analysis of a model with a non-uniform wall thickness becomes a very complicated problem. It was decided to modify the mould design to overcome these (leakage and mould releasing) problems.

The outer shell was made by joining three aluminium plates with screws so as to strip the shell during the releasing operation. "O" rings were used to solvethe leakage problem and they were placed in slots provided along all the mating surfaces of the mould. The solid aluminium block was attached to a top cover plate which was screwed on the side plates of the outer shell during assembly of the mould. Two end plates with rubber gaskets were screwed to the mould ends. The length of the mould was decided from the space available in the electric oven. The aluminium moulds are shown in Plate 3.1. These moulds were successfully employed in casting many photoelastic models of channel sections.

ii.c) Casting procedure

A thermostatically controlled electric oven (Gallenkamp Electric Oven) was used for heating purposes during the casting process. The controlled cooling rate for CT 200 Araldite during casting was recommended as 2°C/hour. It was not possible to achieve this control by manual operation which was available in the oven. A small electrically operated mechanism consisting of an electric motor and a reduction gear box was installed on the thermostat of the oven. This mechanism provided one rotation of the drive shaft in 48 hours which was further reduced to 1 rev. per 96 hours by installing small plastic gears. This arrangement gave the desired automatic temperature control of the thermostat.

The aluminium mould was always cleaned by Gramasol de-greasing agent and the casting surfaces were polished before every casting. Silicon mould release agent was applied to all casting surfaces and the unassembled mould was pre-heated for 15 minutes at 110°C in the oven. All the casting surfaces were polished again with a fine cloth so that the excess mould release agent was removed. Then the mould was assembled by screwing tightly against the "O rings", and an end plate was fitted along with a rubber gasket on one side only, leaving the other

end open for pouring purposes. The assembled mould was then kept in the oven at 140°C for at least half an hour before pouring the plastic in it. This was to ensure that constant temperature was maintained throughout the mould components.

Araldite CT 200 and the hardener HT 901 in proportions of 4:1 by weight were measured in quantities which would be sufficient to fill the mould when mixed in liquid state. Each one of the constituents was heated in a glass beaker to 140°C in the oven.

The glass beaker containing the hardener was always kept covered during heating as very pungent vapours formed when it melted. It took about 45 minutes on the average to obtain a homogeneous solution of each. At this stage the Araldite solution was taken out of the oven and stirred slowly until the temperature dropped to about 130°C. The hardener solution was poured slowly into the Araldite solution and the mixture was stirred constantly to keep the mixture temperature around 130°C. The exothermic reaction tended to increase the mixture temperature if the mixing was done too quickly and with inadequate stirring. The mixture was kept for about 20 minutes at 130°C until a clear bubble-free solution was obtained. The solution was filtered through a cloth filter if some impurities were found in it. The clear mixture was poured slowly into the preheated mould. Care was taken to ensure that as far as possible air bubbles were not trapped inside. The second end plate was screwed in position and the mould was transferred back to the oven and the temperature was set to 126°C.

The mould was allowed to stay at this temperature for about six hours after which the temperature control mechanism was switched on so that the temperature would decrease at 2°C/hour rate to 70°C. The oven and temperature control switch were switched off at this temperature and the mould was allowed to cool to 40°C. It took about 36 hours in all to reach the stage at which the mould was ready for stripping to release the photoelastic model from it.

ii.c) Curing and annealing of photoelastic models

The photoelastic models produced by casting, as described in the previous section, could not be used directly for photoelastic analysis. Residual birefringence was visible in them when they were examined by a transmission polariscope. They had to be further cured and annealed to remove this residual birefringence.

Each of the cast models was placed in the electric oven on a flat surface free from constraints. The temperature was raised to 134°C and the models were kept for about four hours at this constant temperature. It was observed that the models, when cured at temperatures higher than 138°C, deformed permanently. The best results were obtained by controlling the curing temperature carefully between 130°C to 135°C. The temperature of the oven was reduced after four hours by switching on the temperature control mechanism which brought the temperature to 75°C in about 36 hours. The oven

was then switched off and the models were allowed to attain room temperature inside the oven. The models were examined once again for residual birefringence with a transmission polariscope.

It was found that the models obtained after performing the above curing and annealing cycle were almost free from residual birefringence effects. A small amount of birefringence was noticed in some models around tiny impurities which could not be filtered out during the casting procedure. Care was taken during fabrication of joints that spots showing residual birefringence did not occur in the critical region of the joint so that the stress pattern did not get distorted. It was also observed in almost all the models that the free edges of the flanges showed some residual birefringence.

ii.d) Machining of CT 200 models

The rubber gasket used to stop leakage from the ends of the aluminium moulds became imbedded in the plastic models. The two ends of every cast section had to be cut off to remove portions of gasket material. Also, to obtain sections of the desired flange width, the flanges were cut. The cutting of flanges and ends of a cast section was done on a band saw. The models were cut very carefully to avoid chipping of the edges and the introduction of excessive machining stresses.

The edges of cast sections were later smoothed by filing and using fine emery paper. A small residual birefringence remained on the edges cut with a band saw. In some models chipping produced small effects which changed the fringe distribution along an edge.

ii.e) Photoelastic models of isolated joints and a ladder frame

After successfully casting channel sections, it was decided to extend this procedure to cast a model of a complete isolated joint consisting of two channel sections attached to each other.

An aluminium mould was designed for casting a complete joint. Plates (3.3) & (3.4) show this mould in unassembled and assembled form. This mould was used to cast a model of a joint using the casting procedure employed for casting individual channel sections. But releasing the cast model from the mould caused a major problem. CT 200 plastic being brittle could not stand even the small force used to release it. The model broke during the releasing stage. Later, a few more attempts were made to cast a complete joint but unfortunately every model broke during the releasing stage. The failure to free the cast model in one piece was apparently due to the mould release agent although it was used satisfactorily in casting channel sections. Ultimately it was decided to use a suitable adhesive for making models of isolated joints and a ladder frame from cast channel sections.

A heat curing adhesive was recommended |42| for bonding purposes. Its constituents were:

1. Araldite Epoxy Resin AY105
2. Araldite Hardener HY 951.

They were mixed in recommended proportions and the adhesive was applied to the bonding surfaces. The joint was cured at 50°C for twenty hours in the electric oven. Bonds of sufficient strength were obtained after some experience. The models of isolated joints made in this manner are shown in Plate No. (3.2). The cross member in the isolated joints I, II and IV was attached on the outside of the channel section web so that photoelastic measurements could be made on the cross member near the joint.

A model of a ladder frame shown in Plate (3.6) was fabricated from cast channel sections. The ends of cross members were supported and secured carefully in place during the initial stages of curing the adhesive. All the cross members were first attached to one side member and the joints were cured. Then the free ends of the cross members were positioned with respect to the second side member and joints were made. Each section used in the ladder frame was inspected for residual birefringence by a transmission polariscope. The sections used had minimum residual effects. But when the portions of the complete ladder frame were seen through a reflection polariscope, a large number of areas of residual birefringence appeared especially on the side members. This was probably due to the force used to position the cross member ends in the second side member. The entire ladder frame was then subjected to a stress annealing cycle in a large electric oven with coarse thermostatic controls. This procedure helped in reducing residual birefringence on the side members but resulted in deforming the cross members. The cross members sagged in the middle by a small amount and residual birefringence appeared in the middle. The effect of residual birefringence near the cross member ends was quite small. It was expected that during the loading of the frame fringe measurements in the region of the joint would not be affected.